Università degli Studi di Torino
Doctoral School of the University of Torino
PhD Programme in Chemical and Materials Sciences XXXIII Cycle

Synthesis of Covalent Organic Frameworks with Donor-Acceptor Structural Linkers and Preliminary Investigation of Their Electrochemical, Optical and Storage Properties

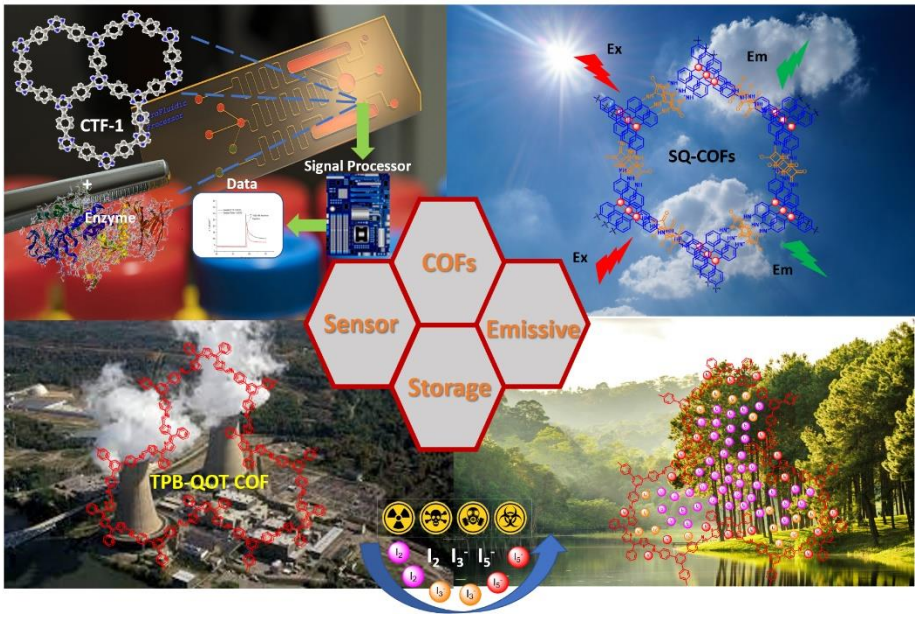

Onur Yildirim

Supervisor:
Prof. Claudia Barolo

Università degli Studi di Torino

Doctoral School of the University of Torino

PhD Programme in Chemical and Materials Sciences XXXIII cycle

Synthesis of Covalent Organic Frameworks with Donor-Acceptor Structural Linkers and Preliminary Investigation of Their Electrochemical, Optical and Storage Properties

Candidate: **Onur Yildirim**

Supervisor: Prof. **Claudia Barolo**

Jury Members: Assist. Prof. **Nadia Barbero**
Università di Torino
Dipartimento di Chimica

Prof. **Marco Milanesio**
Università del Piemonte Orientale
Dipartimento di Scienze e Innovazione Tecnologica

Prof. **Francesca Brunetti**
Università di Roma Tor Vergata
Dipartimento di Ingegneria Elettronica

Head of the Doctoral School: Prof. Alberto Rizzuti
PhD Programme Coordinator: Prof. Bartolomeo Civalleri

Torino, 2021

Abstract

Throughout the present PhD thesis, the synthesis and characterization of different 2D covalent organic frameworks (COFs) as well as investigation of their morphological, photophysical, storage and electrochemical properties are reported and thoroughly discussed. Three different scaffolds have been investigated, namely triazine-based, squaraine, and quinoid-oligothiophene. Different structures will lead to COFs showing peculiar features that make them suitable for tailored application (such as electrochemical enzymatic biosensors, photovoltaics or iodine-capturing sponges). Indeed, all the proposed materials are synthetized by a condensation reaction based on reversible linkage by changing the building blocks or linkers. The proposed approach highlights the versatility of this class of materials as well as their possible tunability by means of thoughtfully designed modification of the chemical structures.

In the first study, we harnessed the simplicity, enhanced conductive property, and organic nature of COFs in electrochemical enzymatic biosensor aiming at detecting superoxide radicals as a model system. Two different well-known semiconductive triazine-based COFs, CTF1 and TRITER-1, were successfully synthesized and characterized using Fourier transform infrared spectroscopy (FT-IR), nuclear magnetic resonance (NMR), X-ray diffraction (XRD), and transmission electron microscopy (TEM). We especially chosen these two COFs which are composed of aromatic units such as benzene (donor) and triazine (acceptor) to test the stability of their bridge, such as C-C (strong covalent bond) and C=N (weak covalent bond) when exploited as sensor matrix. Electrochemical studies demonstrated that CTF-1 improves the electrochemical performance of the enzymatic biosensors and is suitable for electrode design. Using the developed

CTF-1-based biosensor that uses superoxide dismutase (SOD), we measured the levels of superoxide anions that are commonly present in cancerous tissues, with a very promising 0.5 nM detection limit.

To extend the field of application of COFs based on reversible linkage, we designed and synthetized new squaraine-based system with a donor-acceptor geometry to be exploited in photovoltaic devices. Squaraines-based molecules are dye characterized by large emission and narrow band gaps owing to their zwitterionic form and presenting an extended conjugation. For this reason, they are generally used as light-harvesting materials in solar cells. Thus, we aimed at synthetizing squaraine based 2D COFs (SQ-COFs) showing an extended conjugation system by exploiting suitable tritopic linkers to enhance optical properties. SQ-COFs were synthesized based on polycondensation reaction using donor units such as triphenyl benzene, triphenyl amine, triphenyl methane or acceptor unit like triphenyl triazine with squaric acid. A huge effort has been devoted to the optimization of reaction conditions (exploiting both solvothermal and thermal (reflux) method) in order to simultaneously maximize the yield and selectivity of the reaction but also the crystallinity degree of the materials. Synthetized polymers were characterised through FT-IR, elemental analysis, P-XRD, TGA, Solid-state UV-Vis-NIR diffuse reflectance spectroscopy, SEM and CO_2 adsorption-desorption isotherms. In addition to this, ^{13}C-CPMAS (cross polarization magic angle spinning) NMR, ^{15}N-CPMAS NMR and phosphorescence spectroscopy (solid state) were performed. ^{13}C- and ^{15}N-CPMAS NMRs demonstrated that TAPT SQ polymer was successfully obtained. Polymers indicated redshift emissions when compared to model compound. These significant bathochromic shifts and narrow band gaps show that conjugated 2D SQ-polymers can be suitable for future optoelectronic

applications. Indeed, these materials are currently under investigation as active materials in Perovskite Solar Cells.

It should be pointed out that the versatility of COFs is one of the main strengths of this class of materials. As a proof of concept of this, SQ-COFs have been also testes in iodine-uptake. Indeed, they include in their backbone some active sites (heteroatom like nitrogen and oxygen and/or aromatic units) that can interact with iodine. Yet, only modest absorption ability was proved. Therefore, to increase iodine uptake capacity, we designed new building blocks including various active sites such as π-conjugation, aromatic units, heteroatoms such as nitrogen and especially sulfur whose lone pairs have been proved to suitably interact with iodine species. Thus, novel imine-linked COF containing quinoid-oligothiophene linear building block has been developed. Four different quinoid-oligothiophene compounds were designed and one of them (which is composed of thiophene and its quinoid form containing phenyl rings linked with methine bridge) has been selected as case study. This was polymerized using tris(4-aminophenyl)benzene (TAPB) as co-building block. The polymer was characterized through FT-IR, P-XRD, solid state UV-Vis-NIR diffuse reflectance spectroscopy, TGA, SEM-EDX and CO_2 adsorption-desorption isotherms. Once its iodine adsorption capacity was investigated, remarkably high capacity (428 %wt) was detected mainly ascribable to the relevant presence of S atoms, as also proved by TEM analyses. This value is comparable or even higher than the current state of the art. Thus, this kind of building block incorporated into 2D polymer might be very appropriate adsorbent material in terms of gas storage features.

The results obtained throughout the present Ph.D. thesis, both in terms of synthetic and application results, proved the versability and the tunability of

Covalent Organic Frameworks, proposing the latter as one of the main promising class of materials for the next decade.

Summary

Chapter 1
Design, synthesis of Covalent Organic Frameworks

Chapter 2
Electrochemical and storage applications of Covalent Organic Frameworks

Chapter 3
Synthesis of Triazine-based Covalent Organic frameworks and using as semi-conductive materials in electrochemical biosensors.

Chapter 4
Synthesis of Novel 2D Squaraine-based Covalent Organic Frameworks containing donor-acceptor units and their structural, surface and photophysical characterisation.

Chapter 5
Synthesis of Quinoid Oligothiophene-containing 2D imine-linked Covalent Organic Frameworks and their structural, surface and optical characterisation and iodine adsorption studies of TPB-QOT COF

Chapter 6
Summary of obtained 2D Covalent Organic Frameworks and their applications.

Table of Contents

CHAPTER 1

Covalent Organic Frameworks: Design and Synthesis

1.1 Introduction

The existence of ordered porous materials and nanomaterials with controlled porosity and functionalized structure has paved the way for new materials chemistry. These materials having micro-, meso-, and macropores, involving also hierarchical structures, exhibit peculiar functions making them proper for utilization in cutting-edge high technological devices. Porous structures are already existent in Nature and nowadays researches try to mimic them to create useful materials for humankind. Typical examples of porous structures in Nature are honeycomb, sponges, pollen[1] and, royal jelly.[2] During the last years, researchers have performed enormous advancement in the creation of various chemical structures with discrete (zero-dimensional, 0D) to extended (1D, 2D, and 3D) structures by assembling the distinct building units in different ways (Fig. 1.1). There are several examples ranging from 0D[3,4] to 3D[5,6] extended structures, from inorganic[7,8] to organic[9] units, from disordered to regular[7] arrangements, and from nonporous[10] to porous types.[11] Diverse linking strategies for the connection of building units have been followed; based on weak[12,13] (such as π-π stacking) to strong interactions[9,14,15] (e.g. covalent bonding).

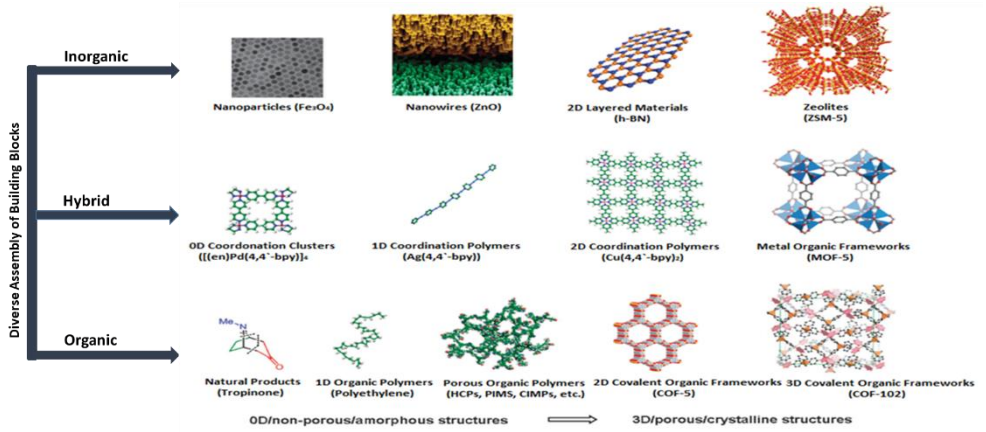

Fig. 1.1 Selected examples for diverse assembly of building units to construct inorganic/hybrid/organic chemical architectures, ranging from the discrete 0D/non-porous/amorphous structures to the extended 3D/porous/crystalline structures.[16]

Covalent organic frameworks (COFs) are novel class of crystalline porous materials and have drawn remarkable attention owing to their distinctive features. They have exceptional potential design that different molecular organic building blocks can be assembled in a great number of diverse possibilities. They are two or three-dimensional novel porous crystalline organic materials composed by light elements (H, B, C, N, and O), metal-free with extended structures in which building blocks are connected by reversible covalent bond formation.[16,17,18,19] Determination of the geometry of the framework is previously possible through the size, symmetry and connectivity of the linkers and so. On the contrary to linear polymers, COFs suggest positional control over their building blocks in two and three dimensions. This control allows the synthesis of structures with high regularity and the fine-adjusting of the chemical and physical properties of the network. Nanoscale channels and regular voids constructed throughout the COF scaffolds present and ideal environment for storage, separation and release processes. On the other side, the large interface is useful for catalysis and sensing

applications. Furthermore, the regularity and connectivity of the organic units make COFs promising candidates for applications based on charge carrier transport, involving optoelectronics and electrochemical energy storage.

COFs were firstly synthesized by the co-condensation of boronic acids with catechols to build a five-membered boronic ester rings linkage between the building blocks, and by self-condensation of boronic esters to boroxines.[9] Afterwards, various distinct reactions have been successfully implemented in the formation of COFs.

These materials have already demonstrated various unique features such as high chemical and physical stability, crystallinity, large surface area, conductivity, and, more remarkably, possibility of functionalization with different building blocks. Significantly, 2D structures with shorter interlayer distances indicate the existence of interactions between the aromatic organic moieties of the layers. Ideally, a 2D COFs with a π-conjugated system could present electronic interactions among the different sheets, so becoming a promising active material and conductive one Supposing that donor and acceptor molecules can be ordered in space in a controlled manner, then the interface between donors and acceptors could be organized at the molecular level obtaining unique properties. We summarised their design, synthetic methods and conditions from the literature.[20]

1.2 Synthesis

Reaction of organic compounds generally takes place with kinetically control which results in formation of irreversible chemical bonds.[21] On the other hand, in reversible reaction covalent linkage is broken up and come together during the reaction and so occurs error-correction under thermodynamic control that

generete final structure without defects[22] and polycondensation reactions provide formation of thermodynamically stable polymers. Therefore, reversible covalent bond is crucial for construction of covalent organic frameworks in terms of orderly layered form. Interestingly, unusually a number of COFs have been synthesized based on irreversible covalent bond linkage such as phanazine, dioxin, and C=C, through nucleophilic aromatic substitution reactions.[23,24,25,26]

1.2.1 Synthetic Methods

1.2.1.1 Solvothermal Synthesis

COFs have been synthesized mostly under solvothermal conditions that relies on the solubility, reactivity of building blocks, and reversibility of the reactions. Reaction time, temperature, solvent conditions, catalyst concentration play significant role in creation of crystalline porous COFs. According to the synthesis process; pyrex tube is generally used as a vessel, suitable monomers, catalyst, solvents or solvents mixtures are added into that tube with proper volume, the mixtures are sonicated for a short time and degassed by freeze−pump−thaw cycles, sealed under flame then kept at a convenient temperature for a certain period. After reaction is ended the tube is cooled at room temperature, and the precipitate is collected by centrifugation or filtration and washed with a suitable solvent or solvents at room temperature or by Soxhlet extraction to exchange high-boiling-point solvents as well as removing oligomers. The residue is dried under vacuum at 80−120 °C.

1.2.1.2 Microwave Synthesis

Solvothermal methods have harsh conditions such as reaction preparation and time that is one of the most significant. For this reason, microwave method has

been developed for the rapid preparation of crystalline porous COFs. Prof. Cooper and co-workers first time attempted to use microwave method by synthesising of boronate-ester-linked COF-5 and COF-102.[27] They have successfully obtained COFs 200 times faster (i.e. 20 minutes reaction) compared to solvothermal method (72 hours). In addition, imine-linked TpPa-COF have been successfully synthesized by using the microwave method.[28] In this method, monomers and solvent or solvents as well as catalyst are added into microwave vial and sealed under inert gas (i.e. nitrogen or argon) or vacuum then heated with stirring for certain time (i.e. 60 min.) at a determined temperature (100-120 °C). After reaction is ended, crude product is collected by filtration using proper solvents and dried under vacuum.

Moreover, three crystalline covalent triazine frameworks (CTFs) that are P1M, P2M, and P4M, have been synthesized via microwave-assisted.[29] The reaction was performed as follows; first of all, a mixture of trifluoromethanesulfonic acid and monomers are added in microwave vessel, sealed and stirred at 110 °C for 30 min. then reaction is stopped and the precipitate is collected, carefully ground into a powder, and washed with ammonia solution. Finally, the powder is washed with water, ethanol, acetone, and THF and dried under vacuum to get CTFs.

1.2.1.3 Ionothermal Synthesis

Ionothermal synthesis method is that ionic liquids are used as both the solvent and reagent or catalyst in the formation of solids and it is related to hydrothermal synthesis that water is used as a solvent. Using ionic liquid as a solvent suggests simple, mild, and green synthetic pathway for the synthesis of COFs on the contrary solvothermal method that has harsh conditions as well as high energy consumptions.

Even if most CTFs are amorphous and do not show more long-range molecular arrangement, two of the CTF families; CTF-1 and CTF-2 have been synthesized under ionothermal conditions and obtained as crystalline porous materials.[30,31] In this method, monomer and $ZnCl_2$ are added into pyrex ampoule, air is evacuated then ampoule is sealed and heated at 400 ^oC for 40 h. The mixture is cooled to room temperature, ground, and washed with water to remove $ZnCl_2$. After that, the powder is stirred in a diluted HCl solution for 15 h to remove more $ZnCl_2$ residue, collected by filtration, washed with water and THF, and dried under vacuum to get CTF-1 and CTF-2. In the reaction $ZnCl_2$ is molten and plays both solvent and catalyze role for the trimerization reaction that is a presumably reversible. CTF-1 has been also synthesized in the presence of p-toluen sulfonic acid catalyst by microwave-assisted. Moreover 3D ionic-liquidcontaining COFs (3D-IL-COFs) have been synthesized by using 1-butyl-3-methylimidazolium bis-((trifluoromethyl) sulfonyl)imide ([BMIm][NTf2]) as a solvent under ambient temperature and pressure.[32]

1.2.1.4 Mechanochemical Synthesis

Mechanochemical synthesis is a technique that solids are processed by incorporation of mechanical and chemical events on a molecular scale. Shortly, products are produced by means of mechanical action that is relevant high pressure and mechanical stress between reactants and balls at room temperature or at temperatures lower than common synthesis. As mentioned above, solvothermal and microwave methods have some hard conditions such as using sealed pyrex tube, certain amount solvent mixtures and temperature as well as inert atmosphere. This method has been developed as an alternative method in order to obtain these materials with simple, economically and environmentally

route instead of using such complicated conditions. The synthetic method is quite simple; the monomers are placed in a mortar and ground by using a pestle at room temperature to obtain COFs. Some COF examples have been synthesized according to this method such as TpPa-1, TpPa-2, TpPa-NO_2, TpPa-F_4, TpBD, TpBD-$(NO_2)_2$, TpBD-Me_2, and TpBD-$(OMe)_2$.[33,34] Furthermore, the liquid-assisted grinding method has been developed to well optimize the conditions. When monomers are grinding, a few of catalyst is added to improve the reaction rate in addition to crytallinity.[35,36,37,]

1.2.1.5 Synthesis under Ambient Conditions

Synthesis of COFs at room temperature are desired and attractive due to fragile building blocks or sensitive substrates even if COFs are obtained under solvothermal conditions. Boroxine-based COF films were prepared using room-temperature vapor-assisted synthesis. In the preparation of BDT-COF and COF-5 films; mixture of acetone and ethanol solution of COFs dropcast on a glass substrate and put into small vessel including mesitylene and dioxane (1:1 v/v), and placed into desiccator then waited for 72 h at room temperature.[38]

One of the efficient ways is to use water-tolerant lewis acids which are metal triflates in order to increase the formation of imine-linked 2D COFs at room temperature. For instance, for the synthesis of TAPB-PDA COF, high temperature (> 70 ^oC) and long reaction time (> 24 h) are needed according to solvothermal method however using $Sc(OTf)_3$ catalyst along with mixture of 1,4-dioxane (DOX) and mesitylene (4:1 v/v) make the reaction conditions benign possible such as performing reaction within 10 min at ambient temperature.[39] Besides synthesis of imine-linked COF-LZU1 is suitable at room temperature using 1,3,5-

triformylbenzene (TFB) and p-phenylenediamine (PPDA) in the presence of CO /water solvent at 4.5 MPa at 24 h.[40]

Gel RT-COF-1 composed 1,3,5-tris(4-aminophenyl)benzene (TAPB) and benzene tricarbaldehyde (BTCA) monomers were prepared at room temperature using acetic acid and m-cresol or dimethyl sulfoxide (DMSO).[41] This synthetic strategy that allows comprising of COFs in the gel form suggests they can be processable as well and flow chemistry is suitable method for that. For instance, a polydimethylsiloxane (PDMS) microfluidic device that is made up of four input channels connecting to a main microfluidic channel has been used to produce COF fibers under ambient pressure and temperature. In the synthesis, TAPB and BTCA monomers are prepared as a solution using acetic acid and injected into two channels on the other hand acetic acid is injected into the other edge channels via a syringe pump. MF-COF-1 was formed like sponge and directly printing on surfaces are possible without losing its high crstallinity and porosity.[42] Furthermore, 3D-printable hydrogels can be performed while adding supramolecular 3D-printing template Pluronic F127 to amorphous imine or β-ketoenamine and transformed into crystalline imine or β-ketoenamine-linked COFs by heating and removing F127 as well as upon solvent annealing.[43]

1.2.2 Linkage Diversities and Reaction Conditions

COFs consist of various building blocks that have some characteristics such as rigid π-backbones and multiple reactive sites. Size of π systems and type of reactive unit effect solubility and generally COFs are produced in a mixture of polar solvent and nonpolar solvent that is suitable for the reversible covalent bond formation. There are some important factors in their synthesis in terms of thermodynamic

control of the reaction such as combinations of solvent, catalyst, reaction temperature, and reaction time that have an impact upon the crystallinity and porosity. To date, COFs have been synthesized based on boroxine,[9] boronate-ester,[9,44,45,46] borosilicate,[47] triazine,[30] imine,[48,49,50] hydrazine,[51] borazine,[52] squaraine,[53] azine,[54] phenazine,[55] imide,[56] double-stage,[57,58] spiroborate,[59] C=C,[23,25,26,60] amide,[61] viologen,[62] hypercoordinate silicon,[63] urea,[64] and 1,4-dioxin linkages[24,65] (Fig. 1.2).

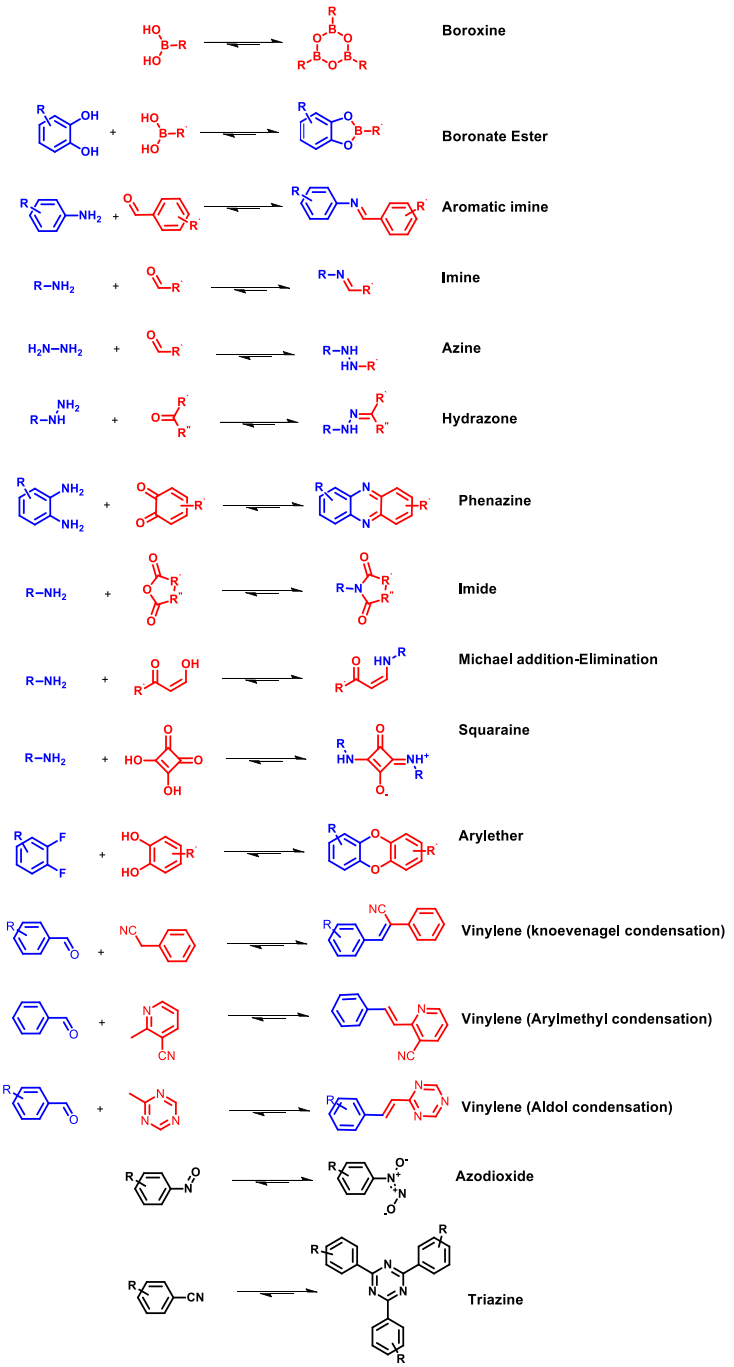

Fig. 1.2 Reported linkage motifs for the realization of crystalline COFs. The reversible condensation reactions were used for the formation of a broad range of COFs.

1.2.2.1 Boroxine Linkage

The first example of COF has been synthesized based on boroxine linkage via self-condensation of benzene 1,4-diboronic acid (Fig. 1.3) and then other six-members boroxine COF examples have been produced.[9,66,67]

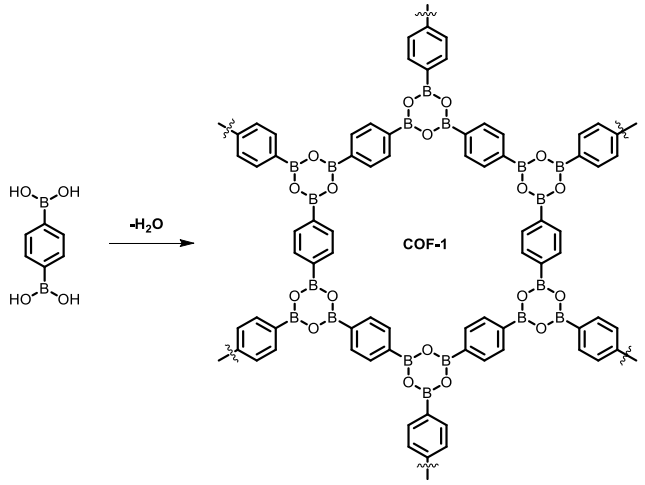

Fig. 1.3 Schematic for the synthesis of COF-1.

COF-1 and PPy-COF have been synthesized from the self-condensation of 1,4-benzenediboronic acid (BDBA) and pyrene-2,7-diboronic acid (PDBA) by using sealed pyrex tube at 120 ^{o}C[9,44] and reactions have been carried out in a mixture of dioxane/mesitylene (1/1 v/v) for 3 days (COF-1), 2 days (PPy-COF). Furthermore, three dimensional COF-102 has been synthesized through self-condensation of TBPM in a mixture of dioxane/mesitylene (1/1 v/v) at 85 °C for 4 days,[66] and 3D COF-103 has been produced by self-condensation of TBPS at the same conditions in a mixture of dioxane/mesitylene (1/3 v/v).

1.2.2.2 Boronate-Ester Linkage

Boronate-ester linked COFs have been prepared through condensation of boronic acids and catechol derivatives. The reaction of 2,3,6,7,10,11-hexahydroxy triphenylene (HHTP) with benzene 1,4-diboronic acid derivatives in a mixture of dioxane/mesitylene at 100 °C for 3 days give COF-5 (Fig. 1.4, Table 1.1).[9]

Table 1.1 Reaction Conditions for COFs based on Boronate-Ester linkage

COFs	Solvents (v/v)	Temperature (°C)	Time (days)
COF-5, AEM-COF-1	Diox/mesitylene (1/1)	100	3 or 7
COF-6	Diox/mesitylene (1/1)	85	5
COF-8, COF-10	Diox/mesitylene (1/1)	85	3
COF-105	Diox/mesitylene (1/1)	85	9
COF-108	Diox/mesitylene (2/1)	85	4
MCOF-1	Diox/mesitylene (2/1)	90	3
DBA-3D-COF 1	Diox/mesitylene (10/1)	95	3
D–A COF, COF-66, T-COFs, MC-COFs-TP, MC-COFs-NiPc	Diox/mesitylene (1/1)	120	3
TT-COF	Diox/mesitylene (1/1)	150	3
ZnP-COF	Diox/mesitylene (1/9)	120	15
CuP-COF	Diox/mesitylene (1/9)	120	2
DTP-ANDI-COF	DMF/mesitylene (1/1)	120	7
DTP-APyrDI-COF	DMAc/o-DCB (1/1)	120	7
Pc-PBBA COF	mesitylene/1,2-dichloroethane (1/1)	85	6
ZnPc-DPB-COF	Diox/MeOH (3/1)	120	3
ZnPc-PPE-COF	Diox/MeOH (5/1)	120	3
DZnPc-ANDI-COF	DMAc/o-DCB	120	14

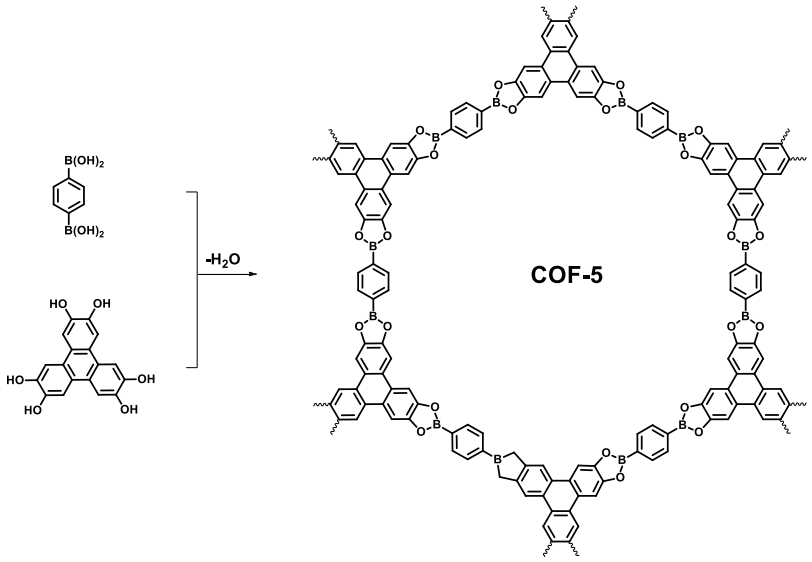

Fig.1.4 Schematic for the synthesis of COF-5

These reactions can be performed by microwave-assisted method in a short time.[68,27,69] To date boronate-ester linkage COFs have been produced using different units such as benzene, biphenyl, thiophene, anthracene, biphenyl acetylene, triphenyl benzene, triphenylene, TPE, porphyrin, and phthalocyanine derivatives resulting in with names TP-COF, D–A COF, TT-COF, T-COFs, HHTP-DPB COF, TPE-Ph COF, H2P-COF, CuP-COF, ZnP-COF, and COF-66 as well as 3D COFs; COF-105, COF-108, MCOF-1, and DBA-3DCOF-1. These COFs (2D and 3D) have been produced under solvothermal conditions in different parameters such as ratio of solvents mixture, reaction temperature or time which are dependent on the monomer formations[70,71,72,73,74] (Table 1.1).

Boronate ester linkage has high planarity and reversibility, so this is more suitable in terms of creation of crystalline structure. Besides Construction of donor-acceptor units in COFs based on that linkage system is more favorable and

bicontinuous donor-on-donor and acceptor-on-acceptor arrays in structure are possible. There are some boronate ester linked COF examples having donor-acceptor relation such as DTP-ANDI-COF, DTP-APyrDI-COF, NiPc-BTDA COF, DMPc-APyrDI-COFs (M = Cu, Ni), DMPc-ANDI-COFs (M = Cu, Ni), and DMPc-APDI-COF (M = Cu, Zn) composed by triphenylene or phthalocyanine as donors and naphthalene dianhydride, benzothiadiazole (BTDA), and pyromellitic dianhydride (PMDA) as acceptors. They have been synthesized in highly polar solvent mixtures, such as N,N-dimethylformamide (DMF)/mesitylene and N,N-dimethylacetamide (DMAc)/o-dichlorobenzene (o-DCB).[75] Boronate ester linked COFs have been also obtained using lewis acid ($BF_3{\cdot}OEt_2$) catalyst via reaction of boronic acids and acetonide monomers (protected catechols).[76,77]

1.2.2.3 Imine Linkage

Reaction of aromatic amines and aldehydes generate imine-linked COFs by using organic acid or Lewis acid catalyst (Fig. 1.5). They can be designed in different topologies which are hexagonal, tetragonal, rhombic, kagome, and trigonal structures.

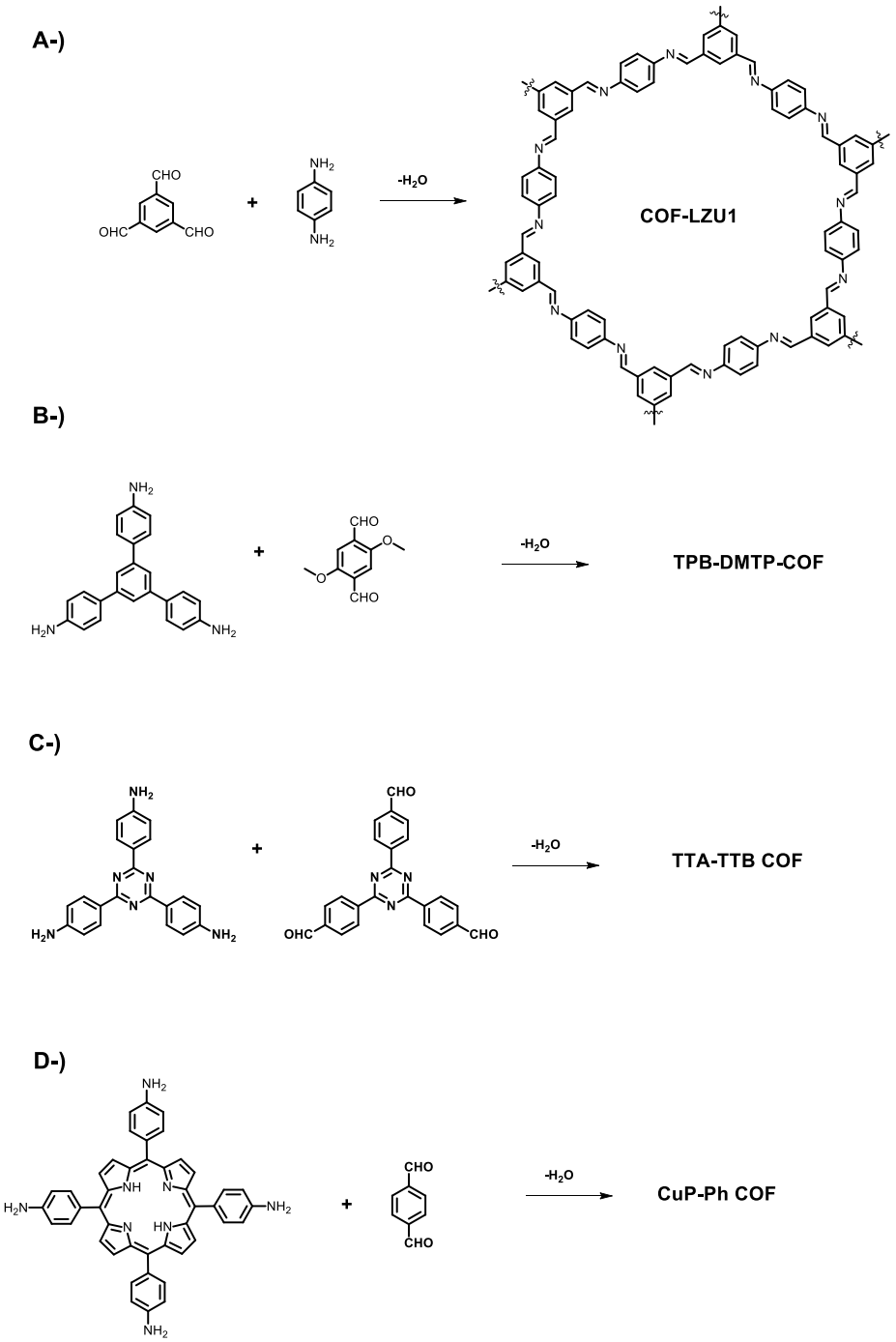

Fig. 1.5 Schematic for the synthesis of imine-linked COFs for A-) COF-LZU1, B-) TPB-DMTP COF, C-) TTA-TTB COF, D-) CuP-Ph COF

Various π-units have been utilized for their construction such as benzene,[78,79,80,81,82,83] triphenyl benzene[84,85,86,87,88,89,90,91,92] triphenyl triazine[93,94,95,96] tetraphenyl pyrene,[97,98,99,100,101] TPE,[61,84,102,103,104] tetrathiafulvalene,[105,106] porphyrin,[107,108,109,110] hexaaza triphenylene (HAT),[111,112] hexaphenyl benzene (HPB),[113] and hexabenzocoronene (HBC)[113] as knots, benzene,[39,78,89,99,107,113,114,115] ortho-substituted benzene,[87,91,96,97,110,116,117] biphenyl,[50,79,84] triphenyl,[84,114] bipyridine[85,97,118] and thiophene[84] derivatives as edges. A variety of solvent mixtures have been used in their solvothermal reactions such as dioxane, dioxane/mesitylene, o-DCB/n-butanol (n-BuOH), ethanol (EtOH), dioxane/o-DCB, THF/mesitylene, DMAc/o-DCB and reactions have been carried out in different temperatures (Table 1.2)

Table 1.2 Reaction Conditions for COFs based on Imine linkage

COFs	Solvents (v/v)	Temperature (°C)	Time (days)	Catalyst
COF-LZU1, ILCOF-1, COF-300, COF-320	Diox	120	3	3 M AcOH
2,3-DhaTta COF, 2,3-DhaTab COF	Diox/mesitylene (0.3/1.7)	120	3	3 M AcOH
Py-2PE COF	mesitylene/Diox/n-BuOH (6.67/4/4)	120	5	6 M AcOH
COF-DhaTab	Diox/mesitylene (0.3/1.7)	120	3	8 M AcOH
PI-2-COF, Py-DHPh	Diox/mesitylene (1/1)	120	3	6 M AcOH
PI-3-COF	Diox/mesitylene (10/1)	120	3	6 M AcOH
COF-LZU8	Diox/mesitylene	120	3	6 M AcOH
TPT-COF-1	EtOH	120	3	3 M AcOH
SIOC-COF-1, SIOC-COF-2	Diox/toluene (1/2)	120	3	9 M AcOH
DAAQ-TFP-COF	DMAc	90 or 120	2	6 M AcOH
TPB-DMTP-COF, Py-An COF	o-DCB/BuOH (1/1)	120	3 or 5	6 M AcOH
TAPB-TFPB, TAPB-TFP, iPrTAPB-TFPB, iPrTAPB-TFP	Diox	110	5	6 M AcOH
HPB-COF	Toluene	120	9	3 M AcOH
HBC-COF	Diox/BuOH (19/1)	120	12	6 M AcOH
CCOF-1, CCOF-2	Diox	100	3	9 M AcOH

LZU-72	Diox/mesitylene	90	3	3 M AcOH
LZU-76	DMAc	100	2	6 M AcOH
COF-505	THF	120	3	6 M AcOH
FL-COF	o-DCB/DMAC (1/1)	120	3	3 M AcOH
TAPB-PDA COF	Diox/mesitylene (4/1)	20	3	3 7.5 μM $Sc(OTf)_3$
LZU-301	Diox	120	3	6 M AcOH
Salen-COFs	DOX/EtOH (4/1)	120	3	3 M AcOH
CCOF-5	Diox	120	3	6 M AcOH
SP-3D-COF-1	o-DCB/BuOH (7/3)	130	3	3 M AcOH
JUC-508	Diox/mesitylene (4/1)	120	3	6 M AcOH

While 2D COFs have many different knots in their constructions, to date in synthesis of 3D COFs that COF-300, COF-320, BF-COF-1, BFCOF-2, LZU-301, 3D-Por-COF, only TAPM and TAA have been used as knots.[78,102,119,120] Furthermore, JUC-508, JUC-509, JUC-509-Y (Y = Mn, Cu, or Eu) which are 3D Salphen-COFs have been obtained with reaction of tetrakis(3-formyl-4-hydroxylphenyl)-methane (TFHPM) and 4,5-difluorophenylene-1,2-diamine (DFPDA) or 4,5-dichlorophenylene-1,2-diamine (DCPDA) using dioxane and mesitylene with acetic acid at 120 °C for 3 days[121] (Table 1.). A series of imine-linked COFs that TpPa-1, TpPa-2, TpBD, LZU-1 (LAG), and DhaTph (LAG) have been also produced through mechanochemical method at room temperature.[34,37]

1.2.2.4 Hydrazone Linkage

Hydrazine linkage COFs have been composed through reaction of aldehydes with hydrazides in the presence of AcOH catalyst. Since obtaining of crystalline form or improving of the crystallinity based on hydrazine linkage, containing of ethoxy group in the ortho position of edge units (e.g., 2,5-diethoxy-terephthalohydrazide (DETH)) are needed. COF-42, COF-43, (Fig. 1.6) TFPT-COF, and COF-JLU4 have been attained according to this strategy via solvothermal

method utilizing mixtures of dioxane and mesitylene or for LZU-21, mixtures of THF and mesitylene at 120 °C.[85,122]

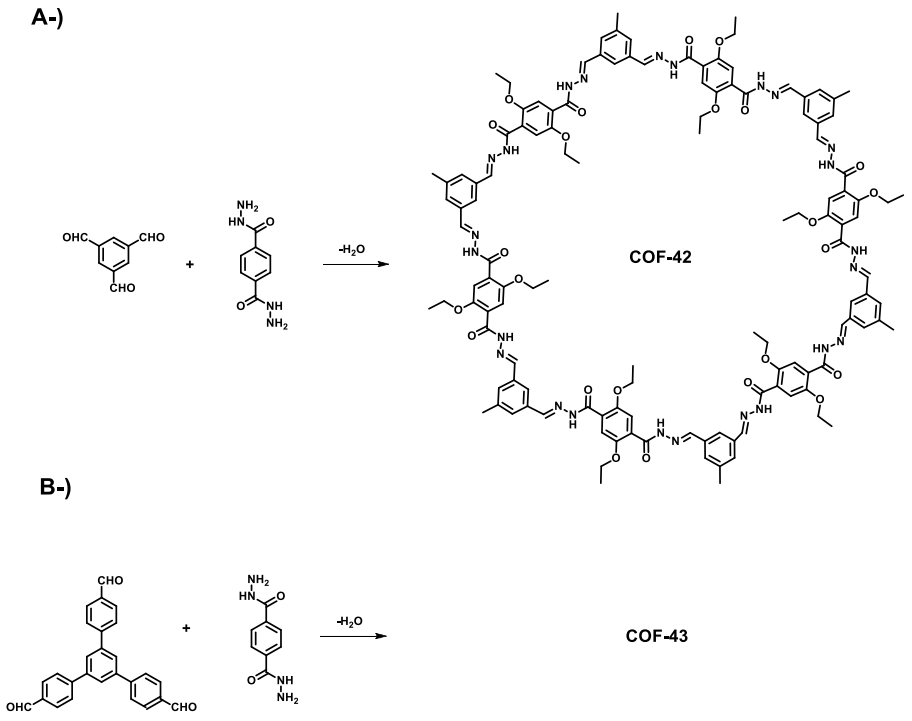

Fig. 1.6 Schematic for the synthesis of hydrazone-linked COFs for A-) COF-42, B-) COF-43

1.2.2.5 Azine Linkage

In construction of azine linkage COFs, generally hydrazine is used along with two aldehyde units and they have exhibited small porous surfaces. As knots, benzene and their derivatives, triphenyl benzene, triphenyl triazine, and pyrene monomers have been used and hexagonal, rhombic, trigonal shapes have been obtained (Fig. 1.7).[123,124,125,126] Their design and synthesis are dependent on different conditions such as temperatures, solvent mixtures and reactivity of the π-knots (Table 1.3).

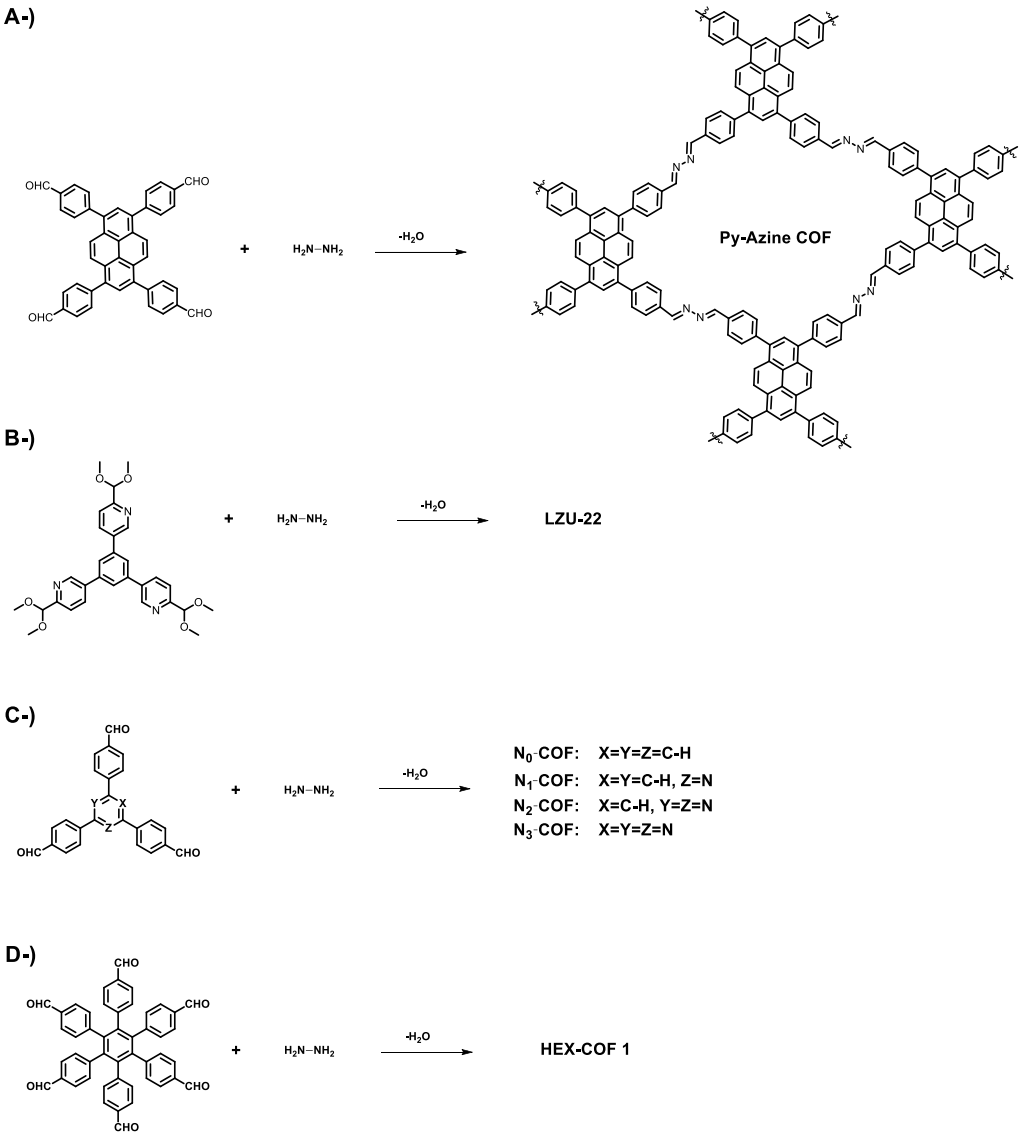

Fig. 1.7 Schematic for the synthesis of COFs based on Azine linkage; A-) Py-Azine COF, B-) LZU-22, C-) N_x-COFs, D-) HEX-COF 1

Table 1.3 Reaction Conditions for COFs based on Azine linkage

COFs	Solvents (v/v)	Temperature (°C)	Time (days)	Catalyst
Py-Azine-COF, NF-COF, TF-COF 1, TF-COF 2, AB COF	o-DCB/n-BuOH (19/1)	120	3 or 7	6 M AcOH
ACOF-1	Diox/mesitylene (1/1)	120	3	6 M AcOH
HEX-COF 1, Nx-COFs (x = 0, 1, 2, 3)	Diox/mesitylene (1/2)	120	3	6 M AcOH
ATFG COF	Diox/mesitylene (12/1)	120	3	6 M AcOH
COF-JLU2	THF/MeOH (1/1)	120	5	6 M AcOH
COF-JLU3	DMF	120	3	3 M AcOH
LZU-22	THF/mesitylene (2/3)	120	7	3 M AcOH

1.2.2.6 Imide Linkage

Reaction of amine and acetic anhydride units build imide-linked COFs and this linkage reversibility is low so high reaction temperatures are necessary (e.g. 250 °C). 2D PI-COF-1, PICOF-2, and PI-COF-3 have been produced via solvothermal method in the presence of N-methyl-2-pyrrolidone (NMP)/mesitylene/ isoquinoline (10/10/1 v/v/v) and acquired as mesoporous[56] (Fig. 1.8). While PI-COf-3 has been synthesized under 250 °C for 7 days, PI-COF-1 and PI-COF-2 have been achieved at 200 °C for 5 days. On the other hand, microporous 3D PI-COF-4 and PI-COF-5 have been prepared in a mixture of NMP/mesitylene/isoquinoline (10/50/1 v/v/v) at 160 °C for 5 days.[127]

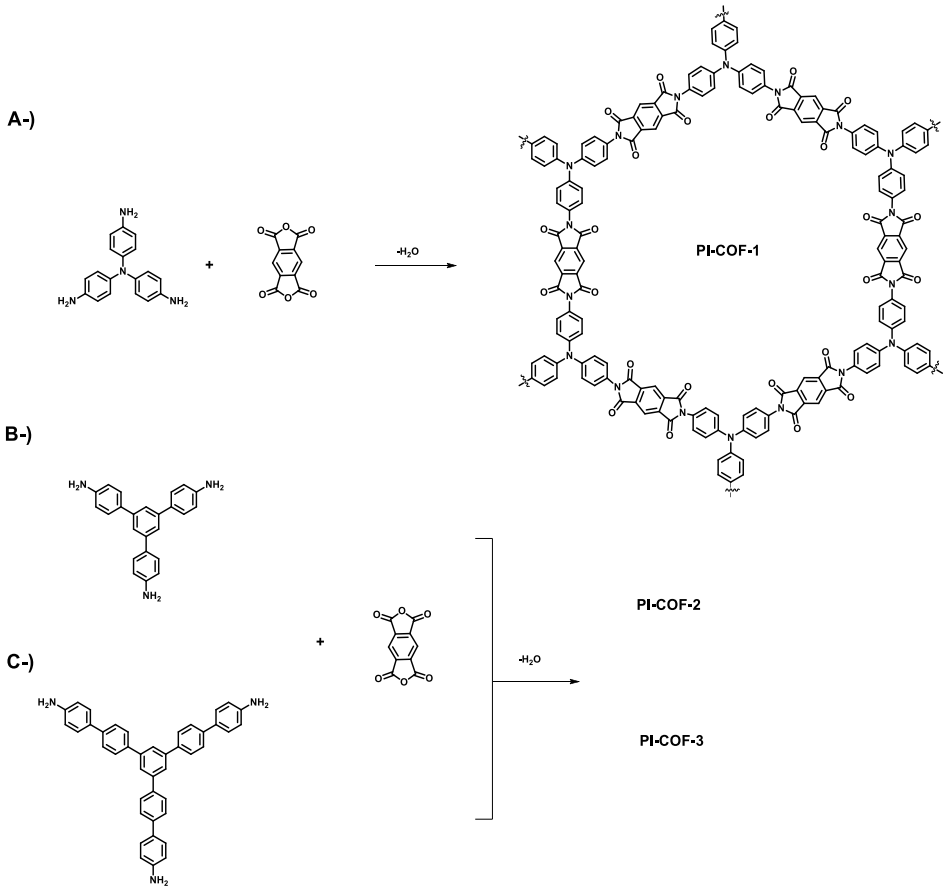

Fig. 1.8 Schematic for the synthesis of COFs based on Imide linkage; A-) PI-COF-1, B-) PI-COF-2, C-) PI-COF-3

1.2.2.7 C=C Linkage

C=C linked COFs have fully π-conjugated system and have been prepared through the Knoevenagel condensation of aldehydes and benzyl cyanides in the presence of a base catalyst. For the first time, sp2c-COF has been synthesized via condensation of tetrakis(4-formylphenyl)pyrene (TFPPy) and 1,4-phenylenediacetonitrile using mixture of mesitylene/dioxane (1/5 v/v) at 110 °C for 3 days in company with catalyst of aqueous NaOH solution (4 M)[25] (Fig. 1.9, A-)). In addition to this example, their family members have been prepared using

different linkers employing different parameters[128] (Fig. 1.9, B-)). For instance, while C=C linked 2DPPV has been produced in o-DCB at 150 °C for 3 days along with Cs_2CO_3 catalyst, TP-COF has been achieved in a mixture of dioxane/chloroform (0.05% chloroform)[26] (Fig. 1.9, B-)) and the porphyrin-based sp2c-COF has been prepared utilizing catalysis of 1,8- diazabicyclo[5.4.0]undec-7-ene (dbu, 3 M) in o-DCB.[129] In the synthesis of hexaazatrinaphthalene 2D CCP-HATN, DMAc and o-DCB have been used as solvents mixture.[130]

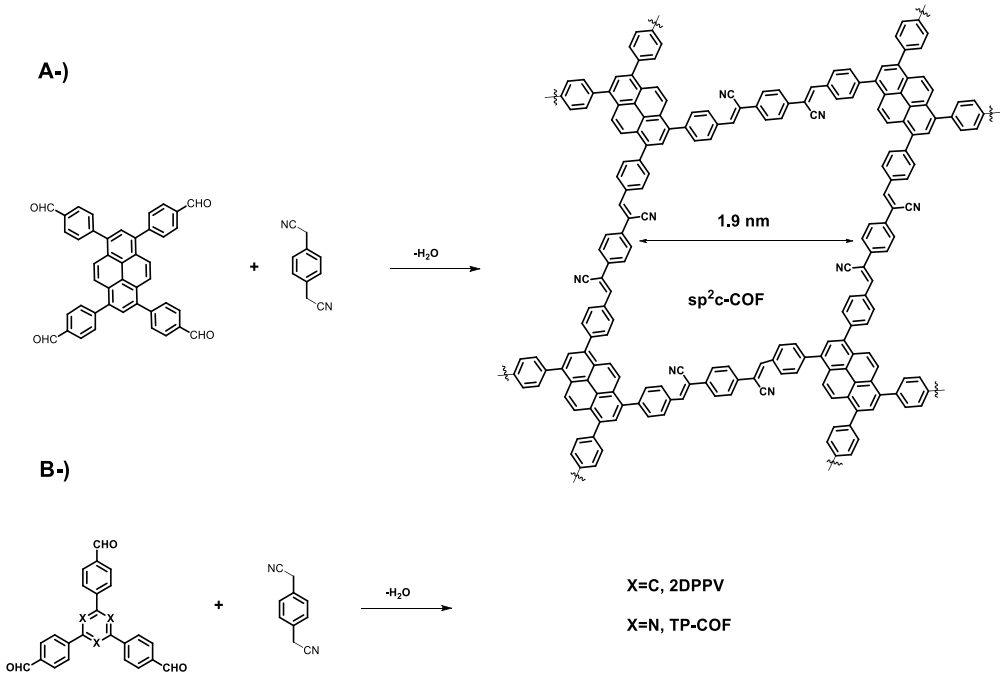

Fig. 1.9 Schematic for the synthesis of C=C-based COFs; A-) sp^2-COF, B-) 2DPPV-COF, C-) TP-COF

As for unsubstituted olefin-linked COFs, they have been prepared according to the aldol condensation. For example, COF-701 has been acquired with reaction of 2,4,6-trimethyl-1,3,5-triazine and 4,4'-biphenyldicarbaldehyde in mixture of mesitylene/dioxane/acetonitrile (18/18/1 v/v/v) and trifluoroacetic acid at 150 °C for 3 days[114] (Fig. 1.10).

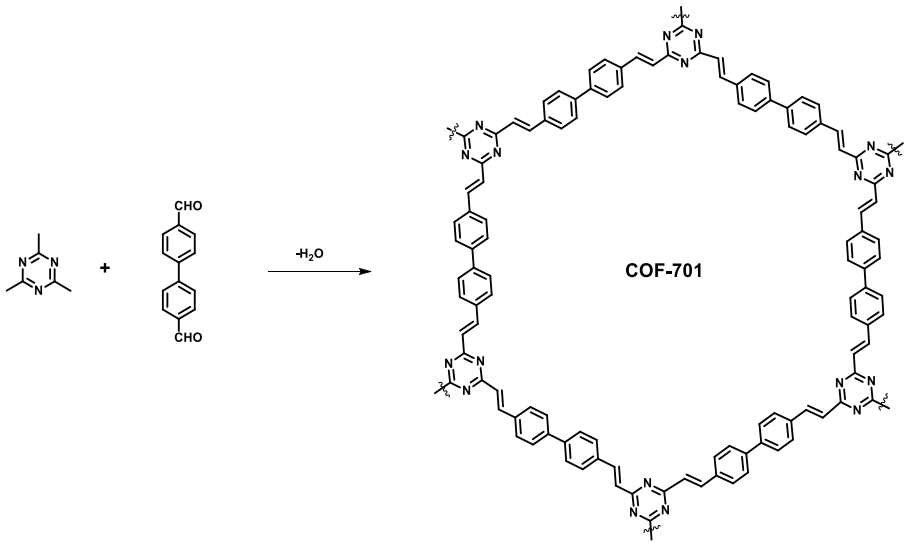

Fig. 1.10 Schematic for the synthesis of C=C-based COFs; A-) sp^2-COF, B-) 2DPPV-COF, C-) TP-COF

Other members of olefin-linked hexagonal COFs; g-C40N3- COF, g-C31N3-COF, and g-$C_{37}N_3$-COF have been produced through condensation of 3,5-dicyano-2,4,6-trimethylpyridine and 4,4''-diformyl-p-terphenyl, 4,4'-diformyl-1,1'-biphenyl, and 1,3,5-tris(4-formylphenyl) benzene using piperidine as a catalyst in the presence of anhydrous deoxygenated DMF at 150 ^oC for 3 days.[23]

1.2.2.8 Dioxin Linkage

Preparing of 1,4-dioxin linkage COFs have been carried out according to condensation reaction using ortho-difluoro benzene or pyridine and catechol building units introducing base catalyst and they have high chemical stability due to their irreversible dioxin linkage (Fig. 1.11). To date, three different dioxin-linked COFs have been obtained; the first one, COF-316 (= JUC-505) has been synthesized via reaction of 2,3,6,7,10,11-hexahydroxytriphenylene (HHTP) and tetra fluorophthalonitrile (TFPN) in dioxane, or N-methylpyrrolidone/mesitylene (2/1 v/v) with triethylamine (COF-316) or K_2CO_3 (JUC-505) at 120 °C for 3 days.[24,65] Add

to this, COF-318 have been made up of condensation of HHTP and 2,3,5,6-tetrafluoro-4-pyridinecarbonitrile in a mixture of dioxane/ mesitylene (1/1 v/v)[24] and JUC-506 has been took place according to the condensation of HHTP and 2,3,6,7- tetrafluoroanthraquinone along with K_2CO_3 catalyst using solvents mixture of NMP/mesitylene (2/1 v/v) at 160 °C for 3 days[65] (Fig. 1.11).

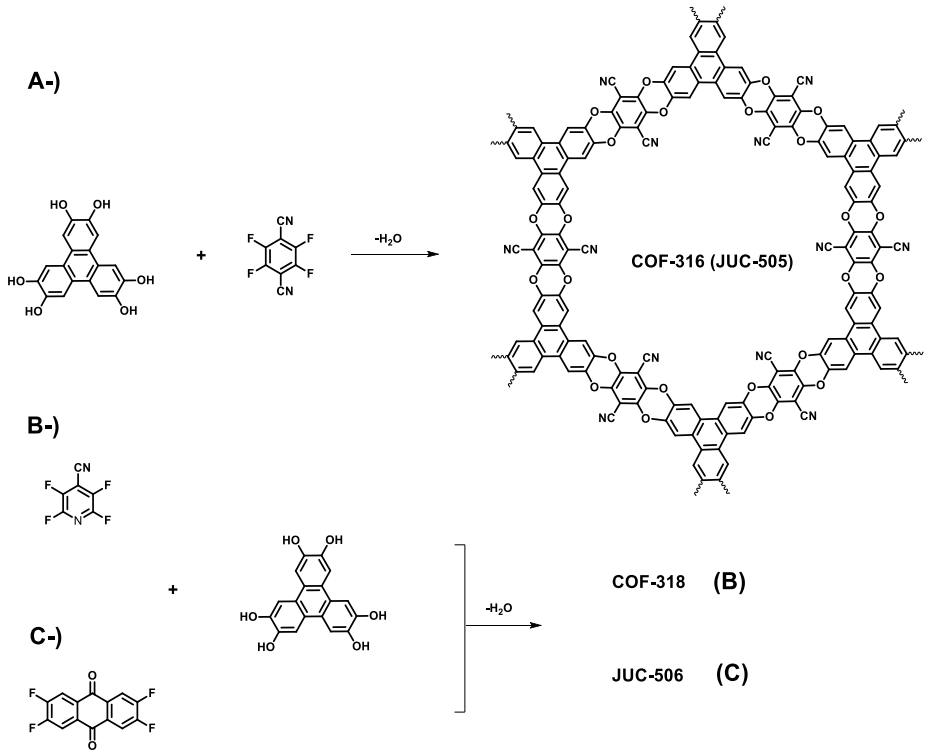

Fig. 1.11 Schematic for the synthesis of Dioxin-linked COFs; A-) COF-316 (JUC-505), B-) COF-318, C-) JUC-506

1.2.2.9 Other Linkages

Various COFs having diverse linkage types or units are also exist in addition to others mentioned above. For instance, covalent triazine frameworks (CTFs) have been prepared through the cyclotrimerization of 1,4-benzonitrile in molten $ZnCl_2$

at 450 °C[30] (Fig. 1.12, A-)). Trimerization reaction of reversibility is very low thus CTFs have low crystallinity and also linkers which constitute the CTFs are limited owing to low crystallinity. Apart from molten $ZnCl_2$ as a catalyst, trifluoromethanesulfonic acid (triflic acid) can be also used and it is possible to carry out the reaction at room temperature or under microwave conditions in the presence of acid catalyst.[29]

Another linkage is phenazine has coherent planar form and this makes the COF structure have high stability as well as π-conjugated system. CS-COF is an example of this linkage and has been constructed by condensation of triphenylene hexamine (TPHA) and tertbutylpyrene tetraone (PT) under solvothermal condition in a mixture of ethylene glycol/3 M AcOH (1/1 v/v) at 120 °C for 3 days[55] (Fig. 1.12, B-)).

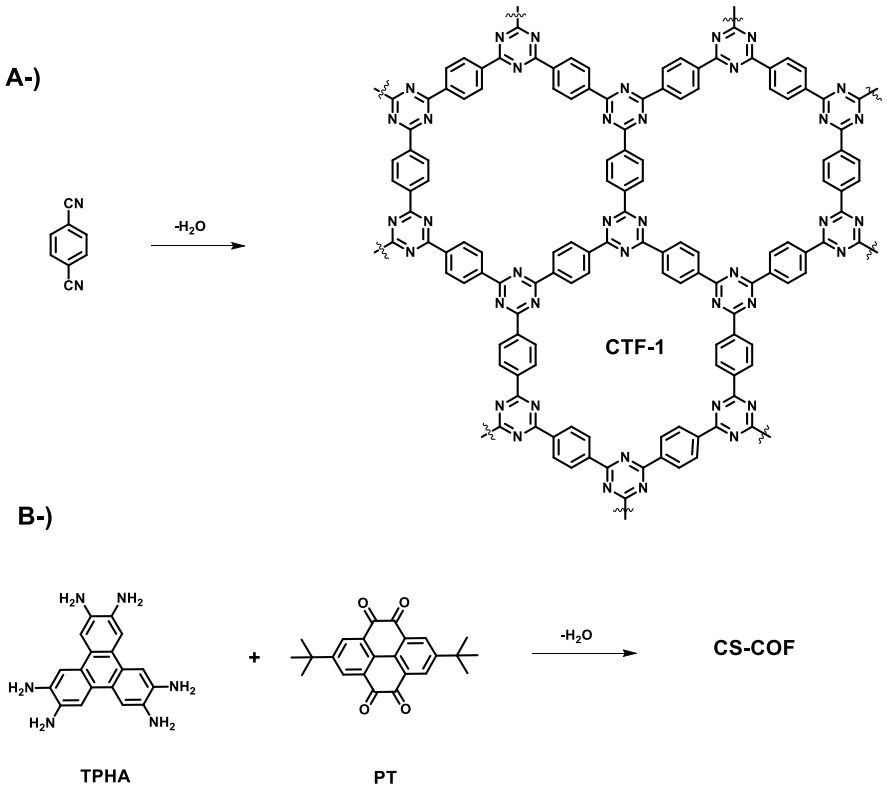

Fig. 1.12 Schematic for the synthesis of A-) CTF-1, B-) CS-COF

Phthalocyanine-based COF-DC-8 has been consist of through the aromatic reaction of 2,3,9,10,16,17,23,24-octaaminophthalocyanine nickel(II) and pyrene-4,5,9,10-tetraone.[131] Furthermore, synthesis of squaraine-linked CuP-SQ COF (Fig. 1.13) has been performed according to the solvothermal method via the condensation of copper(II) 5,10,15,20-tetrakis(4-aminophenyl)porphyrin (TAP-CuP) and squaric acid (SQ) in a mixture of o-DCB/n-BuOH (1/1 v/v) at 85 °C for 7 days.[53] CuP-SQ COF indicates unique feature such as zig-zag and zwitterionic structure.

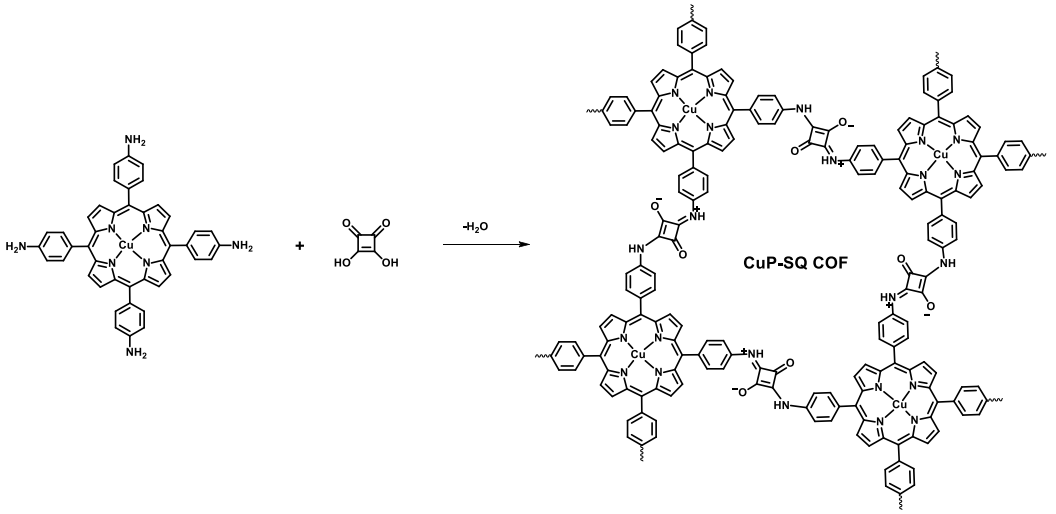

Fig. 1.13 Schematic for the synthesis of CuP-SQ COF

The borazine-linked BLP-2(H) COF has been composed through the thermal decomposition of 1,3,5-(p-aminophenyl)-benzene-borane using mixture of mesitylene/toluene (1/4 v/v) at 120 °C for 3 days.[52] Spiroborate-linked ionic COFs (ICOF-1 and ICOF-2) (Fig. 1.14) have been also prepared under solvothermal conditions in DMF at 120 °C for 7 days.[59] However, the linkage is not highly stable in water and base (1M LiOH for 2 days) when compared the other boron-based linkages.

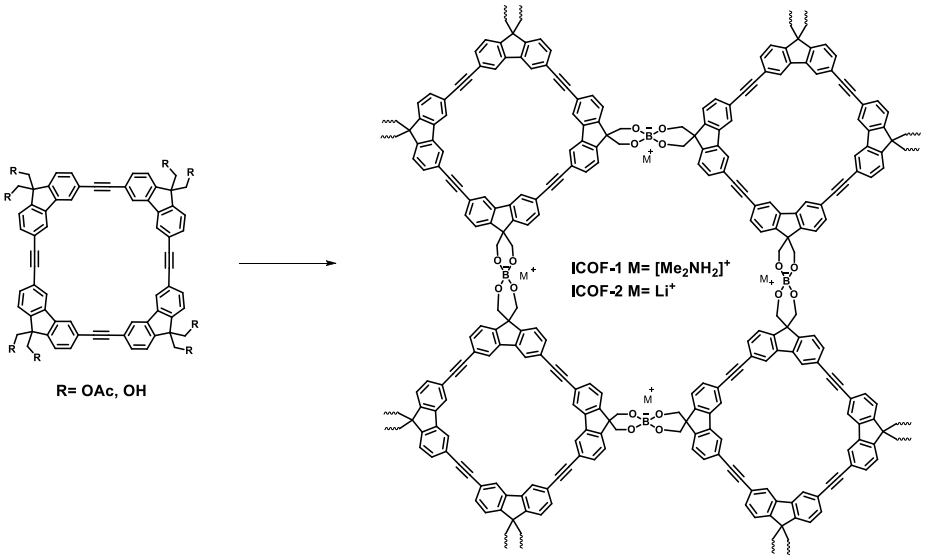

Fig. 1.14 Schematic for the synthesis of ICOFs

Zincke reaction has been used to constitute π-conjugated viologen-based COGF (Fig. 1.15, A-)) and reaction has taken place between 1,1′-bis(2,4-dinitrophenyl)-[4,4′-bipyridine]-1,1′-diium dichloride (BDB) and TAPB monomers through solvothermal or microwave methods.[62] The 2D π-conjugated PD (Fig. 1.15, B-)), BD, and TPA COFs have been synthesized via the Michael addition−elimination reaction using different β-ketoenols and amines under acidic conditions.[132]

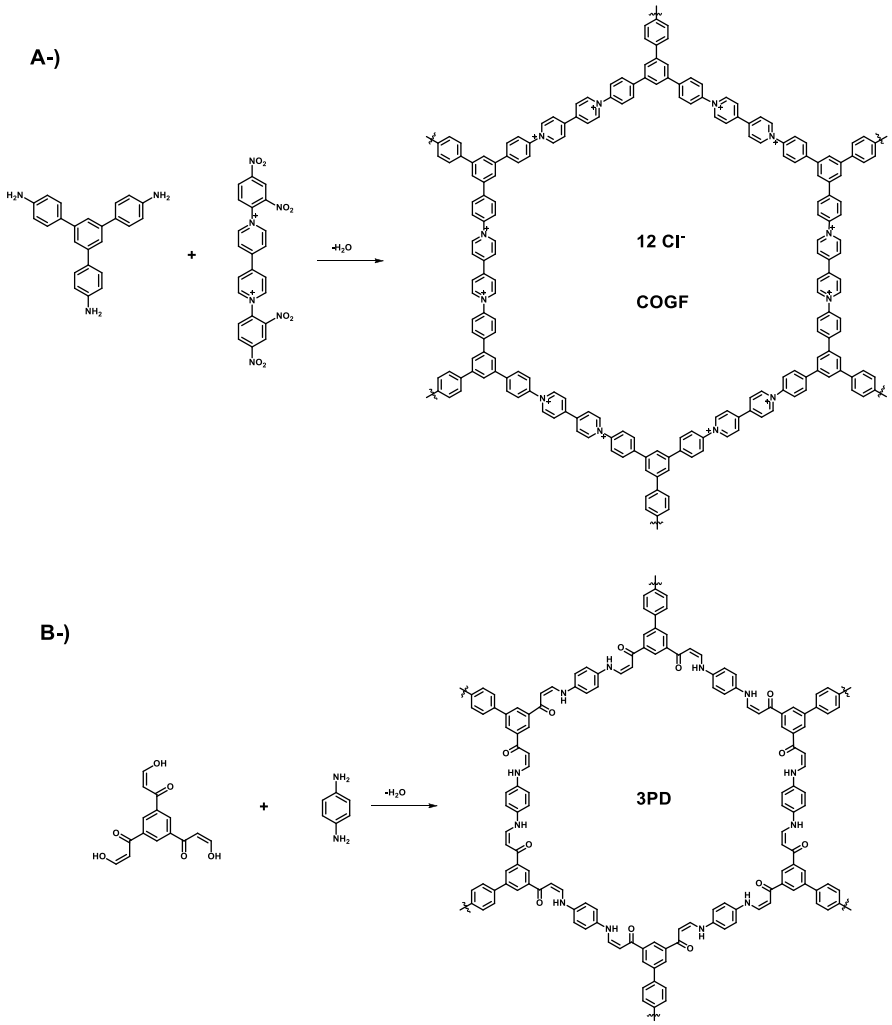

Fig. 1.15 Schematic for the synthesis of A-) COGF, B-) 3PD-COF

Reaction of tetrabromopolyaromatic compounds according to the surface-assisted debromination and aryl−aryl coupling has been led to construction of the C-C linked 2D conjugated aromatic polymer.[133] On the other hand, 2D-COF based on C-C linked (Fig. 1.16, A-)) films have been prepared via Suzuki coupling reaction at a liquid−liquid interface.[134] Another C-C linked π-conjugated covalent organic radical frameworks have been also obtained at a liquid−liquid interface in

dichloromethane/H_2O using acetylenic homocoupling of triethynyl-polychlorotriphenylmethane compounds.[135] COF-117 (Fig. 1.16, B-)) and COF-118 containing flexible urea linkages have been achieved via the condensation of TFP with 1,4-phenylenediurea (BDU) or 1,1′-(3,3′-dimethyl-[1,1′-biphenyl]-4,4′-diyl)diurea (DMBDU).[64]

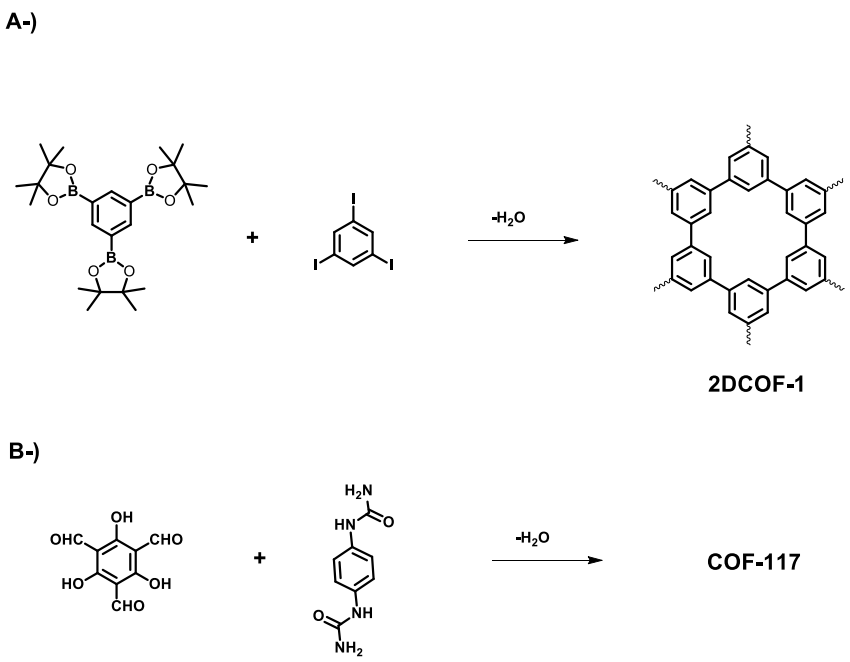

Fig. 1.16 Schematic for the synthesis of A-) 2DCOF-1, B-) COF-117

1.3 Donor-Acceptor Relation in COFs

COFs can be designed and synthesized logically that have an isolated bicontinuous donor (D) - acceptor (A) heterojunction and these donor-on-donor and acceptor-on-acceptor π-columns can suggest pathways for hole and electron transport.[71] For instance, HHTP as a donor at the corner and BTDA as an acceptor at the edges have been vertically incorporated in 2D D−A COFs as donor−acceptor

bicontinuous heterojunctions. The photocurrent showed switch on and off many times without deterioration. This kind of ordered heterojunction system can be important for photovoltaic devices.[74,136] According to the donor–acceptor-types, isoindigo- and thienoisoindigo-based building blocks, Py-pII, Py-pTII and Py-tTII COFs demonstrated low band gaps such as 1.78, 1.48, and 1.36 eV, respectively.[137] In another example, metallophthalocyanines and diimides were used as building blocks that are periodically ordered electron-donor and -acceptor π-columnar arrays in DMPc-ANDICOFs (M = Cu, Ni, Zn).[138,139] When excited of CuPc and NiPc at 355 nm in benzonitrile, those COFs indicated negative absorption bands in transient absorption (TA) spectra with 10-15 nm red shift. DMPc-ADI-COFs contain different metal centers and the one bearing Copper demonstrate longest lifetime (τ) of 33 μs for the charge-separated state, indicating that CuPc is outstanding as an electron donor to construct the long-lived charge separated state with the PyrDI acceptor.[138]

The planarity and proper pore dimension of the building blocks are significant in terms of creation donor-acceptor relation in 2D COFs.[87,140] he TTI-COF was obtained using tris(triphenylamine)triazine (TTI) and trialdehyde based on imine linkage. The layers have been stacked antiparallel to imine linkage and the stacking of the layers are favorable because of planarity of the triazine units causing high crystallinity.[140] Various trigonal or tetragonal-shaped knots have been used to build COFs. For instance, when tetragonal-shaped knot is used, COFs are obtained as armchair instead of propeller geometry which is highly desirable due to interlayer π-π interactions and it was found that electronic properties were identified through the central tetraphenyl pyrene in place of other linkers within COFs, even when incorporated with strong electron withdrawing benzothiadiazole units.[84,98]

One of the COFs based on D-A relation was also prepared using supramolecular units.[141] Electron deficient 2,5,8,11-tetra(formylphenyl)-perylene diimide (PDI) and electron rich perylene units were used to create high crystalline intercalated COF at room temperature. The C=C linked-COFs which indicates fully conjugated system, higher chemical stability than imine-linked has been also produced based on D-A interactions by knoevenagel condensation between aldehyde and benzylcyanides derivatives.[25,128] or instance, sp2c-COFdpy was obtained by knoevenagel condensation using 3,6,8-tetrakis(4-formylphenyl)pyrene (TFPPy) as donor and 2,2'-([2,2'-bipyridine]-5,5'-diyl)-diacetonitrile (BPyDAN) as acceptor. The product was obtained as a red-colored powder and exhibited uniform nanofiber morphology with an average diameter of 150 nm. Optical properties were investigated and its band gap was measured as 2.03 eV. Fullerene is well-known and widely used as electronic acceptors in organic electronics but, incorporating of fullerene into COFs is highly challenging because of non-planarity and crowded π-accumulations.[142] Functionalisation of the fullerene can be applicable procedure to solve this problem. It can be reacted with azido groups and then integrated into the pore channels of N3-ZnPc-COFs. Therefore, it can be built D-A interaction in this N3-ZnPc-COFs.[143] In addition to the fullerene, tetracyanoquinodimethane (TCNQ) is also well-known acceptor and has been attached to the pores of COFs.[144] Optical properties were investigated by diffuse reflectance spectrometer. Much shortened amplitude-averaged lifetime was measured by time-resolved photoluminescence (PL) for both C60 and TCNQ modified COFs and It was determined that charge transfer was taken place from COF donors to C60 and TCNQ acceptors. When TCNQ modified COF was dope with iodine, high conductivity was observed (4 × 10-4 S*cm-1). Moreover, according to the redox activities, this COF indicated less negative reduction and oxidation

potentials compared with pure TCNQ.[144] As a result, It can be considered that anchored acceptors incorporated into pore channels of electron-donating COFs make the insulating COFs semiconducting.

CHAPTER 2

Technological Applications of Covalent Organic Frameworks

2.1 Introduction

Determination of the geometry of the framework is previously possible according to the properties of linkers such as size, symmetry and connectivity and so, on the contrary to linear polymers, COFs suggest positional control over their building blocks in two and three dimensions.[18]

This control allows the synthesis of structures with high regularity and the fine-adjusting of the chemical and physical properties of the network. Nanoscale channels and regular voids constructed throughout the COF scaffolds present and ideal environment for storage, separation and release processes.[145] On the other side, the large interface is useful for catalysis and sensing applications. Furthermore, the regularity and connectivity of the organic units make COFs promising candidates for applications based on charge carrier transport, involving optoelectronics and electrochemical energy storage.[146]

2.1.1 COFs used in Photovoltaics

Self-assembles of molecular Covalent Organic Frameworks (COFs) layers have recently gained attention as a feasible class of semiconducting polymers.[147] The full organic nature of COFs allows to obtain highly tunable structures that could be easily functionalized with both acceptor or donor groups. Straightforwardly, COFs are being deeply investigated to be implemented as conductive polymers in photovoltaic application.

As deeply discussed in the first chapter, COFs are usually synthetized as bulk materials by using boronate esters or imine bond-bridged systems as precursors.[148] Yet, the so obtained COFs usually have poor electric conductivity in the z axis being constituted by stacked 2D layers. In this context, the introduction of imine-bridged pattern offers a feasible approach to partially extend the conjugation throughout the different layers. Indeed, whereas in boronate COFs the charge preferentially moves alongside the plane directions, imine-based COFs also allow lateral diffusion throughout the frameworks. Thereby, boronate ester-based COFs could be considered as small molecule-based electronics whereas imine-based COFs are generally described as conjugated conducting polymers.[147]

Differently from MOFs, just few examples have been reported concerning the implementation of Covalent Organic Frameworks in photovoltaic devices. Jiang et al. reported, for the first time, the synthesis of a photoconductive COF (i.e. PPy-based COF) obtained by self-condensation of pyrene diboronic acid to constitute a boroxine linked COF.[149] This was obtained as micrometric cubic crystals. They measured the photoconductivity of PPy-COF by evaporating a thin film onto an Al electrode and then cover the COF with an Au layer. If irradiated with a Xenon lamp (in the visible region) the COF-modified Al-electrode showed a linear I-V response. Additionally, the on-off ratio was not modified even after multiple switching procedures.

Another photoactive COFs was presented by Ding and co-workers: they synthesized COF using Ni-phthalocyanine through condensation reaction with 1,4-benzenediboronic acid (BDBA).[150] This COF, assembled in an electrode, exhibit a photocurrent of 3 μA when irradiated with a xenon lamp. In a successive study, the same authors discovered that pthalocyanine-based n-channel 2D-NiPc-BTDA

(3,3',4,4'-Benzophenonetetracarboxylic-dianhydride) COFs allowed a faster transport of electrons due to the AA-type stacking. Additionally, the latter absorbs light over a wide range of wavelengths up to 1000 nm.[151] In place of pthalocyanine COF, porphyrin-based ones were made by condensation reaction with benzene diboronic acid (BDBA) to obtain photoactive COFs with different electron and hole mobility following on from the nature of the metal in the porphryin building block.[152]

There are various examples of conductive and photoactive COFs. Nevertheless, their assemblage into complete devices is very challenging due to their insolubility being hardly coated (homogeneously) onto the surface of electrodes or conductive substrates. Following on from this evidence, a feasible approach to avoid the above-mentioned issues, is to directly grow the COF onto the electrode surface. Indeed, Dichtel and co-workers were able to grow oriented COF thin films by using 1,4-phenylenebis(boronic acid) (PBBA) with 2,3,6,7,10,11-hexahydroxytriphenylene (HHTP) (to produce COF-5) and Ni-phthalocyanine-PBBA COF by incorporating single-layer graphene (SLG) supported on copper, silicon carbide, and SiO2 substrates under operationally simple solvothermal conditions.[153] Remarkably, COF layers deposited onto SLG showed improved crystallinity if compared to COF powders. The Ni-phthalocyanine-PBBA-based COF on SLG/SiO2 films absorbed strongly over the visible range of the spectrum being the Ni-phthalocyanine cores chromophores. Therefore, porous phthalocyanine COFs are depicted as suitable candidate to be implemented in organic photovoltaics (OPVs).

Jiang and co-workers synthetized fullerene-loaded CS-COF, a conductive and chemically stable COF obtained by the co-condensation of triphenylene hexamine

(TPHA) and tert-butylpyrene tetraone (PT).[154] Experimentally, the dispersion of CS-COF*C60 in N-methyl-2-pyrrolidone was performed by stirring the solution at 80° C under argon flux for 1 week. Then, a mixture of PCBM (Phenyl-C61-butyric acid methyl ester) in o-dichlorobenzene (40 mg*ml–1) and the obtained suspension (40 mg ml–1 for CS-COF*C60) were spin coated (1,000 r.p.m., 30 s) onto ITO substrate as substrate for organic solar cell. They build up a 1 cm2 sandwiched device with a Al/poly(methyl methacrylate (PMMA; as a glue): CSCOF*C60/Au cell geometry. This device supplies a power conversion efficiency of 0.9% with a very large open circuit voltage of 0.98 V. Very interestingly, conductivity measurements, performed by flash photolysis time resolved microwave method (FP-TRMC), evidence that CS-COF is one of the best hole-transporting organic semiconductors ever reported having a hole-conducting mobility of 4.2 cm2*V-1*s-1. Bein and co-workers successfully obtained thiophene-based COF (TT-COF) to be implemented in a photovoltaic device by co-condensing thieno-[3,2-b]-thiophene-2,5-diyldiboronic acid (TTBA) and hexahydroxytriphenylene (HHTP).[155] They prepared a thin film COF that was employed as photoactive material to produce a photovoltaic cell (i.e. ITO/TT-COF:PCBM/Al) with an overall efficiency up to 0.05% (OCV = 0.62 V). As a result, designing a COF with larger pores and better packing of PCBM into their pores should raise the photoconversion efficiency an assure a better charge transfer.[156] Similarly, Cheng and co-workers synthesized COF by condensing (2,3,9,1016,17,23,24-(octahydroxyphthalocyanito) zinc ($ZnPc[OH]_8$) with a blend of BDBA or a BDBA-derivative that included a pendent azide moiety (N3-BDBA), they inserted covalently-bonded C_{60} units within the COF pores and proved that the charge was effectively transferred.[157] Bein et. al. reported on the synthesis of an oriented thin COF film containing benzodithiophene units and loaded with C60. The synthesis was carried out by co-condensing benzo[1,2-b:4,5-

b']dithiophene-2,6diyldiboronic acid (BDTBA) and HHTP under solvothermal conditions onto an ITO coated glass substrate. Then two different solution (i.e. [60]PCBM and [70]PCBM) were spin coated onto the COF-modified electrode. Thin BDT-COF films presented two important optical absorbance bands in the UV spectral region. Furthermore, the oriented BDT-COF films played a host role for different fullerene-based acceptors molecules. The photoluminescence of the BDT-COF film resulted to be quenched when these acceptors were loaded into COF and this evidence confirmed that charge transfer is taken place.[158]

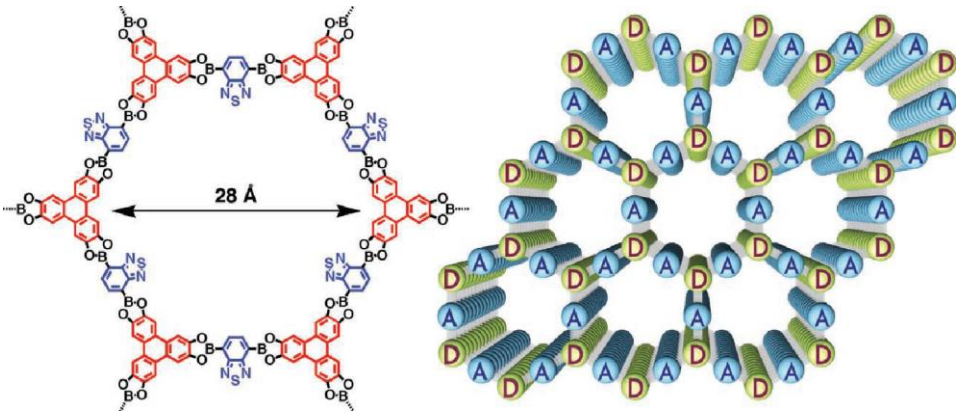

Fig. 2.1 Schematic representation of 2D D-A COF with self-sorted and periodic electron donor-acceptor ordering and bicontinuous conducting channels (right: structure of one hexagon; left: a 3 × 3 grid).[71]

Covalent Organic Frameworks are also synthetized as donor-acceptor building blocks; the obtainment of such COFs with a good crystallinity degree is highly challenging. Indeed, a high crystallinity diminishes the occurrence of internal charge recombination that is detrimental for the photoconductive features of the material. Jiang and co-workers successfully obtained COFs made by columnar arrays of D-A blocks that exhibited vertically ordered p-n heterojunction leading to a remarkably enhanced photoconductivity without any additional dopants.[159]

Another donor-acceptor COF was obtained by Jin and co-workers. They synthesized DZnPc-ANDI-COF, based on zinc phthalocyanine as donor and naphthaline diimide as acceptor.[160] They also reported the substitution of the central metal ion, i.e. Zn, Cu or Ni to compare the physical properties of the different COF.[67] When Zn is replaced by Cu or Ni the acceptor unit is still stable, and the charge separation lifetimes were very similar, even if the meta nature influenced the charge lifetimes. The copper-based COF achieved the longest lifetime, i.e. up to 33 μs. These results evidence how the thoughtful choice of the metal is a key parameter in the design of an effective D-A COF. Very interestingly, Jin et al. reported on a metal free D-A COF system.[161] More in details, they produced COF embodying triphenylene as a donor group and naphtaline diimide (DTP-ANDI-COF) or pyrromellitic diimide (DTP-APyrDI-COF) as acceptor. They investigated fluorescence lifetimes by using time-resolved fluorescence spectroscopy and a value of 0.92 and 1.0 ns was measured for DTP-ANDI-COF and DTP-APyrDI-COF, respectively. Unfortunately, the induced photocurrent measured was null. This evidence how the presence of a metal atom is still required to obtain good photoelectrochemical responses. COF was employed as a photoactive layer in photovoltaic cell by Calik and co-workers. They obtained a TP-Por COF by co-condensation reaction between bis(boronphenyl)porphyrin and HHTP.[162] The so-obtained COF presented segregated donor and acceptor columns in which electrons and holes can move throughout the columns of porphyrins and HHTP, respectively. A thin film of TP-Por COF was grown on an ITO substrate, then a with 20 nm thick coating of ZnO nanoparticles was spin-coated over it, being Al the counter electrode. Even if they observe very low photoconversion this work evidenced that COFs are promising candidate for the photovoltaics application in the forthcoming.

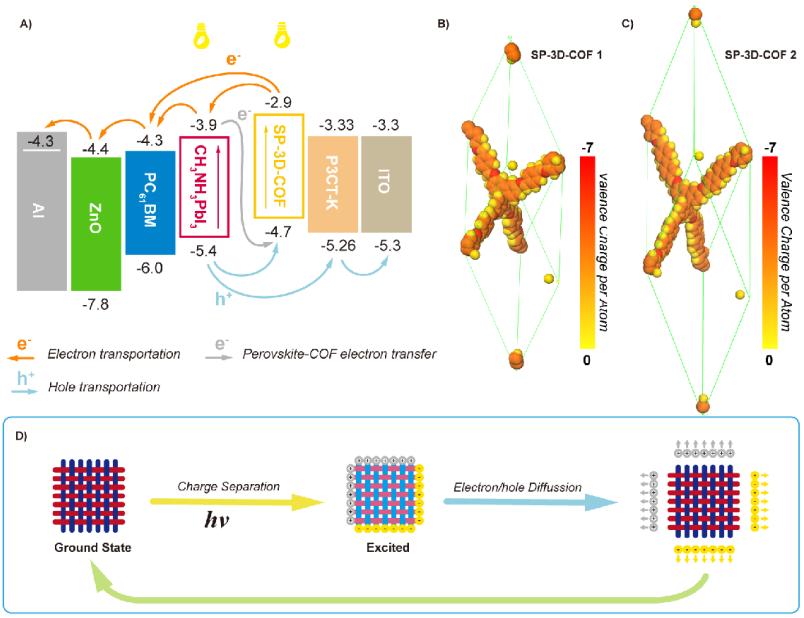

Fig. 2.2 Interplay between the COF layer and other component of PSCs stack. (A) Schematic energy level diagram of SP-3D-COFs doped PSCs with energy levels of SP-3D-COFs calculated from plane-wave DFT; (B,C) geometry optimized framework from the plane-wave DFT calculations of (B) SP-3D-COF 1 and (C) SP- 3D-COF 2; (D) proposed mechanism of photoinduced charge separation.[163]

The totality of the above reported examples deals with the implementation of 2D COFs. Yet, very recently, 3D structures have gained researchers' attention too. Concerning emerging photovoltaics, Wu et. al. has recently reported highly conjugated three-dimensional COFs based-on spirobifluorene and their employment in perovskite solar cells[163] (Fig. 2.2). They employed these COFs as an additive into the perovskite layer. They obtained 3D ordered porous frameworks with an orthogonal configuration of bi-planar spirobifluorene units as tetrahedral nodes. This structure presented several electron-transporting channels in the frameworks with highly ordered array by having rigid and long-range conjugated systems. When a SP-3D-COFs-mdified PSK layer was used in a complete device led

to a power conversion efficiency up to 18.3% for SP-3D-COF 1 and 18.7% for SP-3D-COF 2 that are extremely higher if compared to reference device (PCE = 15.8%).

As far as we are aware, this the first and only example regarding the implementation of a 3D Covalent Organic Frameworks in Perovskite Solar Cells. Yet, following on from the extremely good photoconversion efficiency, it could soon become the milestone for future improvements in this field.

2.1.2 COFs used in Storage Devices

2D polymers indicate various unique features, such as atomic-thick structures, high specific surface areas, plenty of active sites, several available functional building blocks, and tunable porous sizes, etc. Owing to their ordinate structure and modifiable features, 2D polymer or COFs have been also utilized for energy storage and conversion applications.[164]

2.1.2.1 Batteries

Since they have exceptional of long cycle life, large energy densities and light weight, Li-ion batteries (LIBs) have drawn attention and being significant power suppliers for different electronic devices.[165,166,167,168] One of the challenging is development of electrode materials and 2D frameworks as well as polymers could be appropriate electrode materials owing to their high specific surface area, having various redox active sites with different functional groups, and effective ion transfer.[169,170,171] They can be used as both anode and cathode materials. For instance, 2D N-COFs constructed via the condensation reaction between 1,3,5-triformylbenzene and amino derivatives, 2D polyporphyrin COFs, exfoliated 2D redox-active COFs, and DAAQ-ECOFs.[172,173] Layered redox active COFs into 2D few-layer nanosheets (DAAQ-ECOF) to enhance the diffusion-controlled redox

reactions.[174] On the other hand, the exfoliated COFs with few layers were able to lessen the ion/electron migration length as well as enabling the ionic/electronic diffusion. The DAAQ-ECOF indicated outstanding rate capability (a high capacity of ~ 75 mAh/g at 3,000 mA/g), and a good cyclic stability for 1,800 cycles at 500 mA/g without any explicit blanching.

Apart from LIBs, Sodium-ion batteries (SIBs) are favorable because of their Na supplies, cost effective, and their physicochemical properties are akin to Li metals.[170,175,176] But Li has lower radius (0.76 Å) than Na metal (1.02 Å), and this leads to different phase behavior and inferior diffusion properties.[177] 2D polymers can be created with effective ion channels that can be pathway for the Na^+ transport and storage. For this purpose, crystalline 2D-conjugated aromatic polymer 2D-CAP) was obtained through C–C coupling reactions between tetrabromopolyaromatic monomers.[133] The polymer indicated specific sequined form and certain pore size with ~ 0.6 nm, causing aligned one-dimensional (1D) open channels of the stacked sheets that is proper for Na ion transport. Moreover, crystalline 2D triazine sheet showed fast diffusion pathways for Na ions transport and storage due to their robust conjugated porosity with aligned 1D open channels.[178] One of the superior ultrathin nanosheet, 2DPI demonstrated efficient charge transport and storage by delivering a high capacity of 312 mAh/g at 0.1 A/g, along with superior rate capability of 137 mAh/g at 10.0 A/g, and good cycling stability for SIBs because they have redox active sites such as triazine and imide units that coordinate with Na ions as well as having rigid form.[179]

2.1.2.2 Supercapacitors

Supercapacitors have high power density, long-term cycle life and high safety but they have short-term power in contrast to batteries.[180,181,182] β-ketoenamine-

linked 2D COF,[183] redox active pyridine based 2D COFs such as TaPa-Py, DAB-TFP, TpPa-$(OH)_2$ and TpBD-$(OH)_2$,[184,185] DAAQ-TFP,[186] have been utilized in capacitors to date. Thereafter, highly crystalline mesoporous 2D COFs for instance JUC-510, JUC-511, and JUC-512 (JUC = Jilin University China) and few-layer 2D mesoporous COFs were produced through exfoliation process (the average thickness of ≈ 22 nm)[187] and implemented on electrochemical double-layer capacitors (EDLCs). They showed outstanding double-layer charge storage reaching to high areal capacitance of 5.46 (JUC-511) and 5.85 (JUC-512) mF/cm^2 at 1,000 mV/s, high gravimetric power of 55 and 42.2 kW/kg, respectively.

2.1.3 COFs used in Iodine Uptake

The excess of radioactive iodine, which is mostly available in nuclear industries waste, is environmental risk. It could easily penetrate the human body and therefore threat human health. COFs are exceptional adsorbent materials candidate because of their high surface areas, permanent adjustable porosities, controllable structures, high thermal/ chemical stabilities and including several functional groups.[188] There are many COF examples exhibiting high iodine capture properties. For instance, hetero-pore COF (SIOC-COF-7)[189] that has two different types of micropores with surface area of 618 m^2 /g and total pore volume of 0.41 cm^3/g and has high nitrogen content with aromatic rings showed high iodine uptake up to 481 wt%. Ordered 1D nanochannels with p-conjugated pore walls of 3D COF (COF-DL229) was obtained by condensation reaction of 1,3,5,7-tetrakis (4-aminophenyl)-adamantane and 1,4-phthalaldehyde under solvothermal conditions. It exhibited rod-shaped crystallites and BET surface area was measured as 1762 m^2 g^{-1} with total pore volume of 0.64 cm^3 g^{-1} and pore size of 1.4 nm. Its iodine capture capacity was 4200 mg/g (COF-DL229) at 75 ^oC.[190] In addition, 2D

COFs such as TPBDMTP, TTA-TTB, TTA-TFB, TFBCz-PDA, and ETTA-TPA[191] including 1D open channels with different shapes of pore volumes were identified and studied for their uptake capacity of iodine. Among them having 1D hexagonal channels and higher pore volumes ($V_{TPB\text{-}DMTP}$ = 1.28 cm^3 g^{-1} and $V_{TTA\text{-}TTB}$ = 1.01 cm^3 g^{-1}), TPB-DMTP and TTA-TTB demonstrated higher iodine capture capacities of up to 620 and 500 wt%, respectively. However, TTA-TFB exhibited the lowest iodine uptake capacity of 270 wt% because of its lowest pore volume ($V_{TTA\text{-}TFB}$ = 0.55 cm^3 g^{-1}). The channel shapes and pore volumes could play important role for iodine capacities. For instance, TFBCz-PDA have tetragonal (pore volume of 0.74 cm^3 g^{-1}) and ETTA-TPA trigonal shapes (0.95 cm^3 g^{-1}) and they showed the capacities as 370 and 470 wt%, respectively. TJNU-201 and TJNU-202 were produced to use iodine capture and iodine adsorption studies were carried out in a chamber where activated samples were exposed to iodine vapor at 350 K under ambient pressure.[192] According to the gravimetric iodine uptake, 96 hours later, maximum saturation was reached and iodine uptake was measured as 5.625 g g^{-1} for TJNU-201, 4.820 g g^{-1} for TJNU-202. This result is higher than most of the porous polymers or MOFs.[191] Most of COFs have been constituted by simple linkers, flexible building blocks are preferable for iodine capture owing to large lattice sizes, a variety of alternative monomers. Thus, various 2D COFs built by flexible building blocks containing distinctive contents of intralayer hydrogen bonds were produced. Particularly creation of H-bonding in COFs improves crystallinity, surface area, and morphology causing high iodine uptake. Based on this information, flexible building block was created by 4-hydroxy benzaldehyde and triazine unit.[193] The triazine unit is linked with hydroxyl group of 4-hydroxy benzaldehyde and flexible building block was obtained in ester form named 4,4',4''-((1,3,5-triazine-2,4,6-triyl)tris(oxy))tribenzaldehyde. This building block was reacted with

benzidine and 4,4'-diamino-[1,1'-biphenyl]-3,3'-diol to prepare TPT-BD COF and TPT-DHDB COF. They were used for iodine adsorption and iodine uptake was found as 543 wt%. The iodine uptake in water is substantial but at the same time it is challenging. a microporous hydrogen-bonded COF (HCOF-1) was obtained through photo-irradiated single-crystal-to-single-crystal (SCSC) to overcome this challenge.[194] Iodine adsorption was performed in an aqueous environment and HCOF-1 exhibited iodine capacity of 290 wt%, and this high capacity in aqueous environment might be due to the hydrophobic nature of its pores. For this reason, HCOF-1 could be inclined to occurrence of N–H- - -I hydrogen bonding and N- - -I and S- - -I halogen bonding interactions with I_2 molecules. Development of covalent organic polymers containing free ions can be another way to improve iodine adsorption capacity. According to this strategy, two non-porous viologen-based cationic covalent organic polymers, COP_1^{++} and COP_2^{++}, were synthesized through Menshutkin and Zincke reactions using the viologen units which are crosslinked with hexatopic cyclotriphosphazene core moieties.[195] These cationic polymers were transformed into the radical cationic polymers, $COP_1^{\cdot+}$ and $COP_2^{\cdot+}$, and the neutral polymers, COP^0_1 and COP^0_2, by treatment with sodium dithionite ($Na_2S_2O_4$) or excess cobaltocene under a nitrogen atmosphere and iodine adsorption capacities of cationic, radical cationic and neutral polymers were measured as 212, 195, 380, 258, 2.1, and 2.77 wt%, respectively. Today, among the COFs showing the iodine uptake capacity, 3D-Py-COF has highest record with the 1670 wt%. These results show that existence of aromatic rings, high heteroatoms content, well-ordered network as well as microsphere surfaces could be favorable for high iodine capture.[196]

2.1.4 COFs used in Electrochemical Sensor

COFs play significant role as electrochemical sensing in biomedicine as well such as epidermal growth factor receptors, living cancer cells, prostate specific antigens, glucose, ascorbic acid, dopamine, uric acid, hydrogen peroxide etc. porphyrin-based COFs (P-COFs) which have high electrochemical activity, good chemical stability, great bio-affinity were produced to use as aptasensor for the analysis of EGFR and living cancer cells and demonstrated good anti-interferences ability, stability, and reproducibility.[197] In another study, an electroactive 2D COFThi−TFPB nanosheet was synthesized a via dehydration condensation reaction between 1,3,5-tris (p-formylphenyl) benzene (TFPB) and thionine (Thi) and combined with amino-functionalized CNT as a ratiometric electrochemical sensor. It indicated desirable selectivity, reproducibility, and stability.[198] Accessibly active sites make the electroactive COFs suitable for electroanalysis application. They can be prepared using electron-rich species and metal over the framework. For instance, an electroactive iron porphyrin-based covalent organic framework (COFp−FeporNH2−BTA) was produced by aldehyde-ammonia condensation reaction between 1,3,5-benzenetricarboxaldehyde and 5,10,15,20-tetrakis(4-aminophenyl)-21H, 23H-porphine, and post-modified with Fe_2^+. It exhibited a good electrochemical redox property and electrocatalytic activity for the reduction of hydrogen peroxide[199] and demonstrated a wide linear range from 6.85 nM to 7μM with the detection limit of 2.06 nM (S/N = 3) for the detection of hydrogen peroxide. Another electroactive COFs which have multiple redox active states were synthesized through an amine-aldehyde condensation reaction between 4, 4′,4′′-(1,3,5-triazine-2,4,6-triyl) trianiline and 2,5 dihydroxy terethaldehyde (COFDHTA−TTA), and used as a ratiometric electrochemical sensor for the

detection of hydrogen peroxide and pH level based on both current and potential signals.[200] An electroactive COFs were also prepared as composite by a dehydration condensation reaction between 1,3,5-tris(pformylphenyl) benzene (TFPB) and thionine (Thi) combined with carbon nanotubes (CNT) and used as ratiometric electrochemical sensor for ascorbic acid.[198]

CHAPTER 3

Triazine-based 2D Covalent Organic Frameworks as Active Materials in Electrochemical Enzymatic Biosensors

**This chapter was written based on its published version*[201]

3.1 Introduction

Well-ordered porous materials have impressed remarkable attention due to their exceptional properties and great number of existing and potential applications.[6,202,203] Various nanoporous frameworks such as zeolites, covalent organic frameworks (COFs), or metal–organic frameworks (MOFs) have been constructed over the last decades with the purpose of implicitly matching the properties of these materials with their desired applications.[16,29,204,205,206,207,208,209] In the last few years, researchers started to focus on the design and synthesis of COFs, a class of crystalline organic porous materials, due to their structural properties, highly porous surface, chemical, and physical durability as well as having strong covalent bonds. While COFs are generally used for their gas storage and catalysis properties, in addition to other porous materials like zeolites and MOFs, their optoelectronics and energy storage properties have been recently demonstrated.[132,184,210,211] Importantly, 2D structures with shorter interlayer distances imply the existence of interactions between the aromatic organic moieties of the layers. Ideally, a 2D COF with a p-conjugated system and short interlayer distances could exhibit electronic interactions among the different sheets and consequently become a promising conductive material. In general,

COFs are formed by boronic anhydride, boronate ester, imine, hydrazine, hydrazone, and triazine.[210]

There are only a few works applying organic frameworks in electrochemical biosensors in the literature. Researchers utilized from MOFs for electrochemical DNA sensing,[212] determination of nitric oxide in live cells,[213] or for detecting some molecules like parathion,[214] L-cystine,[215] bisphenol A,[216] and hydrogen peroxide[217] by using electrochemical impedance spectroscopy, cyclic voltammetry, and amperometry. The remaining works use optical techniques such as fluorescence and luminescence spectrometry.[218,219]

In this work, we aimed to synthesize triazine-based 2D covalent organic polymers. Covalent triazine framework (CTF-1) that contains phenyl and triazine ring and TRITER-1 were synthesized utilizing Schiff base condensation reaction including phenyl and triazine ring linked with imine bond. Phenyl and triazine rings are considered as donor and acceptor units that make such constructs a potential material in energy storage or photocatalysis technologies, in addition to electrochemical biosensors, due to their electroactive surfaces.[220,221] Using triazine-based organic frameworks as a component of electrochemical enzymatic biosensor matrix, we designed biosensors that use SOD as recognizing element for superoxide radical detection in clinical samples.

3.2 Materials and Methods

4-Aminobenzonitrile, terephthalaldehyde, trifluoromethanesulfonic acid, anhydrous N,Ndimethylformamide (DMF) (%99.8), superoxide dismutase (EC. 1.15.1.1, 75KU) from bovine erythrocytes, xanthine oxidase (EC 1.1.3.22, 0.3 U mg^{-}

[1],from milk), xanthine (2,6-dihydroxypurine) sodium salt, gelatin from porcine bone, glutaraldehyde cross-linking agent were purchased from Sigma-Aldrich. Deionized water was purified using a Milli Pore Simplicity unit to a resistivity C 18.2 MX cm. Electrochemical measurements were carried out with Gamry Instrument using Framework Version 5.50 software.

3.2.1 Experiments

3.2.1.2 Synthesis of covalent triazine framework (CTF-1)

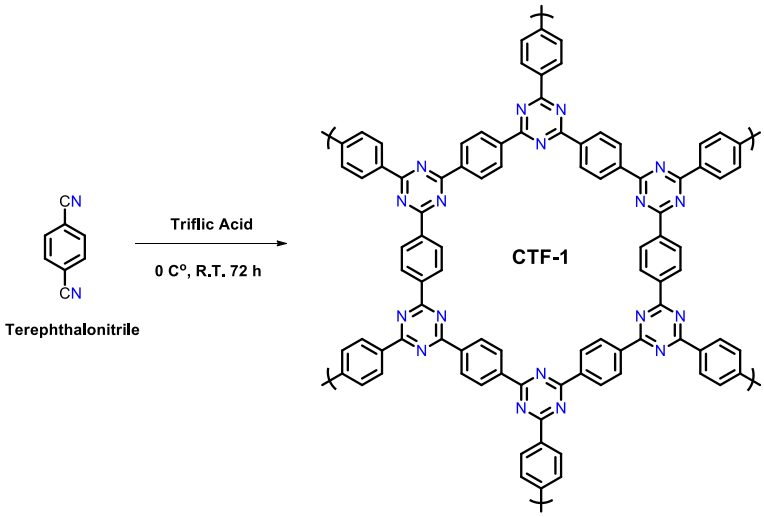

Fig. 3.1 Schematic representation of covalent triazine framework

The polymerization was conducted as described in the literature.[213] Briefly, 6 g (40 mmol) of trifluoromethanesulfonic acid was added dropwise to 1 g (7.81 mmol) of terephthalonitrile (1,4-dicyanobenzene) situated in a predried two-neck round bottom flask in a homemade glove box under nitrogen atmosphere within 45 min at 0 °C. The viscous red solution was enabled to stand at room temperature for 72 h. The obtained solid precipitates were filtered and washed with water several

times, followed by washing steps with ammonia, ethanol, acetone, and chloroform, respectively. Light yellow powder was obtained with a yield of 80%.

3.2.1.3 Synthesis of 1,3,5-tris-(4-aminophenyl)triazine (TAPT)

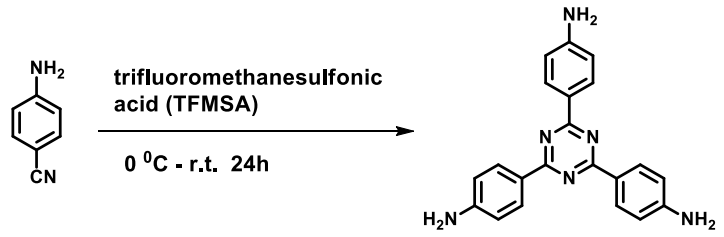

Fig. 3.2 Schematic representation of TAPT

The synthesis of TRITER-1 was performed via a two steps reaction (Fig. 3.2 and Fig. 3.3) as described in the literature.[222] Firstly, 1,3,5-tris-(4-aminophenyl)triazine (TAPT) was obtained and reacted with terephthalaldehyde to attain polymer product. TAPT was synthesized through triflic acid (trifluoromethanesulfonic acid) in compliance with a trimerization of 4-aminobenzonitrile. 2.54 mL (28.75 mmol) of trifluoromethanesulfonic acid was added dropwise to 1.0 g (8.468 mmol) of 4-aminobenzonitrile in a round bottom flask within 30 min at ^{0}C. The mixture was stirred for 24 h at room temperature under nitrogen atmosphere. Thereafter, distilled water was added to the mixture and neutralized by adding 2 M NaOH solution until the pH reaches to 7.0. As the pH increased, the orange precipitate occurred and then turned into pale yellow precipitate by further increase of pH. The final product was filtered and washed several times with distilled water. The purified product was characterized by FT-IR and mass spectroscopy. Yield: 88.35 mol%.

3.2.1.4 Synthesis of covalent organic polymer TRITER-1

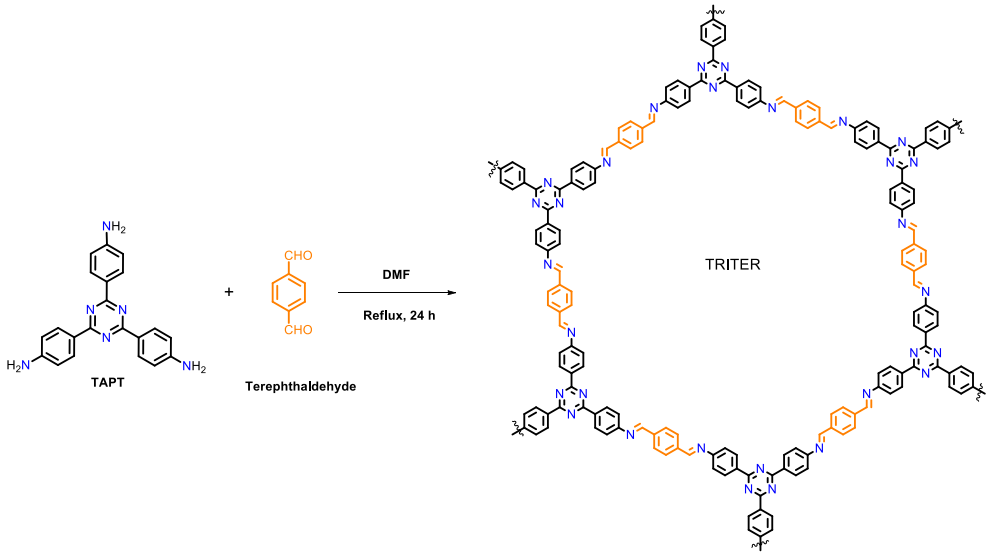

Fig. 3.3 Schematic representation of covalent triazine polymer

TRITER-1 was synthesized according to Schiff-base condensation reaction between TAPT and terephthalaldehyde. 20 mL anhydrous DMF was added to 882 mg (2.49 mmol) TAPT and 501 mg (3.74 mmol) terephthalaldehyde situated in a two-neck round bottom flask fitted with a reflux condenser under nitrogen atmosphere and refluxed for 24 h. Next, the solid product was filtered and washed with hot and cold DMF as well as ethanol to remove any starting material. The polymer was further purified by Soxhlet extraction with methanol for 48 h. Yellow powder 80.32 %.

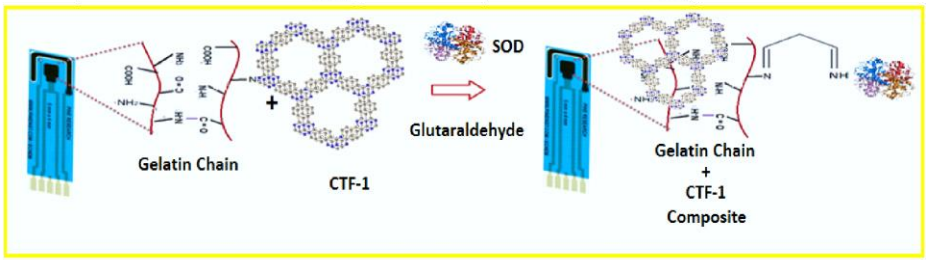

Fig. 3.4 Preparation of composite using screen-printed carbon electrode

3.2.1.5 Development of SOD-immobilized gelatin/COFs enzymatic biosensors

COF-based electrodes were prepared by homogenizing the CTF-1 or TRITER-1 with a sonication probe in phosphate buffer (0.05 M, pH 7.4). The electrodes were prepared by mixing one of the CTF-1 or TRITER-1 COFs, SOD enzymes, and glutaraldehyde cross-linking agent (they all optimized in order to determine the optimal conditions) in an Eppendorf, respectively, where gelatin carrier biopolymers situated. Homogeneity was provided by vortexing for a period of 30 s after each addition. Next, 10 lL of the mixed solution was added dropwise to the electrode surface. Screen-printed carbon electrodes (SPCEs) were employed as transducers for biosensor design taking their advantages of ease of use, low cost, low solution/sample volume, and being disposable that brings another advantage owing to their non-oxidized surface as they do not require cleaning. Enzyme-free electrodes were obtained applying the same protocol without addition of enzymes. The modified electrodes were left at room temperature for 2 h to ensure a stable dry surface. Electrochemical measurements were carried out in a 1 mL electrochemical cell specially designed for SPCEs. In order to trigger the dismutation reaction (Eqs. 1–4), a desired concentration of xanthine in 100 lL buffer was injected into the cell containing 0.9 mL total volume of medium consisting of 0.1 M potassium chloride, 0.5 mM $K_3[Fe(CN)_6]/K_4[Fe(CN)_6]$ as

mediator, and 0.7 U xanthine oxidase enzymes. Electrochemical impedance spectroscopy (EIS) measurements were recorded within the frequency range of 0.01 Hz to 100 kHz at open-circuit potential, and the amperometric measurements were recorded after the electrodes reached stability.

$$\text{Xahnthine} + \text{Xahnthine Oxidase} + O_2 \longrightarrow \text{Uric acide} + O_2^{\bullet -} \quad (1)$$

$$O_2^{\bullet -} + \text{Cu(II)ZnSOD} \longrightarrow O_2 + \text{Cu(I)ZnSOD} \quad (2)$$

$$O_2^{\bullet -} + \text{Cu(I)ZnSOD} + 2H^+ \longrightarrow H_2O_2 + \text{Cu(II)ZnSOD} \quad (3)$$

The overall reaction is:

$$2O_2^{\bullet -} + 2H^+ \longrightarrow H_2O_2 + O_2 \quad (4)$$

The current generated by oxidation of hydrogen peroxide (H_2O_2) at the working electrode held at 650 mV relative to the Ag/AgCl electrode is proportional to the concentration of 2 in solution. Oxidation of H_2O_2 generates the electrons which create a current on the electrode surface which is the principle of superoxide detection reaction.

Biological application of COF-based enzymatic biosensors: the CTF-1-based biosensor response was explored on healthy/meningioma (grade I, WHO 2000) brain tissue obtained from Ankara University, Medical School, Oncology Department. The healthy or cancerous brain tissue (0.5 g) was homogenized in distilled water (3 mL) using a Bandalin homogenizer, which was followed by a centrifugation step in order to remove rough mass. A solution of the homogenized healthy or cancerous brain tissue (100 lL) was injected into the SPCE cell, and the biosensor response was recorded.

3.2.1.6 Biological application of COF-based enzymatic biosensors

The CTF-1-based biosensor response was explored on healthy/meningioma (grade I, WHO 2000) brain tissue obtained from Ankara University, Medical School, Oncology Department. The healthy or cancerous brain tissue (0.5 g) was homogenized in distilled water (3 mL) using a Bandalin homogenizer, which was followed by a centrifugation step in order to remove rough mass. A solution of the homogenized healthy or cancerous brain tissue (100 lL) was injected into the SPCE cell, and the biosensor response was recorded.

3.3 Result and Discussion

3.3.1 Characterization of triazine-based COFs

CTF-1 and TRITER-1 were characterized using FT-IR, ^{13}C CP-MAS NMR, P-XRD, and TEM. as can be seen in the FT-IR spectrum of CTF-1 in Fig. 3.b, the intensity of the carbonitrile band at 2230 cm-1 decreased considerably after terminating the reaction; on the other hand, bands at 1512 and 1352 cm-1 indicated aromatic C–N stretching and bending forms in the triazine unit. According to the NMR spectrum, three carbons were observed in different chemical environments concerning aromatic rings at 129, 139, and 171 ppm as shown in Fig. 3.6. Observing the carbon at 171 ppm exhibited the formation of triazine rings. As a consequence, CTF-1 was successfully synthesized in accordance with FT-IR and ^{13}C CP-MASS spectroscopy.

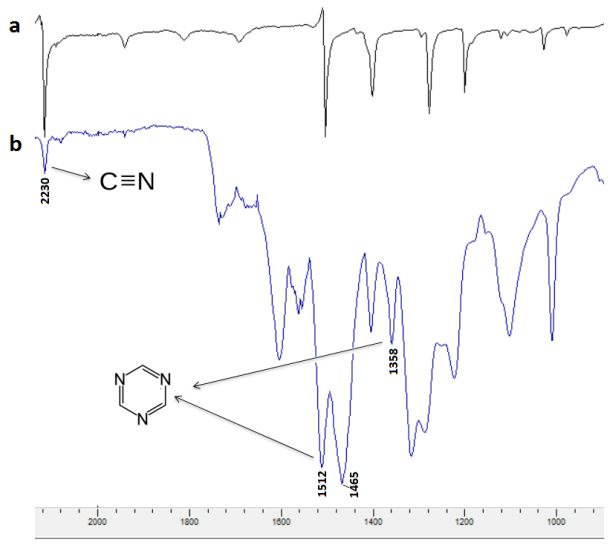

Fig. 3.5 Infrared spectra of a-) 1,4-dicyano benzene (monomer) b-) CTF-1

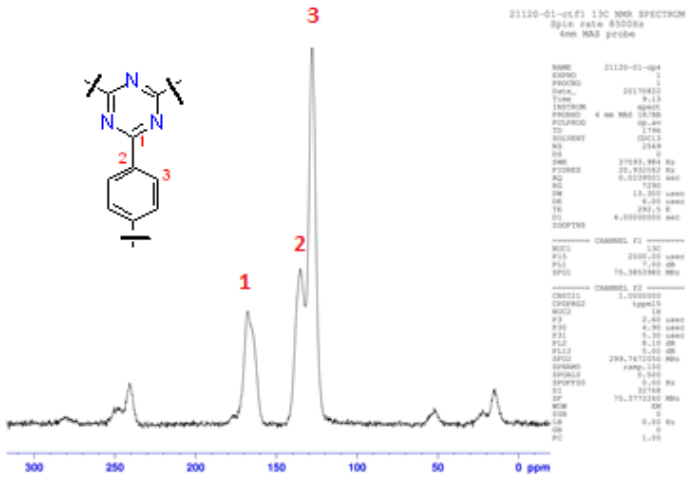

Fig. 3.6 ^{13}C CP-MAS NMR spectra of CTF-1

The XRD pattern of CTF-1 showed a broad band at 25° indicating a high degree of disorder that can be attributed to the interlayer stacking (Fig. 3.7). Similar patterns related to CTF-1 have been previously shown in the literature.[223,224] d001 spacing was calculated as 0.35 nm utilizing Bragg's equation, and a001

corresponding to interlayer distance of aromatic units were determined as 0.4 nm as presented in the literature.[212]

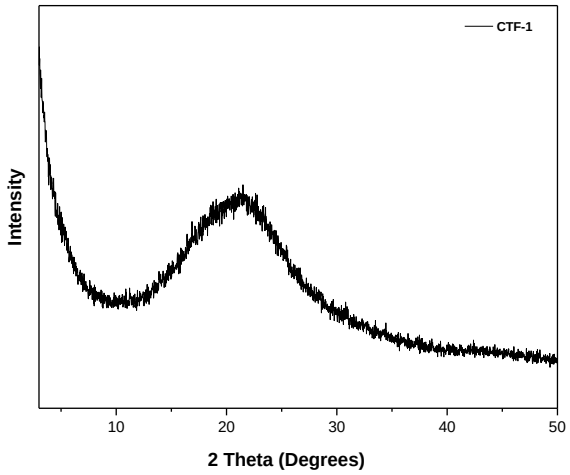

Fig. 3.7 PXRD pattern of CTF-1

High-resolution TEM image supported both the success of synthesis of 2D framework structure and the pore size (Fig. 3.8). The hexagonal pore arrangement that can be seen in a small number of papers was also visible.

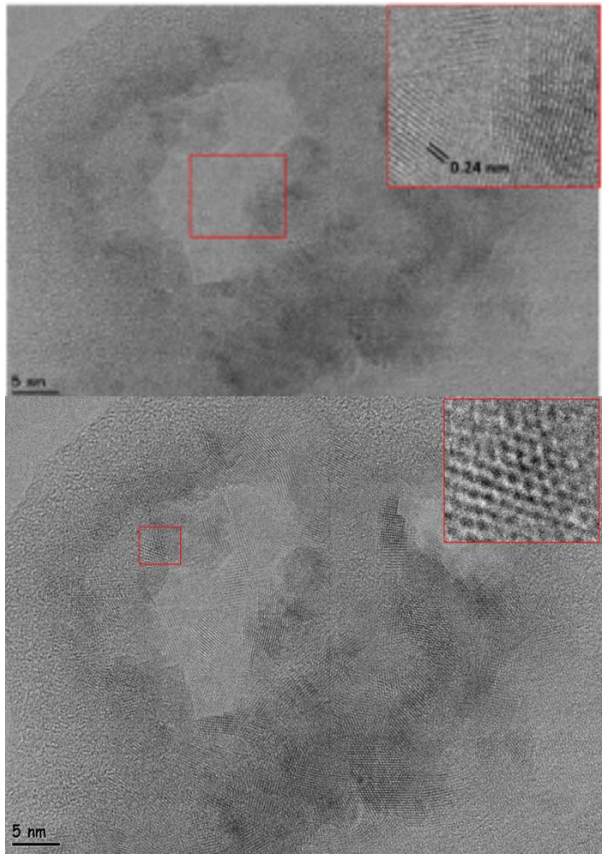

Fig. 3.8 TEM image of CTF-1 layers (scale bar 5 nm)

FT-IR spectra related to TRITER-1, as shown in Fig. 3.9, showed strong peaks at 801, 1360, and 1501 corresponding to triazine rings and peaks at 3210 and 3300, which demonstrated the presence of $–NH_2$ groups on TAPT. Similar to the FT-IR spectrum of TAPT, the peaks at 801, 1360, and 1505 cm^{-1} corresponding to triazine ring were seen. Moreover, the peak at 1705 cm^{-1} demonstrated formation of imine bond in TRITER-1.

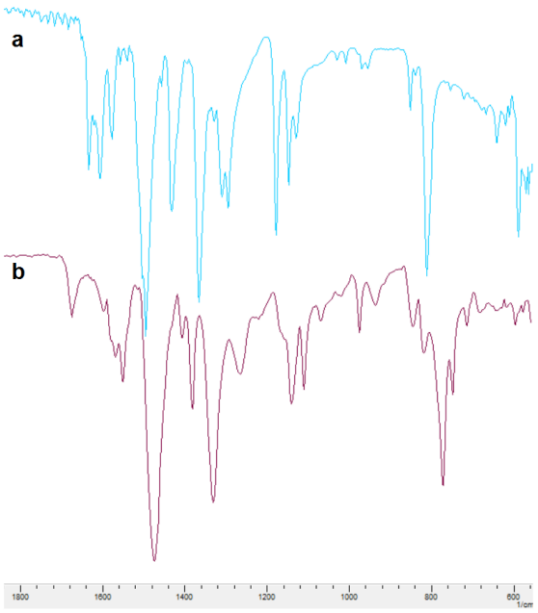

Fig. 3.9 Infrared spectra of TRITER-1

In ^{13}C CP-MAS spectroscopy, strong resonance signals were determined at 171, 159, 153, 139, 129, 118, and 112 ppm, related to carbons in different chemical environments as shown in Fig. 3.10. The presence of peak at 171 ppm indicated the formation of triazine ring and at 159 ppm showed creation of imine bond, while the other peaks belong to phenyl ring. As previously mentioned, we can implicitly understand that TRITER-1 covalent organic framework was appropriately obtained.

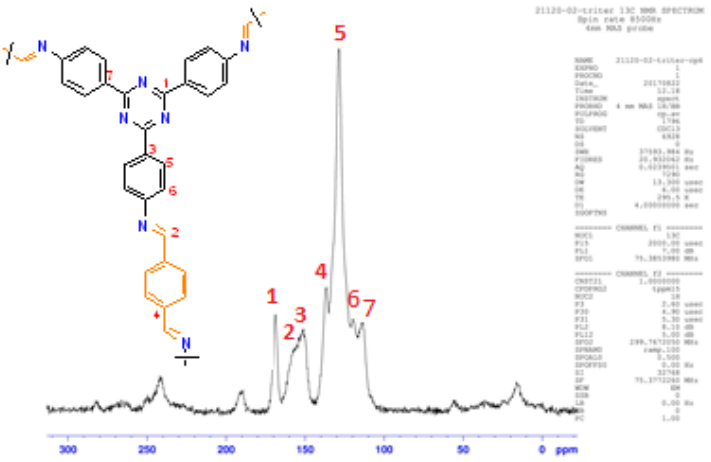

Fig. 3.10 ^{13}C CP-MAS NMR spectra of CTF-1

XRD measurement was carried out for further characterization. Likely to CTF-1, a broaden peak around 22 degree was seen, which indicated a sheet-like structure (Fig. 3.11). d001 value was determined as 0.4 nm. The hexagonal pore arrangement as well as the layered nano-morphology was clearly observed in TEM image, which was another proof of the framework structure (Fig. 3.12).

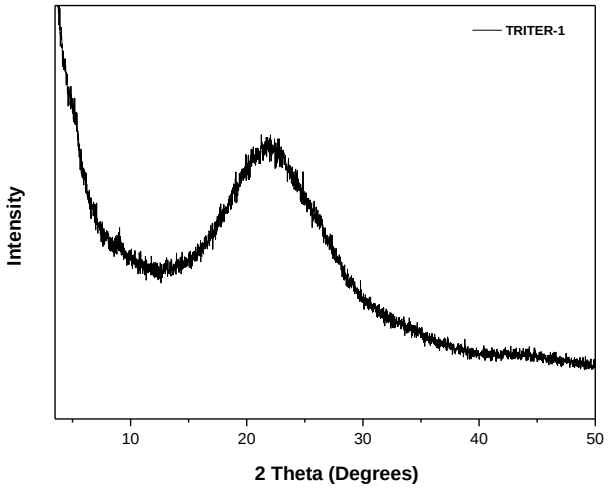

Fig. 3.11 PXRD pattern of TRITER-1

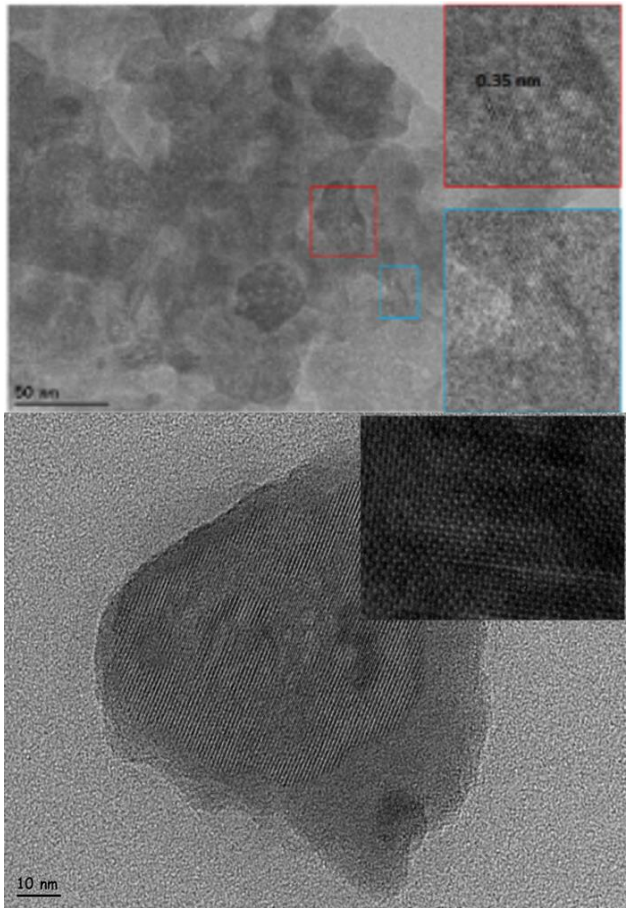

Fig. 3.12 TEM image of TRITER-1 layers (scale bar 50 nm)

3.3.2 Determining the appropriate triazine-based COFs for biosensor design

Kinetic studies using cyclic voltammetry (CV), impedimetric, and amperometric studies were performed to determine the most suitable COF for electrochemical biosensor design. The electron-transfer coefficient and electron transfer rate constant could be determined based on the Laviron theory (Eqs. 5 and 6):[225]

$$Ep_c = E^{"0} + \frac{RT}{\alpha s \eta F} - \frac{RT}{\alpha s \eta F} lnv \qquad (5)$$

$$Ep_a = E^{"0} + \frac{RT}{(1-\alpha s)\eta F} - \frac{RT}{(1-\alpha s)\eta F} ln\nu \qquad (6)$$

where n is the electron transfer number, equal to 2 in this study, R is the gas constant (R = 8.314 J mol^{-1} -K^{-1}), T is the temperature in Kelvin (T = 298 K) and F is the Faraday constant (F = 96493 C mol^{-1}). When $\eta\Delta Ep>200$ mV, the electron-transfer rate, ks, could be estimated with the Laviron's equation (Eq. 7) :[273]

$$k_s = \frac{\alpha\eta F\nu}{RT} \qquad (7)$$

The plots of the peak potential (Ep_a, Ep_c) versus the natural logarithm of scan rate (ln ν) for gelatin/CTF-1/SOD (Fig. 4.13-A) and gelatin/TRITER-1/SOD (Fig. 3.13-B) electrodes were obtained by CV in 0.5 mM $Fe(CN)_6^{3-/4-}$/0.1 M KCl solution in the potential range of - 400 to + 600 mV. Scan rates of 10, 50, 100, 200, 500, and 1000 mV s^{-1} were employed. Utilizing the equations above, the values corresponding to electron transfer coefficients were calculated for CTF-1 and TRITER-1 additive electrodes as $\alpha_{cathodic}$, = 0.14, α_{anodic} = 0.89, $\alpha_{cathodic}$ = 0.24, α_{anodic} = 0.88, respectively. Using Laviron's equations, the electron-transfer rate constant (ks) values were calculated as $ks_{cathodic}$- = 1.10 s^{-1}, ks_{anodic} = 6.93 s^{-1}, $ks_{cathodic}$ = 1.87 s^{-1}, ks_{anodic} = 6.85 s^{-1} for CTF-1 and TRITER-1, respectively. The results showed that the electron-transfer rate constant of the electrode including CTF-1 was higher than that of the TRITER-1 including electrode. However, the difference was less than 2%. The charge transfer resistance (R_{ct}) values related to bare SPCE, gelatin modified SPCE, Gelatin/CTF-1 modified SPCE, Gelatin/TRITER-1 modified SPCE and Gelatin/CTF-1/SOD modified SPCE were measured as 1501 Ω, 2085 Ω, 2009 Ω, 1815 Ω, and 2354 Ω, respectively (Figure 3.13-C). When the COFs were embedded in the

gelatin hydrogel, charge transfer resistance decreased from 2085 Ω to 2009 Ω and 1815 Ω due to the enhanced surface area and increased conductivity. Further reduction of the resistance in the CTF-1 including electrode indicated that CTF-1 had better electrical aspects compared to TRITER-1, in addition to kinetic study. Finally, amperometry study results supported the kinetic and impedimetric study. While the Gelatin/TRITER-1/SOD electrode responded to 1 µM xanthin addition with a peak intensity about 23 µA, the Gelatin/CTF-1/SOD electrode responded with 30 µA, that was nearly 30% higher (Fig. 3.13-D). As a consequent, it was decided that CTF-1 was more suitable for enzymatic electrochemical biosensor design.

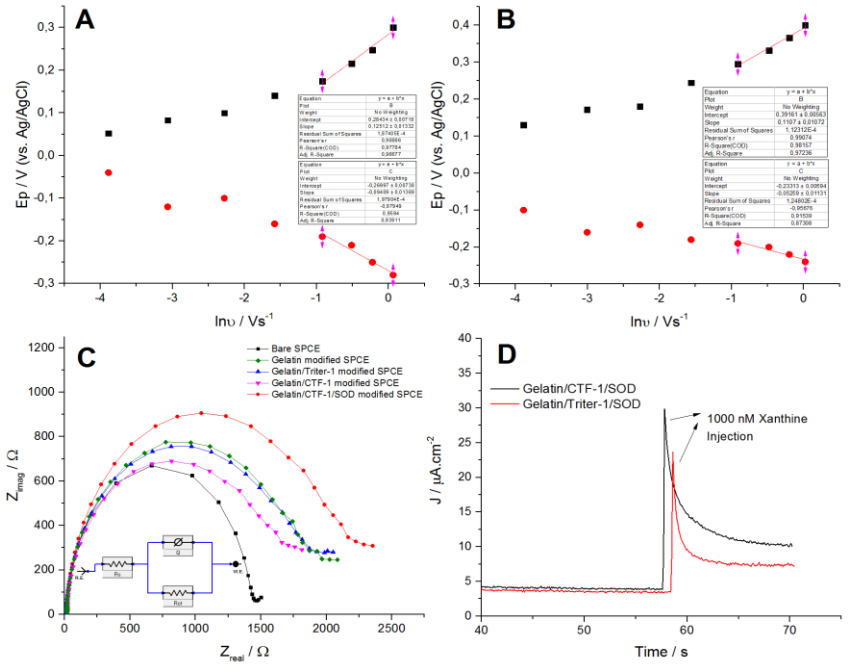

Fig. 3.13 Ep versus ln υ plot enabling kinetic parameters related to CTF-1 (a) and TRITER-1 (b) additive electrodes. (c) EIS spectra showing the modification steps of gelatin–COFs–SOD biosensor. (d) Amperometric responses of gelatin/CTF-1/SOD and gelatin/TRITER-1/SOD electrodes following 1 µM xanthine addition

3.3.3 Optimization, calibration, and validation of the CTF-1-based biosensor

Different parameters affecting the biosensor performance such as concentrations of XOD, glutaraldehyde cross-linker, gelatin, CTF-1 covalent organic frameworks, and SOD enzyme were investigated and the results were provided in (Fig. 3.14).

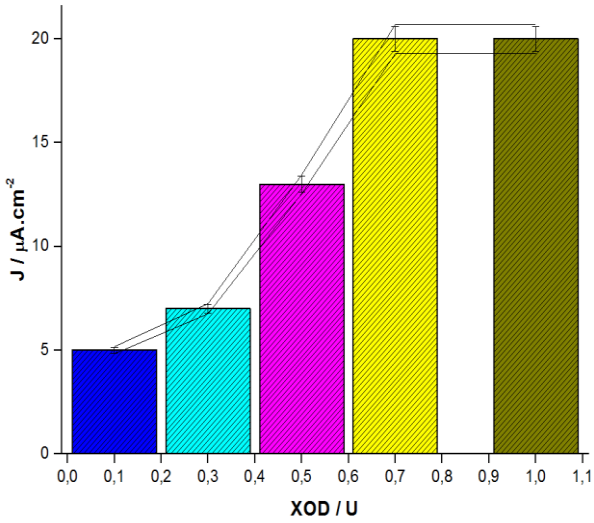

Fig. 3.14 Effect of different XOD concentrations on biosensor performance

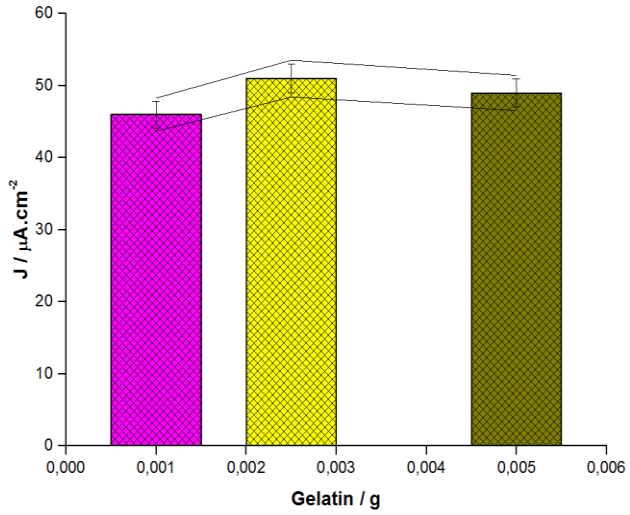

Fig. 3.15 Effect of different gelatin quantities on biosensor performance

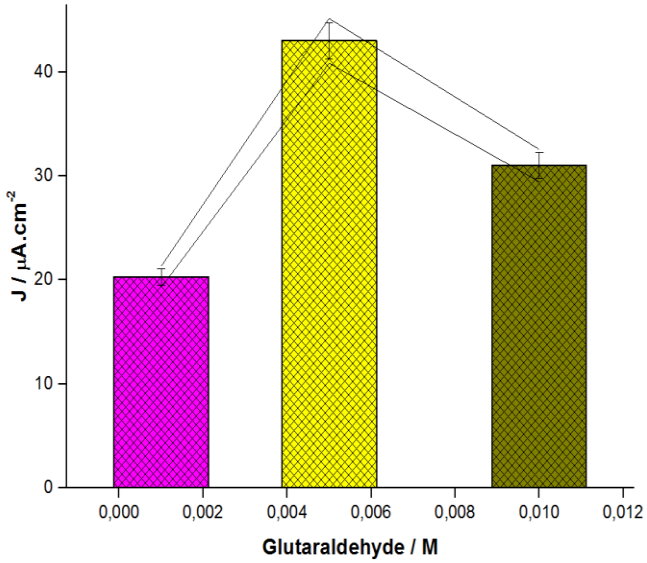

Fig. 3.16 Effect of different glutaraldehyde concentrations on biosensor performance

For this purpose, concentration ranges of 0.1-1 U for XOD, 1-5 mg gelatin, 0.01-0.1 M glutaraldehyde, 5-20 µL CTF-1 (10 mg.mL^{-1}) and 750-6000 U SOD were studied. Maximum amperometric response of 20 µA were obtained for a 0.7 U

XOD concentration, 51 µA for 0.025 g gelatin, 43 µA for 0.005 M glutaraldehyde concentration, 58 µA for CTF-1 (15 µL), 81 µA for 3000 U SOD. Low concentration of XOD didn't generate enough superoxide radicals in the medium, therefore, resulted in a weak amperometric response. The signal intensity remained constant at the concentrations over 0.7 U XOD. On the other hand, low gelatin concentrations caused enzyme leakage due to larger pore size or inefficient binding of enzymes. At higher concentrations, the electrochemical response increased due to an effective amount of immobilized SOD. Similarly, higher glutaraldehyde concentration reduced the amperometric response due to formation of a tight gel structure by excessive amounts of cross-linker. In contrast, lower cross-linker concentrations decreased the signal due to insufficient SOD immobilization. CTF-1, the conductive component of the sensor matrix, did not provide the necessary conductivity when used in lower quantities that might be caused by ineffective surface coverage, while the optimal amounts of CTF-1 increased the amperometric response. Higher amounts of CTF-1 were seen to result in aggregations as a result of van der Waals interactions that decreased the amperometric signal. Lastly, an enzyme optimization study was conducted by examining different concentrations of SOD and the optimum concentration was found to be 3000 U. The amperometric response increased with ascending SOD concentrations up to a limit followed by a decrease in the signal. This behaviour can be attributed to an increased enzyme–enzyme cross-linking in addition to oversaturation within the matrix pores that leads to restriction of product and substrate diffusion.

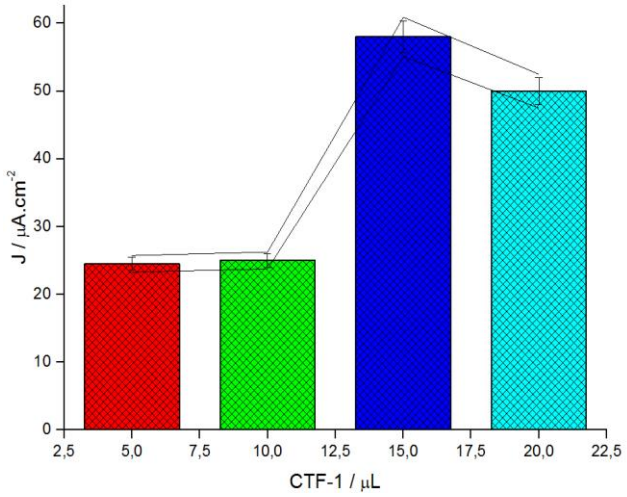

Fig. 3.17 Effect of different CTF-1 concentrations on biosensor performance

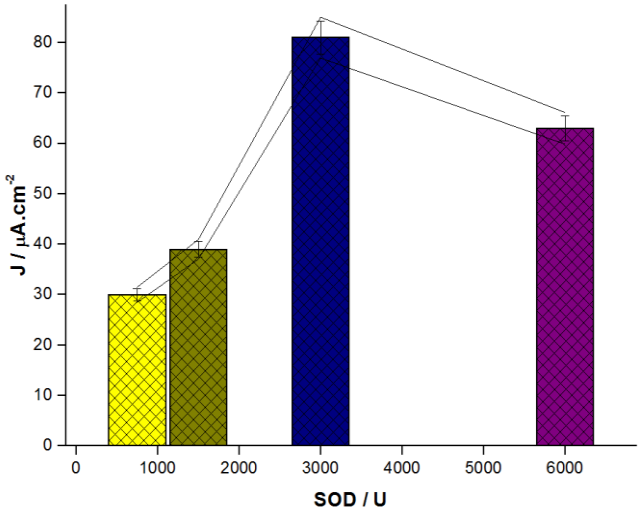

Fig. 3.18 Effect of different SOD concentrations on biosensor performance

Calibration curve, that is essential for evaluating the performance of biosensors, was obtained for 10 nM-100 µM concentration range (Figure 3.19). Non-linear regression equation was expressed for the SOD biosensor as µA= -53.exp(-[Xanthine]/61113)-32(exp(-[Xanthine]/746)), while the regression coefficient was found as 0.9870. The limit of detection was determined as 0.5

nM. In addition, a typical stepwise current response with ascending xanthine concentrations from 0.5 nM to 10 µM was observed, where the steady-state current was reached within 30 s. In order to demonstrate the advantages or disadvantages of our proposed COF-based biosensor, we compared our work with previous reports and presented in Table 3. The data summarized in Table 3 reveal the results of our CTF-1 based biosensor to be better than some of the previously reported detection methods for superoxide radicals.

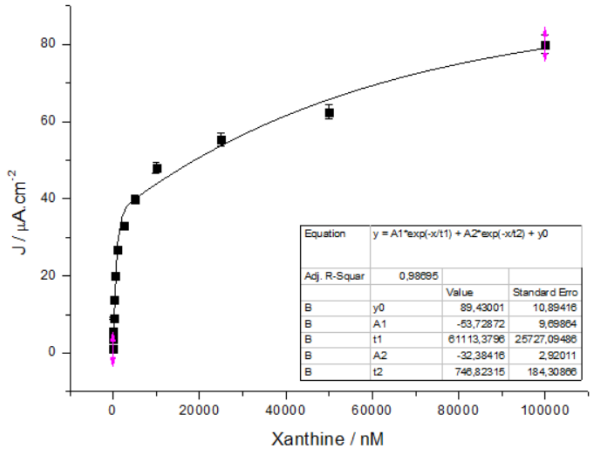

Fig. 3.19 Calibration curve of the developed CTF-1-based electrochemical biosensor

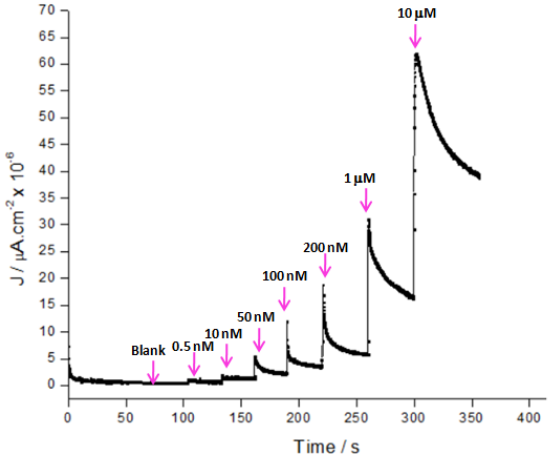

Fig. 3.20 The multistep addition graph showing the consistency of the developed biosensor

Table 3.1 Comparison of CTF-1-based electrochemical biosensor with literature works

Electrode material	Detection method	Linear range	Detection limit	References
FITC doped rattle-type silica colloidal particle	Fluorescence	0.2–20 µM	80 nM	[58]
SOD/PtPd-MWCNTs	Amperometric	40–1550 µM	0.71 µM	[59]
SOD/Fe3O4/Au electrode	Amperometric	0.2–1.4 µM	0.2 µM	[60]
Nanostructured cobalt phosphates	Amperometric	5.76–5396 nM	2.25 nM	[61]
Mn-superoxide dismutase/magnetic polymeric nanotubes	Amperometric	0.15–3.0 µM	0.0136 µM	[62]
Covalent organic framework-based sensor	Amperometric	10 nM–100 µM	0.5 nM	This work

To validate the developed CTF-1 based biosensor, reproducibility, shelf-life and reusability studies were carried out. For reproducibility study, a series of ten electrodes were prepared and electrochemical measurements were conducted under the same conditions (1 µM xanthine). The relative standard deviation (RSD) of the measurements was found to be 0.44% (Fig. 3.21), suggest that the reproducibility of CTF-1 based biosensor was quite good.

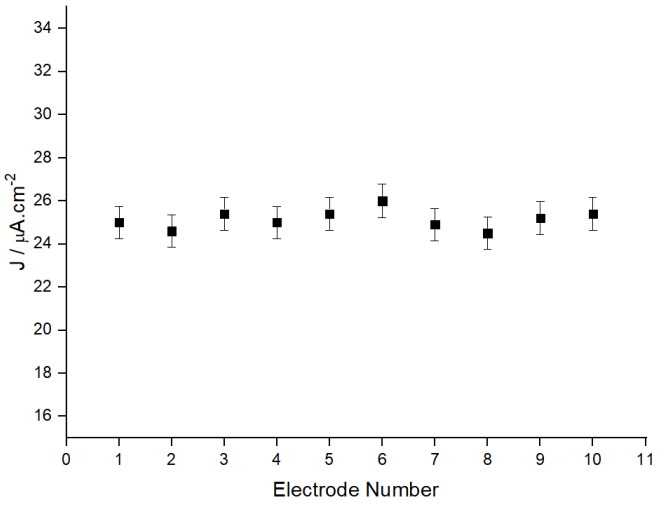

Fig. 3.21 Reproducibility graph of the CTF-1-based biosensor

In order to examine the shelf-life of the electrodes, three independent CTF-1 based electrodes were prepared, and electrochemical measurements were taken for 1 µM xanthine on different time points up to 10 weeks. Measurements were taken on day 1, 3, 5, and 7, then were taken once a week. The biosensor activity which was largely preserved at the end of the 8th week, fell below 80% on week 9 (Fig. 3.22). Thus, it was thought that the CTF-1 based biosensor had a shelf-life of 9 weeks. Lastly, a re-usability study, another important parameter for the biosensors for commercialization, was performed.

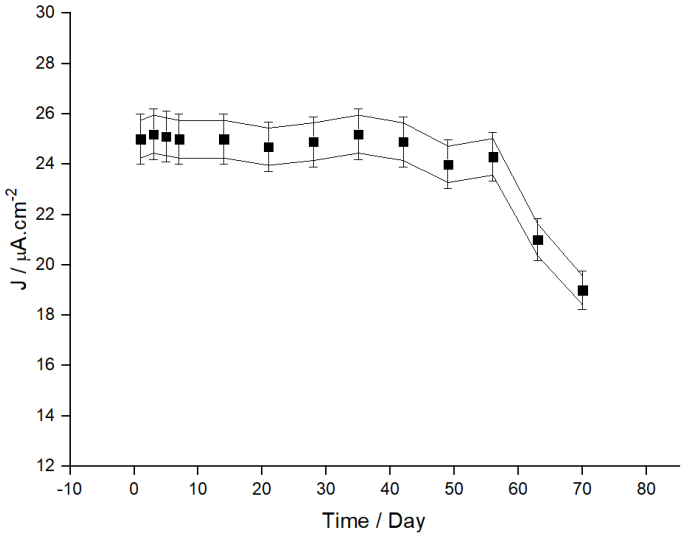

Fig. 3.22 Graph of shelf life of the CTF-1-based biosensor

The amperometric measurements were taken every day during 1 week with the prepared three independent electrodes following injection of 1 µM xanthine. The amperometric response felt below 80% on day 6 (Fig. 3.23), that means the developed CTF-1 based electrochemical biosensor is re-usable for a short-term.

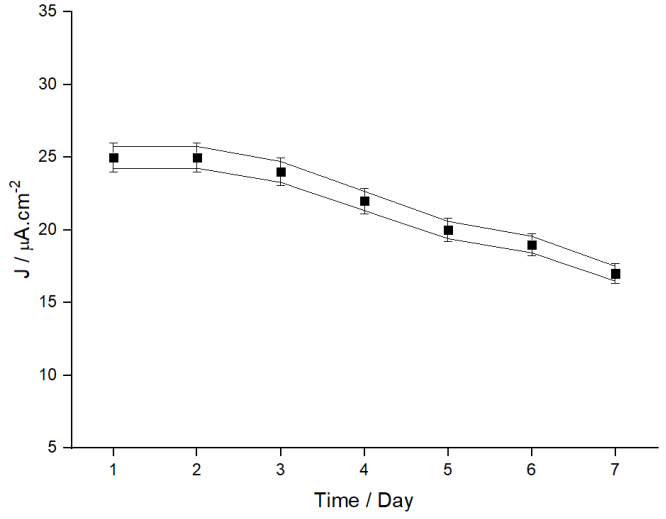

Fig. 3.23 Reusability graph of the CTF-1-based biosensor

3.3.4 Biological application using cancer tissue

In biological application using cancer tissue; In order to test the clinical applicability of the developed CTF-1 based biosensor, experiments with cancerous and healthy tissues were carried out. CTF-1 based electrochemical SOD biosensor responded with nearly 9 times more intensive amperometric current to cancerous tissue compared to healthy tissue (Fig. 3.24). This finding showed the applicability of the developed biosensor for superoxide radical detection in cancerous specimen.

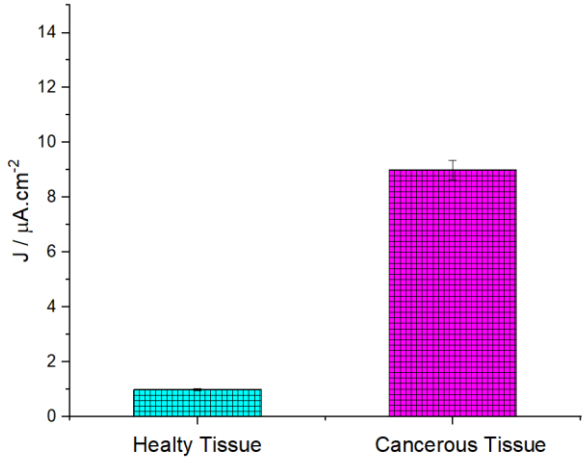

Fig. 3.24 Biological application of the developed CTF-1-basedbiosensor using healthy and cancerous tissue

3.4 Conclusions and Outlook

COFs a promising candidate for numerous applications such as energy storage, electrocatalysis, and electrochemical devices. Yet, their potential for facilitating biosensor design and bioelectrochemical processes has not extensively been investigated. Therefore, in a side project, we harnessed the simplicity, enhanced conductive property, and organic nature of COFs in electrochemical enzymatic biosensor aiming at detecting superoxide radicals as a model system. Covalent triazine framework (CTF-1) that contains phenyl and triazine ring and TRITER-1 including phenyl and triazine ring linked with imine bond. Phenyl and triazine rings are considered as donor and acceptor units that make the final polymer a potential material in energy storage or photocatalysis technologies, in addition to its wide electroactive surfaces. CTF-1 and TRITER-1 were characterized using FT-IR, 13C CP-MAS NMR, P-XRD, and TEM. To determine the appropriate triazine-based COFs for biosensing purposes, kinetic studies using cyclic voltammetry (CV), impedimetric, and amperometric techniques were performed to determine the most promising COF.

As a result, we have developed a novel biosensing platform that includes a covalent organic framework, CTF-1, as a new generation single-layered conjugated organic structure. CTF-1 enables advantages to the sensor matrix such as advanced conductivity. CTF-1, when compared to TRITER-1, was more electro-conductive which was revealed by a kinetic study and thus chosen as sensor matrix. Consequently, superoxide radicals were successfully detected in cancerous tissue utilizing the developed CTF-1-based SOD biosensor; hence, applicability of COFs in electrochemical enzyme biosensors was demonstrated.

CHAPTER 4

Squaraine-Based Covalent Organic Frameworks; Synthesis, Characterization and Photophysical Studies of Novel Squaraine-Based 2D Covalent Organic Frameworks

4.1 Introduction

There are various methodologies reported for the preparation of covalent organic frameworks or polymers. They have been generally synthesized based on boronate ester, boroxine, imine, triazine, and hydrazone linkages.[9,30,48,85,] Among them, Schiff base reaction is one of the most adjustable approaches owing to facile, one-pot, catalyst-free, quantitative synthesis.[226] Squaraines are appealing dyes with a zwitterionic resonance structure and have extensive applications in areas such as imaging, nonlinear optics, photovoltaics, photodynamic therapy, and ion sensing.[227] Therefore, they could show very attractive features once incorporated in covalent organic frameworks or polymers. There are some studies about squaraine-based COFs and they have been generally used as organoctalysis for organic synthesis[228] or photocatalysis for singlet oxygen generation[53], hydrogen evolution and water splitting.[229,230]

Squaraines are generally obtained through the condensation of squaric acid (SA) with aromatic, heteroaromatic, or olefinic compounds in a simple one-step reaction. Prof. Yiang and his group developed a new reaction consisting of squaraine unit for COFs.[53] Model compound was attained via condensation of SA with p-toludine and revealed that squaraine (SQ) with a planar form exhibited zigzagged zwitterionic resonance structure (Fig. 1.13). Based on this linkage, they

synthesized copper(II) 5,10,15,20-tetrakis(4-aminophenyl)porphyrin (TAP-CuP) as a building block, then obtained CuP-SQ COF under solvothermal conditions through the condensation of SA and TAP-CuP in o-dichlorobenzene/n-butanol (1:1 by vol.) at 85 ^{o}C for 7 days and built a crystalline 2D conjugated COF with a tetragonal mesoporous skeleton (pore size; 2.1 nm, BET surface area; 539 m2 g-1 , pore volume; 0.6410 cm3 g-1). Zigzagged formation was also observed in this CuP-SQ COF and this provides that conserve the layered structure from sideslip making it highly stable in solvents.

Extended conjugation system in 2D form exhibits a low band gap corresponding to 1.7 eV based on onset wavelength and improved absorbance capability. Based on electrochemical studies, it is mentioned that CuP-SQ COF containing electron-deficient skeleton may enable two-directional electron flow through the stacked column and over the 2D plane. In addition UV–Vis absorption spectroscopy showed that the CuP-SQ COF demonstrated a highly broadened Soret band at 467 nm which provides a delocalization of the π electrons in the COF and it was red-shifted by over 28 nm relative to that of TAP-CuP and at least 100 nm from the band exhibited by SQ. It was used as a heterogeneous catalyst for the activation of molecular oxygen and when exposed visible photons, it was found that CuP-SQ COF can generate the triplet excited state bringing about the activation of molecular oxygen.

In a similar way, SQ-COF based on hydrazone linkage was synthesized using porphyrin building block and squaric acid (Mn-CPF2) or terephthalaldehyde (Mn-CPF1) via bottom-up approach under solvothermal conditions[231] (Fig. 4.1).

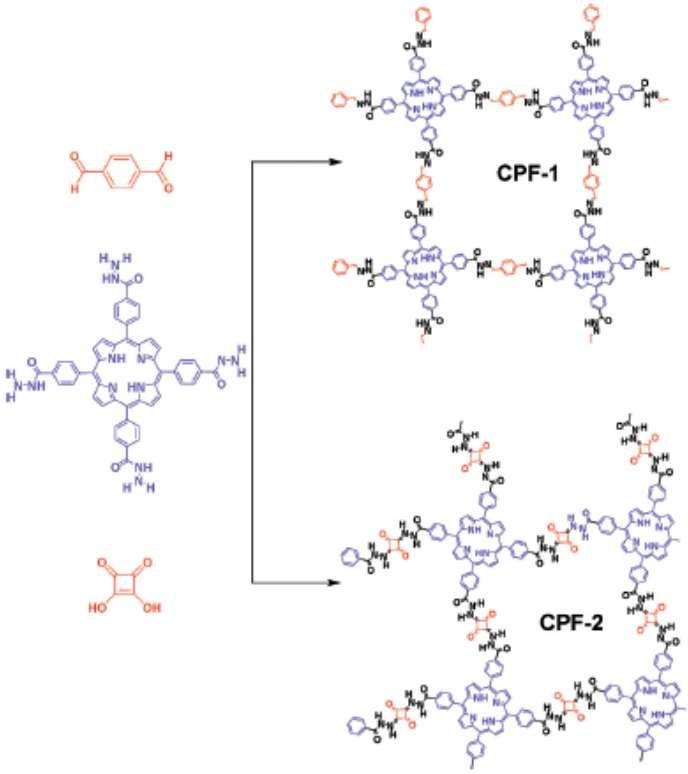

Fig. 4.1 Schematic representation of molecular building blocks of CPF-1 and CPF-2.[231]

These porphyrinic frameworks with coordinated manganes (III) ions (Mn–CPF-1 and Mn–CPF-2) were used as a catalysis for the selective oxidation of olefins. CPF-1 and CPF-2 which is metal-free porphyrin COFs exhibited poor diffraction peaks ($40° > 2\theta > 15°$) in XRD pattern while Mn–CPF-1 and Mn–CPF-2 did not show any clear diffraction peaks that may be an amorphous network. BET surface area of CPF-1 and CPF-2 were measured as 158 $m^2 g^{-1}$ for CPF-1 and 92 $m^2 g^{-1}$ for CPF-2. However, surface area of manganese (III) ions (Mn–CPF-1 and Mn–CPF-2) COFs were not measured because of showing low surface area of CPF-1 and CPF-2. For their thermal stability, TGA curves of the activated CPF-1 and Mn–CPF-1 did not demonstrate no weight loss until 350 °C while the frameworks of CPF-2 and Mn–

CPF-2 showed weak thermal stability that decompose around 230 °C. Based on catalytic activity findings, Mn–CPF-1 indicated most effective result than Mn–CPF-2 among those analysis including homogeneous and heterogeneous systems.

Bifunctional squaramide units have shown good biomimetic hydrogen-bonding organocatalytic performance,[232] thanks to their hydrogen-bond accepting and donating functionality via their carbonyl and N–H groups. For the first time this squaramide unit was incorporated into COF by Li and co-workers and used as a heterogeneous catalyst for hydrogen-bonding organocatalysis in Michael addition reactions under mild conditions.[228] They designed and synthesized a new diamino linear building block composing of a squaramide unit, 3,4-bis((4-aminophenyl)amino)-cyclo-but-3-ene-1,2-dione (Fig. 4.2). COF-SQ was obtained through the condensation reaction of 1 and 2 in a mixed solvent of mesitylene and 1,4-dioxane in the presence of 6.0 M acetic acid as catalyst within a flame-sealed glass ampule at 120 °C for 3 days.

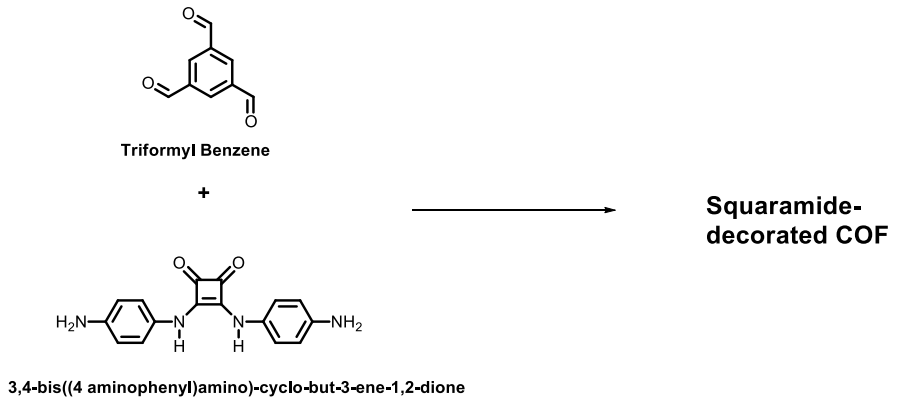

Fig. 4.2 Schematic representation of squaramide-decorated COF

Solvent stability was tested and COF-SQ showed good solvent stability in common solvents such as toluene, acetone and THF and any change of peak intensity or position was not observed in PXRD pattern.

Catalytic activity studies were conducted to understand whether catalytic activity originated from the squaramide or other sites. They prepared COF without squaramide units and catalytic activity was not observed or showed low efficiency because of lack of catalytic activity. In addition to this, it would be easily recovered by centrifugation and reused for at least 4 times without remarkable loss of catalytic activity.

COFs have been alternatively obtained through condensation reactions of squaric acid and porphyrin based on imine, hydrazine linkage or prepared as a squaraimide building block and synthesized based on imine-linked. In this study, squaric acid and metalloporphyrins (M; Co, Ni, Zn) have been used for construction of octa-hydroxy decorated metalloporphyrin based C-C linked two-dimensional polymers (Co; 2DP1, Ni; 2DP2, Zn; 2DP3, respectively)[229] (Fig. 4.3). Free-standing polymer films with crystalline layered structure were obtained by reflux monomers of porphyrin and squaric acid in a vacuum sealed Pyrex tube for three days.

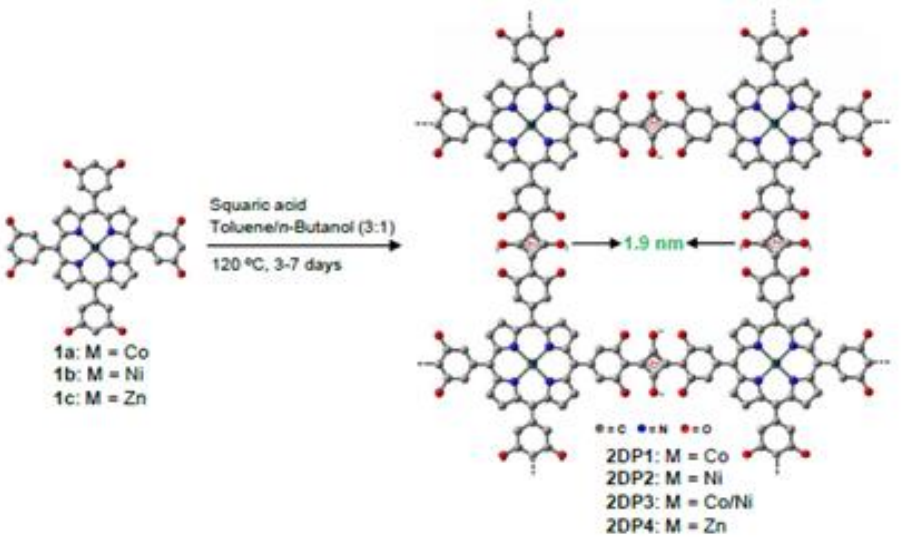

Fig. 4.3 Schematic representation of squaramide-decorated COF[229]

Optical properties were carried out by solid state UV-Vis spectroscopy and large broad peak closing to the NIR region was observed in spectra. In addition, transmission electron microscope (TEM) was used to determine multilayer stacks of the polymers and a single crystalline characteristic for 2DP1 was seen in the selected-area in electron diffraction pattern. Different metal ions in the centre of porphyrin were scrutinized for adjustment of H_2 evolution and found out that bimetallic (Co and Ni) porphyrin polymers increased the performance achieving 670 µmol of H_2 production.

In another study, this squaraine-linked metalloporphyrin (2DP1) was utilized for water splitting application and Photocatalytic release of H_2 and O_2.[230] It indicated long-term durability of 20 cycles in 300 days and efficiency was lowered negligibly. Therefore, it is believed that it showed outstanding performance.

To date, as far as is known there are no studies about squaraine based covalent organic frameworks or polymers synthesized through condensation reaction of squaric acid and trigonal-shaped linkers. However, there is theoretical study about 2D Squaraine-Bridged Covalent Organic Polymers with Promising CO_2 Storage and Separation Properties.[233] Three SQ-COPs were suggested named SQ-COP-1, SQ-COP-2 and SQ-COP-3 by the combination of linear squaraine unit and heterocyclic molecules ($H_3B_3O_3$, $H_3B_3N_3$ and $H_3C_3N_3$) (Fig. 2.4). It was studied by means of grand canonicalMonte Carlo (GCMC) simulations and estimated to possess big pore sizes (13.8-15.0 A^o), large free volumes (5.07- 10.94 $cm^3\ g^{-1}$) and high BET specific surface areas (8585- 8938 $m^2\ g^{-1}$)

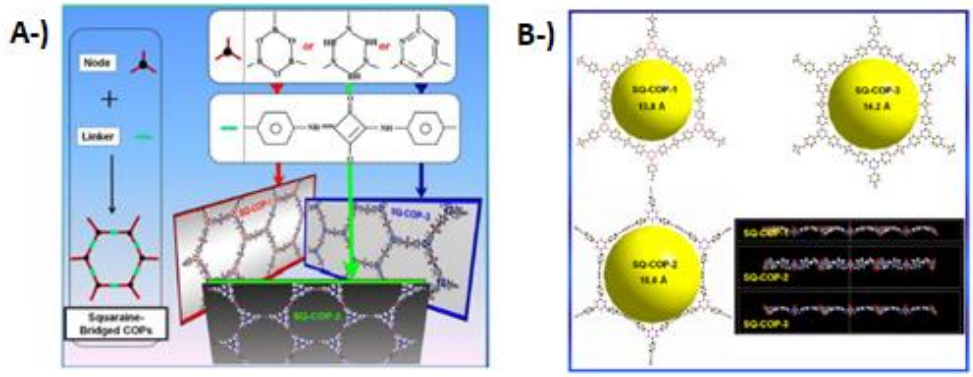

Fig. 4.4 Photographs of A-) building blocks for three 2D squaraine bridged covalent organic polymers, B-) the top and side view of optimized configurations for three 2D SQ-COPs respectively (yellow balls represent the pores space and size)

According to the theoretical studies, these SQ-COPs indicate promising gas storage and separation properties of H_2, CH_4, N_2 and CO_2 at ambient conditions. Particularly at 298 K and 30 bar, their CO_2 uptake reaches 804, 575 and 633 mg/g respectively.

As a consequence, SQ-COFs or polymers have been synthesized based on different linkage systems such as imine, hydrazone or even C-C based and used for organocatalysis or photocatalysis due to outstanding features of the squaraine unit. Mainly porphyrin and its derivatives have been used as knots with squaric acid as edge. In the first study, CuP-SQ COF has been synthesized in the formation of zig-zag, flat and twisted having high stability extended π-conjugation and lower band gap energy with enhanced absorbance. It was studied for the activation of molecular oxygen and exhibited great catalytic activity. After right, porphyrin-SQ COF has been obtained based on hydrazone linkage and utilized as organocatalysis for the selective oxidation of olefins. Contrary to the former study, this polymer did not show crystallinity and high specific surface area and thermal stability, however, it was successful for conversion of alkenes to the epoxide products. These polymers took place by condensation reaction of amino monomers and squaric acid. Moreover, squaramide were also obtained as a building block containing amino terminal groups and used with triformylbenzene for construction of squaramide-decorated COF through schiff base reaction and highly crystalline and porous squaramide-COF was attained owing to its reversible linkage system. COF which does not contain squaraine unit was also synthesized and their biomimetic organocatalysis studies were investigated for Michael addition reactions using both squaramide and without squaramide COFs. The COF obtained without the squaramide unit did not show any catalytic performance or very low performance in some reactions. Thus, this study proves that squaraine units in COFs can be important for catalysis studies. Squaraine-COFs were synthesized based on not only –imine or –hydrazone linkages but also C-C linkage. Octa-hydroxy-decorated metalloporphyrin based C-C bond linked two-dimensional polymers were obtained as free-standing films and they exhibited broaden

absorbance which is close to NIR. They could enhance the performance of the H_2 evolution as well as water splitting by releasing H_2 and O_2.

4.2 Materials and Methods

All chemicals, reagents and solvents were purchased from different suppliers, and used without further purification. The reaction of linkers and building blocks were monitored by thin-layer chromatography (TLC) performed on silica gel TLC-PET foils GF 254, particle size 25 mm, medium pore diameter 60 Å. Vibrational IR spectra were collected in transmission mode using a Thermo Scientific Nicolet 6700 spectrometer. The ^{1}H and ^{13}C NMR spectra were recorded on a JEOL Resonance 600 (^{1}H NMR operating frequency 600 MHz) at 298 K or Bruker Avance 200 spectrometer at 200 MHz. Small molecules of UV/Vis absorption spectra were measured with a double-beam Perkin–Elmer Lambda 20 UV/Vis spectrophotometer equipped with a 1-cm quartz cell. Mass spectra were recorded using an LCQ Advantage MAX Ion Trap Spectrometer (Thermo Fisher Scientific, Dreieich, Germany) equipped with an electrospray ion source. Elemental analysis was performed using a Thermo Nicolet FlashEA 1112 Series. Powder X-ray diffraction (PXRD) patterns were taken with a Panalytical X'Pert PRO MPD diffractometer equipped with a CuKα source operating in reflectance Bragg-Brentano geometry employing Ni filtered Cu Kα line focused radiation at 1600 W (45 kV, 40 mA) power. A Micromeritics ASAP 2020 apparatus was used to measure both N_2 and CO_2 adsorption isotherms at 273 K on Carbon. Thermogravimetric analysis (TGA) data was recorded with a TA instruments Q600 thermobalance in dry N_2 flow (100 mL/min) with a ramp of 10°C/min from 30 to 800°C. Polymers were analysed by solid state UV/Vis measurements on Cary 5000 UV-Vis-NIR

spectrometer from Agilent. Emission spectra as well as luminescence lifetimes were obtained by using a HORIBA Jobin Yvon IBH Fluorolog-TCSPC spectrofluorimeter. Luminescence lifetimes were determined by time-correlated single-photon counting.

4.2.1 Experimental

4.2.1.1 Synthesis of Monomer 4,4',4''-(1,3,5-triazine-2,4,6-triyl)trianiline(TPT)

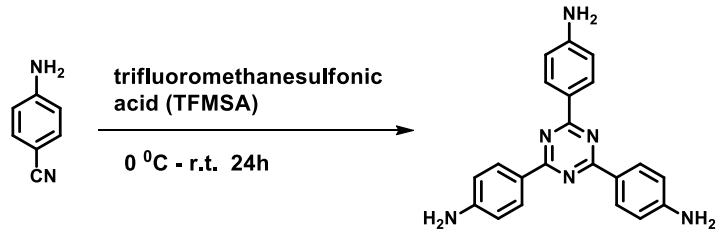

Fig. 4.5 Schematic representation of TAPT

TAPT was synthesized via superacid catalyzed trimerization of 4-aminobenzonitrile. In a typical synthesis, 4-aminobenzonitrile was taken in a round bottom flask at 0 ºC. Then 2 mL (22.2 mmol) trifluoromethanesulfonic acid was added dropwise for 20 min maintaining the temperature at 0 ^{o}C. The resultant mixture was stirred for 24 h at room temperature in an inert atmosphere. After that, 20 mL distilled water was added to the mixture and it was neutralized by adding 2M NaOH solution until the pH reaches to 7. Initially, with increase in pH, the orange precipitate dissolves to give a bright orange solution, which upon further increase in pH gives a pale-yellow precipitate. The resultant pale yellow product was filtered and washed several times with distilled water (85% yield) ^{1}H NMR (200 MHz, DMSO-d6) δ: (ppm) 8.35 (d, J = 8.6 Hz, 6H), 6.69 (d, J = 8.7 Hz, 6H), 5.91 (s, 6H), LC-MS: m/z = 355,11 $[M + H]^{+}$ UV-Vis: λmax (DMSO) = 350 nm FT-IR

(cm^{-1}): 3460, 3320, 3202, 3030, 1630, 1602, 1579, 1487, 1430, 1358, 1307, 1290, 1177, 1149, 1126, 1026, 1009, 959, 843, 806, 637, 584

4.2.1.2 Synthesis of Model Compound of Squaraines

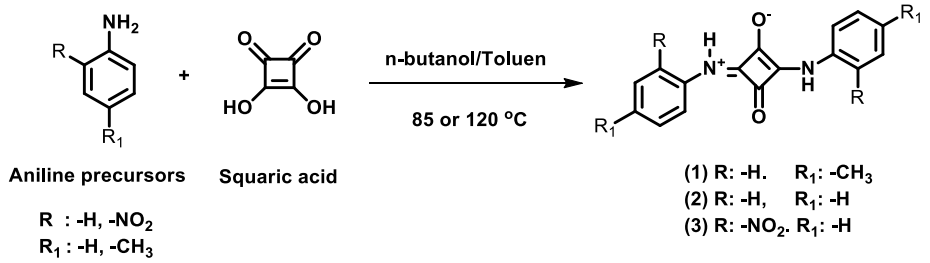

Fig. 4.6 Schematic representation of Model Compound

(1,2): Squaric acid and p-toluidine or sublimated white crystal p-aniline in n-butanol/toluene (8 ml, 1:1) was refluxed for 15 h. The afforded precipitate was collected by filtration and washed with CHCl3 and hexane to give SQ as light yellow (1, 92%), yellow solid (2, %90). (1); ^{1}H NMR (200 MHz, DMSO-d6) δ: (ppm) 10.22 (s, 2H), 7.42 (d, J = 8.3 Hz, 4H), 7.13 (d, J = 8.5 Hz, 4H), 2.27 (s, 6H)

(3): A mixture of 2-nitroaniline (1.33 g, 9.63 mmol, 2.2 eq) and squaric acid (0.5 g, 4.38 mmol, 1 eq) in n-BuOH/toluene (10 ml, 1:1) was stirred at 120 ^{o}C for 3 hours. After cooled to r.t., the reaction mixture was filtered. The resulting solid was washed with diethyl ether and dried in air. 1.43 g (yield: 93%) of 1,3-bis(2-nitroanilino)-cyclobutenediylium 2,4-diolate was collected as red solids with metallic luster.

4.2.1.3 Synthesis of Squaraine-based Covalent Organic Frameworks

Mechanism:

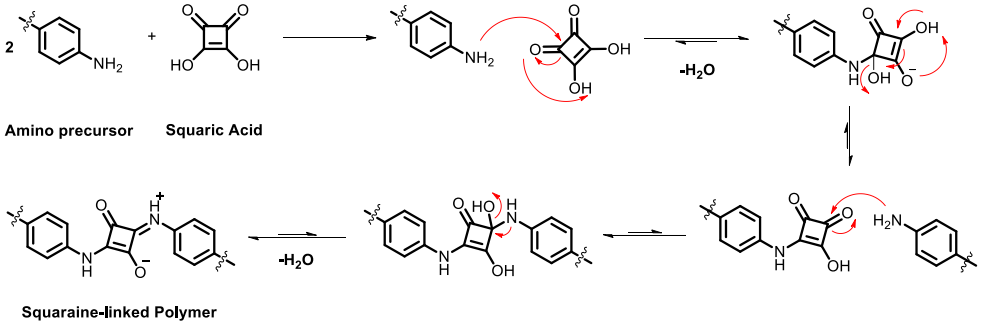

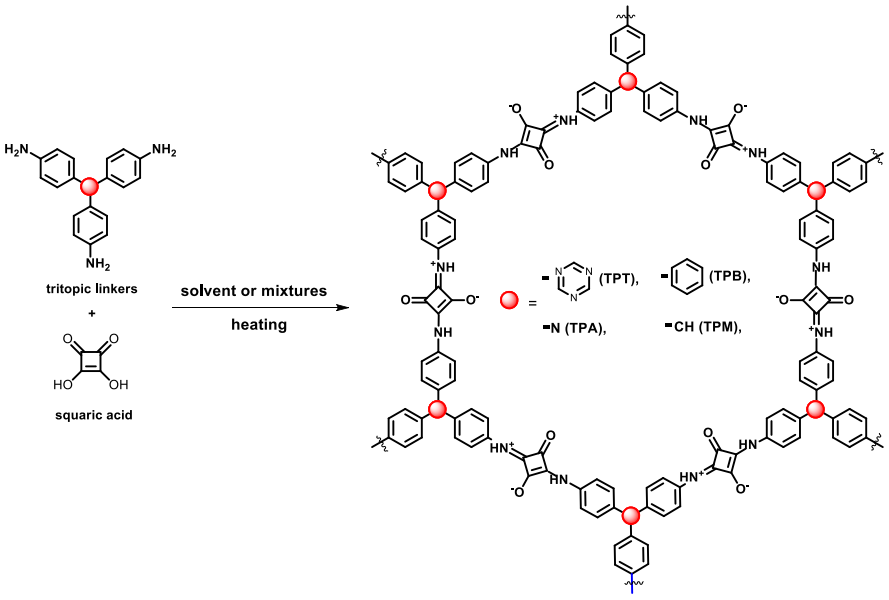

Fig. 2.7 Schematic representation SQ-COPs

Thermal:

OY 52-55: The mixture of TAPT and squaric acid in solvent mixture was degassed in 20 ml Biotage microwave vial by argon. The vial was sealed off, heated and stirred in an oil bath at 85 °C. The precipitate was filtered by vacuum, washed with DMF, DMSO, THF, acetone several times and dried at 120 °C under vacuum for 24 h.

Solvothermal:

OY 64-69: TAPT and squaric acid (1.5 eqv.) were dissolved via sonication in a mixture of solvents (solvents were degassed by three freeze-pump-thaw cycles in 20 ml Biotage microwave vial). The vial was sealed off and placed in a pre-heated oven. After cooled to room temperature, the precipitate was filtered by vacuum, washed with DMF, THF, acetone, diethyl ether for several times. They were kept in DMF for 2 days, washed THF, acetone again and filtered by vacuum, and dried at 120 °C under vacuum for 24 h.

OY 132-158: Reaction was performed as above but solvents were degassed by three freeze-pump-thaw cycles in 50 ml schlenk tube before reaction. Starting compounds were dissolved in degassed solvents and sealed off the vial, degassed by freeze-pump-thaw cycles for 3 times more and placed in a pre-heated oven. After cooled to room temperature, the precipitate was filtered by vacuum, washed with DMF, THF, acetone, diethyl ether several times, and dried at 120 °C under vacuum for 24 h.

OY 228-261: Reaction was carried out in 5 ml biotage microwave vials. Reagents and DMAc were added to vials then sonicated in hot water for 15 minutes. n-BuOH was added and degassed by freeze-pump-thaw cycles for 3 times by needle,

warmed to r.t. and placed in a pre-heated oven. After reaction was finished, washed with hot DMF until the solvent was seen as transparent then washed with anhydrous THF, Methanol and Acetone respectively, and dried under vacuum at 80 ^{o}C for one night.

Table 4.1 Synthetic conditions for construction of SQ-COPs by solvothermal metod

Entry OY-	Tritopic Linkers (mmol, mg)	Squaric acid (mmol, mg)	React. Time	Solvent mixtures and Ratios	Temp.	Color	Yield
48	TAPT 0.28/100	0.42/48	24 h	o-DCB/ t-Butanol (10 ml 1:1)	85	light orange	24 %
52	TAPT 0.28/100	0.42/48	168 h	o-DCB/ t-Butanol (10 ml 1:1)	85	orange	48%
53	TAPT 0.28/100	0.42/48	72 h	dioxane/ t-Butanol (10 ml 1:1)	85	dark brown	21%
55	TAPT 0.28/100	0.42/48	72 h	dioxane/ n-Butanol (10 ml 1:1)	85	dark red	76%
64	TAPT 0.28/100	0.42/48	120 h	Dioxane/ Mesitylene (10 ml 1:1)	120	Dark red-brown	45%
65	TAPT 0.28/100	0.42/48	120 h	Dioxane/ o-DCB (10 ml 1:1)	120	light brown	46%
66	TAPT 0.28/100	0.42/48	120 h	n-Butanol/ Mesitylene (10 ml 1:1)	120	brown	56%
67	TAPT 0.28/100	0.42/48	120 h	n-Butanol/ o-DCB (10 ml 1:1)	120	dark brown	73%
68	TAPT 0.28/100	0.42/48	120 h	Dioxane/ Mesitylene	120	orange	56%

				(10 ml 2:1)			
69	TAPT 0.28/100	0.42/48	120 h	Dioxane/ Mesitylene (10 ml 1:2)	120	light orange	32%
132	TAPT 0.56/200	0.84/96	168 h	Dioxane/ Mesitylene (8 ml 3:1)	120	dark orange	31%
133	TAPB 0.57/200	0.86/98	168 h	Dioxane/ Mesitylene (8 ml 3:1)	120	brown	35%
134	TAPA 0.68/200	1.02/118	168 h	Dioxane/ Mesitylene (8 ml 3:1)	120	dark brown	38%
135	TAPM 0.69/200	1.03/119	168 h	Dioxane/ Mesitylene (8 ml 3:1)	120	dark brown	29%
147	TAPT 0.07/25	0.105/12	120 h	Dioxane/ Mesitylene (2 ml 3:1)	120	orange	19%
148	TAPB 0.07/24.6	0.105/12	120 h	Dioxane/ Mesitylene (2 ml 3:1)	120	brown	16%
149	TAPA 0.07/20.3	0.105/12	120 h	Dioxane/ Mesitylene (2 ml 3:1)	120	purple	15%
150	TAPM 0.07/20.2	0.105/12	120 h	Dioxane/ Mesitylene (2 ml 3:1)	120	-	-
152	TAPT 0.07/25	0.105/12	120 h	o-DCB/ n-butanol (2 ml 1:1)	120	-	-
153	TAPT 0.07/25	0.105/12	120 h	Mesitylene/ n-BuOH (2 ml 1:1)	120	-	-
154	TAPT 0.07/25	0.105/12	120 h	o-DCB /dioxane (2 ml 1:1)	120	-	27%

155	TAPT 0.07/25	0.105/12	120 h	Mesitylene/benzylalcohol(2 ml 1:1)	120	-	30%
156	TAPT 0.07/25	0.105/12	120 h	THF/EtOH (2 ml 1:1)	120	-	
157	TAPT 0.07/25	0.105/12	120 h	DMAc/ mesitylene (2 ml 1:1)	120	-	27%
158	TAPT 0.07/25	0.105/12	120 h	dioxane/ n-BuOH (2 ml 1:1)	120	-	-
228	TAPT 0.141/50	0.211/24.1	168 h	DMAc/ Mesitylene (3 ml 1:1)	120	Light orange	71%
229	TAPT 0.141/50	0.211/24.1	168 h	DMAc/EtOH (3 ml 1:1)	120	Brown	77%
230	TAPT 0.141/50	0.211/24.1	168 h	DMAc/ n-BuOH (3 ml 1:1)	120	Orange	78%
231	TAPT 0.141/50	0.211/24.1	168 h	DMAc/ Water (3 ml 1:1)	120	(Noprecipitate)	-
232*	TAPT 0.141/50	0.211/24.1	168 h	o-DCB/ n-BuOH (3 ml 1:1)	120	Golden sand	93%
236	TAPT 0.141/50	0.211/24.1	168 h	DMAc/ n-BuOH (3 ml 5:1)	120	(Tan-Beige)	44%
237	TAPT 0.141/50	0.211/24.1	168 h	DMAc/ n-BuOH (3 ml 3:1)	120	light brown (sand)	40%
238	TAPT 0.141/50	0.211/24.1	168 h	DMAc/ n-BuOH (3 ml 1:5)	120	light brown (sand)	93%
239	TAPT 0.141/50	0.211/24.1	168 h	DMAc/ n-BuOH (3 ml 1:3)	120	orange	88 %

240	TAPT 0.141/50	0.211/24.1	168 h	DMAc/ n-BuOH (5 ml 1:1)	120	light brown (sand)	53%
241	TAPT 0.141/50	0.211/24.1	168 h	DMAc / o-DCB (3 ml 1:1)	120	light brown (sand)	78%
242	TAPT 0.141/50	0.211/24.1	168 h	DMAc (3 ml)	120	orange	32%
258	TAPT 0.141/50	0.211/24.1	168 h	DMAc/ o-DCB (3 ml 5:1)	120	light brown (sand)	44%
259	TAPB 0.142/50	0.214/24.3	168 h	DMAc/ n-BuOH (3 ml 1:1)	120	Dark brown	78%
260	TAPA 0.172/50	0.248/29.4	168 h	DMAc/ n-BuOH (3 ml 1:1)	120	dark red	94%
261	TAPM 0.173/50	0.259/29.5	168 h	DMAc/ n-BuOH (3 ml 1:1)	120	dark green	84%

DMAc; dimethylacetamide, o-DCB; ortho dichlorobenzene, n-BuOH; n-Butanol. EtOH; Ethanol *Reaction was firstly performed in microwave at 160 ºC for 30 min. then heating in oven

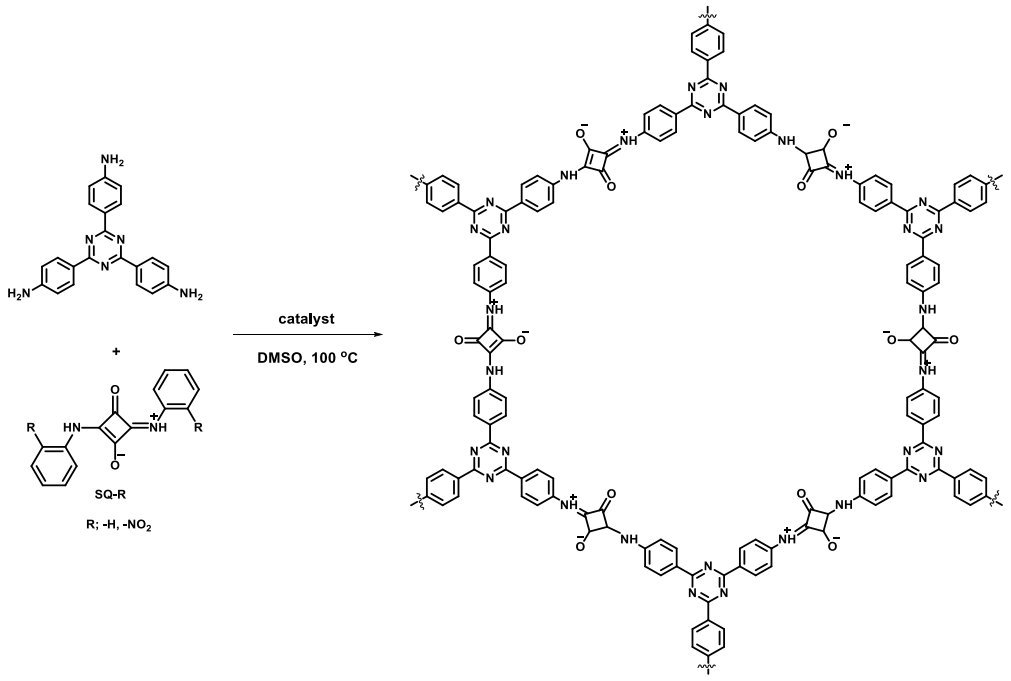

Fig. 4.7 Schematic representation of TPT-SQ COP by imine exchange procedure

Imine-exchange method:[234]

To pre-dried a 20 mL biotage microwave vial was charged with TAPT and either SQ-NO_2, or SQ-H and catalyst. The vial was sealed and anhydrous DMSO was added. Finally, air was removed by Argon exchanging by needle. The solution was heated at 100 ^oC in an oil bath or in an oven.

Table 4.2 Synthetic conditions for construction of TPT-SQ COP by imine exchange procedure

Entry OY-	TAPT (mg, mmol)	SQ-NO_2 (mg, mmol)	SQ-H (mg, mmol)	Catalyst (ml)	Solvent	Result
262	50/0.141	74.84/ 0.211	-	-	DMSO (10 ml)	N.R.[1]
263	25/0.07	37.15/0.105	-	PbI_2 (30mg/ml, 0.05ml)	DMSO (3 ml)	N.R.[2]
264	25/0.07	37.15/0.105	-	CH_3COOH (6M,0.2ml)	DMSO (3 ml)	N.R.[2]
265	25/0.07	-	27.9/0.105	PbI_2 (30mg/ml, 0.05ml)	DMSO (3 ml)	N.R.
266	25/0.07	-	27.9/0.105	CH_3COOH (6M,0.2ml)	DMSO (3 ml)	N.R.

[1]Reaction was performed in oil bath.[2]Reaction was carried out according to the published procedure in literature with slightly changing[]. N.R.; No Reaction.

Polymerisation reaction was not observed. This may be due to irreversible linkage of squaraine. Solubility may also play an important role because starting compounds are not highly soluble, even homogeneous suspension was not formed.

Reflux:

A pre-dried flask was charged with either TAPT, TAPB, TAPA or TAPM, squaric acid and DMF (15 ml). This mixture was degassed by Argon bubbling and heated at 150 °C for 24 h. The precipitate was filtered by vacuum and washed with DMF, THF, acetone, diethyl ether several times and dried at 120 °C under vacuum for 24 h.

Table 4.3 Synthetic conditions for construction of SQ-COPs by reflux

Entry OY-	Tritopic Linkers (mmol, mg)	Squaric Acid (mmol, mg)	Color	Yield
141	TAPT 1.41/500	2.11/241	tile red	87%
142	TAPB 0.85/300	1.28/146	dark brown	38%
143	TAPA 1.03/300	1.55/171	dark purple	30%
144	TAPM 1.72/500	2.59/295	dark green	50%

4.3 Result and Discussion

we developed novel two dimensional squaraine-based covalent organic polymers containing trigonal-shaped electron donor tectons, which can be suitable for optoelectronic devices, particularly solar cells. As far as is known Squaraine-based 2D COFs or COPs have especially been constituted by (metallo)porphyrins till today[53,188,191,192] however, we designed and produced these polymers by composing of trigonal electron donor linkers as metal-free under mild synthetic conditions and investigated their photophysical features addressing to optoelectronic devices. To identify reaction conditions, and structural regularity of polymer, highly planar trigonal linker of TAPT was used and optimized conditions were implemented for overall polymer reactions. Reaction was conducted according to the electrophilic aromatic substitution (i.e. condensation reaction between squaric acid and amino precursor of trigonal linkers) as catalyst-free in solvent or solvent mixtures under (solvo)thermal or reflux conditions. In Structural

and thermal analyses; first, obtained polymers were characterised by FT-IR and elemental analyses. Solid state ^{13}C- and ^{14}N-NMR as well as P-XRD were performed on selected polymers then their thermal stabilities were analysed by TGA. Afterwards, their surface analyses were examined by nitrogen and CO_2 adsorption-desorption isotherms for the surface area and pore distribution. The analysed polymers were investigated for optical properties through diffuse reflectance and solid-state fluorescence spectrometers. Reaction reversibility[20,235] is one of the main conditions to obtain crystalline two-dimensional polymers due to thermodynamic equilibrium. Another one is the planarity[20,235] of the monomers. It could be also added solubility[20] of the monomers to those factors. Imine or boroxine reactions have higher reversibility but lower chemical stability of the chemical bond of the bridge among the linkages (Fig. 1.2). In contrast, Squaraine reaction has low reversibility but higher chemical stability. Considering these factors, knowing that squaric acid is a planar[236] compound, we also chose a highly planar trigonal linker which is Tris(4-aminobenzene)triazine (TAPT)[237] so that we could examine regularity of polymer structure. Moreover, TAPT is known one of the acceptor unit[238] as trigonal linker and reaction of TAPT and squaric acid gives squaraine unit[239] and so it can be possible to create acceptor-acceptor relation on polymer backbone. This gave us an opportunity to compare optical properties as well in comparison to obtained polymers based on donor-acceptor relation created by other linkers. As mentioned in the experimental section, polymers were obtained under thermal and solvothermal methods. To determine the best conditions, TAPT and squaric acid were used. In thermal conditions; reactions of OY 52-55 (Table 4.1) were performed using polar solvent mixtures or polar and nonpolar solvent mixtures in microwave vials in oil baths by stirring leading to a kinetic control of the reaction. After reactions were ended, different colours were

observed in dried polymers. While reaction yield was so low in dioxane/t-BuOH mixtures, when t-BuOH was substituted with n-BuOH the yield increased and darker colour was observed. This proved that the combination of solvent mixture has a huge impact on the reaction yield and the nature of the final product. This can be clarified with the low solubility reason of starting compounds, especially squaric acid has very low solubility in organic solvents. Even if reaction solution in o-DCB/t-BuOH was sonicated for a long time (> 30 min) or the vial was heated, the monomers could not be dissolved clearly, even not homogeneous dispersion could be obtained in this mixture and it can be clearly seen in Fig. 4.8 precipitate was observed. On the contrary, a clear solution was achieved in dioxane/n-BuOH (Fig. 4.8, A-); OY 55) solvent mixture after heating the reaction tube. Another important factor was the reaction time, while polymer was obtained with low yield and light orange colour in short time, getting reaction time extended showed higher yield with dark orange-brown colour in acquired polymers (Fig. 4.8 B-)).

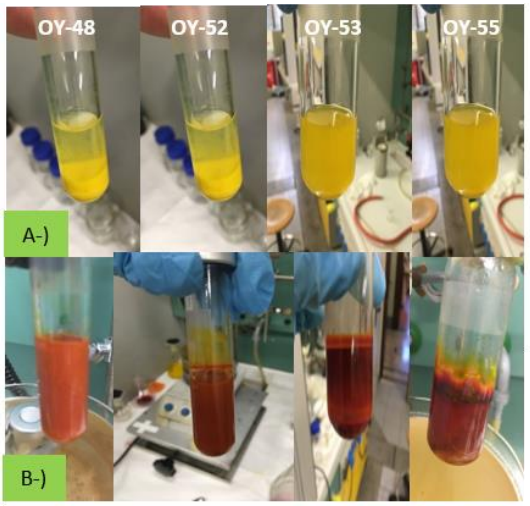

Fig. 4.8 Photograph of preparation of TPT-SQ COPs by thermal condition in microwave vials; A-) before commencing the reaction B-) after ending reaction

Considering solvothermal conditions, mostly used solvent mixtures in literature were chosen[20] and reaction was performed for longer times. To drive the reaction toward thermodynamic equilibrium, combinations of high and low polar solvents as well as high and low boiling ones are preferred and reactions are generally carried out in high or low pressure. The solvothermal method requires a sealed system to avoid interaction of moisture and oxygen[235] with reaction solution as well as keeping within the reaction mixture water that occurs during reaction in the closed system aiming at increasing reversibility in order to attain a highly ordered material. Oxygen and carbon dioxide create gaps in solvent molecules caused disordered alignment in the structure, thus, degassing the solvents is a suitable and required treatment to get rid of such undesired dissolved gases that could lead to the formation of by-products Solvents can be degassed in another system before using in reaction or degassed all together with reagents in sealed environment. Hence, biotage vial is appropriate vessel as reaction environment leading to a proper degassing of solvents. Once these conditions were met, reaction was carried out in conventional oven which is very suitable for nanostructure synthesis such as gas chromatography and reaction oven including fan which circulate the hot air to keep fixed the temperature within closed system.

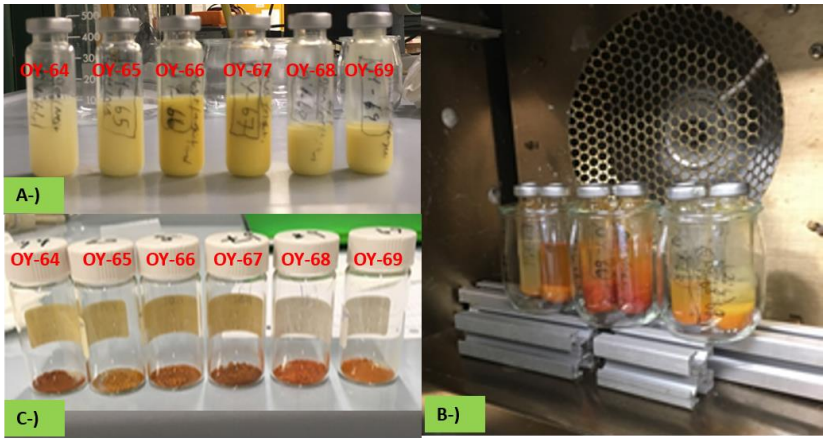

Fig. 4.9 Photograph of preparation of TPT-SQ COPs by solvothermal method in microwave vials; A-) before commencing the reaction B-) placed in the oven, C-) after the work-up process as powder form in stored vials

In the reactions of OY 64-69, high polar and low polar solvent combinations were used and prepared samples were kept in the oven for a relatively long time After the workup, polymers were dried and activated in a vacuum oven. Due to the presence of unreacted monomers, they were washed with high polar solvent of DMF and kept in it for 2 days. One of the most effective solvent combinations is dioxane and mesitylene mixture because of controlling the diffusion of monomers into the solution. In reactions of OY 132-135, all trigonal linkers were used besides TAPT and the amount of higher polar solvent was increased in the mixtures in order to enhance solubility of the monomers. Despite raising polarity, monomer residuals were seen in the resulting product (Fig 4.10, A-)).

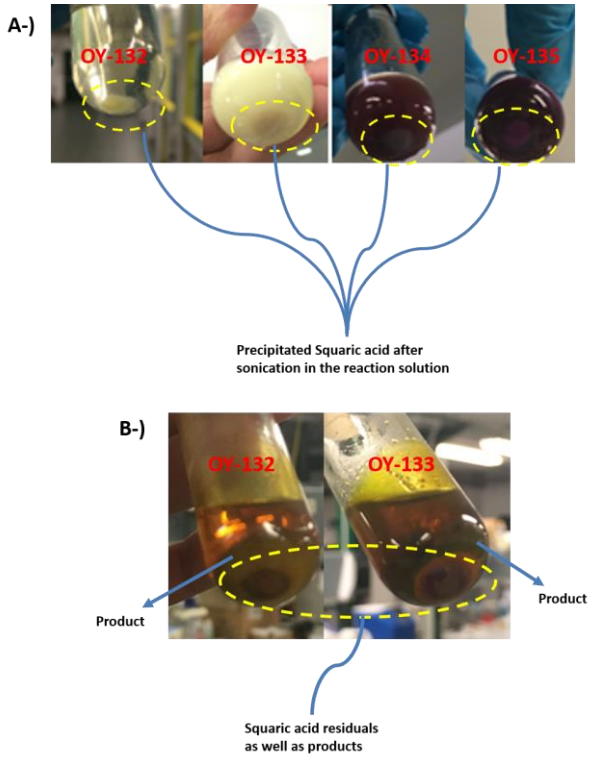

Fig. 4.10 Photograph of showing of squaric acid residuals in preparation of TPT-SQ COPs by solvothermal method; A-) before commencing the reaction B-) after ending reaction

Subsequently, monomer quantities were reduced considerably in OY 147-158 to force solubilization of the monomers in addition to approach obtaining high regularity, however, squaric acid precipitated in reaction solution combinations obtained products. The insolubility of squaric acid makes the complete polymerisation hard. To overcome this issue, we focused on the solubility of squaric acid. While squaric acid could not be dissolved in most known organic solvents at room temperature,[236] it was found out that it is clearly dissolved in the hot highly polar solvents such as dimethylformamide (DMF), dimethyl sulfoxide (DMSO), and dimethylacetamide (DMAc). As a matter of fact, a round 20-25 mg squaric acid could be solubilized in approximately 1-2 ml DMAc at nearly 60-80 ^{o}C (Fig. 4.11, A-)). According to these findings, the last reactions were carried out

based on DMAc with a combination of solvents polar or low polar solvents. In compliance with the structural regularity, completion of the reaction, yield, reproducibility, the satisfied results were obtained in DMAc/n-BuOH mixtures. Monomers have a high soluble capability once this mixture is heated and sonicated .During the heating process, monomers start to dissolve and the clear solution becomes blurry, suspension occurs that indicatesthe polymer reaction to be started, then they were placed in preheated oven.

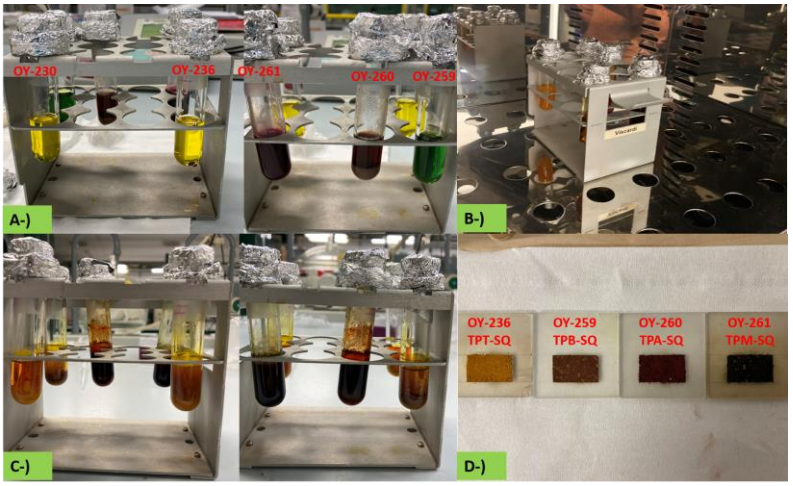

Fig. 4.11 Photograph of preparation of SQ-COPs by the solvothermal method in microwave vials placed in the racks; A-) before commencing the reaction left; front of the rack, right; back of the racks B-) the rack placed in the oven, C-) after ending reaction left; front of the rack, right; back of the racks, D-) activated as a powder form for the measurement of PXRD

Polymers were successfully produced not only by solvothermal or thermal but also by reflux in DMF. Reflux is one of the most common methods for chemical reactions and DMF is mostly used as a solvent in especially cross-linked polymer synthesis due to its high boiling point, high dissolution power of numerous classes of substrates, and its ability to solvate ions.[240,241] Reactions were repeated several times to control reproducibility and while same results were obtained by

solvothermal method particularly in synthesis of TPA-SQ and TPM-SQ polymer, produced polymers by reflux indicated different outcomes like changing colour resulted in different optical properties.

Above, reaction conditions, methods, product scalability as well as producibility were stated. The characterisation outcomes demonstrating physical, chemical, optical, and morphological properties will be discussed in the sections of structural, thermal, surface analyses, and optical properties.

4.3.1 Structural Analysis

Infrared Spectroscopy is one of the substantial techniques to identify functional groups in substances.[242] To observe exploitation of the active functional groups in the product, and understand whether reaction is completed or not, this technique could be very useful at the beginning. Condensation reaction of two monomers gives the squaraine unit formation in this reaction. There are two active functional groups in the precursors; one is primary amine, another one is the ketone. Their reaction generates neutral secondary amine and its positive charged form as well. Reaction completion could be easily comprehended by observing whether especially primary amine -N-H stretches reduce or even almost disappear in the region of 3000-3500 cm^{-1} (Fig. 4.12, B-)).

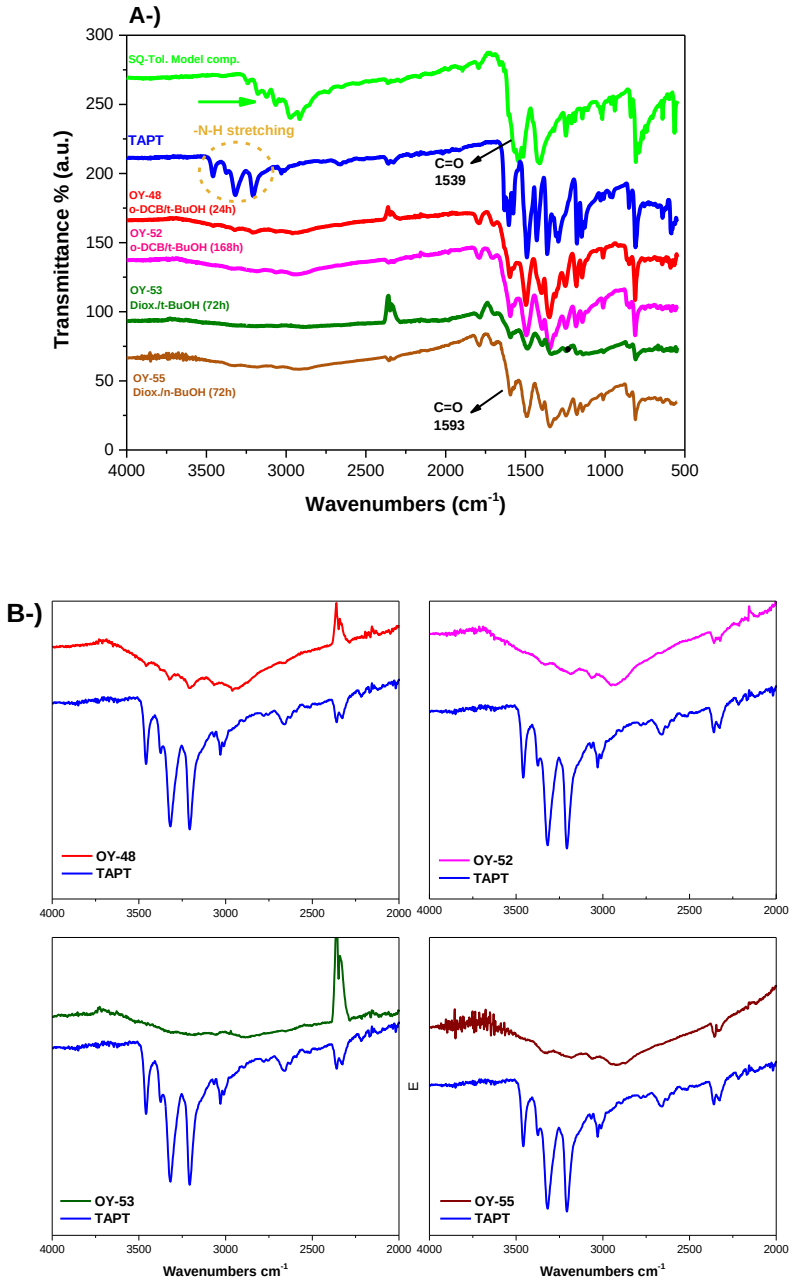

Fig. 4.12 Infrared spectra of TPT-SQ COPs obtained by thermal condition; A-) comparison of model compound (green), monomer of TAPT (blue), OY-48 (red), OY-52 (pink), OY-53 (dark green), OY-55 (brown), B-) comparison -NH_2 stretching between monomer of TAPT and TPT-SQ COPs

For instance, in the first polymer reactions (OY 48-55), It can be clearly seen that -N-H stretching of monomer TAPT has almost disappeared or reduced significantly (still the terminal groups can be seen) in spectrum (Fig. 4.12, B-)) and the new broadened peak between 3000-3500 cm^{-1} is attributed to the overlapped stretching vibration of secondary -N-H as well as aromatics -C-H in polymer. Moreover, stretching vibrations of the carbonyl group of squaraine is shifted toward the blue region (1593 cm^{-1}) with respect to the model compound (-C=O 1539 cm^{-1}) because of the extended conjugation. The peak at about 1491 cm^{-1} reveals the existence of C=C stretching in aromatic rings. The characteristic C=N stretching band was arisen at 1710 cm^{-1} indicating the occurrence of polycondensation reaction (Fig. 4.12, A-)).

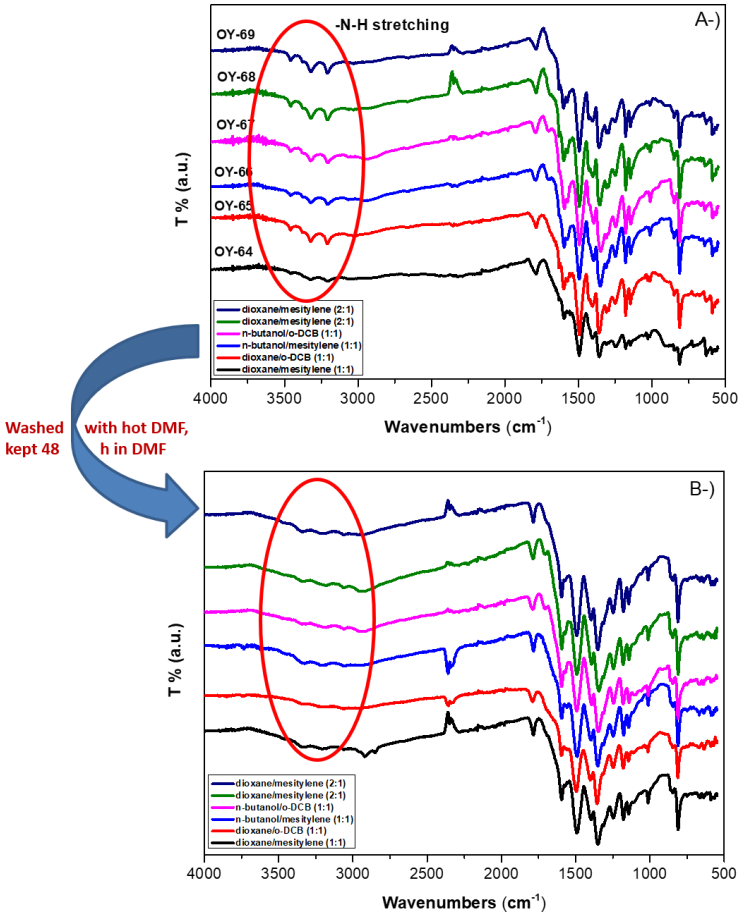

Fig. 4.13 Infrared spectra of TPT-SQ $COPs_{solv}$ indication comparison of -NH_2 stretching before washing and keeping in DMF for 2 days A-), after B-)

These findings give information about the yield of the polymerization reaction. It is possible that during reaction oligomers or starting compounds can be trapped into pore or even not consumed completely, thus, it could be identified the specific functional groups in the spectrum. In the reaction of OY 64-69, mostly oligomers or monomers were observed and the –N-H primary amine stretching vibration was still detectable in the IR spectrum (Fig. 4.13) evidencing that these active groups were not polymerized completely or small molecules, oligomers were still present.

When products were washed with hot DMF and then kept products in DMF solution for 2 days, the intensity of the vibration ascribed to these amino groups diminished considerably (Fig. 4.13).

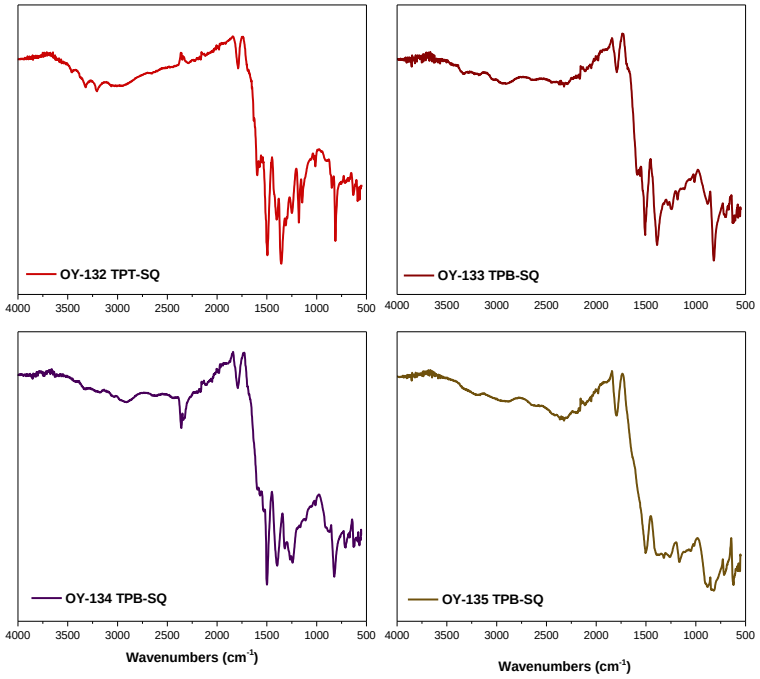

Fig. 4.14 Infrared spectra of SQ-COPs synthesized by solvothermal method in Dioxane/mesitylene 3:1

In spectrums of OY 132-135, primary amine groups are not clearly identified except for OY 141 (Fig. 4.14). The solubility of monomers of TAPT is lower than other linkers and this is the reason why primary amine -N-H groups of oligomers or monomer residuals were observed; in other reactions using different linkers, these vibrations were only barely detectable. In addition, C=C stretches in the aromatic rings in the region between 1400-1600 cm^{-1} are not clear and the -C=N bond in between 1675-1680 cm^{-1} is not visible (Fig. 4.14).

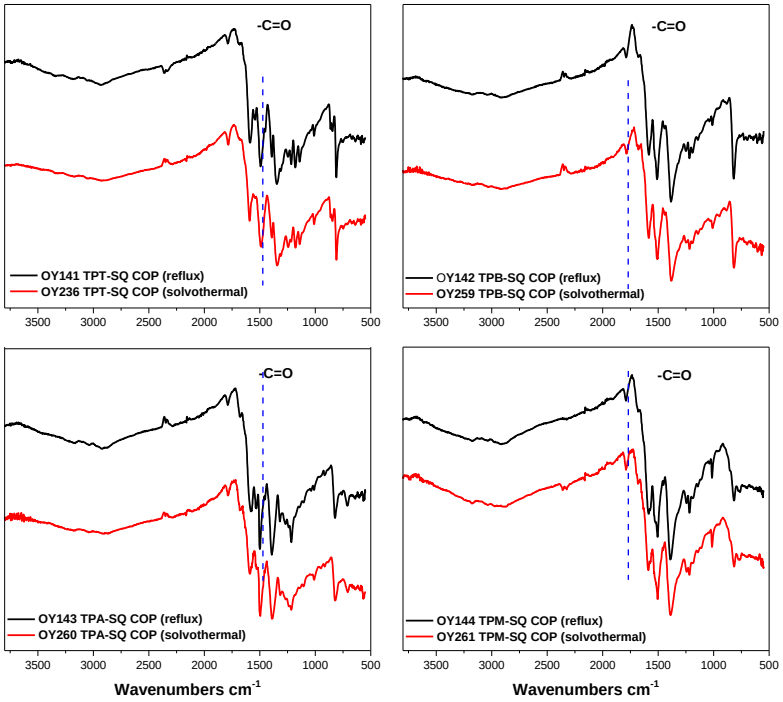

Fig. 4.15 Comparison of infrared spectra of SQ-COPs synthesized by solvothermal method (red) and reflux (black)

On the other hand, the spectrums of polymers produced by reflux (OY 141-144) and solvothermal method (OY 228-261) are well matched (Fig. 4.15). Primary amine bonds of monomers have almost disappeared and the -C=N bond related to occurrence of squaraine units in the polymer can be clearly seen in spectra (Fig. 4.16).

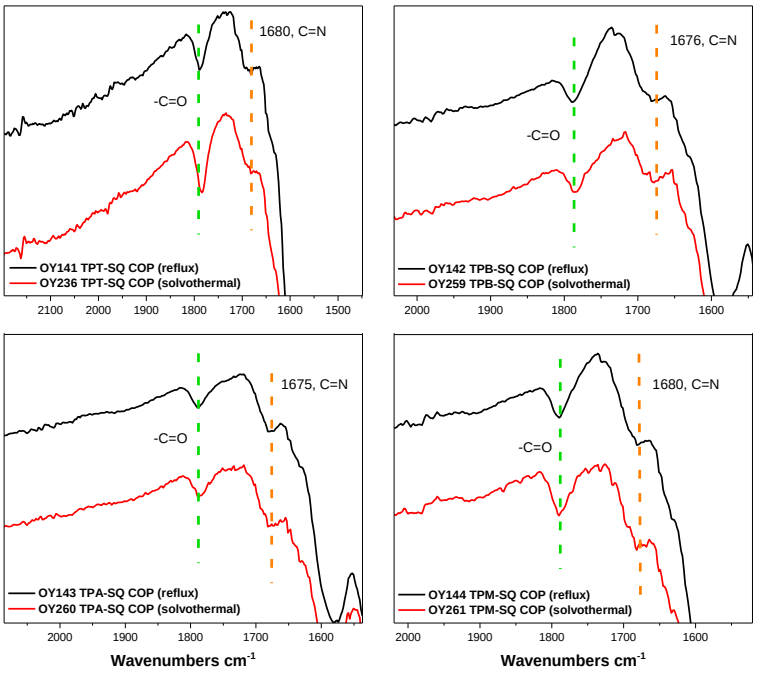

Fig. 4.16 Infrared spectra of SQ-COPs indicating carbonyl and imine stretching frequency (solvothermal method (red) and reflux (black))

According to the FT-IR spectrums, we could identify the structure relying on functional groups. In addition to FT-IR spectroscopy analysis, elemental analysis (Table 4.4) was performed to elucidate whether the reaction is completed or not as well as to support IR results and elemental composition of polymers was ascertained by combustion elemental analysis. C, H, N elemental analysis data indicates that the found results are too close to calculated ones obtaining relatively higher hydrogen and lower carbon and nitrogen content (Table 4.4). This can be possible due to incomplete combustion of polymer samples, and solvent or gas molecules such as H_2O, O_2, CO_2, trapped inside pores of prepared materials. However, while most of the prepared samples demonstrate very close results to calculated ones, nitrogen and hydrogen contents in OY133-135 are too lower than

calculated values. The most accurate way regarding clarification of the outcomes is C/N values and while most of the prepared samples of C/N values are same or very close to the calculated ones, the values of the OY 133-135 are extremely higher, just as functional groups are not clear in FT-IR spectrums.

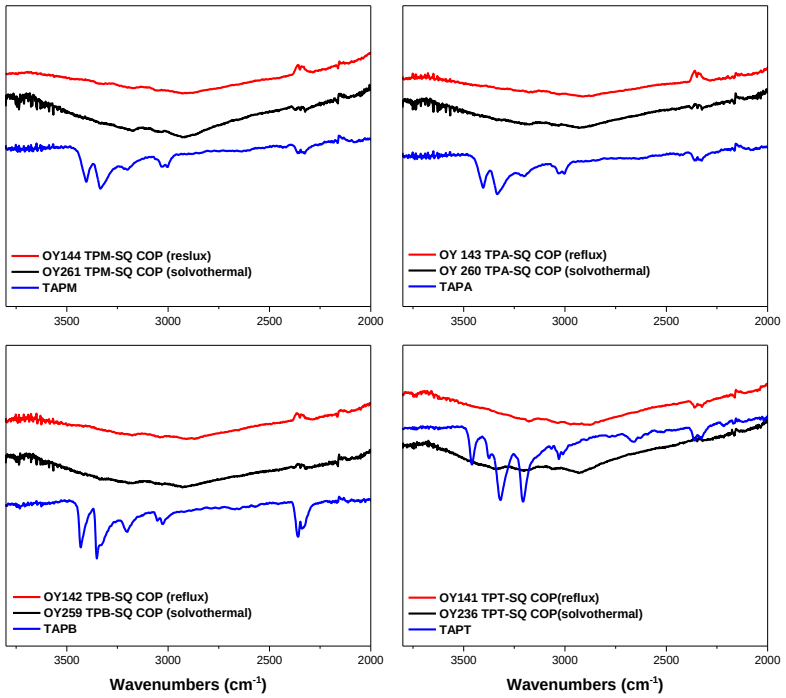

Fig. 4.17 Comparison of infrared spectra of SQ-COPs with starting compounds indicating imine stretching frequency (solvothermal method (red), reflux (black), and starting compounds (blue))

Table 4.4 Elemental analysis of prepared polymers

Sample No (SQ-COPs)	Composition	C (%)	H (%)	N (%)	C:N
OY-48 TPT-	**Calculated**	68.79	3.21	17.83	3.8
	Calculated (1xH_2O)	61.36	4.58	15.90	3.8
	Found	63.59	4.16	16.73	3.8
OY-52 TPT-	**Calculated**	68.79	3.21	17.83	3.8
	Calculated (1xH_2O)	61.36	4.58	15.90	3.8
	Found	60.53	3.82	14.95	4.0
OY-53 TPT-	**Calculated**	68.79	3.21	17.83	3.8
	Calculated (1xH_2O)	61.36	4.58	15.90	3.8
	Found	62.18	4.00	15.34	4.0
OY-55 TPT-	**Calculated**	68.79	3.21	17.83	3.8
	Calculated (1xH_2O)	61.36	4.58	15.90	3.8
	Found	68.25	4.43	17.00	4
OY-132 TPT-	**Calculated**	68.79	3.21	17.83	3.8
	Calculated (1xH_2O)	61.36	4.58	15.90	3.8
	Found	62.44	4.02	14.91	4.1
OY-133 TPB-	**Calculated**	76.91	3.87	8.97	8.6
	Calculated (1xH_2O)	68.56	5.18	8.00	8.6
	Found	47.35	2.24	1.52	31
OY-134 TPA-	**Calculated**	70.76	3.71	13.75	5.1
	Calculated (1xH_2O)	67.28	4.71	13.08	5.1
	Found	50.29	4.32	4.33	11.6
OY-135 TPM-	**Calculated**	73.88	3.97	10.34	7.1
	Calculated (1xH_2O)	70.25	4.95	9.83	7.1
	Found	42.99	1.84	0.37	116

Continuing Table 4.4

Sample No (SQ-COPs)	Composition	C (%)	H (%)	N (%)	C:N
OY-141 TPT-	**Calculated**	68.79	3.21	17.83	3.8
	Calculated (1xH_2O)	61.36	4.58	15.90	3.8
	Found	61.70	3.90	16.91	3.6
OY-142 TPB-	**Calculated**	76.91	3.87	8.97	8.6
	Calculated (1xH_2O)	68.56	5.18	8.00	8.6
	Found	68.38	4.47	8.44	8.1
OY-143 TPA-	**Calculated**	70.76	3.71	13.75	5.1
	Calculated (1xH_2O)	67.28	4.71	13.08	5.1
	Found	62.17	4.32	12.88	4.8
OY-144 TPM-	**Calculated**	73.88	3.97	10.34	7.1
	Calculated (1xH_2O)	70.25	4.95	9.83	7.1
	Found	65.97	4.44	9.89	6.8
OY-236 TPT-	**Calculated**	68.79	3.21	17.83	3.8
	Calculated (1xH_2O)	61.36	4.58	15.90	3.8
	Found	62.67	3.97	14.54	4.3
OY-259 TPB-	**Calculated**	76.91	3.87	8.97	8.6
	Calculated (1xH_2O)	68.56	5.18	8.00	8.6
	Found	70.28	4.56	8.23	8.5
OY-260 TPA-	**Calculated**	70.76	3.71	13.75	5.1
	Calculated (1xH_2O)	67.28	4.71	13.08	5.1
	Found	64.99	4.36	12.11	5.3
OY-261 TPM-	**Calculated**	73.88	3.97	10.34	7.1
	Calculated (1xH_2O)	70.25	4.95	9.83	7.1
	Found	67.01	4.61	9.41	7.1

We scrutinized the chemical environment of prepared polymers, starting compounds of tritopic linkers, squaric acid as well as model compound using ^{13}C CP-MAS NMR and ^{13}N-CPMAS NMR spectroscopy, carried out in solid state. The secondary amine carbon corresponding to TAPT and carbonyl carbon or enol carbon belonging to squaric acid at 151, 187 and 192 ppm almost completely

disappeared in the ^{13}C-CPMAS NMR spectrum (Fig. 4.20), very low residue was observed and this is supposed to be the terminal groups in polymer that are unreacted functional groups. On the other hand, a new peak at 141 ppm emerged, indicating the formation imine linkages (Fig. 4.20).

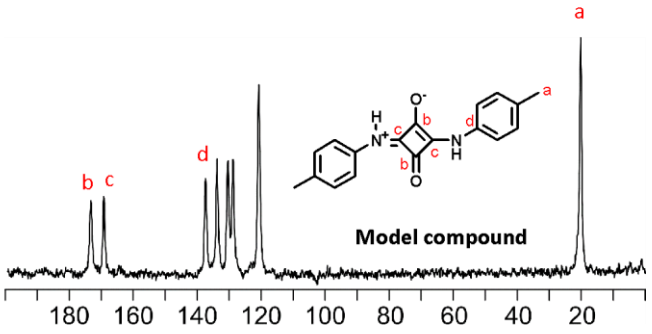

Fig. 4.18 ^{13}C-CPMAS NMR of model compound of Tol-SQ

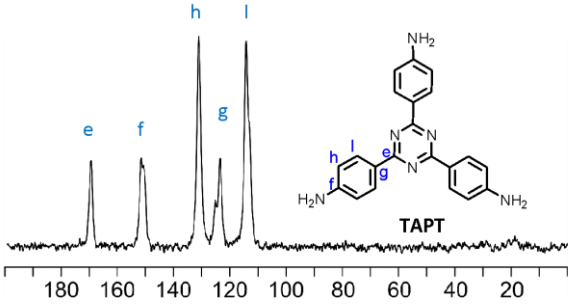

Fig. 4.19 ^{13}C-CPMAS NMR of TAPT

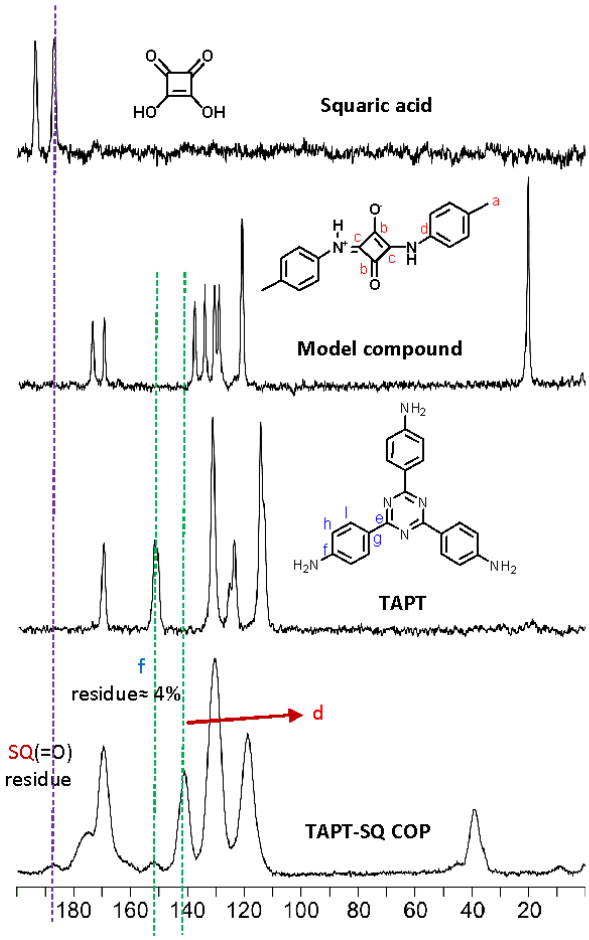

Fig. 4.20 Comparison of ^{13}C-CPMAS NMR indicating carbon of functional groups from up to down; squaric acid, model compound of Tol-SQ, starting compound of TAPT, TPT-SQ polymer, respectively

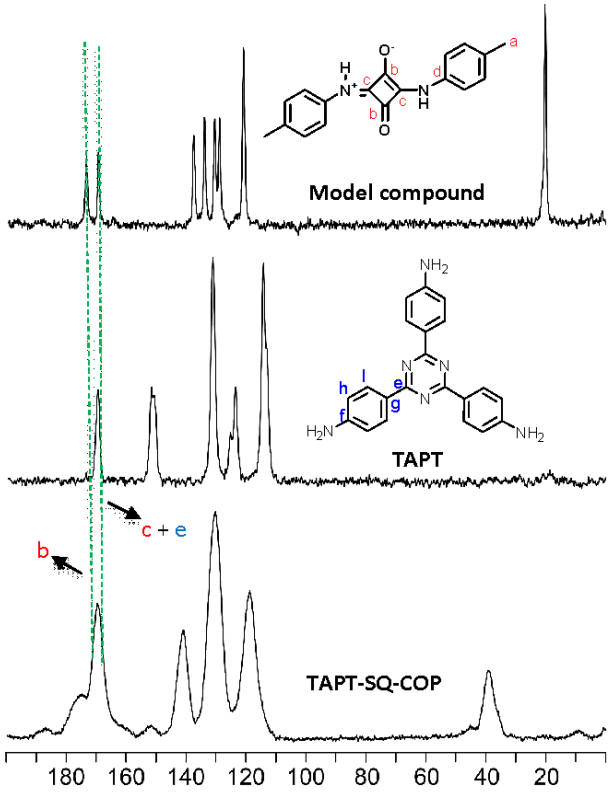

Fig. 4.21 Comparison of ^{13}C-CPMAS NMR indicating new carbons occurred in TPT-SQ polymer from up to down; model compound of Tol-SQ, starting compound of TAPT, TPT-SQ polymer, respectively

In addition, disappearance of secondary amine nitrogen related to the TAPT was observed as well in ^{15}N-CPMAS NMR spectrum and a new peak ascribed to primary amine group which is positive charged nitrogen arose at around 128 ppm (Fig. 4.22). The disappearance of the amine nitrogen peak in ^{15}N-CPMAS NMR and its carbon in ^{13}C-CPMAS NMR as well as emergence of an imine nitrogen peak, and also its carbon demonstrates that polycondensation of TAPT and squaric acid were accomplished successfully.

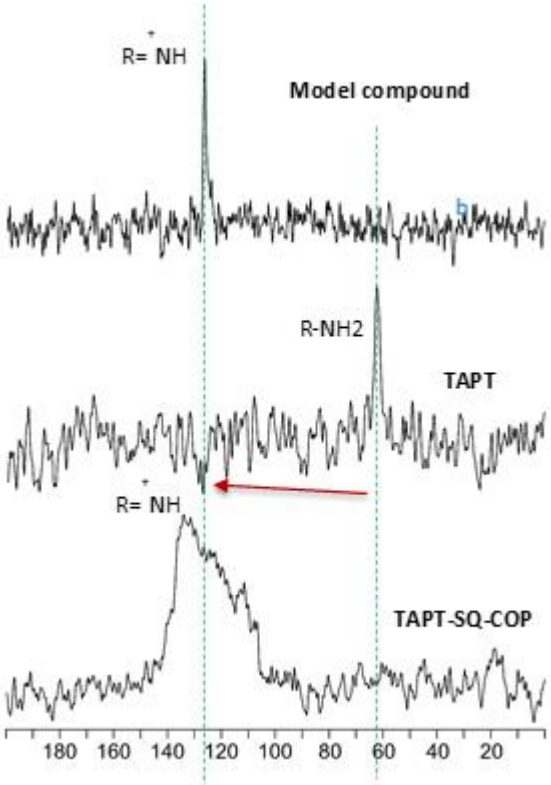

Fig. 4.22 Comparison of ^{15}N-CPMAS NMR indicating new charged nitrogen occurred in TPT-SQ polymer from up to down; model compound of Tol-SQ, starting compound of TAPT, TPT-SQ polymer, respectively

4.3.2 PXRD Analysis of Prepared Polymers

X-ray powder diffraction (XRD) is a rapid analytical technique mainly utilized for phase identification of a crystalline material and can give information on unit cell dimensions.[243] It is mainly employed for organic, inorganic small molecules who usually results in highly ordered and even crystalline structures. Structural regularity is analyzed by powder X-ray diffraction (PXRD). The topology of the layers is identified by the structure of the linkage and linker molecules, and typically a hexagonal pattern is constituted because of the symmetry of the linker

moieties. Planarity, rigidity of linker molecules as well as reversibility of linkage play a key role for obtaining regular crystallinity in covalent organic frameworks.

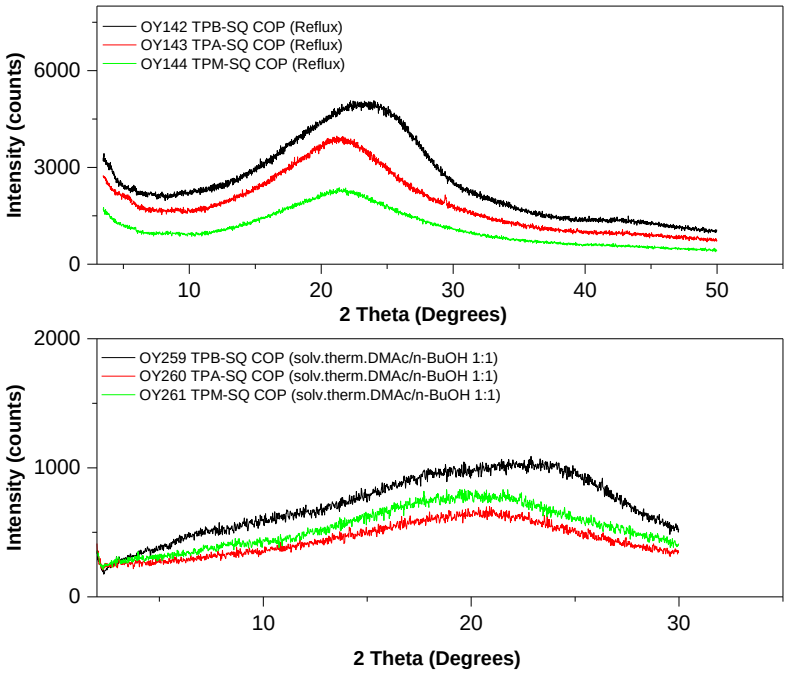

Fig. 4.23 PXRD patterns of SQ-COPs$_{reflux}$ (up), SQ-COPs$_{solv}$ (down)

The trigonal linkers, except TAPT, which were used for polymerisation are not planar and squaraine linkage has no high reversibility that cause kinetic reaction control in comparison to imine linkage; therefore, disordered morphology of polymers was expected and TPB-, TPA-, TPM-SQ COPs demonstrated predominately amorphous nature (Fig. 4.23). Due to nonplanar tritopic linkers, the squaraine unit could twist and rotate during the condensation reaction. This also has an impact on the regularity of resulting polymer structure. On the other hand, since TAPT and squaric acid are highly planar molecules, it is expected that their reaction provides highly planar structure resulting in regular morphology in 2D

form. Therefore, we mostly focused on the synthetic conditions of the latter reaction by changing solvent mixtures, their ratios and quantities as well as monomer amounts. Firstly, we investigated the XRD of the precursor to compare their patterns with polymer results and squaric acid revealed more intense and sharper diffraction peaks than TAPT owing to its high crystallinity (Fig. 4.24)

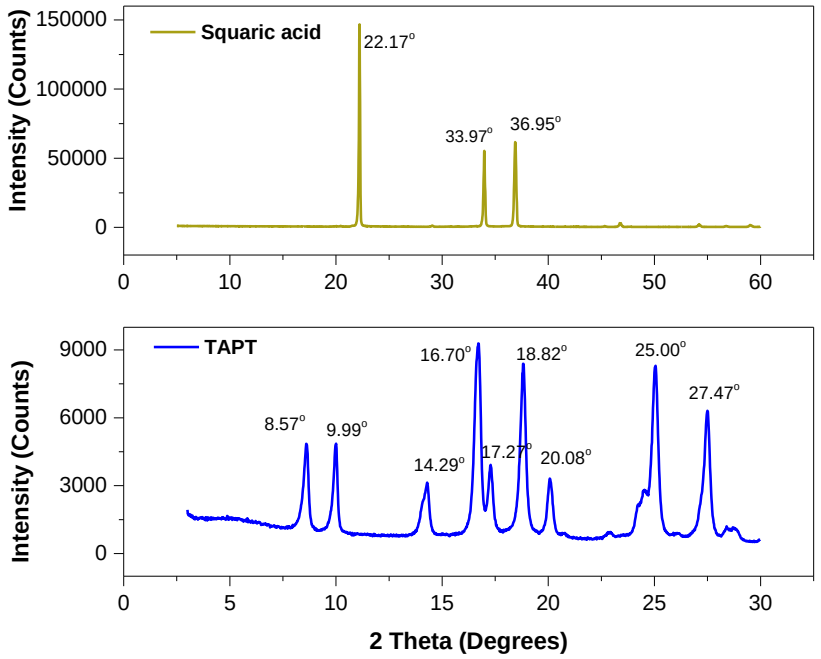

Fig. 4.24 PXRD patterns of starting compounds of squaric acid (up) and TAPT (down)

Even though we analysed the effect of the solvent mixtures to the resulting product in the first reactions (OY 48-55), they exhibited amorphous morphologies (Fig. 4.25). While OY48 indicated a broadened peak (FWHM=10.96), the OY-55 showed larger broadened peak (FWHM=15.38) based on estimated their FWHM calculation. This could be due to polar solvent mixtures that lead to a kinetic control of the reaction.

Divergence slits block X-rays with angle different from the direction identified by source and sample. The size of the divergence slit affects peak intensity and peak shapes the closer the slit the smaller the angular aperture and more parallel (but less intense) the beam. Narrow divergence slits reduce the intensity and the length of the X-ray beam hitting the sample to produce sharper peaks. There are two slits in front of the X-Ray source.

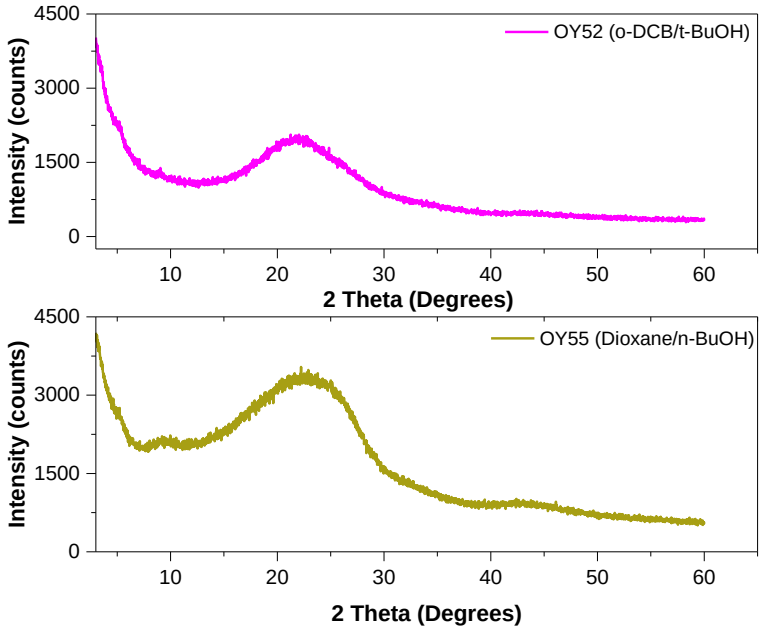

Fig. 4.25 PXRD patterns of TPT-SQ COPs synthesized by thermal condition; OY-52 (up), OY55 (down)

On the other hand, considering the polymers synthetized by solvothermal method, patterns of OY 64-69 TPT-SQ COPs indicated broadened peaks around 15-30 degrees (Fig. 4.26). Polymerisation was not successfully completed, mostly oligomers or residuals of starting compounds were found beside desired product. They were washed with hot DMF and kept in DMF for 2 days. This washing process can cause aggregation resulting in irregularity so, this could also be reason why amorphous form were seen in patterns.

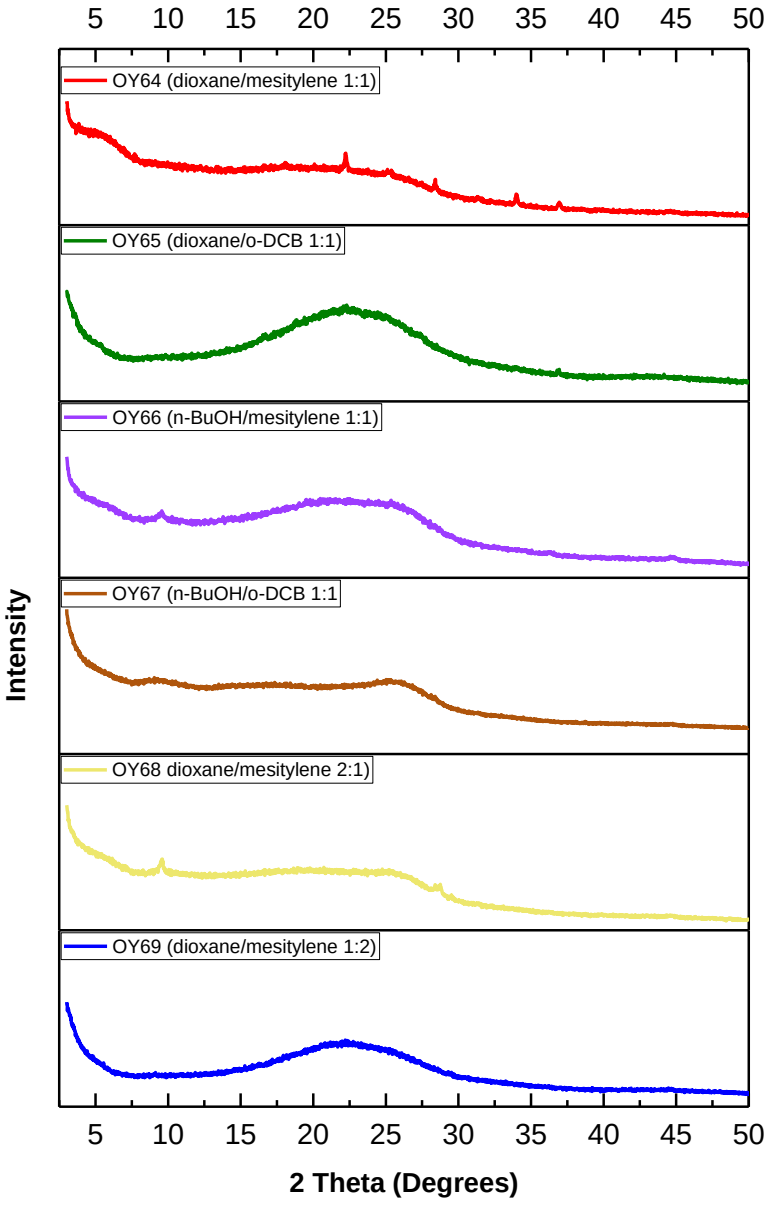

Fig. 4.26 PXRD patterns of TPT-SQ COP_{solv} from up to down; OY-64-69, respectively

Solubility of squaric acid in DMAc also has an impact on the crystallinity. Whereas the obtained TPT-SQ polymers in polar solvent combination of DMAc with

mesitylene or EtOH, revealed broadened peaks that are clearly visible at around between 25° – 26° (Fig. 4.27) and they did not show any diffraction peaks, the polymer produced in DMAc/n-BUOH (1:1) mixtures indicated a very low intensity peak at around 3.09° that could be associated with (100) plane along with broaden peak at 25.95° (Fig. 4.27, C-)).

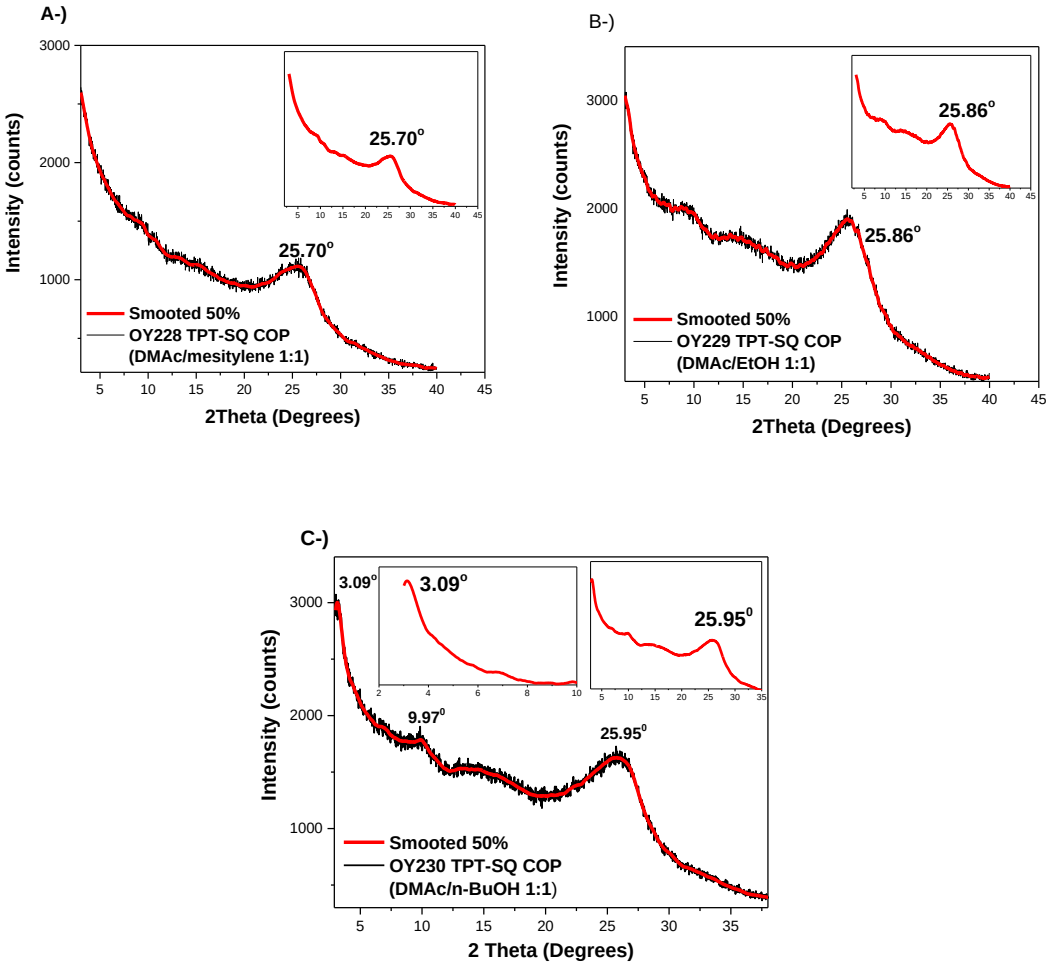

Fig. 4.27 PXRD patterns of TPT-SQ COP_{solv}; A-) OY228, B-) OY229, C-) OY230 (measured using 1/16 and 1/32 slits)

Peaks at around 2θ = 25-26o for polymers are usually ascribable to interlayer stacking, similarly to PXRD patterns of other layered, aromatic systems such as aromatic porous polymers and COFs.[30] Most of the COFs generally exhibit mesoporous surfaces (2-5 nm pore size)[20] and this is corresponding to the low angles diffraction peaks in PXRD pattern according to the de Bragg`s equation.[244] Divergence slits block X-rays with angle different from the direction identified by source and sample. The size of the divergence slit affects peak intensity and peak shapes the closer the slit the smaller the angular aperture and more parallel (but less intense) the beam. Narrow divergence slits reduce the intensity and the length of the X-ray beam hitting the sample to produce sharper peaks. There are two slits in front of the X-Ray source. To see any diffraction peaks at low angles, mostly very narrow slits are used in order to localise the beam on the surface of the sample in very low angles and 1/16 and 1/32 mm slits were used in these analyses. We also analysed the sample OY230 (DMAC/n-BuOH 1:1-3ml) (Fig. 4.28) using two 1/16 slits to reduce the intensity in low angles since we can identify the broadened peak in the high angle region as well as a sharp peak in low angle region. The peak observed at low angles (3.09^{o}) is less intense compared to the high broadened peak at 25.95^{o}. This demonstrates that there is no long-range order. Increasing the solvent volume from 3 ml to 5 ml in the same mixture (OY240) revealed a sharper peak at 26.69^{o} (Fig. 4.29).

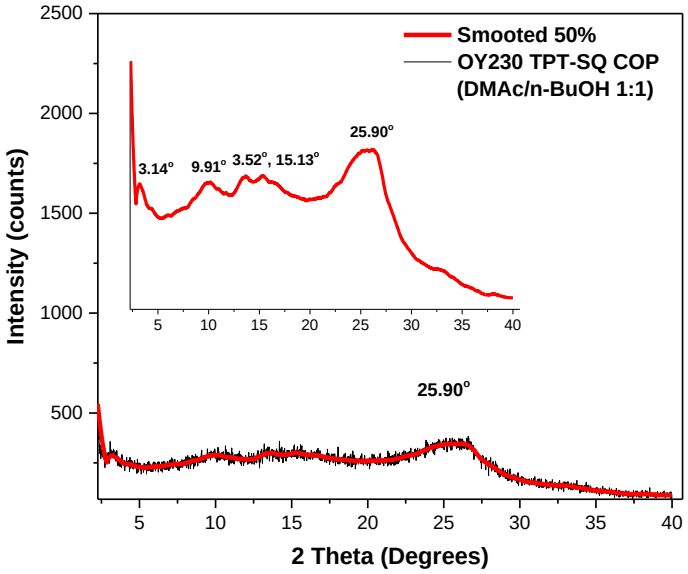

Fig. 4.28 PXRD pattern of TPT-SQ COP_{solv} in DMAc/n-BuOH 1:1, 3ml (measured using 1/16 and 1/16 slits)

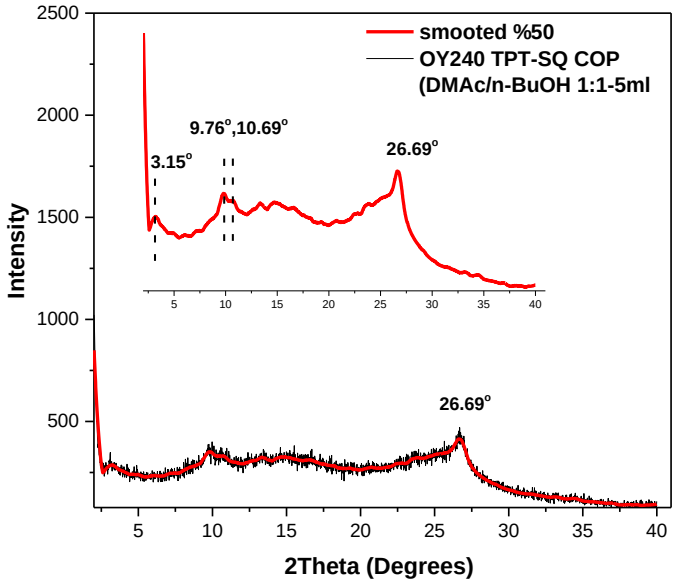

Fig. 4.29 PXRD pattern of TPT-SQ COP_{solv} in DMAc/n-BuOH 1:1, 5ml (measured using 1/16 and 1/16 slits)

Reaction in DMAc/n-BuOH was repeated by changing the ratio of solvent combination to understand whether regularity is improved or not. Raising of the more polar solvent leads to sharper peaks at similar degrees, especially at between 25-27° (Fig. 4.30, 4.31) that is related to interlayer stacking distance of the layers (distance of aromatic unit) associated with (001) plane[245] and it has lower intensity but it is sharper. The employment of TAPT as linker also revealed two intense sharp peaks at around 25° and 27.47° (Fig. 4.24) which determines distance of two aromatic phenyl and triazine rings. This sharp peak was observed at around 26.74° in TPT-SQ polymer (Fig. 4.30, 4.31) (OY 236-237) and it is similar graphitic-like layers with a spacing of around 0.33−0.34 nm which is very close that of the graphitic materials (≈0.38 nm)[246]

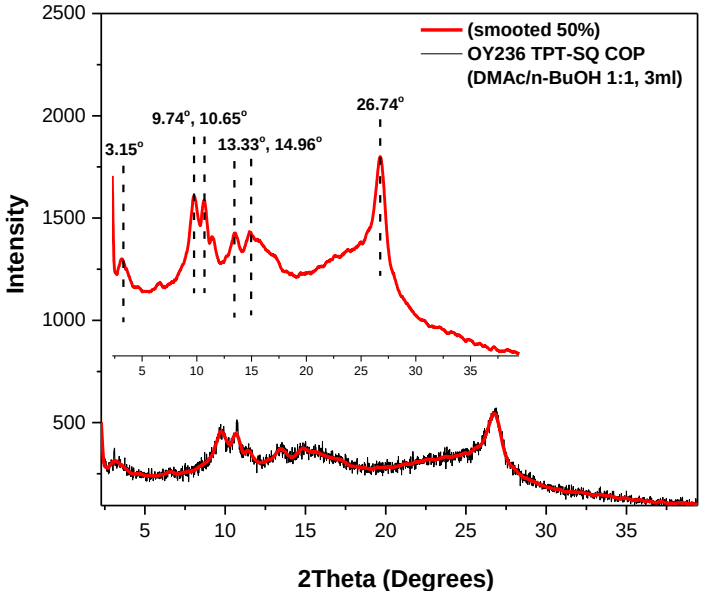

Fig. 4.30 PXRD pattern of TPT-SQ COP_{solv} (OY 236)

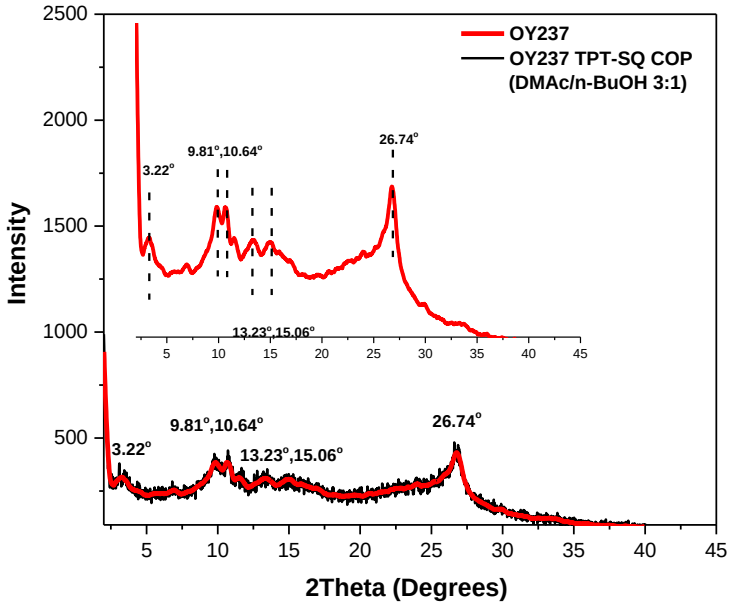

Fig. 4.31 PXRD pattern of TPT-SQ COP_{solv} (OY-237)

Measurement was also performed in low angle between 2-12° 2θ to make those peaks more comprehensible and, as seen in Fig. 4.32, peaks are clearer even if they are not really sharp.

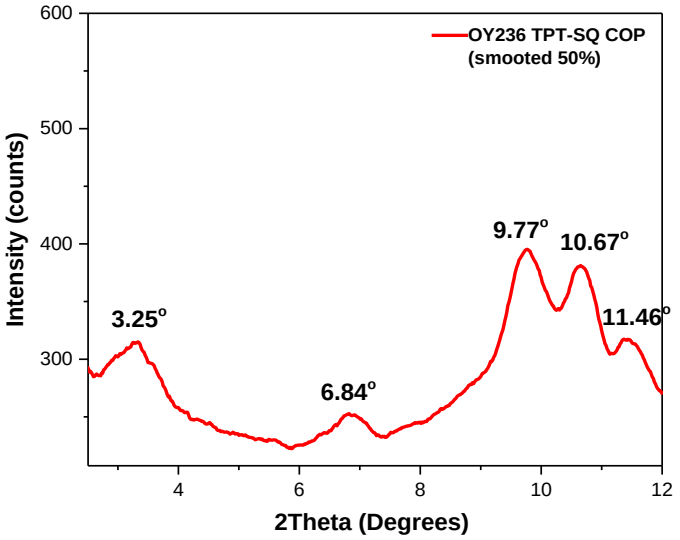

Fig. 4.32 PXRD pattern of OY-236, TPT-SQ COP_{solv} (measured in low angle between 2-12 2 theta)

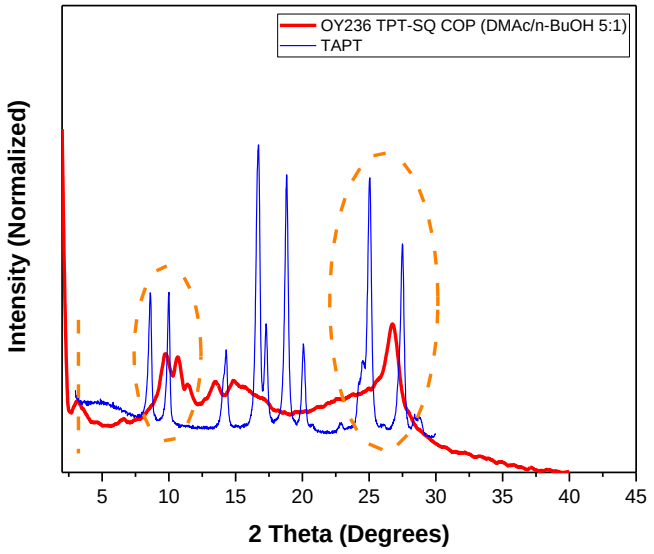

Fig. 4.33 Comparison of PXRD patterns TPT-SQ COP (OY-236, red), starting compound of TAPT (blue)

The peaks corresponding to polymer were shifted by comparison with the ones of the linker (TAPT). The sharp peaks that arose between 15° and 25° in the PXRD pattern of TAPT were not observed in the corresponding polymer (Fig. 4.33). This proves that polymer can have own characteristic peaks and there are no residuals coming from linker. The regular crystalline lattice is generally possible when individual layers are stacked. Most of the 2D-COFs have been exhibited AA (eclipsed, P6/mmm) interlayer stacking.[247] This geometrical arrangement enlarges the affinity of the molecular existence and give rise to straight channels, orthogonal in the COF layers, as known from the literature.[9,47] Imine-linked COFs are constituted by carbon and nitrogen linkages. These lead to polarization in the structure and the AA stacking arrangement boost the attractive London dispersion interaction between the layers, and causes repulsive Coulomb force because of the polarized linkages; moreover, in the charged form of layers, this repulsive force is higher due to the overlapping of identical charges;[248,249] thus, it is possible that layers can slip and result in different stacked geometry such as AB or ABC.[250] Layered 2D crystalline frameworks generally reveals one important sharp peak in low angle which is associated with (100) plane.[237] In Layered COFs, atoms become more intense in (100) plane describing pore size.[251] Slipping of layers in this TPT-SQ polymer is highly possible due to zwitterionic and zig-zag form of squaraine unit.[53] In case of the random displacement of the 2D layers, the peak corresponding to (100) plane could not be observed or seen with a very low intensity. In this case, various peaks could be arisen in pattern regarding different planes. This may be reason why different peaks were seen in this pattern. In addition, layers could not be stacked in different geometry, regularity could be observed but exfoliation might occur that layers may be dispersed randomly.[246]

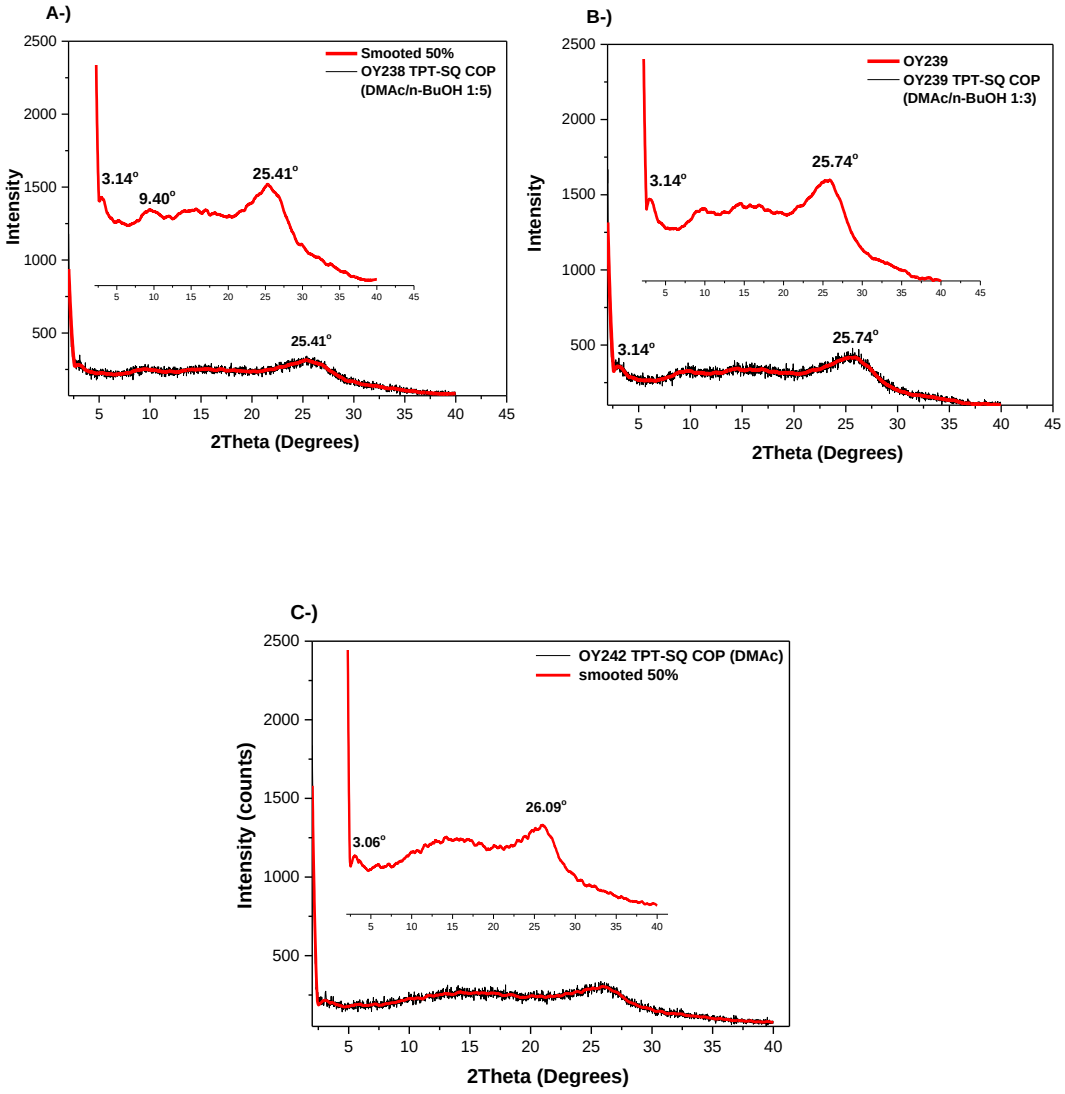

Fig. 4.34 PXRD patterns of TPT-SQ COP_{solv}; A-) OY238, B-) OY239, C-) OY242

While the volume of DMAc in the mixture of DMAc/n-BuOH impacted the reaction (thermodynamic reaction controlled) and caused revealing some characteristic peaks (Fig. 4.31), decreasing volume of DMAc did not affect the reaction (Fig. 4.34).

The reaction was repeated using DMAc (OY242) (Fig. 4.34, C-)) without any addition of solvent and any change was not observed. This shows the efficiency of n-BuOH as a solvent in combination with DMAc promoting the regular molecular arrangement of TPT-SQ polymer.

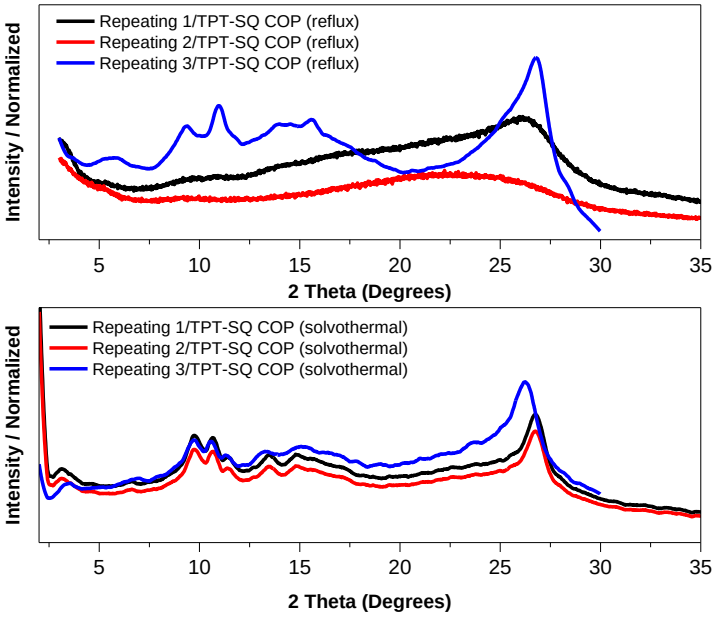

Fig. 4.35 PXRD patterns of SQ-COPs$_{reflux}$ (up), SQ-COPs$_{solv}$ (down)

The reactions of both reflux and solvothermal were repeated three times in order to control the reproducibility. Resulting polymers by reflux did not indicate the same patterns as seen Fig. 4.35. While the first and second reaction indicated amorphous morphologies, the last one showed some characteristic peaks as obtained in the solvothermal method. Furthermore, there is a small difference between first and second reaction relevant to interlayer distance of the layers. The polymers reproduced by the solvothermal method revealed almost the same characteristic peaks. There are only small differences in the last reaction related to interlayer stacking distance at around 25°-27° (Fig. 4.35).

4.3.3 Surface and Thermal Analysis of Prepared Polymers

Gas sorption analysis is one of the most common techniques applied to porous polymers to measure the specific surface area and the porosity of a material. The amount of gas employed to fill the pores can be utilized to quantitatively determine the surface area, pore size, and pore volume of a given material. Langmuir and Brunauer-Emmett-Teller (BET) equations are two common methods to measure the specific surface area;[252,253] Langmuir adsorption models assume that only a monolayer of adsorbates can appear on top of the surface. On the contrary, the BET model describes multilayer formation. When multilayers are formed, BET presumes that they are not formed through directly covering the surface, but by covering extra layers. On the other hand, Langmuir considers that multilayers can only form as the first adsorbed layer, causing an unrealistic surface area.[253]

We probed the surface analysis of the polymers to determine their surface area and pore size distribution. At the beginning, surface areas were measured through nitrogen adsorption–desorption isotherms. The SQ-COPs except TPT-SQ indicated highly amorphous morphologies. Irreversibility of linkage but especially nonplanarity of linkers leads to disarrangement in materials. Planarity of the linker of TAPT as well as squaric acid can make the polymer more regular among the used linkers. The TPT-SQ reactions obtained in DMAc/n-BuOH solvent combinations indicate better regularity revealing some diffraction peaks in PXRD pattern. Despite observation of these peaks in pattern, they appear on amorphous broadened peaks, and the specific peak corresponding to the (100) plane could not be observed at low angles which shows pore size of the framework. This demonstrates the low-range crystallinity of the SQ-polymers due to the random displacement of the 2D layers resulted in exfoliation and it may hinder the pore accessibility.[246]

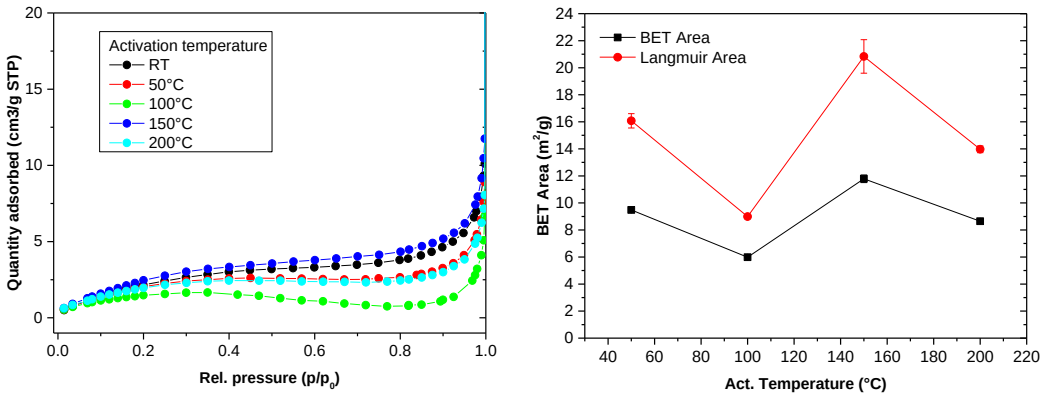

Fig. 4.36 Nitrogen adsorption isotherm of TPT-SQ COP_{reflux} (left), BET and Langmuir surface area of TPT-SQ COP_{reflux} (right)

Therefore, the surface area of TPT-SQ polymer produced by reflux was measured as 11 m^2/g (Fig. 4.36) which is extremely low in comparison to those COFs in literature.[254] For the calculation of surface area, nitrogen adsorption was not suitable for these SQ-polymers. Indeed, Nitrogen could not pass through the pores easily due to the presence of very narrow pores; thus, we employed CO_2 at 273 K to estimate the surface area and pore distributions of synthetized polymers. Based on CO_2 adsorption and desorption isotherms, the BET surface area and total pore volume as well as pore size were calculated using non-local density functional theory (NL-DFT) (Table 4.5).

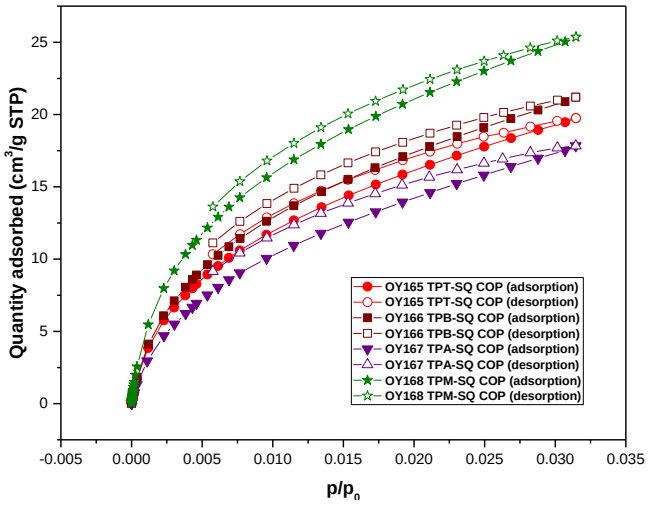

Fig. 4.37 CO_2 adsorption-desorption isotherms of SQ-COPs$_{solv}$

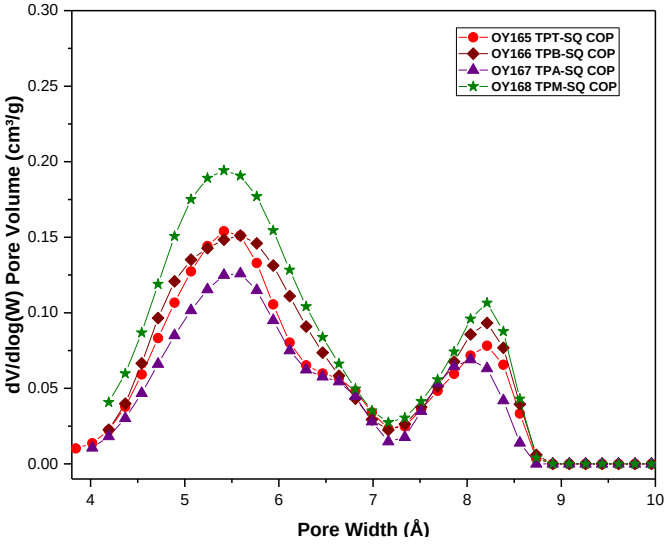

Fig. 4.38 Pore size distribution based on CO_2 adsorption isotherm of SQ-COPs$_{solv}$

BET surface areas of SQ-COPs$_{solv}$ were calculated as between 125-159 m^2/g with a total pore volume of 0.025-0.040 cm^3/g and their pore sizes were found as between 5.4-8.2 Å which shows there can be interpenetration in SQ-COPs causing

such very low micropores and especially containing more active binding sites of SQ-COPs demonstrates the reason for the CO_2 adsorption selectivity instead of N_2.

Table 4.5 Surface analysis data of SQ-COPs$_{solv}$

Polymer (SQ COPs)	BET SSA (m^2/g)	Total pore volume (cm^3/g)	Micropore size (Å)
TPT	129 ± 2	0.030	5.4 – 8.2
TPB	137 ± 2	0.032	5.5 – 8.2
TPA	125 ± 2	0.025	5.5 – 8.0
TPM	159 ± 2	0.040	5.4 – 8.2

One of the most common features of porous polymers is gas storage and removal of volatile iodine whose environmental risk is highly significant.[188] We also worked on iodine adsorption using SQ-polymers produced by both reflux and solvothermal methods. Although the capacity of gas storage in porous polymers is directly related to their surface area, it is possible to achieve a high gas storage capacity in 2D polymers with low surface area owing to their extended 2D networks containing various active sites on the surface. SQ-polymers include different active sites in knots and they have a zwitterionic form that can be attractive for interaction with highly polarizable iodine molecules. Moreover, adsorption studies gave us secondary information about the surface area of the polymers. The capturing was performed in gas phases of molecular iodine. SQ-COPs (10 mg) and excess iodine were placed into two open weighing vials in a closed larger vial at the same time. They were heated in an oven at 100 °C. We then removed the larger vial at a specific time point, cooled it to room temperature, weighed it, and compared the changes to the weight before and after iodine adsorption.

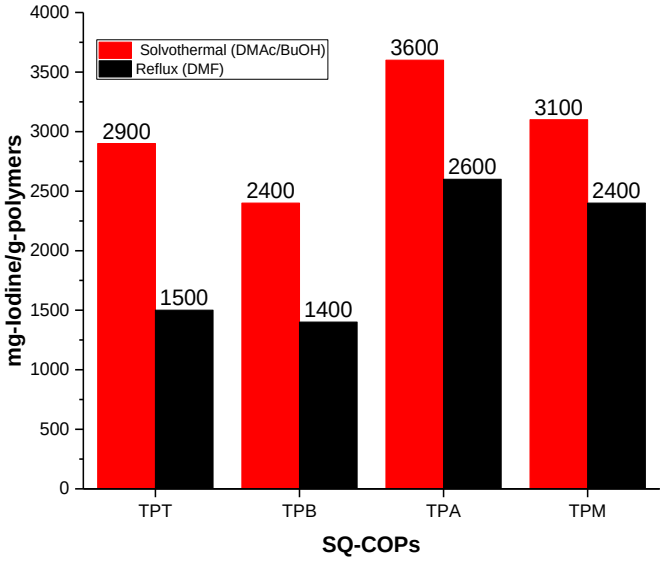

Fig. 4.39 Comparison of iodine adsorption capacities of SQ $COPs_{reflux}$ (black column), SQ $COPs_{solv}$ (red column)

As seen in Fig. 4.39 high iodine adsorption capacity was obtained in polymers synthesized by solvothermal method in DMAc/n-BuOH (red column). The polymers produced by reflux indicated lower adsorption capacity in comparison to the solvothermal method (black column). According to the adsorption capacities, it can be comprehended that the surface areas of polymers attained by solvothermal method might be higher than those produced by reflux. Moreover, The TPA-SQ polymers demonstrated higher capacity than other polymers. This could be related to linker including polymer apart from surface area. The triphenyl amine contains nitrogen which can interact with iodine molecules. On the other hand, Triphenyl methane might create a radical on its carbon element due to including acidic protons and this can be interactive for the iodine molecule as well thus, showing higher capacity than other polymers of TPT-SQ and TPB-SQ.

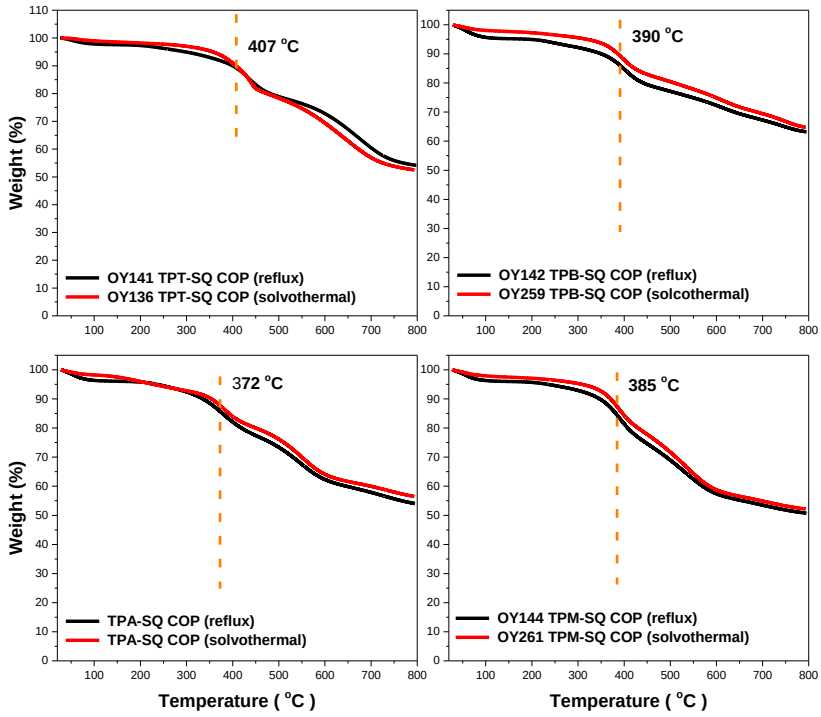

Fig. 4.40 Comparison of TGA curves; SQ $COPs_{reflux}$ (black), SQ $COPs_{solv}$ (red)

Above all, thermal stability of organic materials is essential for high-heat resistance in electronic applications, especially solar cells owing to sun exposure during process.[255] Covalent organic frameworks or polymers constituted organic nature indicate high thermal stability in comparison with MOFs and coordination polymer because the latter are simply linked by weak metal-coordination bonds.[256,257] TGA analysis of polymers produced by reflux and solvothermal were performed and they exhibit high thermal stability as expected (Fig. 4.40).

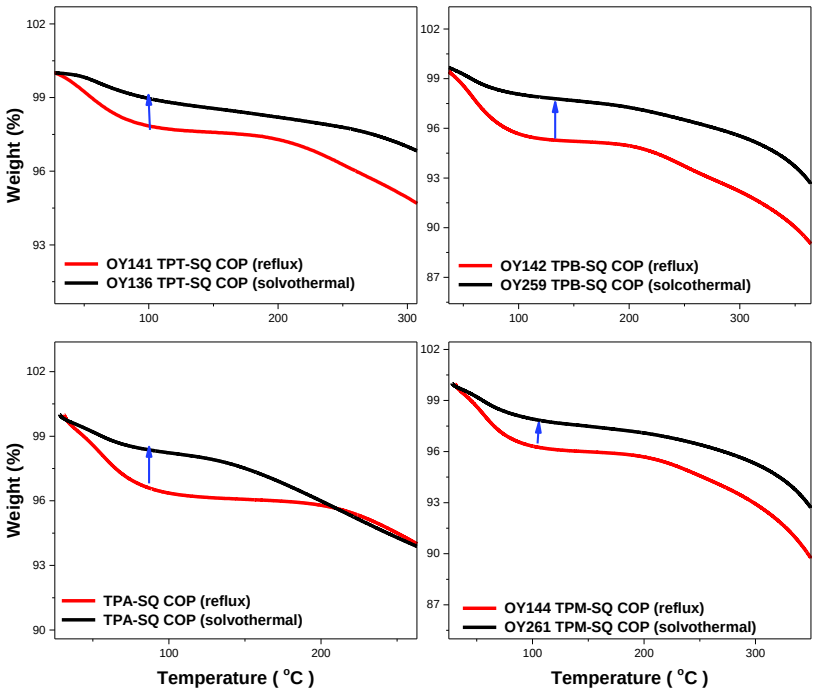

Fig. 4.41 Comparison of TGA curves indicating difference between SQ $COPs_{reflux}$ (black), SQ $COPs_{solv}$ (red) in low temperature

The onset point of the weight loss temperature (decomposition temperature Td) was 407 °C, 390 °C, 372 °C, 385 °C for TPT-, TPB-, TPA-, and TPM-SQ COPs, respectively (Fig. 4.40). Very low weight loss was observed, particularly in polymers obtained by reflux in DMF at lower temperatures (Fig. 4.41). This could be possibly due to the entrapping of solvent in the pores. However, nitrogen content was found lower than calculated values by elemental analysis and this proved that moisture or gases like O_2 or CO_2 could be trapped into pores.

As a result, in this section, we analysed thermal stabilities and structural regularity relying on surface morphology of the polymers. It has come out that solvent combinations and ratios, as well as planarity of linkers, demonstrate an

effect on structure arrangement. The iodine adsorption study, which can be relevant to surface areas depending on adsorption capacities, indicated different capacities between two reaction methods and it suggests that the solvothermal method might be more effective in terms of obtaining wider surfaces. After we analysed their surface morphologies, optical properties of the prepared polymers were investigated in detail through diffuse reflectance and solid-state fluorescence spectrometers.

4.3.4 Optical Properties of Prepared Polymers

As we mentioned previously, most of the porous organic polymers are insoluble materials. Optical characterisation of solid materials is possible based on their diffractions and reflections. Diffuse reflectance spectroscopy is a technique that was developed to be able to measure optical properties of materials as powder form. Measurement is fulfilled by a special apparatus of spherical sample holder attached to the instrument (Fig. 4.42) that makes it possible to collect reflected light from the powder. This spherical sample holder directs the sample beam which is non-adsorbed light coming from the sample. These reflected lights are assessed by reference beam and adsorption can be calculated to prepare the spectrum and calculation of Bandgap is possible based on Kubelka-Munk theory by converting reflectance of materials.

Fig. 4.42 Photograph of diffuse reflectance spherical sample holder; front filled with sample (left in up), side (left in middle), back (left in down), inserted to instrument (right)

Thus, we carried out diffuse-reflectance UV-Vis measurements in solid state in order to investigate optical properties of prepared polymers. Squaraines (SQs) usually demonstrate intense absorption and fluorescence in the near infrared caused by narrow band-gap due to resonance stabilized zwitterionic form.[258,259,260] The Electron-deficient cyclobutene ring of the squaraine unit is attractive in terms of being created tunable optical properties by incorporating various donor units. For this purpose, we functionalized the squaraine unit with donor linkers as 2D materials to improve their optical properties that aim at obtaining low band-gap in polymers.

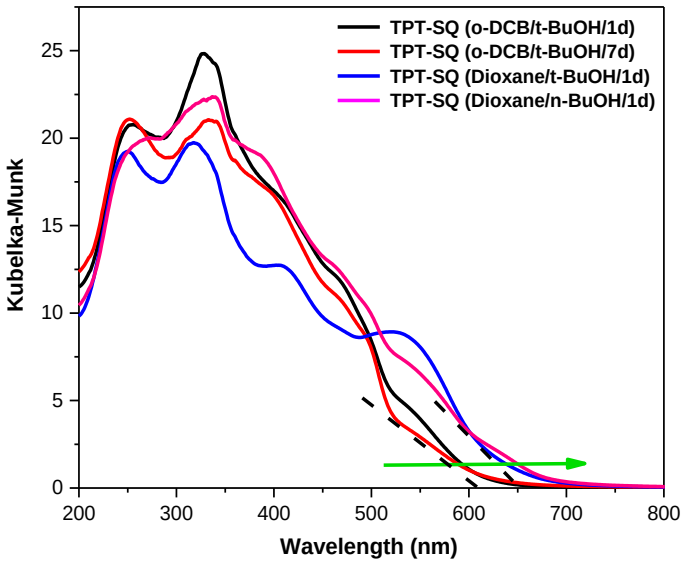

Fig. 4.43 Diffuse reflectance spectra based on kubelka-munk of SQ-COPs synthesized by thermal condition

In the first products, OY48-55, small differences were observed (Fig. 4.43) especially in their absorption edges. As seen in the spectra, even if the first two produced TPT-SQ polymers demonstrated different colours such as orange and dark orange, it was not observed a huge difference in absorption edges. However, the change of the solvent mixtures, increasing the polarity, leads to a small difference in absorption edges as approximately 70 nm.

We compared the optical properties of TPT-SQ COPs obtained in different conditions. The resulting polymers showed different colours such as red tile (OY141), light brown (OY236), dark red (OY55) and 100 nm shifting of absorption edges was seen in the spectrum (Fig. 4.44). The last example of TPT-SQ polymer synthesized by reflux (OY141) also showed similar properties but demonstrated

low iodine capacity that can be related to low surface area and different surface morphology.

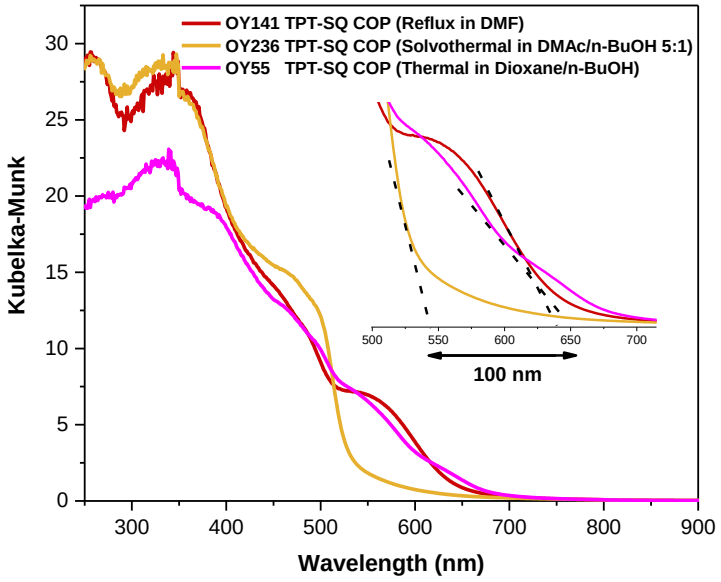

Fig. 4.44 Comparison of diffuse reflectance spectra based on kubelka-munk of SQ-COPs; produced by reflux (dark red), solvothermal (light brown), thermal (pink)

Even if it was not observed long-range order or high crystallinity, in the case of making a correlation between structural regulation and optical properties of TPT-SQ polymers, it can be mentioned that there might be no direct relations between regularity and optical properties in these TPT-SQ polymers.[261,262] Because regularity can be possible when aromatic units are stacked periodically in the same arrays in layered materials.

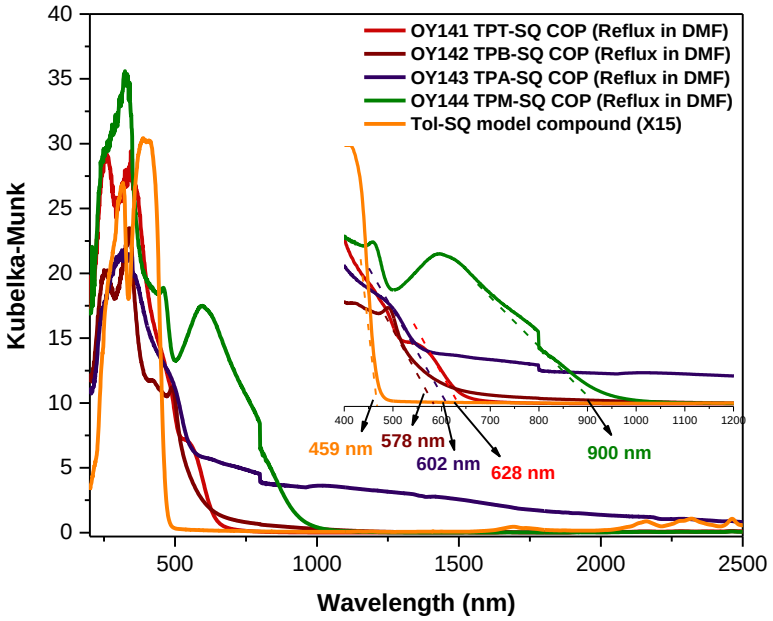

Fig. 4.45 Comparison of diffuse reflectance spectra based on kubelka-munk of SQ-COPs$_{reflux}$ and model compound

Based on this, in the regular system of TPT-SQ polymer, it is expected that triazine units are stacked as well as squaraine units in the same column. While acceptor triazine and squaraine units can`t interact with each other vertically in regular arrangement due to stacking of each of the units with themselves, in the case of randomly dispersed, they might interact with each other; this gives rise to a more red-shifted absorption edge because of electrostatic interaction in different morphological form.[262]

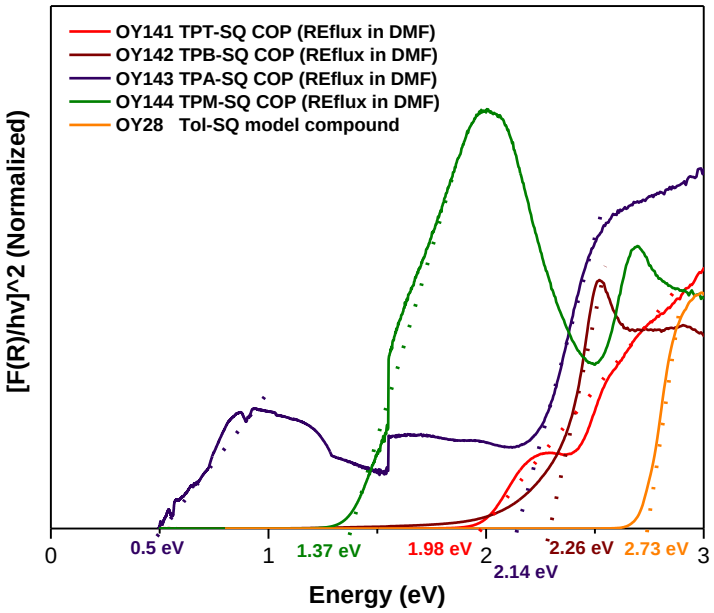

Fig. 4.46 Estimation of band-gaps of SQ-COPs$_{reflux}$ and model compound based on Tauc plot

Later, we investigated optical properties of polymers which were obtained by reflux and various absorption edges were achieved differing from 578 nm to 900 nm (Fig. 4.45). All polymers exhibited red-shifted absorption edges compared to the model compound and their optical band-gaps were estimated through Tauc Plot (Fig. 2.46) as 2.73 eV (model compound) > 2.26 eV (TPB-SQ) > 2.14 eV (TPA-SQ) > 1.98 eV (TPT-SQ) > 1.37 eV (TPM-SQ). These outcomes clearly demonstrate the effect of optical properties (optical band gap) adjusting in extended conjugation of SQ-polymers, through the construction of one material with various combinations of electron-donating and accepting linkers.

Diversity of linkers in polymers exhibit tunable optical properties revealing larger absorption than its model squaraine compound constructed with aromatic rings. Although the triazine unit was used to investigate acceptor-acceptor relation

in the polymer backbone, it demonstrated absorption-edge close to the NIR region owing to containing extra aromatic-donoring rings. It can be clearly seen spectral shift with functionalization; for instance, when phenyl ring replaces triazine unit, polymer showed higher absorption-edge with 50 nm difference (Fig. 4.45). On the other side, the polymers built with triphenylamine (TPA-SQ) and methane linkers (TPM-SQ) were supposed to cause limited conjugation on polymer backbone owing to unconjugated linkers, interestingly, they follow this rising of high absorption-edge with large difference such as 270 nm for triphenylmethane, and 1800 nm (with very low intensity) for triphenylamine by reaching out 2500 nm absorption edge and all polymers enlarged the maximum absorption (Fig. 4.45).

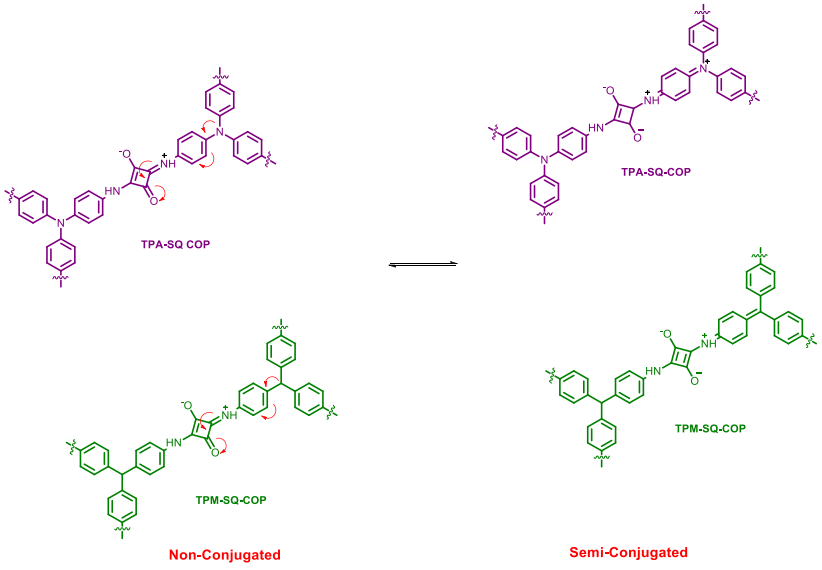

Fig. 4.47 Cross-conjugation (resonance form) of TPA-SQ COP (purple), and TPM-SQ COP (green)

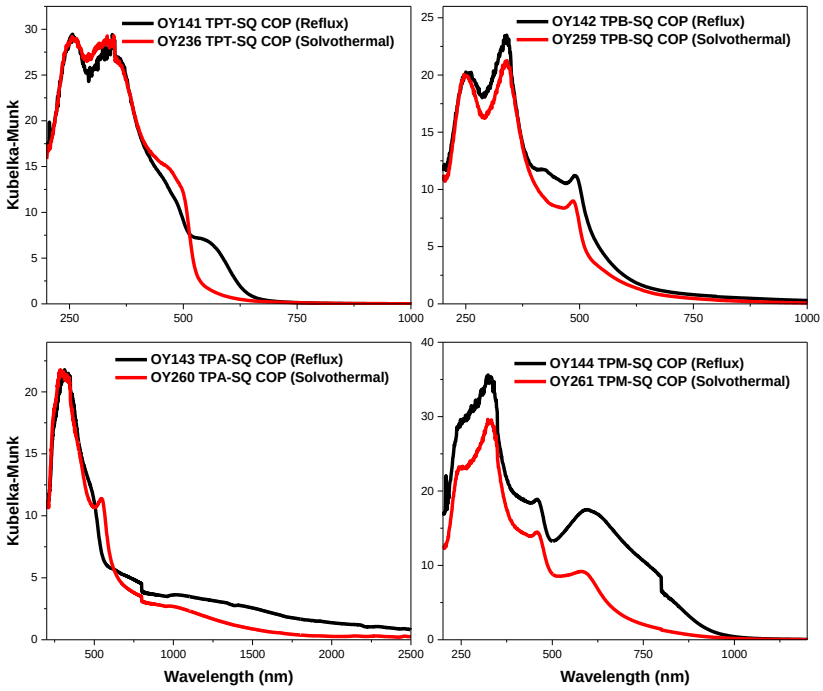

Fig. 4.48 Comparison of diffuse reflectance spectra of SQ-COPs$_{reflux}$ (black), SQ-COPs$_{solv}$ (red) based on kubelka-munk theory

TPB-SQ and TPT-SQ polymers could have naturally conjugated due to absorption edge of TPA-SQ and TPM-SQ polymers should be due to providing extra conjugation on materials and this might be possible by the means of cross-conjugation on the structure (Fig. 4.47).[132,263,264,265,266]

The TPT-SQ and TPA-SQ polymers produced by the solvothermal method demonstrated similar optical properties to ones refluxed despite the observation of dissimilarity in TPB-SQ and TPM-SQ polymers, and particularly, larger absorption was attained in produced TPM-SQ polymer by reflux (Fig. 4.48) Their optical band-gaps were estimated by Tauc`s plot as 2.73 eV (model compound) > 2.38 eV (TPB-SQ) > 2.35 eV (TPT-SQ) > 2.00 eV (TPA-SQ) > 1.80 eV (TPM-SQ) (Fig. 2.49). While the

band-gap of TPA-SQ polymer is lower, the band-gaps of the other polymers were higher than the ones of refluxed polymers.

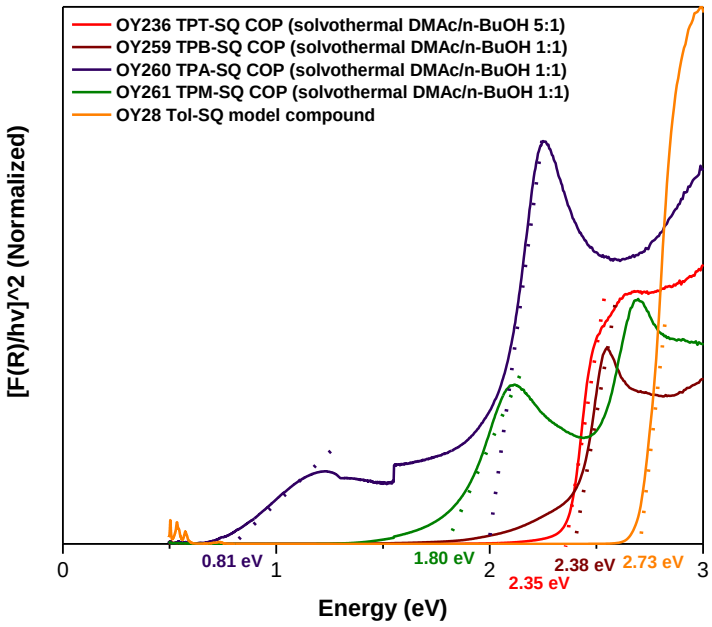

Fig. 4.49 Estimation of band-gaps of SQ-COPs$_{solv}$ and model compound based on Tauc plot

In their iodine adsorption studies, we analysed their surface areas. There are two possibilities in their adsorption. If there is a strong chemical bond-like interaction between adsorbate and adsorbent, it is a chemisorption whereas if a Van der Waals interaction is predominant, a physisorption occurs. Observation of both these processes is theoretically possible in SQ-polymers due to their surface area, extended networks as well as containing various active sites. Based on this, when polymers were exposed to iodine vapours, their absorption edges were red-shifted in UV-Vis Diffuse Reflectance spectra (Fig 2.50). This might be related to the p-type doping impact that adsorbed iodine species cause rising charged density and generate additional energy state in the valence band of the polymers; therefore,

their adsorbed form enables to spread out light absorption region resulting in narrower optical bandgaps than their neutral forms (Fig. 4.51).[267]

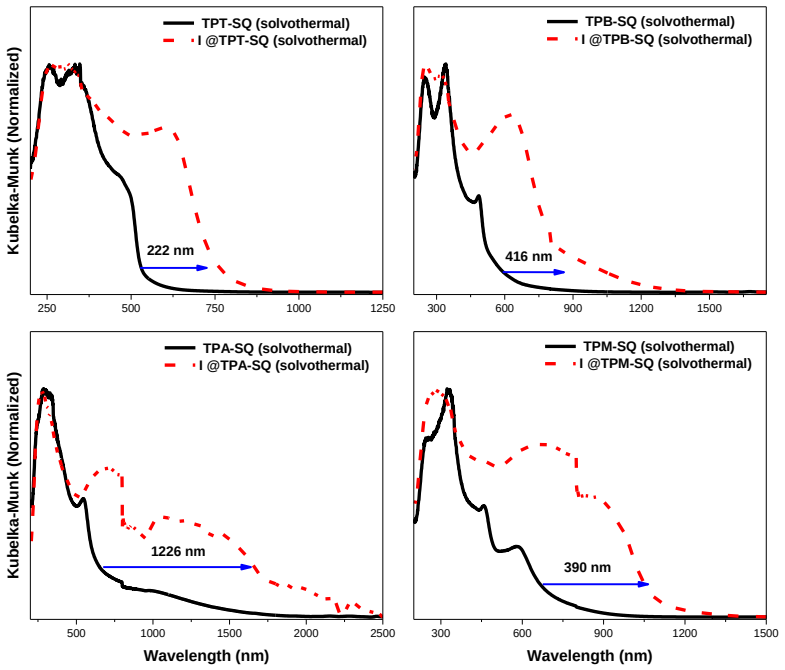

Fig. 4.50 Comparison of diffuse reflectance spectra of SQ-COPs$_{solv}$ (black-solid), iodine-doped (red-dash)

Fluorescence properties of polymers were investigated by using solid-state photoluminescence emission (PLE) spectroscopy and red-shift emission was observed in all polymers revealing different maximum wavelengths. There is no direct correlation between obtained polymers by reflux and solvothermal method. The TPT-SQ$_{reflux}$ polymer exhibited PL spectra comprising two distinct emission bands at around 516 and 630 nm, where the former defines stronger emission intensity (Fig. 4.52). While The TPT-SQ$_{reflux}$ polymer revealed an emission peak at 516 nm with a small shoulder at 630 nm; in the TPT-SQ$_{solv}$ only one maximum emission was seen in the spectrum (Fig. 4.50).

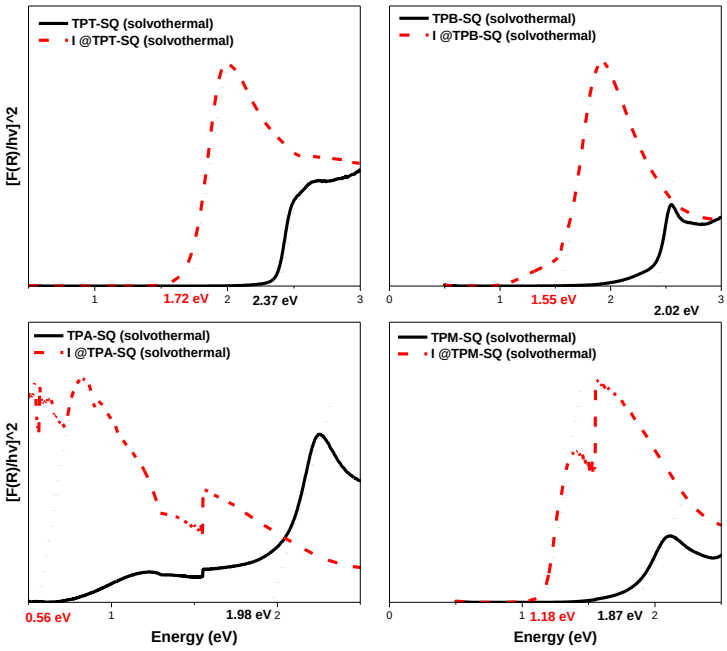

Fig. 4.51 Comparison of estimated band-gaps of SQ-COPs$_{solv}$ (black-solid), iodine-doped form (red-dash) by Tauc plot

On the other hand, TPB-SQ$_{reflux}$ polymer indicated lower emission wavelength (Fig. 4.52) than the one obtained by solvothermal (Fig. 4.53), the TPA-SQ$_{solv}$ and TPM-SQ$_{solv}$ polymers showed higher emission wavelengths (Fig. 4.49) than those synthesized by reflux (Fig. 2.53, Table 2.6). Even though, TPT-SQ$_{reflux}$ polymer revealed two PL spectra that latter indicated low intensity, the emission wavelength is higher than TPB-SQ$_{reflux}$ and they, produced by solvothermal method, are also the same. Thus, it can be understood that the triazine unit on the center of the tritopic linker affects the excited state allowing larger emission wavelengths which can be due to planarity causing a more pronounced π-π stacking. On the contrary, the highest emission wavelength was obtained in TPA-SQ polymers (Fig. 4.54). This might be owing to cross-conjugation on polymer

structure that can lead to occurrence of extra charged form on nitrogen and oxygen elements of the linkers as well as enhancing π-π interaction between molecules.[266]

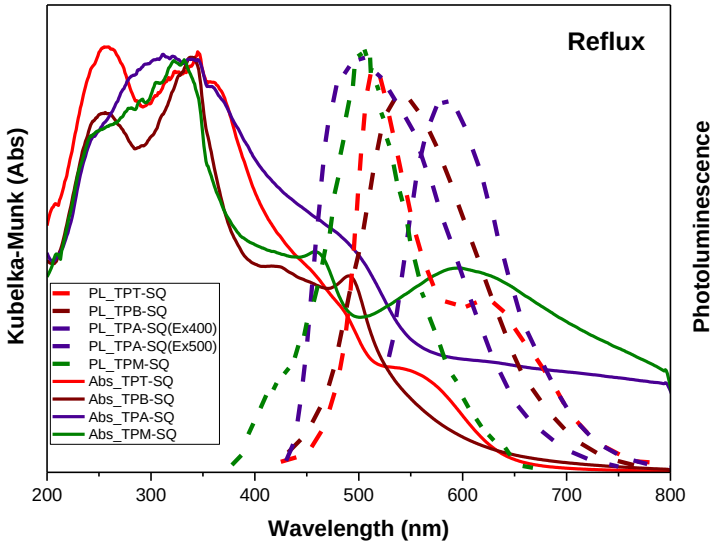

Fig. 4.52 Comparison of kubelka-munk-based diffuse reflectance and photoluminescence spectra of SQ-COPs$_{reflux}$

In addition to this, nonplanarity, high dihedral angle, sp^3 orbital hybridization of the carbon atom causing the lowest rigid structure of triphenylmethane linker, as well as low conjugation, might be the reason why TPM-SQ polymers exhibited the lowest emission wavelength among the other polymers (Fig. 4.54).

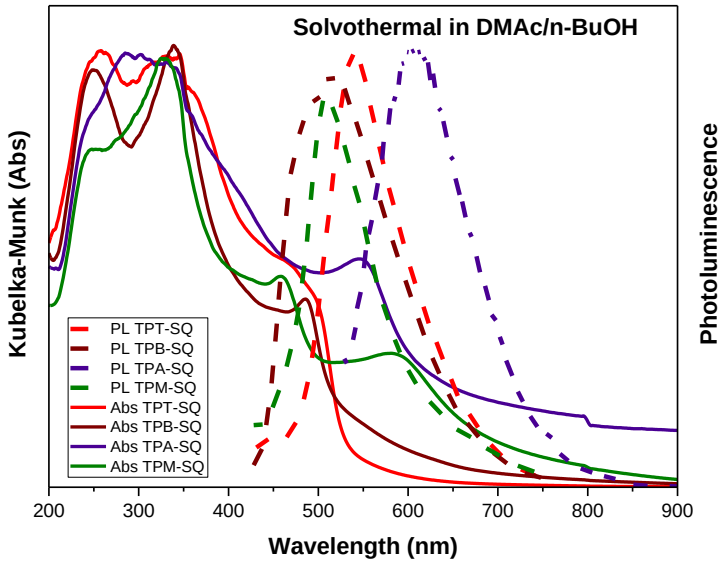

Fig. 4.53 Comparison of kubelka-munk-based diffuse reflectance and photoluminescence spectra of SQ-COPs$_{solv}$

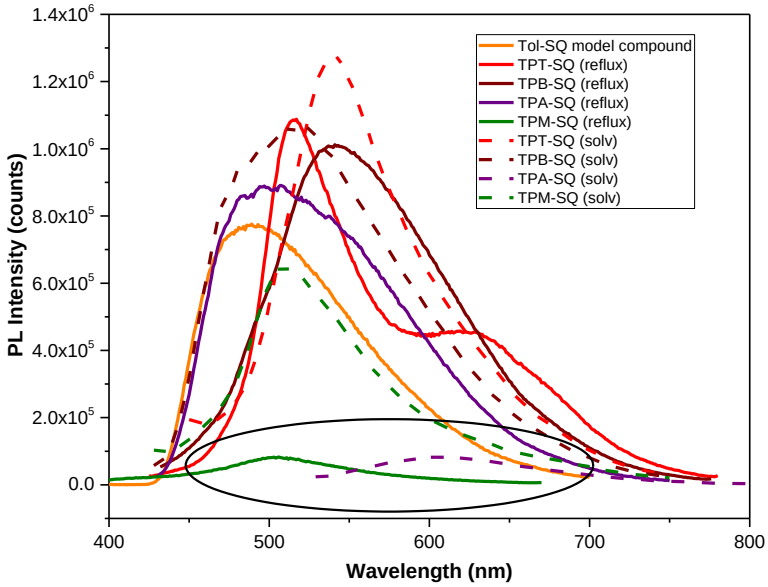

Fig. 4.54 Photoluminescence spectra of SQ-COPs$_{reflux}$ (solid), SQ-COPs$_{solv}$ (dash)

Though the polymers have emission in the large wavelengths, in comparison of polymers and model compound (Table 4.6), it is clearly seen that TPM-SQ_{reflux} and TPA-SQ_{solv} have very low intensity showing that they are not highly fluorescent (Fig. 4.54); yet, most of them exhibited more red-shift emission than the model compound of Tol-SQ (Fig. 4.54). This proves that donor-acceptor construction in extended conjugation of 2D SQ-polymers sizeably influences the emission properties.

Table 4.6 Calculated optical properties of prepared SQ-polymers

Conditions	Polymer	λ_{max} (nm)	λ_{onset} (nm)	λ_{Ex} (nm)	λ_{Em} (nm)	$E_{g(direct)}$ (eV)	$E_{g(direct/I@doped)}$ (eV)
Reflux	Model compound Tol-SQ	400	459	385	490	2.73	-
	TPT-SQ	350, 562	628	400	516, 630	1.98	-
	TPB-SQ	340,492	570	400	544	2.26	-
	TPA-SQ	340	602	400, 500	510, 585	2.14, 0.5	-
	TPM-SQ	330,600	900	350	505	1.37	-
Solvothermal	TPT-SQ	340	530	400	542	2.35	1.72
	TPB-SQ	340,486	532	400	518	2.38	1.55
	TPA-SQ	320,550	686	500	614	2.00, 0.8	0.56
	TPM-SQ	335,460, 584	705	400	511	1.80	1.18

It is clearly seen that donor-acceptor features impacts on the optical properties by obtaining distinct band gaps in polymers (Table 4.6)

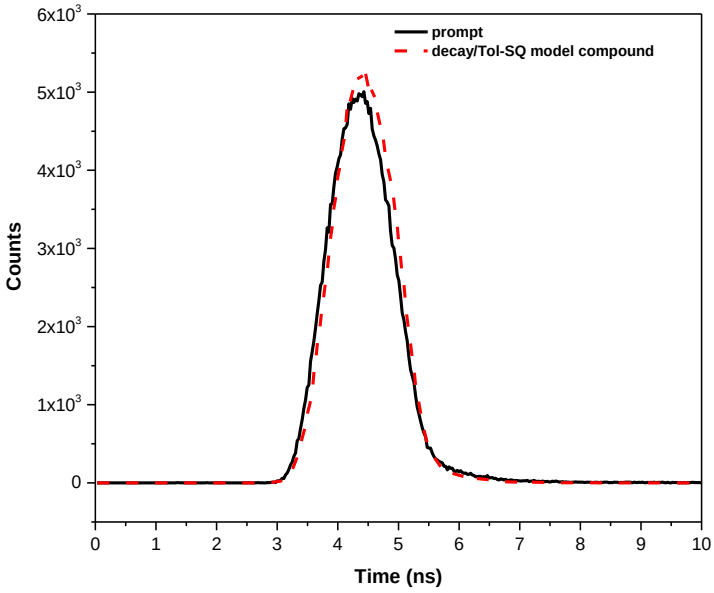

Fig. 4.55 Lifetime profile of the Tol-SQ model compound

Furthermore, time-correlated single photon counting (TCSPC) was carried out in order to calculate estimated lifetimes of prepared polymers and model compounds. The obtained decay curves were fitted with a double-exponential for TPM-SQ_{reflux}, TPM-SQ_{solv} and TPM-SQ_{solv} and triple-exponential function for other polymers. Yet, we could not observe any change between the fitting and prompt curves in Tol-SQ model compound (Fig. 4.55). The reason might be that there is no fluorescence feature owing to lack of conjugation in solid form.

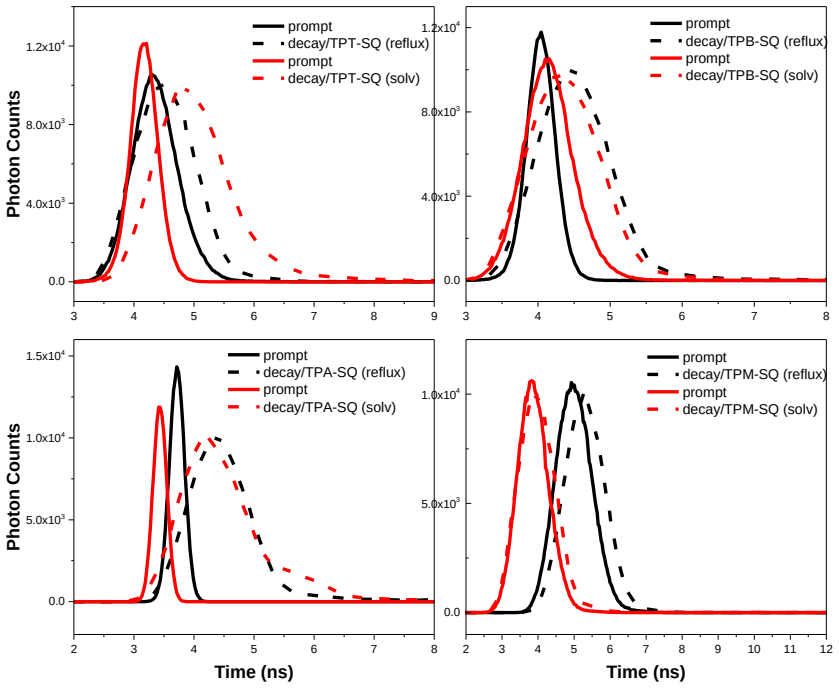

Fig. 4.56 Lifetime profile of the SQ-COPs$_{reflux}$ (black; solid-prompt, dash-decay), SQ-COPs$_{solv}$ (red; solid-prompt, dash-decay)

The longest lifetimes were observed for the TPA-SQ$_{reflux}$, which indicates a long-time decay constant of 7.30 ns (5.65%) (Fig. 4.53, Table 4.7). The additional lifetime constants are 2.31 ns (12.43%) and 0.29 ns (81.93%). The TPT-SQ$_{solv}$ follows this high lifetime with 5.35 ns (2.15%) and additional times are 1.31 ns (10.34 %), 0.45 ns (87.51%). While most of the average life times of polymers obtained by reflux were detected higher than them synthesized by solvothermal, the TPT-SQ$_{solv}$ exhibited approximately three-fold increase in lifetime decay than TPT-SQ$_{reflux.}$ This indicates that regularity causing lower interlayer stacking distance influences the fluorescence features in the material due to π-π interaction of molecules.

Table 4.7 Time-correlated single photon counting data for SQ-polymers

Conditions	Polymer	λem (nm)	τ_1 (ns)	B_1 (%)	τ_2 (ns)	B_2 (%)	τ_3 (ns)	B_3 (%)	τ_{avg} (ns)
Reflux	TPT-SQ	514	0.07	90.91	0.46	8.44	3.48	0.65	0.12
	TPB-SQ	540	0.93	2.33	0.28	93.35	3.29	4.32	0.30
	TPA-SQ	579	2.31	12.43	7.30	5.65	0.29	81.93	0.94
	TPM-SQ	501	0.16	99.67	2.64	0.33	-	-	0.17
Solvothermal	TPT-SQ	539	0.45	87.51	1.31	10.34	5.35	2.15	0.64
	TPB-SQ	519	0.21	97.98	1.95	2.02	-	-	0.25
	TPA-SQ	609	2.02	0	0.23	99.99	7.40	0	0.23
	TPM-SQ	512	0.18	99.19	2.29	0.81	-	-	0.20

These results relevant to large bathochromic-shift and low band gaps indicate that Squaraine units linked with different donor units can delocalize the electrons through the 2D-network frameworks resulting in good light-harvesting and semiconducting features. Hence, we thought that they can be suitable as hole transport layers in perovskite solar cells. For this reason, they are actually under investigation by our collaborators (at CHOSE, University of Rome, Tor Vergata) to test their employment as HTMs in perovskite solar cell.

4.4 Conclusion and Outlook

In summary, as small molecules, the squaraine compounds have demonstrated remarkable optical properties because of their zwitterionic form and their conjugation. Their polymeric constitution has been generally obtained based on one dimensional form and even if they can be effective in desired applications, their extended network can be more effective and essential in optoelectronic applications. For this reason, we have comprehensively investigated how to build these squaraines as 2D layered materials and we found that their 2D form for the first time has been produced for the last 10 years. However, after the first research just few studies have been presented till today and they have been mostly produced based on (metallo)porphyrin units. Hence, we aimed to produce these 2D SQ-polymers by diversifying their knots and, for this purpose, we designed and developed a new class of 2D Squaraine Covalent Organic Polymers bearing trigonal linkers based on donor-acceptor relation (SQ-COPs), which can be suitable for optoelectronic devices, especially solar cells. The linkers were particularly chosen due to containing aromatic electron-donor units leading to donor-acceptor interaction in overall materials. Polymers were synthesised as catalyst-free through condensation between trigonal amino precursors and squaric acid and their structural characterisation was carried out by FT-IR, combustion elemental analysis, ^{13}C-CPMAS (cross polarization magic angle spinning) NMR, ^{15}N-CPMAS NMR, their surface and thermal analysis were performed by P-XRD, nitrogen adsorption-desorption isotherms and TGA analysis. The optical properties of obtained polymers were investigated by Solid-state UV-Vis-NIR diffuse reflectance and photoluminescence spectroscopies. We studied reaction conditions relying on different parameters such as temperature, solvent or solvent mixture, solvent

ratio, and polarity as well as monomer quantities. Different methods like reflux (or thermal) and solvothermal were employed. It can be highlighted that low solubility of squaric acid plays a critical role on reaction completion, yield and structure regularity and it was realized that high polar solvents are more effective in these SQ-polymer synthesis. As known, the trigonal linkers except TAPT are nonplanar, they demonstrated highly amorphous morphologies and the SQ-polymer constructed with TAPT revealed some characteristic peaks in the PXRD pattern indicating that regular formation might take place on the amorphous bulky surface. In this case, we comprehended how important is the selection of the solvent combination because the solubility of linkers and stabilization of the overall bulky structure substantially determine structural order. Moreover, due to their organic nature, these SQ-polymers exhibited very high thermal stabilities.

As regards surface area and morphology, they can indicate lower surface area than porous organic polymers owing to their limited construction possibilities, condensation reaction which results in zigzag form thus leading to disconformity in materials and natural zwitterionic occurrence causing shifting of stacking layers because of electrostatic repulsion. Therefore, we found the BET surface area of TPT-SQ_{reflux} very low. In addition, we carried out iodine adsorption studies to compare surface area of the polymers which were synthesized through different methods such as reflux and solvothermal and the polymers obtained by solvothermal exhibited higher adsorption capacities than refluxed polymers. This shows that a solvothermal method with proper solvent combination can be an effective method in terms of reaching a higher surface area than reflux.

Optical properties of Squaraine compounds can be tuned by incorporation of various organic components. Based on this, polymers were constructed by

triphenyl linkers which contains triazine (TAPT), benzene (TAPB) units and nitrogen (TAPA), carbon (TAPM) elements on the center of linkers and resulted polymers exhibited tunable optical properties. They exhibited redshift emission in comparison with model compounds. Surprisingly, cross-conjugation was observed in TPA-SQ and TPM-SQ polymers causing larger absorption edges than those two polymers. The order of the band gaps of polymers as estimated from the onset wavelength in the diffuse reflectance spectra based on Tauc`s plot and very narrow band gaps were obtained. Apart from iodine doped form, these significant bathochromic shifts and narrow band gaps indicate an extended π-conjugation over the 2D skeletons of the COP. As far as we know there are just few studies based on squaraine-COFs or COPs and there is no result indicating such a narrow band gap characteristic. We believe that these optical features might be suitable for future optoelectronic applications. Moreover, based on these findings, the SQ-COPs can harvest visible photons. Following on from that, the SQ-COPs are actually under investigation by our collaborators (at CHOSE, University of Rome, Tor Vergata) to test their employment as HTMs in perovskite solar cell.

We have realized that incorporation of squaraine units into covalent organic frameworks can be very fruitful in terms of electrical applications due to their unique form. Thus, in the future, we are planning to design novel SQ-polymers altering the linkers. We will create alternative building blocks to construct novel SQ-polymer based on linkage diversity such as imine, or even C=C sp^2. Moreover, in this study, we have discovered that amino-squaraine can be formed through various alternative reaction routes which can be proper for the construction of highly porous crystalline covalent organic frameworks. For instance, squaraine can be obtained by squaric esters instead of its acidic form. Its ester form is highly

soluble and the solubility problem of squaric acid would be figured out. The important thing is while water is released which plays an important role in the occurrence of crystalline form because of increasing reversibility in reaction with squaric acid, with its ester form, alcohol will be released in reaction and nucleophilic reactivity of alcohol is lower than water. In this case, a certain amount of water can be added to the reaction with ester form to solve this problem and then, their electrochemical behaviour can be investigated in case of obtaining highly crystalline covalent organic frameworks.

CHAPTER 5

Thiophene-Based Covalent Organic Frameworks; Synthesis, and Iodine Uptake Studies of Imine-linked 2D Covalent Organic Framework Containing Quinoid Oligothiophene

5.1 Introduction

As mentioned above, covalent organic frameworks have exceptional features such as high surface area, regular structural arrangement, chemical stability, functionality. Even though the first purpose of the development of COFs was relevant to the investigation of enhancement of gas storage capacity and catalysis performance of novel materials, the incorporation of a functional building block in an extended network, linkage diversity makes them convenient and promising candidate materials for the optoelectronic and energy storage applications as well. In this case, creation of novel building blocks incorporated into COFs that are functional and can have extended conjugation leading to wide absorption capability in the UV spectrum, low oxidation potential, and high oxidation stability, is highly desirable in terms of being effective and active materials for electrochemical applications. Therefore, including heteroatoms is essential in building blocks of COFs or 2D polymers and sulfur-containing molecules like thiophene and their derivatives are very appropriate in order to meet those requirements.

After first developed boroxine and boronate ester-linked COFs based on aromatic rings such as benzene and its derivatives, thiophene-containing boronate-linked Porous crystalline COFs were also introduced.[268] As building

blocks, thiophene, bithiophene, thienothiophene and hexahydroxytriphenylene were used. While higher crystallinity was achieved with symmetric bithiophene and thienothiophene, thiophene-based one exhibited lower crystallinity because of rotation of the thiophene ring leading to disorder morphology in COF. Their off white coloured natural forms indicated wide bandgap as insulators. Thiophene is a donating group and its doped form can be conductive due to low oxidation. For this purpose, materials were oxidized with strong oxidizer such as 2,3-dichloro-5,6-dicyano-1,4-benzoquinone (DDQ) and chloranyl causing dark coloured compounds. Optical properties were probed by Ultraviolet-visible-near infrared (UV-Vis-NIR) diffuse reflectance spectroscopy and materials indicated large absorption bands. For instance, the thienothiophene incorporated COF revealed an absorption band centered at 850 nm. These findings suggest that thiophene-based COFs or polymers can be very proper in terms of reaching high charge or electron transfer in electronic applications.

Exploration of imine-linked COFs paved the way for conductive 2D layered materials owing to high conjugation. Therefore, many COFs applications have been presented based on imine-linked bearing thiophene and derivatives. For instance, Prof. Cooper and co-workers produced crystalline covalent organic framework (COF) based on a benzobis (benzo thiophene sulfone) moiety as water splitting catalysts.[269] They obtained also linear polymers as well as COFs using different building blocks and found that crystalline COFs exhibited a much higher activity for photochemical hydrogen evolution than its amorphous or semicrystalline counterparts. The COF was stable under long-term visible light irradiation and demonstrated steady photochemical hydrogen evolution with a sacrificial electron donor for at least 50 hours. High quantum efficiency of fusedsulfone-COF was

reached due to its crystallinity, its strong visible light absorption, and its wettable, hydrophilic 3.2 nm mesopores. These COFs that have high pores make them dye-sensitized, causing further 61% improvement in the hydrogen evolution rate up to 16.3 mmol g^{-1} h^{-1}. The COF also persisted its photocatalytic activity when cast as a thin film onto a support.

Most of the COFs have been produced based on hexagonal or tetragonal geometrical shapes, however, first time new construction named K*agome shape* has been introduced using novel building block 1,1,2,2-tetraphenylethene (4PE) by Prof. Bein and co-workers;[84,270] this new and tetragonal form exhibited better electric and charge transfer than hexagonal one.[271] In their study, benzodithiophene was incorporated into Kagome-shape COF and it was utilized as photoelectrode. Highly oriented COF films were capable of absorbing light in the visible range to produce photoexcited electrons that diffuse to the surface and are transferred to the electrolyte, causing proton reduction and hydrogen evolution. Photoelectrochemical activity of the 2D-COF films and their photocorrosion stability in water proposed a novel class of photo absorber materials with versatile optical and electronic properties that are adjustable by the choosing of proper building blocks and their three-dimensional stacking.

Oligothiophene is a very appropriate conjugated molecule for optoelectronics and energy storage devices. Their usage in linear polymers is highly prevalent and containing of alkyls chain of oligothiophene which is asymmetric and symmetric has been used as building blocks in COFs.[272] While asymmetric building block did not show crystallinity, the symmetric one demonstrate highly crystallinity. Indeed, the alkyl chain in asymmetric building blocks disturbs stacking of the layers resulting in amorphous morphology. In optical studies, first time formation of a

charge transfer state was observed between the COF subunits across the imine bond. In addition, thiophene-based acceptor units, such as 4Hthieno[3,4-c]pyrrole-4,6(5H)-dione (TPD) and thieno[3,4-b]thiophene (TT) was integrated into COF using pyrene unit and obtained tunable optical absorption and emission properties that can be convenient in optoelectronic devices.

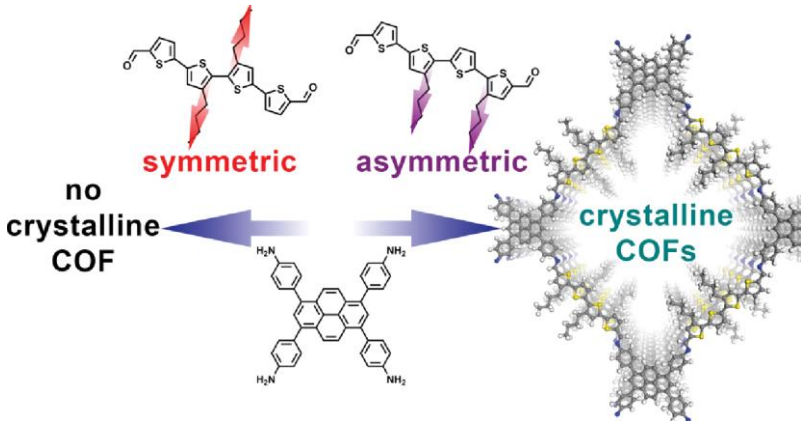

Fig. 5.1 Schematic representation Oligothiophene-Bridged Conjugated Covalent Organic Frameworks[272]

Albeit COFs are generally created based on small molecules, integration of complex building blocks are highly desirable because of large absorption capability and enhancement of charge or electric transfer; yet it is quite challenging due to restriction of construction possibilities and their bulky surface causing disorder morphologies. Nevertheless, in the case of preparing rigid, planar complex linkers as well as knots, it can be possible to obtain porous crystalline frameworks that can be very useful especially for optoelectronic devices. For instance, donor–acceptor-type isoindigo- and thienoisoindigo-based building blocks were incorporated into COFs.[137] These materials were intensely coloured solids with a high degree of long-range order and a pseudo-quadratic pore geometry and they indicated near-

infrared-absorbing resulting in low bandgap. The building blocks were formed by isoindigo molecule linked with different aromatic units such as benzene-benzene, benzene-thiophene or thiophene-thiophene (named Py-PII, Py-pTII and Py-tTII COFs, respectively). Among these COFs the Py-tTII demonstrated red-shift in UV-spectrum in the comparison with other COFs. This is due to steric repulsion from the edge of building blocks bringing about an increase of the planarity thus, boosting π-π interlayer interaction. Thienoisoindigo-COF fullerene heterojunction was employed as the photoactive component, and it was created the first COF-based UV- to NIR-responsive photodetector. It was found that the spectral response of the device is reversibly switchable between blue- and red-sensitive, and green- and NIR-responsive. These outcomes are very promising in terms of electrochemical studies for information technology or spectral imaging.

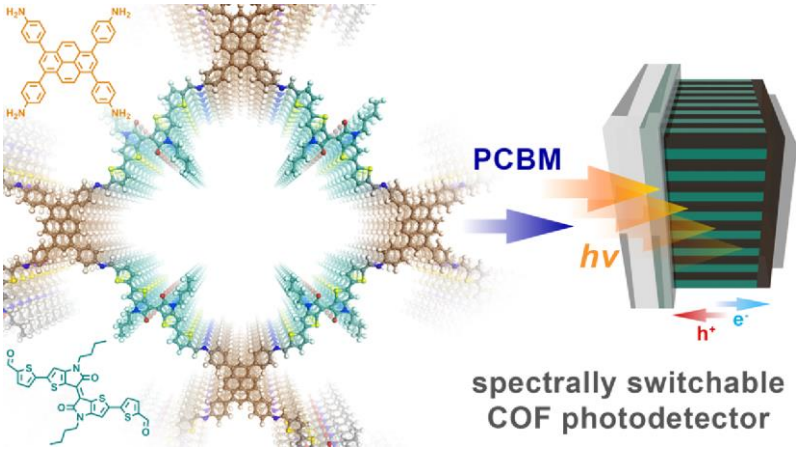

Fig. 5.2 Schematic representation Near-Infrared-Absorbing Covalent Organic Frameworks[137]

In another work, donor–acceptor-type diketopyrrolopyrrole (DPP) and tetraphenylporphyrin (TPP) units were used to build COFs.[273] Integration of such a dye molecule into COF with porphyrin unit enabled to improve absorption edge

reaching 800 nm. Surprisingly, the obtained COF indicated spontaneous aggregation into hollow microtubular assemblies with outer and inner tube diameters of around 300 and 90 nm, respectively. Optical properties of starting compounds, model compound and DPP-TAPP-COF were investigated by diffuse reflectance spectra and the COF showed red-shift absorption obtaining maximum λ=670 nm. It is mentioned that this is due to being rationalized by planarization of the π-system and pronounced aggregation of the individual layers within the COF[53] and because of increasing absorption, DPP-TAPP-COF more efficiently harvested photons in the visible and near-IR region.

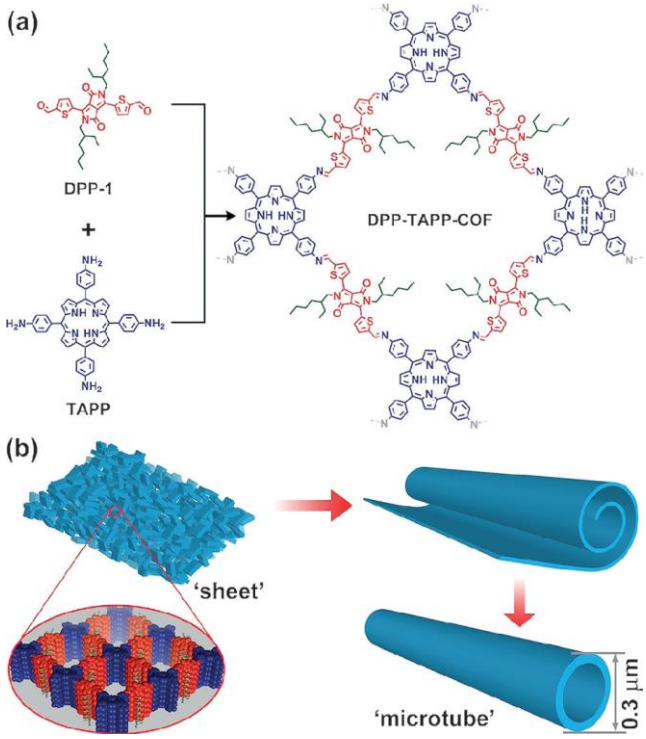

Fig. 5.3 a) Synthesis and b) proposed self-assembly of DPP-TAPPCOF into microtubes.[273]

Integrated stimulus-responsive molecules into COFs can be useful because of additional function and photo-responsive unit of (1,2-bis(5-formyl-2 methylthien-

3-yl)cyclopentene) was used for the construction of COF.[274] It exhibited photo-induced transformations without structural destruction, namely, UV light can switch “ON” the high electrical conductivity and there is also reversibility under UV light like “ON” and “OF”. So, this reversibility could be controlled through a circuit containing a light-emitting diode (LED).

Thiophene-containing COFs have been synthesized based on not only imine or boronate ester but also C=C sp^2 linkage which is highly stable and fully conjugated. In this study, novel bithiophene- and biphenyl-bridged donor–acceptor-containing 2D sp^2-carbon-linked conjugated polymer (2D CCP) were presented.[275] The COF was synthesized through the knoevenagel polymerization between the electron-accepting building block 2,3,8,9,14,15-hexa(4-formylphenyl) diquinoxalino[2,3-a:2′,3′-c]phenazine (HATN-6CHO) and the electron-donating linker 2,2′-([2,2′-bithiophene]-5,5′-diyl)diacetonitrile (ThDAN) and 2,2'-([1,1'-biphenyl]-4,4'-diyl)diacetonitrile. In the comparison with, biphenyl-bridged 2D CCP-HATN-BDAN (2D CCP-BD), the bithiophene-based 2D CCP-Th showed a wide light-harvesting range (up to 674 nm), an optical energy gap (2.04 eV), and 2D CCP-Th exhibited a good H_2-evolution photocurrent density up to ≈7.9 μA cm^{-2} at 0 V versus reversible hydrogen electrode.

Apart from electrochemical applications, thiophene-based COFs or polymers demonstrate high iodine uptake capacity as well due to including active sites (sulfur groups, aromatic units, conjugation and imine-linkage etc.), high surface area and micro-spherical morphologies.[188] For instance, conjugated microporous polymers bearing thiophene-moieties (SCMP-COOH@1-3) was produced by a homo-coupling polymerization reaction.[276] Then the SCMP-COOH@1-3 were directly pyrolyzed without any templates to obtain the porous carbon networks, named as

SCMP-600@1,2 and 3. SCMP-600@1-3 indicated BET surface area of 362–642 m^2 g^{-1}, have a permanent porous structure and plenty of sulfur and oxygen units in the structures as effective sorption sites, and demonstrated an absorption performance for iodine vapour with an uptake up to 204 wt%. To increase the active sorption sites, S-rich linker benzo[1,2-b:3,4-b':5,6-b'']trithiophene-2,5,8-tricarbaldehyde (BTT) and N-rich linker 1,3,5-tris-(4-aminophenyl) triazine (TAPT) as building blocks to obtain a COF adsorbent (BTT-TAPT-COF), bearing abundant S and N active sites and extended π-conjugation with inherent microporosity. It indicated high crystallinity, large surface area, and thermal stability.[277] It exhibited rapid reversible volatile iodine uptake with an adsorption capacity of 276 wt% because of the high surface area, including of electron-rich heteroatoms and the extended π-conjugated system. After five cycles, BTT-TAPT-COF almost retained the same iodine adsorption capacity with the original adsorbent. More Recently, porous organic polymers composed by 4,4',4'',4'''-(ethene-1,1,2,2-tetrayl) tetraaniline (ETT) and thiophene moieties such as thiophene (TTDP-1), thienothiophene (TTDP-2) and dithienothiopene (TTDP-3) were introduced to aim at using as adsorbents in iodine capture and Iodine adsorption capacities showed differences according to the porosity of the COF which is owing to flexibly tuning the stacking degree and number of sulfur contents. The adsorption capacities of TTDP-1, TTDP-2, and TTDP-3 was measured as 536, 470, and 425 wt%, respectively.[278]

Throughout the present study, we designed and synthesized a linear building block which composes thiophene and its quinoid form to use as a linker in covalent organic framework. One of the crucial aims in conjugating polymers is to obtain a small bandgap leading to conductivity that can be proper for electrochemical

applications. Semiconducting polymers with quinoidal building blocks demonstrated high conductive properties. Quinoid unit is the oxidative state form of the heteroaromatic or aromatic units and exhibits different bond length alternations that break the aromaticity, decreasing the highest occupied molecular orbital (HOMO)–lowest unoccupied molecular orbital (LUMO) gaps that potentially empower injections of both electrons and holes.[279] There are several linear conductive polymer examples related to including quinoid segments[280,281] yet, there are not various studies about two-dimensional conjugated semiconducting polymers.

These quinoid thiophene-based oligomers are one of the model compounds of small bandgap polymers[282] and exhibited optical absorption maximum (λmax) of 470. Prof. Jenekhe firstly suggested one of the possible synthetic approaches to obtain small bandgap polymers to prepare poly(heteroarylene methines) which directly incorporate quinoid moieties in the polymer backbone. [280,283] This class of polymers has been theoretically predicted to have bandgap values around 1 eV.[284] There are various recognized conjugated quinoid compounds which have been reported in the literature [282,285,286,287,288] and some of them are shown in Fig. 5.4

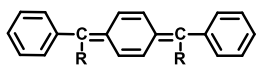

1a. R=H

1b. R=Ph

1c. R=CN

1d. R=COOR

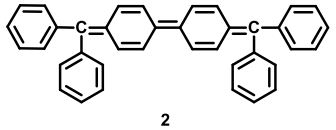

2

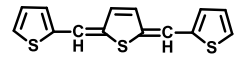

3

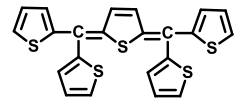

4

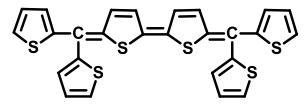

5

((λmax) 2,3,4,5 = 574, 433, 472, 580)

Fig. 5.4 Schematic representation of conjugated quinoid compounds

These compounds are generally highly coloured due to their λ-electron delocalized structures. Two of the most eminent compounds are Thiele hydrocarbon (Fig.5.4-1b) and Chichibabin hydrocarbon (2). These two compounds are highly colored (orange for 1 b and blue-violet for 2), however both compounds are oxygen sensitive. Fernandez et. al presented for the first time the synthesis of 1,4-bis(phenylmethylene)-2,5- cyclohexadiene (Fig. 5.4-1a).[288] Yet others could not be successful to obtain these structures. The high reactivity of the quinoid segment may clarify the failure of these attempts. It has been mentioned that the stability of 1a can be raised sterically or electronically by substitution with a phenyl group or cyano group at the methine bridge.[282,286,287,288] This idea has been verified to be successful. For instance, compounds 1c and 1d are stable to oxygen and compound 1c is also highly stable to moisture and does not easily homopolymerize. In Fig. 3.4, the monomers 3, 4, and 5 have obtained by Hanack et al. with thiophene, pyyrole, or isothianaphthene.[287] These compounds have a high planarity and good λ-electron delocalization (λ_{max} = 400-580 nm). Although the monomer 3 (Fig. 5.4) is unstable in air, 4 (Fig. 5.4) is more stable because of steric hindrance of the substitution of the thiophene ring at the methine carbon and so this boosts the stability. Chen and Jenekhe presented three new different quinoid thiophene oligomers in addition to those examples.[280] Quinoid structures are formed thiophene (6), bithiophene (7) and terthiophene (7) units (Fig. 5.5) and there is phenyl ring on methine bridge.

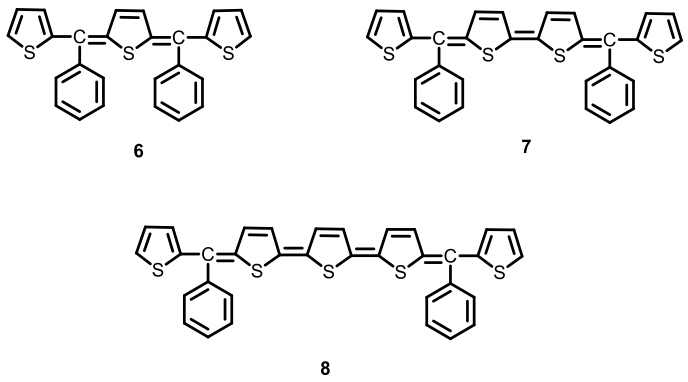

Fig. 5.5 Schematic representation Quinoid oligothiophene compounds

Having in mind these structural models, we aimed to design new building blocks incorporated into 2D covalent organic polymer that can show different electrochemical properties such as donor-acceptor role due to having different moieties in methine bridge of the molecules such as donor phenyl group or acceptor cyano group.

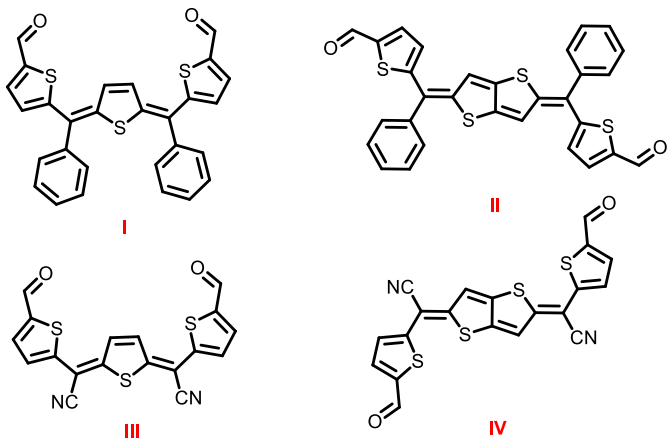

Fig. 5.6 Schematic representation of new quinoid oligothiophene compounds containing formyl group

These four linear ditopic linkers including two functional groups are composed of a quinoid of thiophene or thienothiophene in the center of the molecule and

thiophene bearing formyl group in the methine bridge. Their reaction with tris(4-aminophenyl)benzene (TAPB) give 2D hexagonal polymers that can have different electrochemical properties with different linear building blocks and exhibit satisfied iodine adsorption capacities because of high sulfur and aromatic contents, active sites such as imine linkage and alkene groups.

5.2 Materials and Methods

All chemicals, reagents and solvents were purchased from commercial suppliers, and used without further purification. The reaction of linkers and building blocks were monitored by thin-layer chromatography (TLC) performed on silica gel TLC-PET foils GF 254, particle size 25 mm, medium pore diameter 60 Å. Vibrational IR spectra were collected in transmission mode using a Thermo Scientific Nicolet 6700 spectrometer. The ^{1}H and ^{13}C NMR spectra were recorded on a JEOL Resonance 600 (^{1}H NMR operating frequency 600 MHz) at 298 K or Bruker Avance 200 spectrometer at 200 MHz. Small molecules of UV/Vis absorption spectra were measured with a double-beam Perkin–Elmer Lambda 20 UV/Vis spectrophotometer equipped with a 1-cm quartz cell. Mass spectra were recorded using an LCQ Advantage MAX Ion Trap Spectrometer (Thermo Fisher Scientific, Dreieich, Germany) equipped with an electrospray ion source. Elemental analysis was performed using a Thermo Nicolet FlashEA 1112 Series. Powder X-ray diffraction (PXRD) patterns were taken with a Panalytical X'Pert PRO MPD diffractometer equipped with a CuKα source operating in reflectance Bragg-Brentano geometry employing Ni filtered Cu Kα line focused radiation at 1600 W (45 kV, 40 mA) power. A Micromeritics ASAP 2020 apparatus was used to measure both N_2 and CO_2 adsorption isotherms at 273 K on Carbon. SEM measurements

were performed using FESEM TESCAN S9000G microscope (Microanalysis; OXFORD Detector Ultim Max Software AZTECT) equipped with Schottky source (Resolution: 0.7 nm AT 15keV in beam mode, Mode: Analysis Samples have been sputtered with 20 nm of gold). Thermogravimetric analysis (TGA) data was recorded with a TA instruments Q600 thermobalance in dry N_2 flow (100 mL/min) with a ramp of 10°C/min from 30 to 800°C. Polymers were analysed by solid state UV/Vis measurements on Cary 5000 UV-Vis-NIR spectrometer from Agilent.

5.2.1 Experimental

5.2.1.1 Synthesis of Poly(EDOT)methine

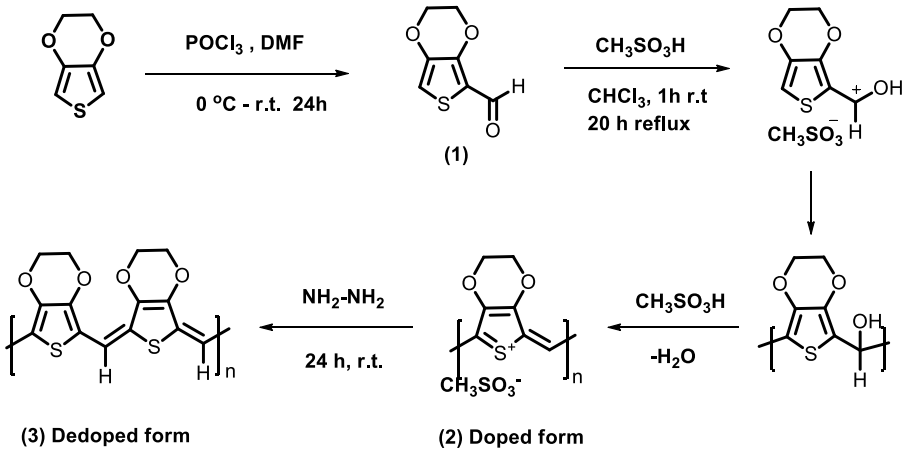

Fig. 5.7 Schematic representation of poly(EDOT)methine

(1):[289] To 3,4-Ethylenedioxythiophene (1.33 g, 9.36 mmol) dissolved in dry DMF (9ml) at -10 °C, $POCl_3$ (0.9 mL, 9.64 mmol) was added dropwise in ice bath. The mixture stirred 1 h at -10 °C, ice water (20 mL) was added and the mixture stirred overnight at room temperature. The aldehyde was filtered off, dissolved in CH_2Cl_2 and dried (Na_2SO_4). The CH_2Cl_2 filtrate was eluted through a short silica "plug" to

remove coloured impurities, (white to slightly tanned crystals, %75). ^{1}H NMR (200 MHz, $CDCl_3$) δ: (ppm) δ 9.91 (s, 1H), 6.80 (s, 1H), 4.37 (m, 2H), 4.28 (m, 2H).

(2): To a stirred solution of EDOT-2-carbaldehyde (250 mg, 1.47 mmol) in $CHCl_3$ (25 ml) at room temperature, methanesulfonic acid (0.1 ml, 150 mg, 1.56 mmol) was added under argon atmosphere. After stirring at room temperature for 1 h, the solution mixture was refluxed overnight 20 h. (The black precipitate, %82).

(3): Doped polymer was dedoped with hydrazine-hydrate (2 ml) in Ethanol solution under argon at 3 h and then washed with ethanol and water, and dried in vacuum to afford 110 mg product (Black precipitate) Anal. calcd for (3) [H–(C7H5O2S-0.75H2O)40–CH=NNH2]: C, 50.20; H, 3.97; N, 0.42; S, 19.14. Found: C, 47.98; H, 3.05; N, 0.74; S, 19.05.

5.2.1.2 Synthesis of Tris(4-(Thien-2-yl)Phenyl)Amine (TTPA)

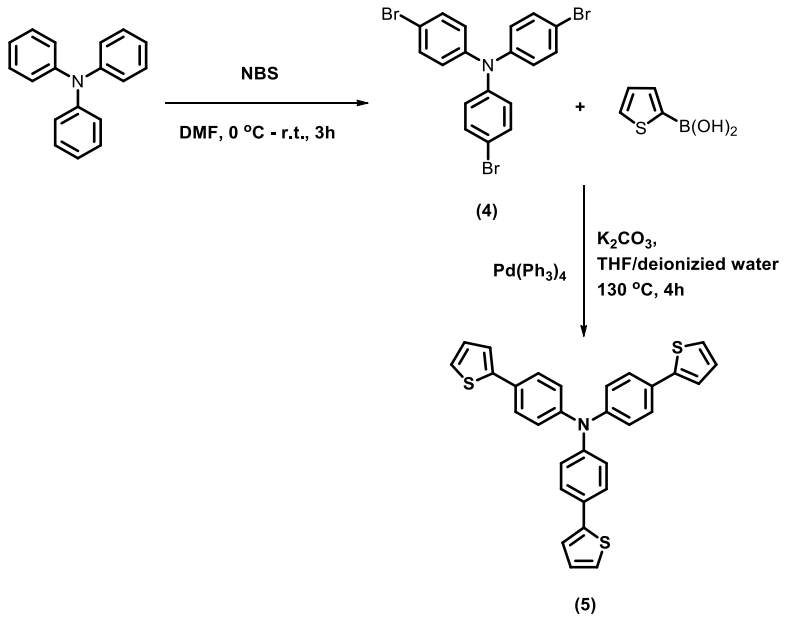

Fig. 5.8 Schematic representation of TTPA

(4): To a solution of triphenylamine in DMF (50 ml) at 0 ^{o}C, NBS (5.34 g, 30 mmol) in DMF (15 ml) was dropwise added. The mixture was stirred for 3h at room temp then ice water was added to the mixture to produce a white precipitate. After filtration and drying, the obtained white solid was recrystallized from petroleum ether to afford tris(4-bromophenyl) amine. (white solid to light purple, %92). 1H-NMR (200 MHz, CDCl3,): δ 7.36-7.34 (d, 6H), 6.93–6.91 (d, 6H).

(5): Thiophen-2-boronic acid (1.02 g, 8 mmol) was mixed with Tris(4-bromophenyl)amine (0.63 g, 1.03 mmol) and K2CO3 in THF/deionized water in a 100 ml two neck round bottom flask. Pd(PPh3)4 was added to the stirred suspension, which was then heated rapidly under argon atmosphere. After cooling to room temp. Deionized water (50-100 ml) was added to precipitate the main part of the product and then the mixture was washed by water and extracted with dichloromethane consecutively. The product was then dried with Na_2SO_4 and purified on biotage column chromatography using petroleum ether - CH2Cl2 5:1 as eluent to obtain the final product as a light yellow powder (%80 yield). 1H NMR (200 MHz, CDCl3) δ 7.62 (d, J = 8.6 Hz, 6H), 7.53 (m, 3H)-7.42 (m, 3H), 7.14-7.12 (m, 6H), 7.10-7.08 (m, 3H).

5.2.1.3 Synthesis of methine-linked 2D covalent organic polymer containing quinoidal moieties

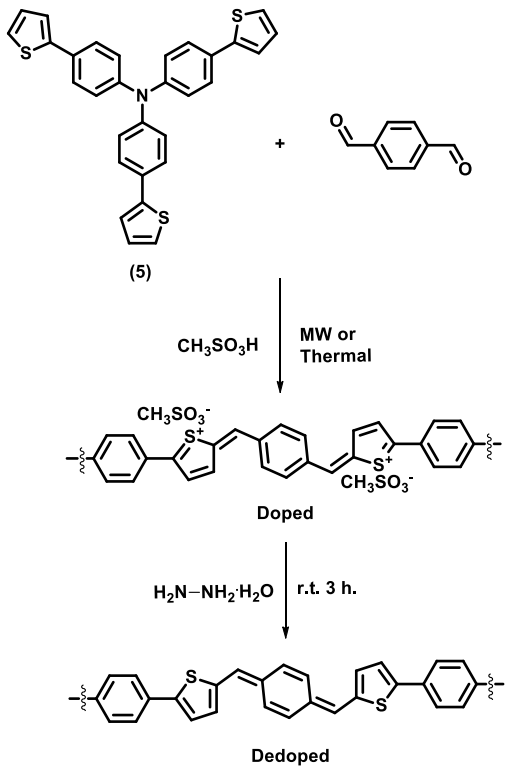

Fig. 5.9 Schematic representation of methine-bridged TTPAQ covalent organic polymer

Doped: Starting compounds (5) and terephthaldehyde were put inside a 5 ml glass microwave tube and kept in a vacuum oven for 30 min then solvent was added as well as acid catalyst and sealed under nitrogen. This mixture was heated in an oil bath with stirring for 3 days in thermal condition, for 40 min. in a biotage microwave reactor. After the reaction ended, it was filtered, and washed with chloroform thoroughly. (black powder).

Dedoped: The doped form was reduced to dedoped form to be turned to quinoid-architecture using 2 ml hydrazine-hydrate (NH2-NH2.H2O) in ethanol (brown powder)

Table 5.1 Synthetic conditions for construction of methine-bridged TTPAQ COP

Entry	TPAT (mg, mmol)	Aldehyde (mg, mmol)	CH_3SO_3H (mmol, eqv.)	React. Condt.	Solvent	Temp.	Time	Product amount
1	20, 0.04	11, 0.08	1.54, 20	MW	$CHCl_3$ (1.5 ml)	90 °C	40 min	43 mg
2	20, 0.04	11, 0.08	0.8, 10	MW	$CHCl_3$ (1.5 ml)	90 °C	40 min	42 mg
3	20, 0.04	11, 0.08	0.38, 2.5	MW	$CHCl_3$ (1.5 ml)	90 °C	40 min	33 mg*
4	20, 0.04	11, 0.08	0.8, 10	MW	Diox. (1.5 ml)	90 °C	40 min	49 mg
5	20, 0.04	11, 0.08	0.8, 10	Therm.	$CHCl_3$ (5 ml)	90 °C	3 days	25.6 mg
6	20, 0.04	11, 0.08	0.8, 10	Therm.	Diox. (5 ml)	120 °C	3 days	23 mg

*MW; biotage microwave reactor, Therm.; Thermal, React. Condt.; reaction conditions, Diox.; Dioxane, Temp.; Temperature. * : starting compounds were observed.

5.2.1.4 Synthesis of linear building blocks of quinoid-oligothiophene

Synthesis of 5,5'-((1E,1'E)-thiophene-2,5 diylidenebis (phenyl methanylylidene))bis(thiophene-2-carbaldehyde);

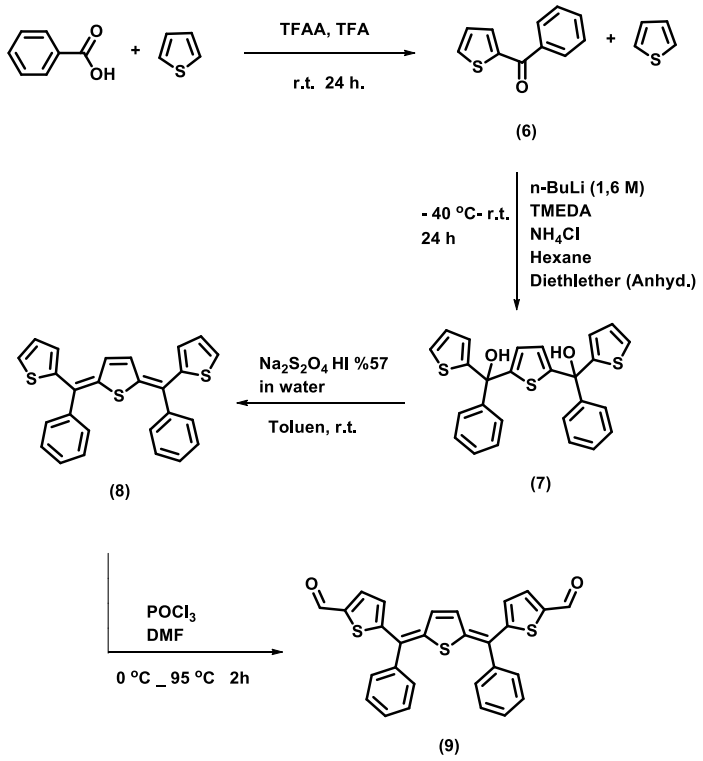

Fig. 5.10 Schematic representation of thiophene-based quinoid-oligothiophene containing phenyl ring on methine bridge

(6): 100 ml one neck flask was charged with benzoic acid (4.14 g, 34 mmol) thiophene (16.2 g, 50.96 mmol) TFAA (16 ml) and TFA (10.8 ml). The reaction mixture was stirred at room temperature for 24 h and monitored by TLC. Solution colour was straw-colour after 1 hour later the colour was turned dark blue-green. Upon completion, the excess of TFAA and TFA was distilled, extracted with DCM, dried in Na_2SO_4 after removed the solvent the residue was recrystallized from petroleum ether (4.6 g, %72) ^{1}H NMR (200 MHz, DMSO-d6) δ: (ppm) 8.08 – 8.03

(m, 1H), 7.80 – 7.72 (m, 2H), 7.68 – 7.63 GC-MS: m/z = 188 $[M + H]^+$. (m, 1H), 7.63 – 7.56 (m, 1H), 7.55 – 7.45 (m, 2H), 7.25 – 7.19 (m, 1H).

(7): Anhydrous hexane was added to a 50 mL two-necked, round-bottomed flask under argon protection then tetramethylethylenediamine (TMEDA) (1.55 mg, 13.33 mmol, 2 ml), thiophene (0.45 g, 5.4 mmol), and n-butyllithium (8 ml, 13.20 mmol) were added to the stirred solution at room temperature. The reaction mixture was refluxed for 1 h and then cooled to -40_^{0}C. The solution of phenyl thienyl ketone (6) in anhydrous diethyl ether was added dropwise to the reaction mixture. Then, the mixture was warmed up to room temperature and stirred overnight. After the reaction was quenched with 1 M NH_4Claq. (20 mL), the organic layer was extracted with chloroform and ethyl acetate. The combined organic layer was dried over Na_2SO_4 and the solvent was evaporated. (It was used without purification for next step)

(8): After drying under vacuum, the obtained crude alcohol product (7) was dissolved in toluene and a solution of $Na_2S_2O_4$ and 57% HI in distilled water (50 mL) was added. The two-phase system was vigorously stirred at room temperature for 24 h. An orange coloured reaction mixture was neutralized with $NaHCO_3$ and extracted several times with diethyl ether. The combined organic layer was dried over Na_2SO_4. After evaporation of the solvent, the product was chromatographed on a silica gel (dichloromethane : PE - 1 : 5), (0.316 g, 45 %) 1H NMR (200 MHz, DMSO-d6) δ: (ppm) 7.63 (dd, J = 5.0, 1.1 Hz, 2H), 7.48 – 7.32 (m, 6H), 7.32 – 7.16 (m, 4H), 7.09 (dd, J = 5.0, 3.8 Hz, 2H), 6.94 (dd, J = 3.8, 1.1 Hz, 2H), 6.36 (s, 2H), UV-Vis: λmax (THF) = 470 nm, FT-IR (cm-1): 3098, 3059, 3019, 1599, 1540, 1481, 1488, 1436, 1141, 1076, 1023, 807, 749, 690

(9): $POCl_3$ (1.64 g, 10.73 mmol, 1 ml) was added dropwise into a solution of compound (8) in DMF (1.2 ml) in a flamed-dried reaction flask at 0 °C. During the addition, the temperature was kept below 10 °C, after which the mixture was stirred for 30 min at r.t. before being heated at 90–95 °C for 90 min. After cooling down, the mixture was poured into crushed ice (50 mL), and made weakly alkaline with a NaOH solution (1 M). After partitioning between CH_2Cl_2 and water, the organic layer was dried over Na_2SO_4. The solvent was removed under vacuum and isomers took place. The isomers were chromatographed (PE:DCM – 1:6) to obtain stable one isomer (9) (0,1 g, 61%) 1H NMR (200 MHz, DMSO-d6) δ: (ppm) 9.86 (s, 2H), 7.96 (d, J = 4.3 Hz, 2H), 7.48 – 7.37 (m, 6H), 7.28 (dd, J = 6.5, 2.8 Hz, 4H), 7.10 (d, J = 4.1 Hz, 2H), 6.51 (s, 2H), LC-MS: m/z = 482,04 $[M + H]^+$ UV-Vis: λmax (THF) = 523 nm, FT-IR (cm-1): 3070, 2824, 1650, 1499, 1406, 1220, 1132, 1038, 796, 750, 698, 664, 617

***** Isomers were transformed into one stable one under vacuum oven at 100 °C for one night (91%)

Synthesis of 5,5'-thieno[3,2-b]thiophene-2,5 diylidenebis (phenyl methanylylidene))bis(thiophene-2-carbaldehyde):

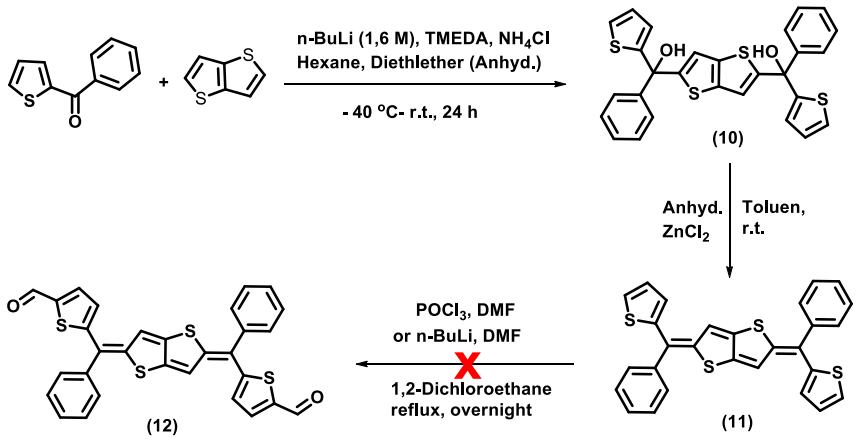

Fig. 3.11 Schematic representation of thienothiophene-based quinoid-oligothiophene containing phenyl ring on methine bridge

(10): To a solution of Thieno[3,2-b]thiophene (0.7 g, 5 mmol), tetramethylethylenediamine (TMEDA, 2 ml, 1.55 mmol) in anhydrous diethylether (50 mL) was slowly added n-BuLi (2.5 M, 5 mL, 54 mmol) at −40 °C. After the mixture was stirred at room temperature for 2 h, it cooled −40 °C again and Phenyl(thiophen-2-yl)methanone (2.1 g, 11.7 mmol) was slowly added in anhydrous ether solution. The mixture was allowed to gradually warm to room temperature and stirred overnight. After the addition of a saturated aqueous solution of NH_4Cl, the mixture was extracted with CH_2Cl_2. The combined organic layer was washed with brine and dried over Na_2SO_4. The crude product was suspended with a small amount of $CHCl_3$, and the insoluble solid was collected by filtration to give (10) (1.49 g, 58%) as an off- white solid. 1H-NMR (600 MHz, DMSO-d6) δ: (ppm) 7.42-7.37 (m, 3H), 7.24 (q, J = 5.3 Hz, 3H), 7.13 (s, 1H), 6.95 (s, 1H), 6.89 (dd, J = 5.1, 3.6 Hz, 1H), 6.78 (dd, J = 3.6, 1.3 Hz, 1H)

(11): To the dried 20 ml microwave vial, (10) (0.2 g, 0.39 mmol) was added and suspended in anhydrous toluene (8 ml) and degassed with argon then anhydrous $ZnCl_2$ (0.29 mg, 1.55 mmol) was added. The tube was sealed, purged argon to remove air and stirred one day at room temperature. The dark purple clear solution was filtered to remove Zn residuals and filtrate was evaporated to dryness. The residue was purified by column chromatography (silica gel, Hexane:DCM = 3:1), dark purple powder with isomers (0.12 g, 67%). 1H-NMR (600 MHz, $CDCl_3$) δ: (ppm) 7.44-7.27 (m, 13H), 7.14 (t, J = 2.7 Hz, 1H), 7.02 – 6.97 (m, 4H), 6.93 – 6.91 (m, 1H), 6.89 – 6.84 (m, 1H), 6.31 (s, 1H), 6.18 (d, J = 1.5 Hz, 1H)

(12): Final product of quinoid oligothiophene based thienothiophene was tried to synthesize according to Vilsmeier–Haack reaction or using n-BuLi in DMF in different conditions, however, it could not be obtained. Starting compound was observed or polymerisation occurred.

Synthesis of 2,2'-(thiophene-2,5-diylidene)bis(2-(5-formylthiophen-2-yl)acetonitrile):

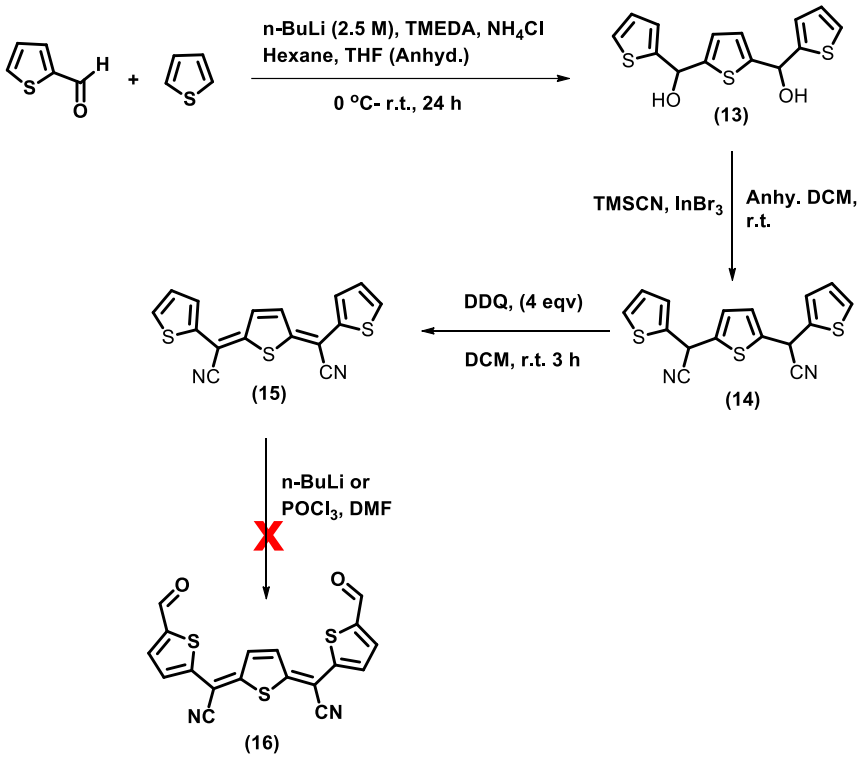

Fig. 3.12 Schematic representation of thiophene-based quinoid-oligothiophene containing phenyl ring on methine bridge

(13): To a solution of Thiophene (0.55 g, 0.52 ml, 5 mmol), tetramethylethylenediamine (TMEDA, 2.5 ml, 1.94 mmol) in anhydrous Hexane (25 mL) was slowly added n-BuLi (2.5 M, 7 mL, 75.6 mmol) at −40 °C. After the mixture

was refluxed for 1h, it cooled −40 °C again and 2-thiophenecarboxaldehyde (1.8 g, 1.5 ml, 16 mmol) was slowly added in anhydrous THF solution. The mixture was allowed to gradually warm to room temperature and stirred overnight. After the addition of a saturated aqueous solution of NH_4Cl, the mixture was extracted with CH_2Cl_2. The combined organic layer was washed with brine and dried over Na_2SO_4. The crude product was suspended with a small amount of $CHCl_3$, and the insoluble solid was collected by filtration to give (3) (1.49 g, 55%) as an off-white solid. ^{1}H-NMR (600 MHz, CDCl3) δ: (ppm) 7.29 (dd, J = 5.0, 1.4 Hz, 1H), 6.97 – 6.85 (m, 2H), 6.76 (s, 1H), 6.20 (d, J = 4.0 Hz, 1H), 5.34 (d, J = 4.3 Hz, 1H)

(14): A solution of the alcohol 12 (0.1 g, 0.32 mmol) in anhydrous dichloromethane is added slowly to a solution of InBr3 (0.022 g, 0.064 mmol) and trimethylsilyl cyanide (0.13 g, 1.28 mmol) in anhydrous dichloromethane at room temperature under an atmosphere of argon. The reaction was monitored by TLC. After complete conversion the solvent was removed carefully under reduced pressure and the crude product was purified by flash column chromatography on silica gel (PE/DCM = 5:1) to get product (13) as a red solid (0.625 g, 60%). ^{1}H-NMR (600 MHz, $CDCl_3$) δ: (ppm) 7.31 – 7.25 (m, 1H), 7.11 – 7.08 (m, 1H), 7.02 – 6.99 (m, 1H), 6.98 – 6.91 (m, 1H), 5.50 (s, 1H)

(15): To the mixture of 13 (0.11 g, 0.34 mmol) and 2,3-dichloro-5,6-dicyano-1,4-benzoquinone (DDQ) (0.16 g, 0.69 mmol) was added degassed anhydrous DCM (20 mL) in an argon atmosphere. The orange solution turned into a brown solution. The resulting solution was stirred at room temperature for 3 h and controlled by TLC. After completion of reaction, triethylamine (TEA, 0.5 mL) was added to quench the reaction. The solvent was removed under vacuum and the residue was purified by chromatography (TEA deactivated silica gel, hexanes/EtOAc 3:1 as eluent) to

give the fully conjugated product (14) as a dark red-purple powder containing isomers (55 mg, 50%). ^{1}H-NMR (600 MHz, $CDCl_3$) δ: (ppm) 7.31 – 7.25 (m, 1H), 7.11 – 7.08 (m, 1H), 7.02 – 6.99 (m, 1H), 6.98 – 6.91 (m, 1H), 5.50 (s, 1H)

(16): Final product of quinoid oligothiophene containing cyano group was tried to synthesize according to Vilsmeier–Haack reaction or using n-BuLi in DMF in different conditions, however, it could not be obtained. Starting compound was observed or decomposed.

Synthesis of model compound; (N,N'E,N,N'E)-N,N'-((5,5'-((1E,1'E)-thiophene-2,5 diylidenebis (phenyl methanylylidene))bis(thiophene-5,2-diyl))bis(methanylylidene))bis(4-methylaniline) [Tol-QOT]:

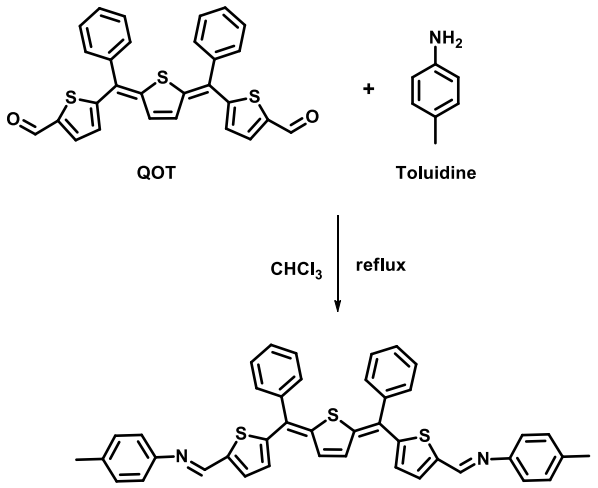

Fig. 3.13 Schematic representation of model compound; Tol-QOT

QOT (40 mg, 0.08 mmol) and toluidine (9.76 mg, 0.09 mmol) were dissolved in chloroform (10 mL). The mixture was refluxed for 24 h. After cooling to room temperature, solvent was evaporated under vacuum, purified by flash chromatography using hexane/DCM 1:2, yield: 36.9 mg (70%).

5.2.1.5 Synthesis of quinoid oligothiophene-containing 2D covalent organic polymer (TPB-QOT COP)

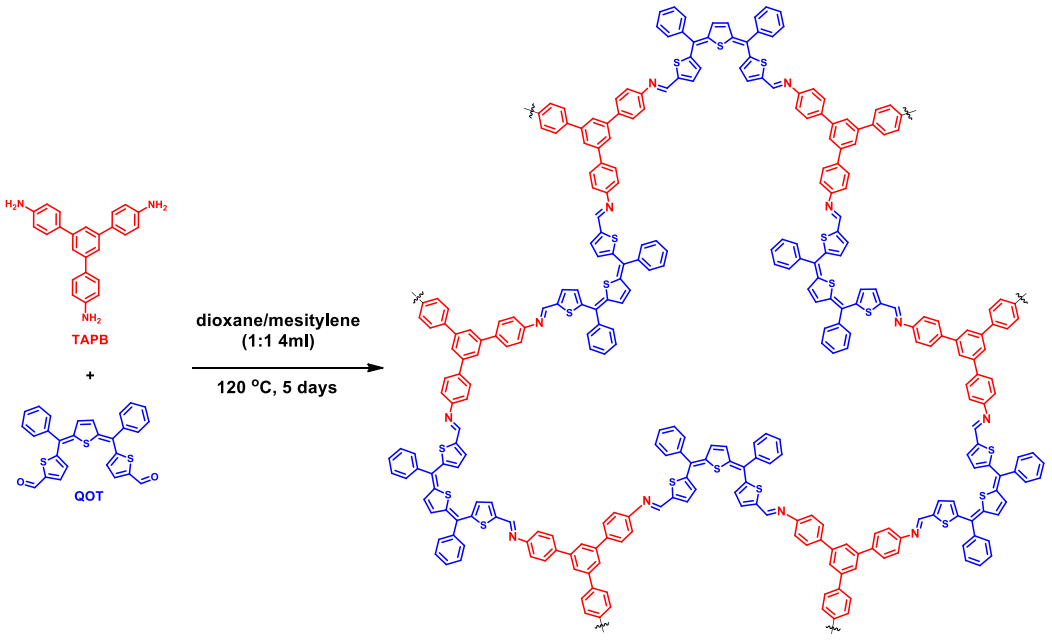

Fig. 5.14 Schematic representation of TAPB-QOT covalent organic framework

To a pre-dried biotage microwave vial, TAPB and QOT were added and the vial was sealed off. The air was evacuated by argon using a needle from the sealed vial. Solvent mixtures (dioxane/mesitylene, 4 mL, 1/1 in vol.) were added via syringe (solvents were degassed by three freeze-pump-thaw cycles before using). Suspended solution was degassed by three freeze-pump-thaw cycles for 3 times. Monomers were dissolved via sonication and then 6M CH3COOH (0.1 ml) was added. The vial was sealed off and heated in an oil bath or in an oven at a certain time for 5 days without stirring. The precipitate was filtered by vacuum, washed with anhydrous dioxane, THF, diethyl ether for several times, and dried under

vacuum at 120 °C for 24h, dark-violet colour powder. Anal. calcd for $C_{44}H_{28}N_2S_3$: C, 77.61; N, 4.11; H, 4.14. Found: C, 72.69; N, 3.93; H, 4.02.

Table 5.2 Synthetic conditions for construction of TAPB-QOT COP

Sample QOT	TAPB (mmol)	QOT (mmol)	Amount/ Ratio	Heating (°C)	Product Yield
Isolated Isomer	0.055	0.085	19.44/40 mg 1;1.5	80	67 % (40mg)
Isolated Isomer	0.11	0.17	38.88/80 mg 1;1.5	120	60% (71 mg)
Isomer Mixtures	0.11	0.17	38.88/80 mg 1;1.5	120	51% (60 mg)

5.2.1.6 Iodine adsorption process of TPB-QOT covalent organic polymer

TPB-QOT polymer (5 or 10 mg) was placed into a small open vial and the whole system weighed; then, this small vial was placed into a larger vial where excess iodine solids (500 mg) were present and closed. They were heated in an oven at 75 °C. It was removed it at a specific time point, cooled it to room temperature, weighed it, and compared the changes to the weight before and after iodine adsorption. 5 mg polymer was adsorbed around 21.4 mg iodine that is corresponding to 4280 mg in 1 g polymer. The I_2-loading weight of samples was calculated by the following equation:

$$\alpha = \frac{(m_2 - m_1)}{m_1} x100\ W\%$$

(α = the iodine uptake, m1 = the mass of polymer before adsorption of iodine, m2 = the mass of polymer after adsorption of iodine).

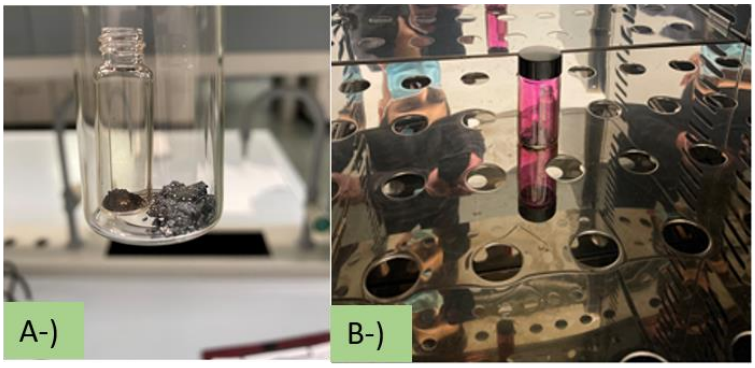

Fig. 3.15 Photograph of A-) small vial filled with polymer which is inside of the large vial filled with iodine pieces, B-) vial after iodine adsorption process in oven

5.3 Result and Discussion

In this chapter we have introduced a novel 2D covalent organic polymer by incorporating quinoid oligothiophene and characterised by structural, surface and thermal analysis as well as optical properties. In addition, we monitored its iodine adsorption capacities due to its exceptional features such as high sulfur, aromatic unit contents, active sites like alkene, imine linkage and particular formation of the building block. Before we created TAPB-QOT polymer, we firstly focused on polycondensation of poly(EDOT)methine then created its 2D form. Reaction was performed and characterized following the literature procedure. In poly(EDOT)methine reaction, EDOT carboxaldehyde is self-assembly polymerized according to condensation reaction and firstly polymer containing alcohol intermediate or oligomers took place then these alcohol groups were doped by excess of methanesulfonic acid which was converted into conjugated doped form. After treating with hydrazine hydrate, these doped forms turned into fully-conjugated Poly(EDOT)methine that contain heteroaromatic-quinoid-heteroaromatic arrays, respectively. These black colours of doped and de-doped

polymers have almost the same (relatively low) bandgap value which is around 0.8 eV.[289] To understand of synthesis whether it was successful or not, we characterised by Infrared spectroscopy and elemental analysis and results are compatible with literature one.[289]

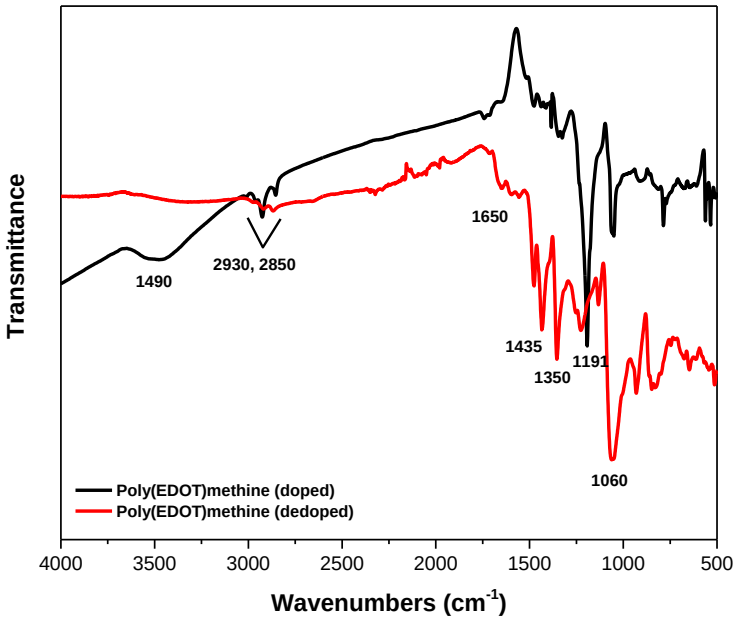

Fig. 5.16 Infrared spectra of poly(EDOT)methine-doped (black), -dedoped (red)

The infrared spectra of doped and de-doped polymers were compared (Fig. 5.16) and they are suitable. A strong band at 1060 cm^{-1} due to C–O vibration of substituents, and thiophene properties at around 1350 and 1435 cm^{-1} were observed in both polymers but in doped form these peaks are weak because of delocalization and the aromatic C-C vibration at 1650 cm^{-1} is very weak in both samples, indicating highly delocalized form. The strong band at 1191 cm^{-1} were observed in doped form owing to $CH_3SO_3^-$ dopant and disappears in the de-doped system.[289]

Based on this procedure, we designed 2D polymers that can be polymerized by co-condesation reaction using two different linkers. For this purpose, we chosen Tris-thienyltriphenyl amine which is highly electron-donor linker and terephthalaldehyde. We created this tritopic linker containing thiophene (Fig. 5.17 (II)) for condensation reaction with terephthalaldehyde instead of tritopic linker containing thiophene carboxaldehyde (Fig. 5.17 (II)) to avoid formation of di-addition to the carbonyl bond (Fig. 5.21), when thiophene is in tritopic linkers, only one addition reaction might occur and it can be doped by excess of methanesulfonic acid due to steric hindrance.

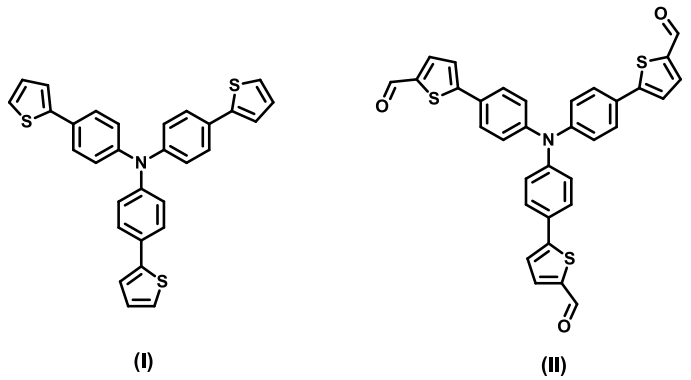

Fig. 5.17 Structure of TTPA (I) without formyl group, (II) with formyl group

Reaction was performed by microwave or conventional thermal heating conditions by changing dopant (CH_3SO_3H) amount, heating process or solvent. When we used a highly excess dopant (e.g. 20 eqv.), the polymer was obtained with 153% yield (Table 3.1) that shows doping was accomplished successfully;[289] when the dopant quantity was reduced to 10 eqv. the yield was not changed so using less than 20 eqv. can be enough to turn the hydroxyl group into doped form. On the contrary, in case of decreasing of the dopant quantity to the 2.5 eqv. product was obtained with low quantity and even starting compounds were

observed showing reaction does not quantitatively occur with low quantity of dopant. The use of dioxane in reaction resulted in high yield; this can be due to solubility of water in dioxane that mild its reactivity causing hydrolysis. On the other hand, in thermal heated reactions, carried out in $CHCl_3$ or dioxane, yield was very low, which might be proof that doping could not occur. This suggests that microwave-assist can be the more effective approach for polymerization.

To identify the stretching vibrations of functional groups, we characterized the polymer by infrared spectroscopy and as we observed characteristic peak of $CH_3SO_3^-$ dopant in doped form of poly(EDOT)methine, the methine-bridge TPTAQ polymer also exhibited this peak in spectrum at 1160 cm^{-1} and also it vanished after de-doped (Fig. 3.18). =C-H stretching vibration corresponding to alkene was observed more clearly in de-doped form, suggesting the occurrence of methine bridge in polymer. Most of the characteristic peaks related to doped and de-doped form were compatible with poly(EDOT)methine, however, the strong band at 3430 cm^{-1} displays still existence of -OH groups that means hydroxyl groups could not turn into doped form or after dedoping with hydrazine hydrate it might be decomposed by air or moisture which turns into alcohol form.

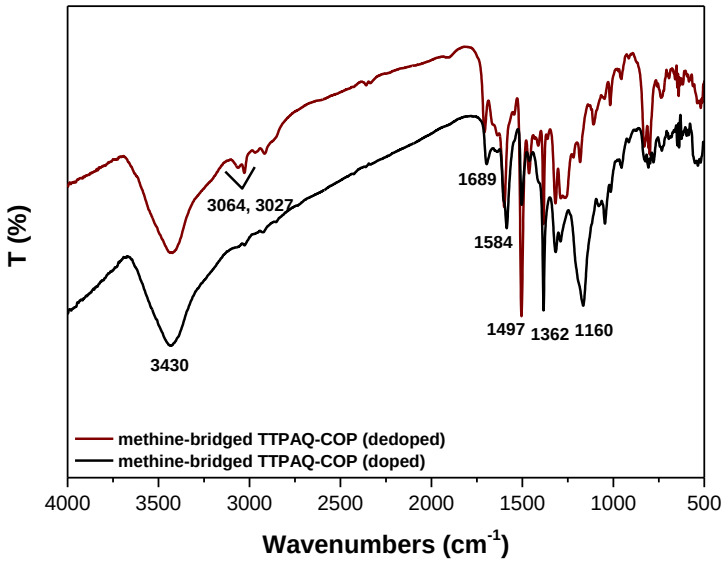

Fig. 5.18 Infrared spectra of methine-bridged TTPAQ-COP-doped (black), -dedoped (brown)

We performed combustion elemental analysis in order to determine composition of polymers and the element contents C, H, N, S of doped polymer which was obtained using $CHCl_3$ (Table 5.2, sample 2) and dioxane (Table 5.2, sample 3) were found similar and the numbers are close to the calculated doped polymer one (Fig. 5.19 (I)) obtaining slightly lower C and S content. On the other side, the found numbers of polymers synthesized by thermal conditions are also close but found higher C contents than other polymers. We also calculated element contents of possible structural forms of the polymer such as nitrogen doped form (Fig. 5.19 (II)), hydrolysed form (Fig. 5.19 (III)) or hydrogenated form (Fig. 5.19 (V)) and even if it can be possible of these structural forms, there is difference between found carbon content and calculated one because in the hydrogenated or hydrolysed form carbon content found remarkably lower than calculated content yet, sulfur content are compatible and while sulfur content was found lower,

carbon content was higher than the calculated values in the nitrogen doped form. In addition, the found values of de-doped form are also similar with calculated content attaining relatively lower carbon, higher nitrogen content.

Table 5.2 Elemental analysis of methine-bridged TTPAQ polymers

Sample	Found			
	% C	% H	% N	% S
2	52	3.52	1.73	15.12
4	53	3.85	1.85	15.20
5	65.10	3.87	2.18	14.50
6	69.10	4.70	1.70	11.42
4 (dedoped)	67.30	4.09	5.85	11.55

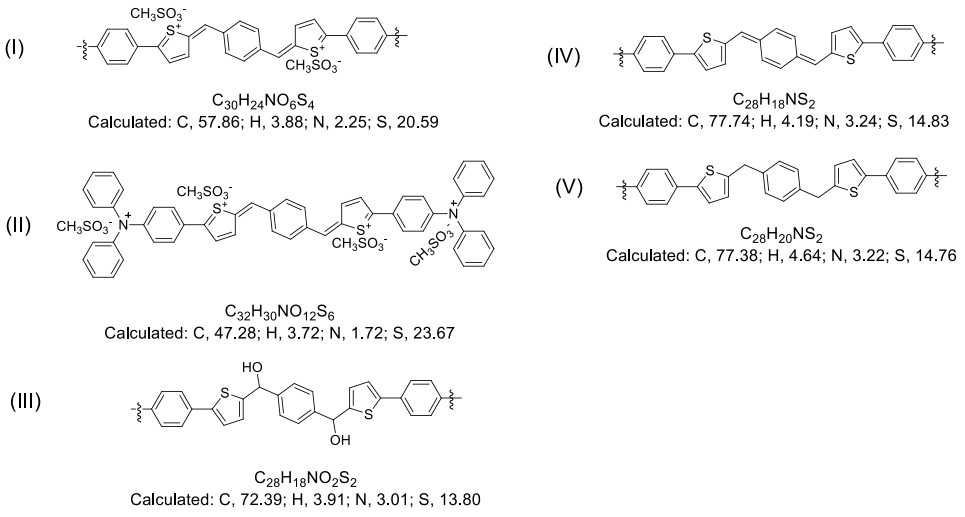

Fig. 5.19 Element analysis calculated with different structure of polymer

Optical properties of doped and dedoped polymers were investigated by diffuse reflectance spectroscopy. If the reaction occurs as expected in Fig. 5.19 (I), it is supposed that de-doped (conjugated) forms exhibit large absorption because of higher conjugation based on the quinoid form.[289] However, while doped form demonstrated absorbance in IR region, dedoped (conjugated) form indicated blueshift in UV-Vis region (Fig. 5.20). This difference indicates that quinoid form could not take place completely as expected (in Fig. 5.19 (IV), it could occur as a suggested reaction pathway in Fig. 5.21 containing quinoid form instead.

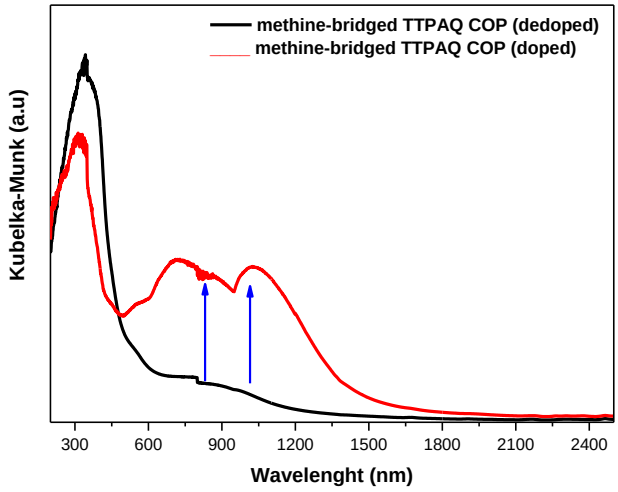

Fig. 5.20 Diffuse reflectance spectra of methine-bridged TTPAQ-doped (red), -dedoped (black)

Therefore, we believe that reaction might be very complex and not occur as expected, although found values in elemental analysis data are compatible with expected doped and de-doped form, it could not be doped completely or more explicitly, mixtures can take place, causing lower conjugation in the overall polymer backbone.

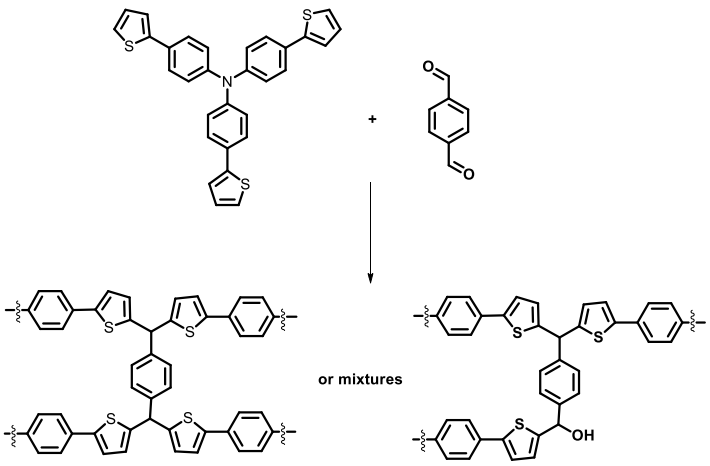

Fig. 5.21 Schematic representation of suggested reaction pathway of methane and methanol-bridged TTPA polymer

Furthermore, we also investigated their structure by PXRD and they revealed predominantly amorphous phases (Fig. 5.22) This was expected because C-C based reaction is ruled by a kinetic control. So, this reaction might not be stable in the formation of the desired product.

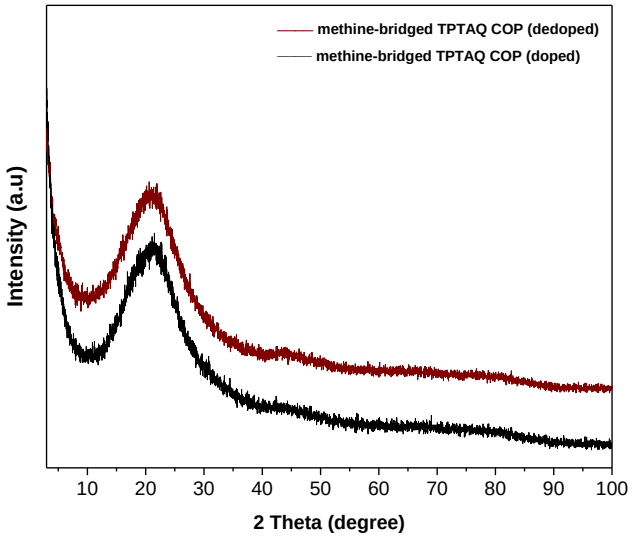

Fig. 5.22 PXRD pattern of methine-bridged TTPAQ COP-doped (black), -dedoped (brown)

Afterwards, as we mentioned in the introduction section, we focused on designing and synthesis of new building blocks which are thiophene, thienothiophene, and their quinoid form and incorporation into covalent organic frameworks based on imine linkage. The first asymmetric building block consisted of thiophene and its quinoid form connected methine bridge and there are phenyl rings on this bridge to make the structure stable. Without substituent on methine bridge the structure is not stable, it is decomposed very easily and these phenyl rings show electron donor feature in overall material. Due to asymmetric form, isomers occur from methine bridge (alkene Z-E isomers) and one of them was detected to have highest intensity among other forms by ^{1}H-NMR spectroscopy as seen in Fig. 5.23 and tried to purify through column chromatography. However, purification by chromatography is difficult and causes low yield. In literature there are similar molecules having quinoid moiety that gives isomers and it is isolated by reflux using toluene as solvent at 120 °C.[290] When mixtures are heated in solvent, unstable isomers turn into one isomer form that is most stable and having lowest energy. This procedure was followed but it could not be successful to convert isomers into a stable one. Nevertheless, when the compound was put into a vacuum oven as a powder and heated up to 100 – 120 ^{o}C under vacuum oven overnight, the isomers were turned into a stable form that has highest intensity in NMR spectrum (Fig. 5.24).

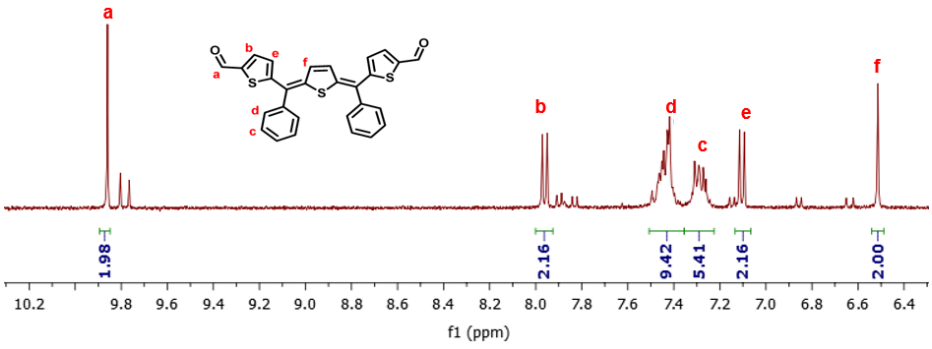

Fig. 5.23 ^{1}H-NMR of QOT (crude)

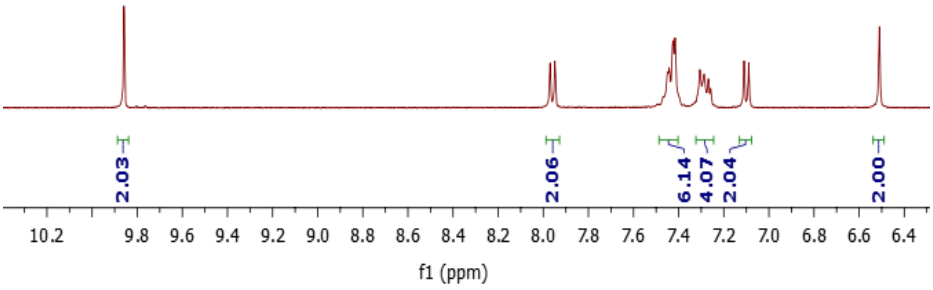

Fig. 5. 24 ^{1}H-NMR of QOT (isolated)

To understand isomer stability, theoretical calculations were carried out and relative energies of isomers were calculated and the structure F was found to have lowest energy and to be the more stable form (Fig. 5.25, Table 5.3).

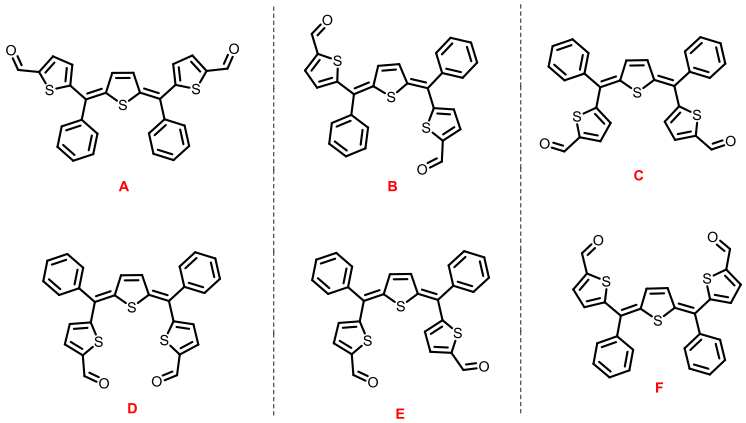

Fig. 5.25 Building block of QOT containing isomers

Table 5.3 Isomers data of QOT which is calculated relative energies

Isomers	Relative Energy, (kcal/mol)	Dipole Moment
A	1.684612	8.174
B	0.566767	2.5124
C	0.956262	9.3142
D	1.758533	0.5861
E	0.207141	4.1477
F	0	8.8298

As seen in Table 5.3, there is not only one stable isomer but also others have relatively low energy that were identified with too low intensity in ^{1}H-NMR spectrum (Fig. 5.23) and it was possible to interconvert them one into another. NMR spectrum indicates that there is only one isomer after the heating process (Fig. 5.24).

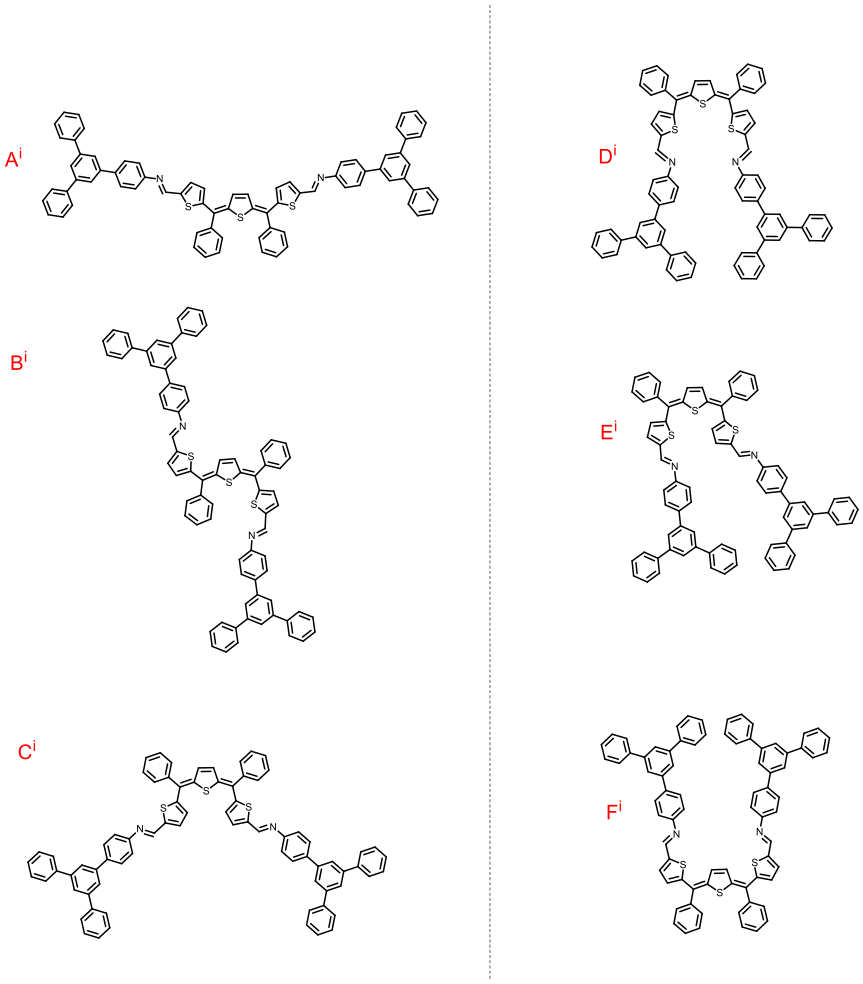

Fig. 5.26 Model compounds of QOT containing isomers

Furthermore, we calculated relative energies of isomers of model compounds. While the building block F has lowest relative energy (Table 5.3), in its model compound this energy changes (Table 5.4) and when this structure F is prepared as a model compound, relative energy is still relatively low but it turns not to be the lowest one in comparison with other structural forms (Table 5.4). In addition, while the lowest relative energy of the model compound is E^{I},

it is not one of possible structures due to steric hindrance, and also the other model compounds of B^{I} and F^{I} which have low relative energies are not possible either, because of steric hindrance. This model compound form is not suitable to construct 2D covalent organic polymer and other 2 possible forms (A^{I}, B^{I}) can`t be proper because they cause distortion in overall bulky structure. On the other side, the most likely form can be structure C^{I} because in this form both relative energy is quite lower than others and the geometry is more appropriate to build a 2D polymer. Therefore, we proposed the more appropriate model of 2D polymer as seen in Fig. 5.14

Table 5.4 Isomers data of model compounds of QOT which is calculated relative energies

Isomers	Relative Energy, (kcal/mol)	Dipole Moment
A^{i}	2,08	1,65
B^{i}	0,69	0,82
C^{i}	0,41	0,16
D^{i}	2,53	3,33
E^{i}	0	0
F^{i}	1,73	1,75

Model compound was also obtained using toluidine and the building block of QOT. In the IR spectrum (Fig. 5.27), it can be clearly seen that carbonyl stretching frequency at 1652 cm^{-1} is highly reduced in model compound and a new peak corresponding to imine linkage appears at 1578 cm^{-1}.

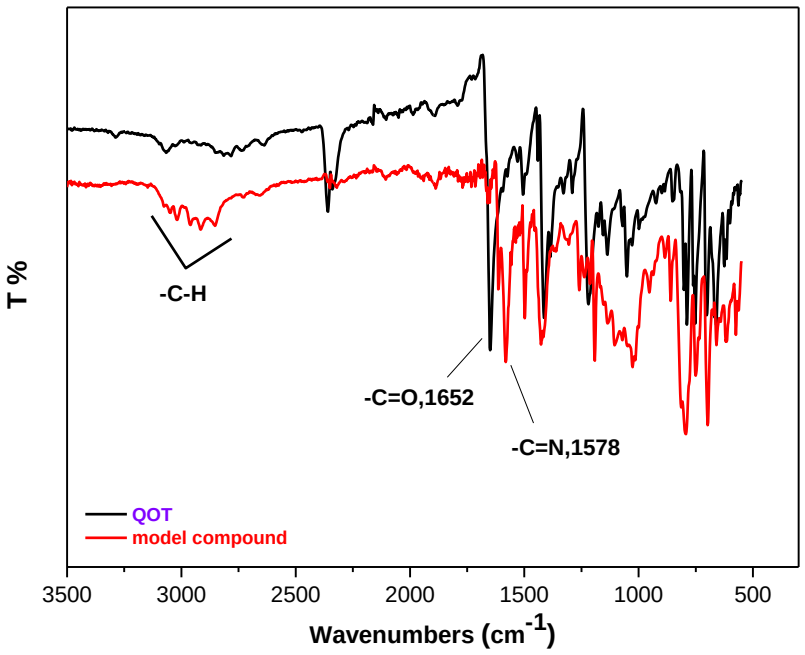

Fig. 5.27 Infrared spectra of QOT (black)

Even if isomers were obtained, new imine linkage corresponding to the model compound was also identified by ^{1}H-NMR. As seen in Fig. 5.28 the carbonyl proton disappeared and a new imine linkage proton was created at around 8.7 ppm. This indicates that the schiff-base reaction was fulfilled successfully.

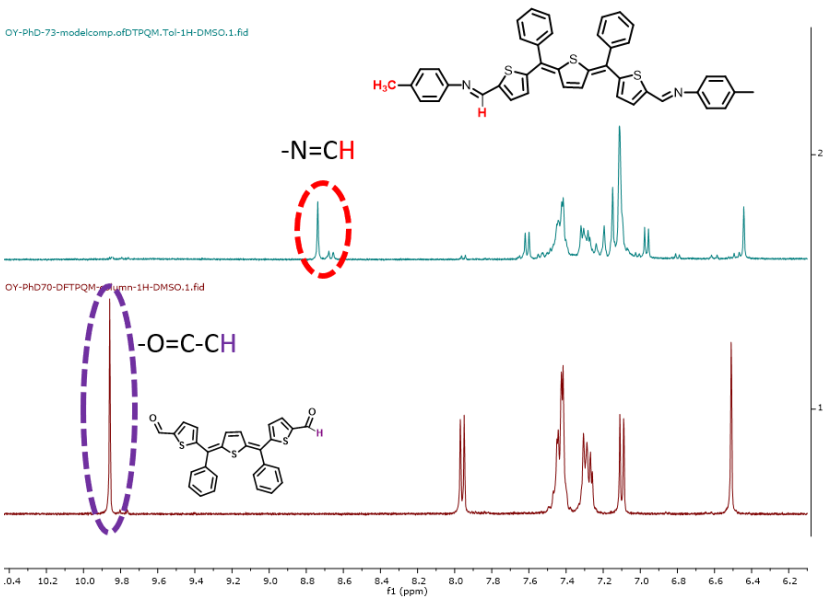

Fig. 5.28 Comparison of -NMR of model compound (up), QOT (down)

In the comparison of absorbances of QOT (without formylated), QOT (without formylated), and model compound (Tol-QOT), the model compound exhibited higher absorbance with larger absorbance edge in spectrum. This shows that imine linkage containing phenyl ring leads to extended conjugation resulting in larger absorbance. Hence, using electron donor linker such as triphenyl benzene for the construction of 2D polymer can provide high conjugation causing larger absorbance that can lead to conductive features.

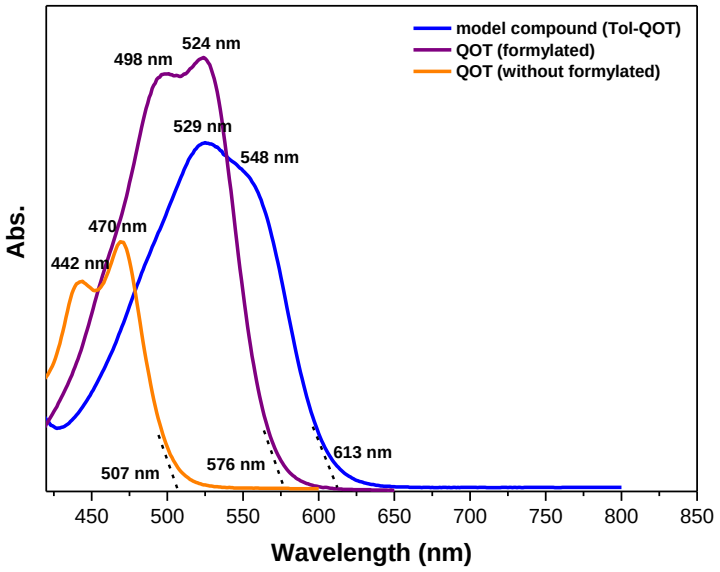

Fig. 5.29 UV-Vis spectrum of model compound (blue), QOT-formylated (purple), QOT-without formylated (orange)

With respect to other proposed building blocks that are composed bythienothiophene and its quinoid form as well as thiophene containing cyano group on methine bridge, we attempted to synthesize their formylated form to build the 2D polymer; however, we could not obtain them because in the formylation method the structure was mostly decomposed, polymerized or even residual of starting compound was observed. Even if we tried to use different methods or conditions, the desired product could not be obtained.

5.3.1 Characterisation of pristine TPB-QOT 2D covalent organic polymer

The stable isolated building block (Fig. 5.25, C) was integrated into a 2D polymer named TPB-QOT using TAPB (tris-aminotriphenyl benzene) which is a tritopic linker as knot. Reaction was carried out in different temperature such as 80 and 120 ^{o}C

and characterized by FT-IR, combustion elemental analysis, P-XRD, SEM, SEM-EDX, CO_2 adsorption-desorption isotherm, solid state UV-Vis, and TGA.

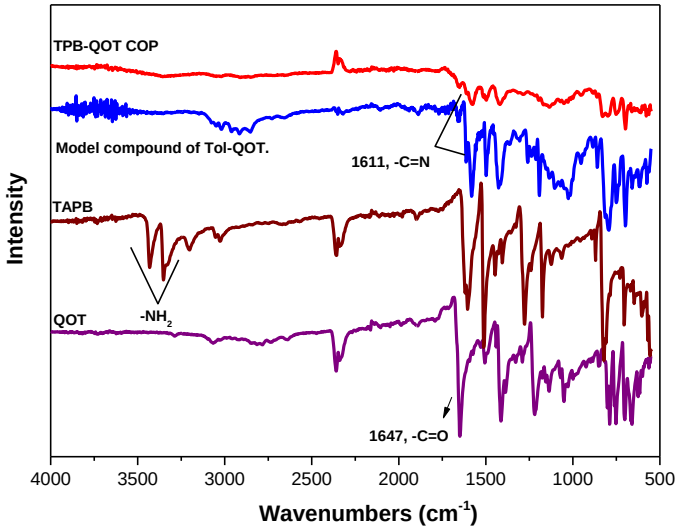

Fig. 5.30 Infrared spectra of TPB-QOT COP (red), model compound (blue), TPB (brown), QOT (purple)

As seen in the infrared spectrum, the disappearance of N−H stretching bands of TPB-QOT COP compared to its linker (-NH_2) indicated the formation of imine bonds (Fig. 5.30). On the other hand, the carbonyl stretching band was also considerably reduced in the infrared spectra of the polymer compared to the building block of the carbonyl bond.

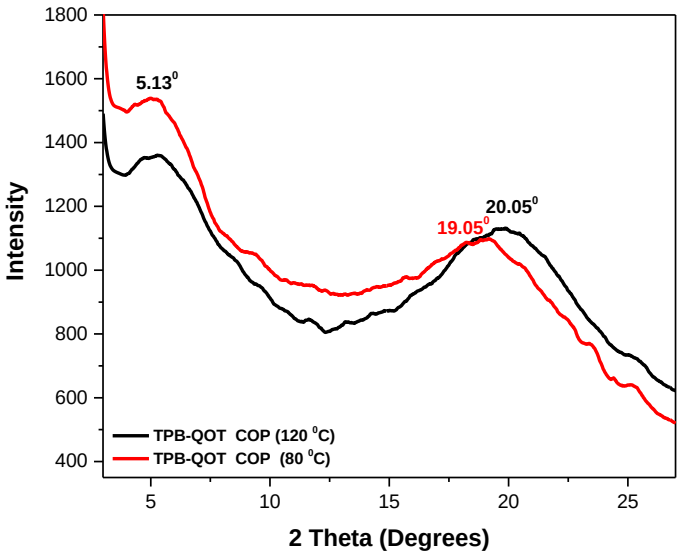

Fig. 5.31 PXRD pattern of TAPB-QOT COP

A powder X-ray diffraction (PXRD) was employed to determine the structural regularity of TPB-QOT polymer. The PXRD pattern demonstrates two broad diffraction peaks at around 5.13° and 20.5° or 19.05° corresponding to the (might be 100 or 110) and (001) planes, respectively (Figure. 5.31). The polymer synthesized at 80 °C revealed a broad peak at 19.05° in its pattern. This shows that interlayer stacking distance is higher, thus, layers are not stacked well in the comparison with polymer obtained at 120 °C, this could affect regularity as well as electrochemical properties due to change in the magnitude of π-π interaction. Therefore, reaction temperature can play a significant role in regular arrangement. Revealing broad peaks of TPB-QOT polymer show that occurrence of the low-range crystallinity due to the random displacement of the 2D layers (i.e., exfoliation), which can hinder the pore accessibility. In addition, d spacing for the (001) plane was calculated as ~4.44 Å, which is slightly higher than that of graphitic materials

(d002 ≈ 3.8 Å) referring the formation of a more exfoliated structure of the TPB-QOT polymer.[34]

Scanning Electron Microscopy (SEM) was used to investigate the morphology of TPB-QOT COP and it was composed of uniformly agglomerated spheres with different sizes (Fig. 5.32). This uniform occurrence indicates that the building block of quinoid oligothiophene in polymer is stable; there might not be an isomer mixture in the construction of polymer. In addition, The SEM-EDX pattern demonstrates the existence of the C, S, and N elements (Fig. 5.33), which carbon and sulfur contents higher proving the structure of TPB-QOT COP

.

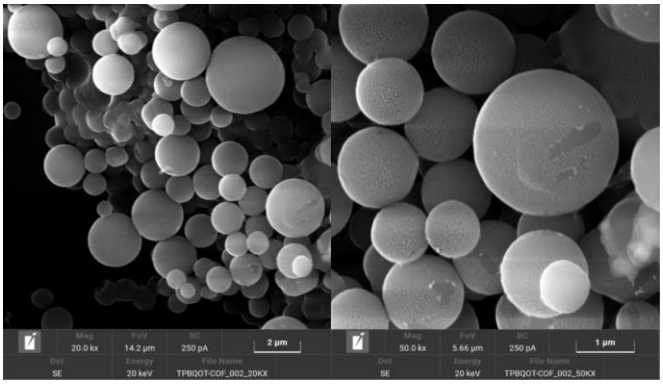

Fig. 5.32 SEM images of TPB-QOT COP; (left) 2 µm, (right) 1µm

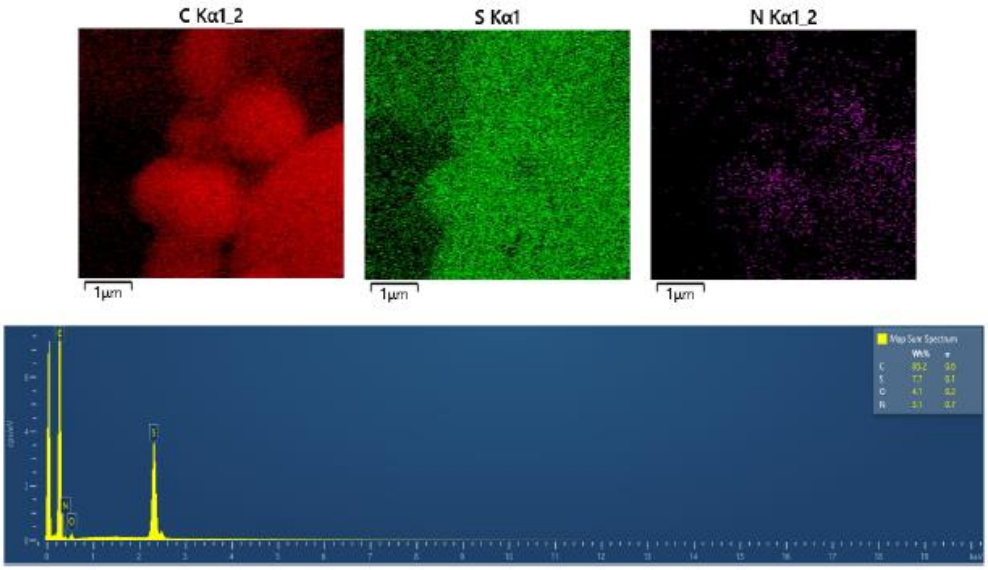

Fig. 5.33 SEM-EDX pattern of TPB-QOT COP

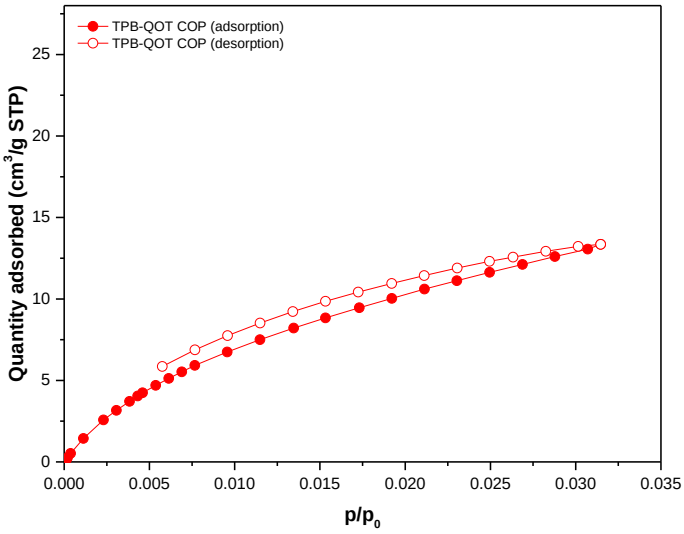

Fig. 5.34 CO_2 adsorption-desorption isotherm of TPB-QOT COP

The surface area of TPB-QOT COP was calculated as 106 m^2/g with a total pore volume of 0.018 cm^3/g and pore size of 5.6-8 Å by CO_2 adsorption-desorption isotherm using non-local density functional theory (NL-DFT) (Fig. 5.34, 5.35). As we observed in SQ-COPs, N_2 adsorption could not be employed in case of the TPB-QOT polymer to calculate the surface area and pore distribution, so the reason might be owing to the formation of building blocks bent inside pore incorporated COP causing very small cavities.

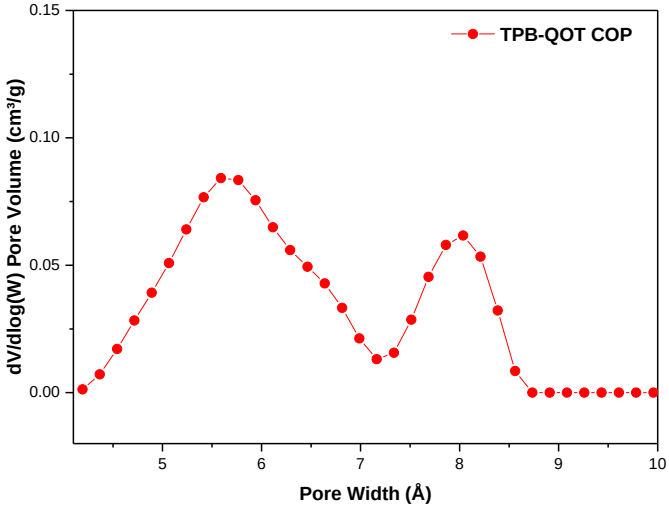

Fig. 3.35 Pore size distribution based on CO_2 adsorption isotherm of TPB-QOT COP

Thermal stability of TPB-QOT polymer was investigated by thermogravimetric analysis (TGA), suggesting that the polymer is stable up to ~ 400 ^oC under nitrogen (Fig. 5.36). Exhibiting such high stability is promising and significant in terms of using it as active material in electronic applications.

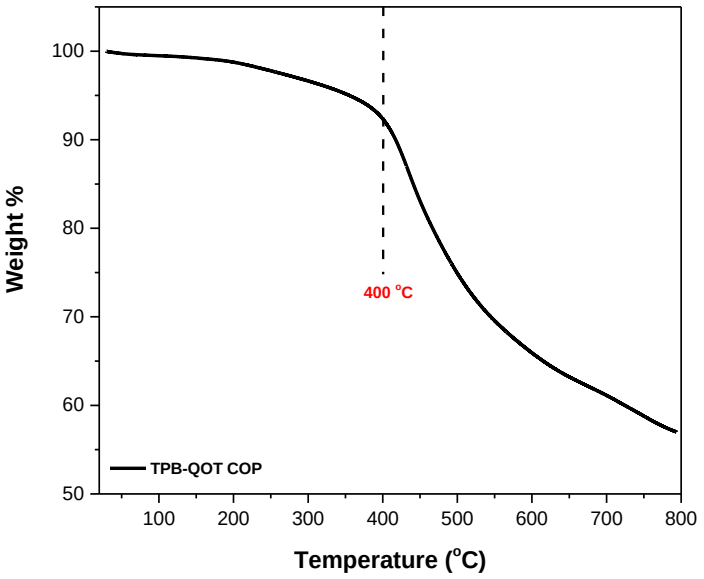

Fig. 5.36 TGA profile of TPB-QOT COP

To evaluate optical properties of TPB-QOT COP the solid-state diffuse reflectance spectrum (DRS) was used and as seen in Fig. 5.37, polymer revealed a large absorption profile with an absorption edge at ~ 935 nm. Optical direct and indirect band-gaps of polymer were determined as 1.43 (direct), 1.23 (indirect), respectively by the Tauc's plot as indicated in Fig. 5.38. Such a low optical band gap is highly desirable for electron or charge transfer which may be appropriate for the optoelectronic and storage devices.

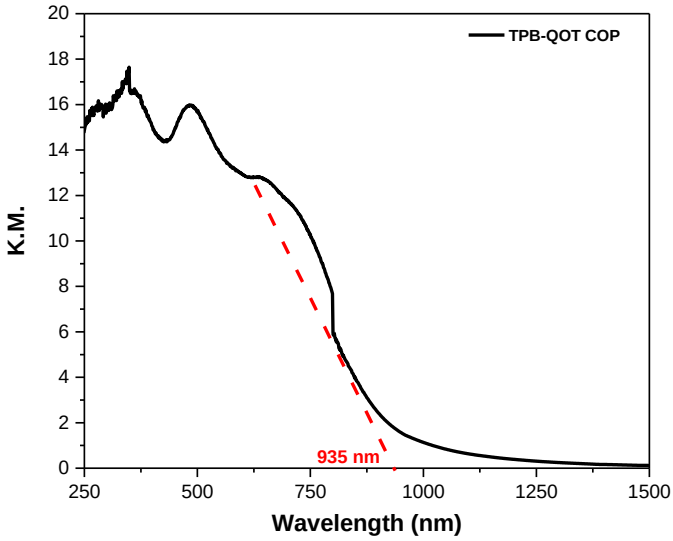

Fig. 5.37 Diffuse reflectance spectrum of TPB-QOT COP

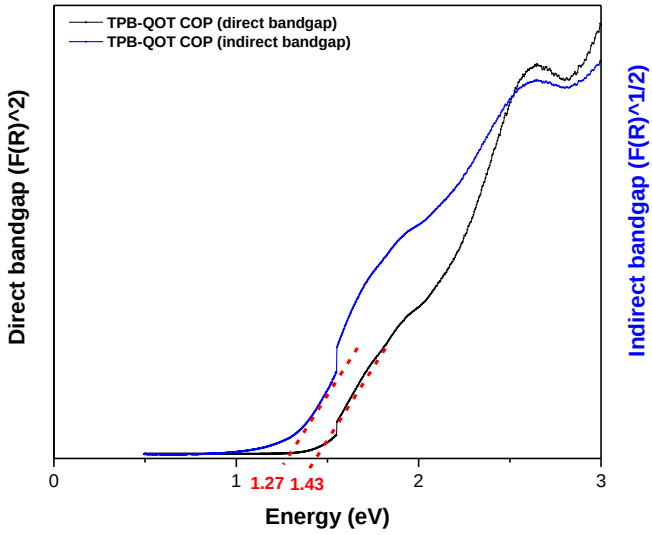

Fig. 5.38 Tauc plot of TPB-QOT COP

5.3.2 Iodine adsorption study and characterisation of iodine-adsorbed TPB-QOT 2D covalent organic polymer

One of the most powerful industrial wastes is radioactive iodine. It (129I and 131I) is highly volatile and a serious environmental risk that causes thyroid cancer.[291] Therefore, its removal is significant but challenging. Some silver-doped adsorbents have been used to turn iodine into AgI but, it exhibited very low maximum capacity like 1.18 g/g (per gram Ag).[292] Thus, new materials are necessary to increase uptake iodine capacity and porous materials are extremely successful to adsorb iodine showing high capacity.[188,293] It is possible to design effective materials functionalising the building block to control pore size, connectivity and topology.[188] For this purpose, we designed and synthesized the building block of quinoid oligothiophene to incorporate into covalent organic polymer that can be very suitable for iodine uptake due to confirmation of building block which is bended form and containing active sites, sulfur and aromatic contents which iodine can interact and bending of building block creates micro-sphere surfaces which are desirable for iodine adsorption.

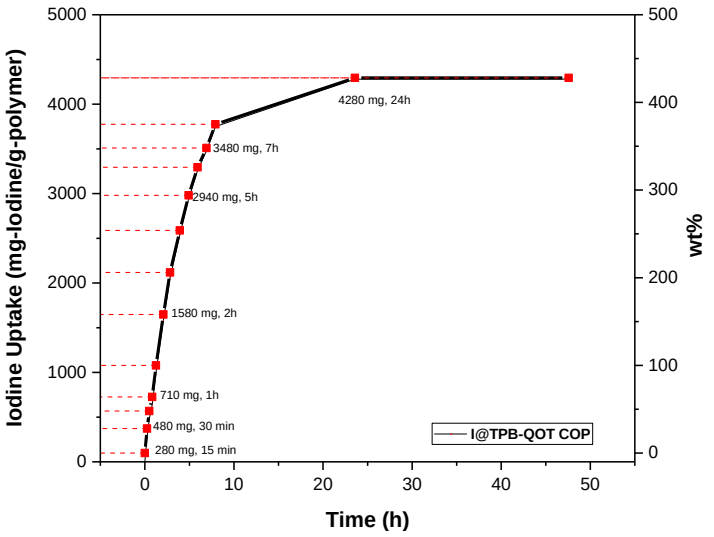

Fig. 5.39 Gravimetric changes of iodine uptake capacity (10 mg) at 75 ^{o}C and 1 atm

To evaluate Iodine adsorption capacity of TPB-QOT COP gravimetric measurement was utilized. The vial filled with TPB-QOT COP (10 mg) was placed in a large vial with an excess of iodine and the adsorption process was conducted at 75 °C in the oven under normal pressure. Gravimetric measurements were recorded at different time durations, and the outcomes demonstrated that the iodine uptake of TPB-QOT sample went up quickly during the first 8 h (Fig. 5.39), and low raising of uptake was observed then, reaching equilibrium. The increase of iodine uptake continued constantly over the first 24 hours, after that, no weight change was observed and adsorption capacity was calculated as 428 wt% (Fig. 5.39). As far as we know, the iodine capacity of TPB-QOT COP is the highest capture value among the POPs.[188]

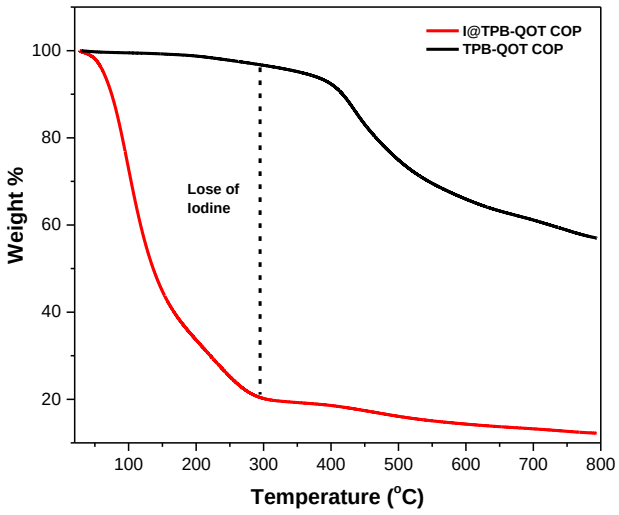

Fig. 5.40 Comparison TGA curves of I@TPB-QOT COP (red) and pristine of TPB-QOT COP (black)

Thermogravimetric analysis was performed to compare weight loss of pristine TPB-QOT polymer and its iodine adsorbed form and there is a significant weight loss difference between iodine adsorbed polymer and pristine polymer. The weight loss of iodine adsorbed polymer at between 50 and 300 ^{o}C is around 76% and this loss is compatible with iodine adsorption results. The weight loss of I@TPB-QOT at 400 ^{o}C also demonstrates there is no chemical decomposition after removing iodine, which means remaining the same chemical properties of the pristine form (Fig. 5.40). In addition, the diffuse reflectance spectrum indicates that I@TPB-QOT COP enlarged the absorption compared to the pristine form because interaction of iodine with sulfur groups creates additional energy states in the valence band of the polymer (Fig. 5.41). This also proves the existence of iodine-doped polymer.

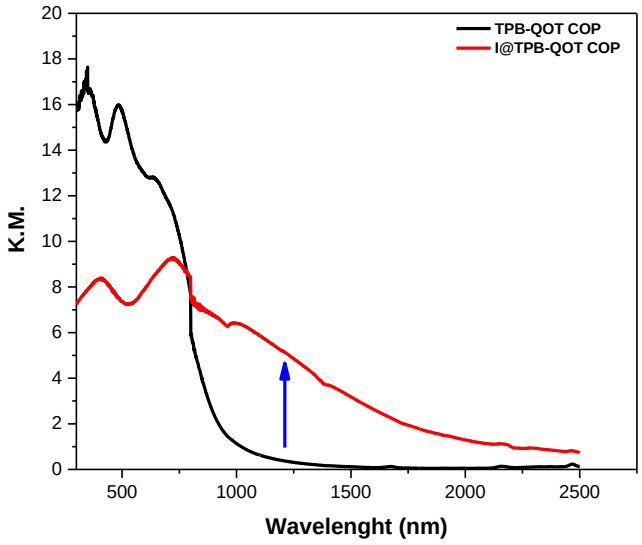

Fig. 5.41 Diffuse reflectance spectra of TPB-QOT COP (black), I@TPB-QOT COP (red)

SEM images of TPB-QOT COP and its iodine-doped form were compared. It can be clearly seen that the spherical morphologies of pristine TPB-QOT COP disappeared in the I@TPB-QOT COP due to the loading of polyiodide on the surface of polymer (Fig. 5.42). Moreover, the SEM-EDX pattern shows the existence of the I element apart from the C, S, and N elements and the intensity of the I element is higher than S and N element, indicating that the surface of the pristine polymer is captured with high iodine (Fig. 5.43)

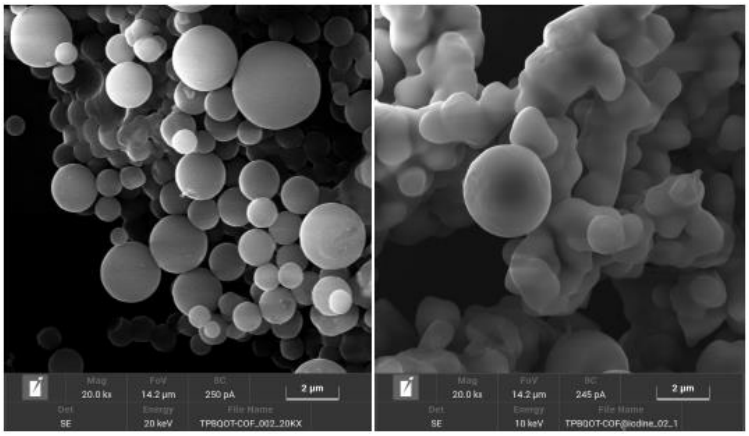

Fig. 5.42 SEM images of TPB-QOT COP; (left, 2 µm), I@TPB-QOT COP (right, 2 µm)

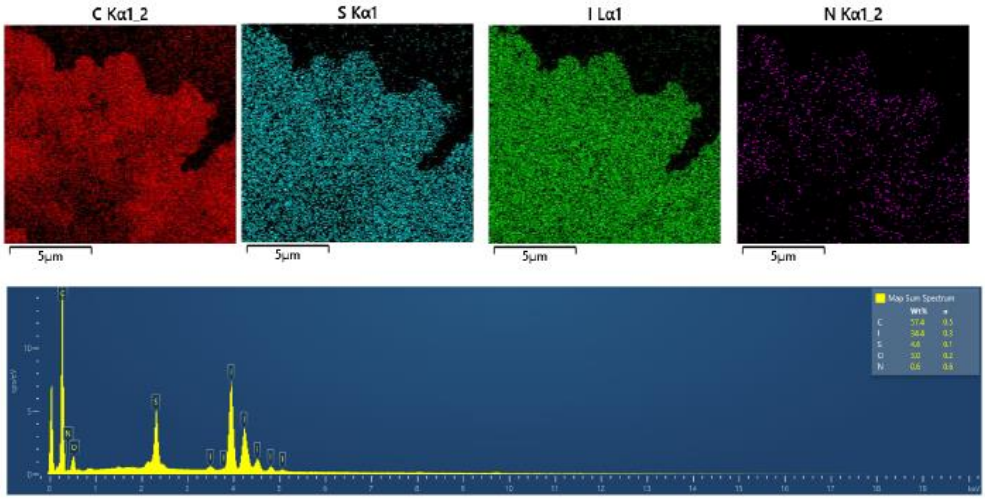

Fig. 5.43 SEM-EDX pattern of I@TPB-QOT COP

The adsorption study was repeated 5 times for 24h in the same process and uptake results did not change dramatically indicating remarkable reproducibility 4320 mg/g, Fig. 5.44). On the other hand, the cycle stability was performed 5 times

and after five cycles, the polymer can still retain 79% iodine adsorption performance (Fig. 5.45).

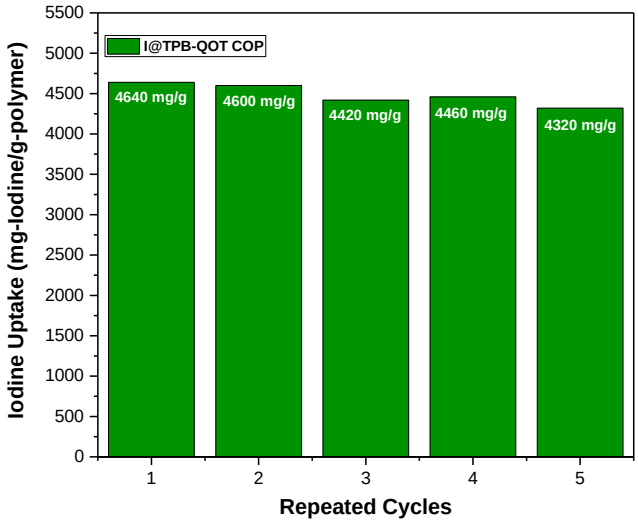

Fig. 5.44 Repeating iodine uptake of TPB-QOT COP in the same process

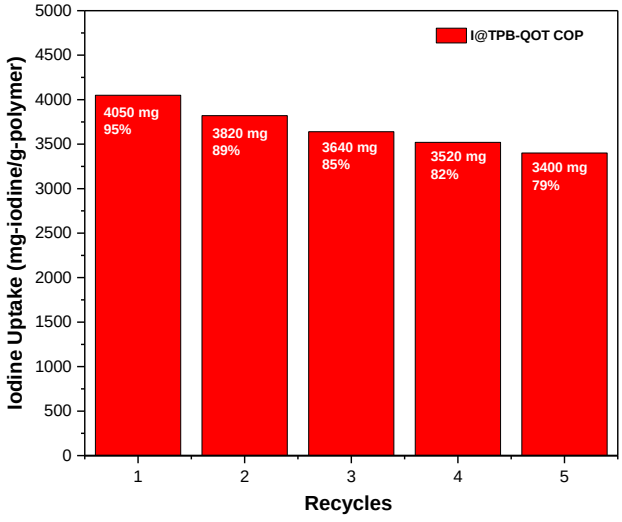

Fig. 5.45 Recycles of iodine adsorption of TPB-QOT COP

For releasing of iodine from TPB-QOT polymer, the 5 mg material was immersed in 3 ml EtOH and stirred vigorously on plate. This process went on for a certain time and 1 mg polymer adsorbed iodine was dissolved in 20 ml EtOH then analysed by UV-Vis spectrometer (Fig. 5.46).

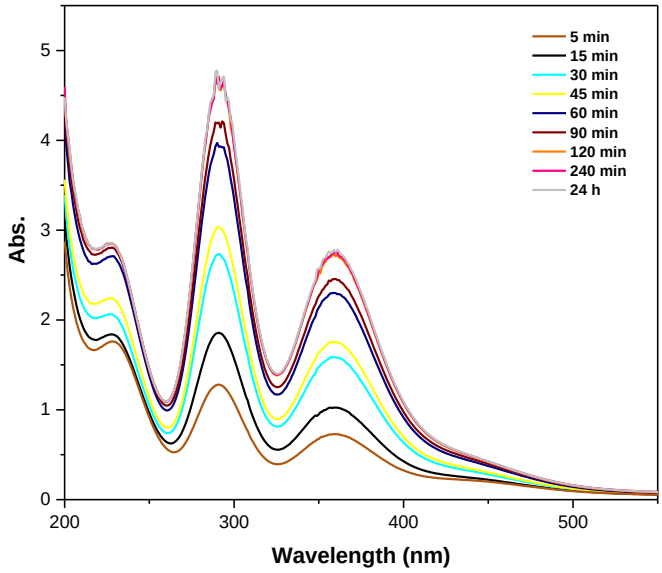

Fig. 3.46 UV–vis spectra of iodine released from iodine-adsorbed TPB-QOT COP in ethanol.

The adsorbed iodine was released easily from TPB-QOT polymer in EtOH at room temperature. When immersed in EtOH, colour of the solution rapidly changed from colourless to orange-brown indicating iodine is released into EtOH. After 1 hour later, the Intensity of colour in EtOH was higher and no colour change was observed after 24 hours that shows no more iodine is released (Fig. 5.47). After

washing with ethanol, the polymer was used 5 times, and its capacity was calculated as 340 wt% which remains 84% of its initial iodine capacity.

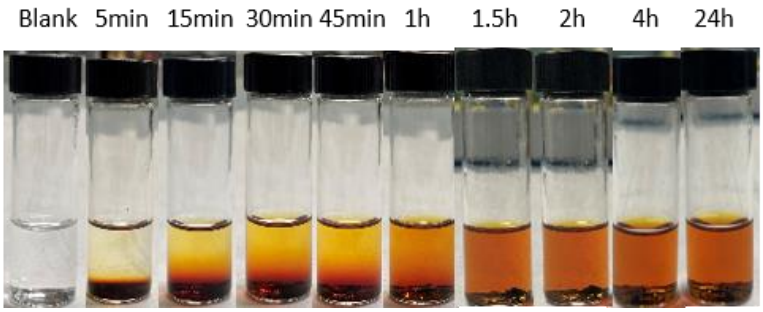

Fig. 3.47 Photographs indicating the iodine release of iodine-adsorbed TPB-QOT COP in ethanol.

The iodine adsorption was also performed in the solution. We first calibrated the iodine solution of hexane in different concentrations then, prepared the polymer for the iodine adsorption in solution. 5 mg polymer was added to an iodine solution of hexane (1.2 mg/2ml) and performed gradually adsorption by time-dependent UV-Vis absorption spectra (Fig. 5.48, (c)). Thereafter, 5 mg polymer was added to the iodine solution of hexane (20 mg/2ml) to determine its maximum adsorption capacity in solution. 0.1 ml was taken from this solution and diluted with 2 ml hexane to measure the absorbance according to the Beer-Lambert Law equation.

$$A = \varepsilon c l$$

A = Absorbance
ε = Molar absorption coefficient ($M^{-1}cm^{-1}$)
c = Molar concentration (M)
I = Optical path length (cm)

As seen in Fig. 5.44 (d), after 48h later the concentration of iodine solution of hexane decreased and reached maximum iodine adsorption capacity with 248

wt%. This indicates that the TPB-QOT polymer exhibited still high iodine adsorption capacity in solution. A lower adsorption capacity in solution than in vapor phase can be due to impact of the solvent encapsulation.[278]

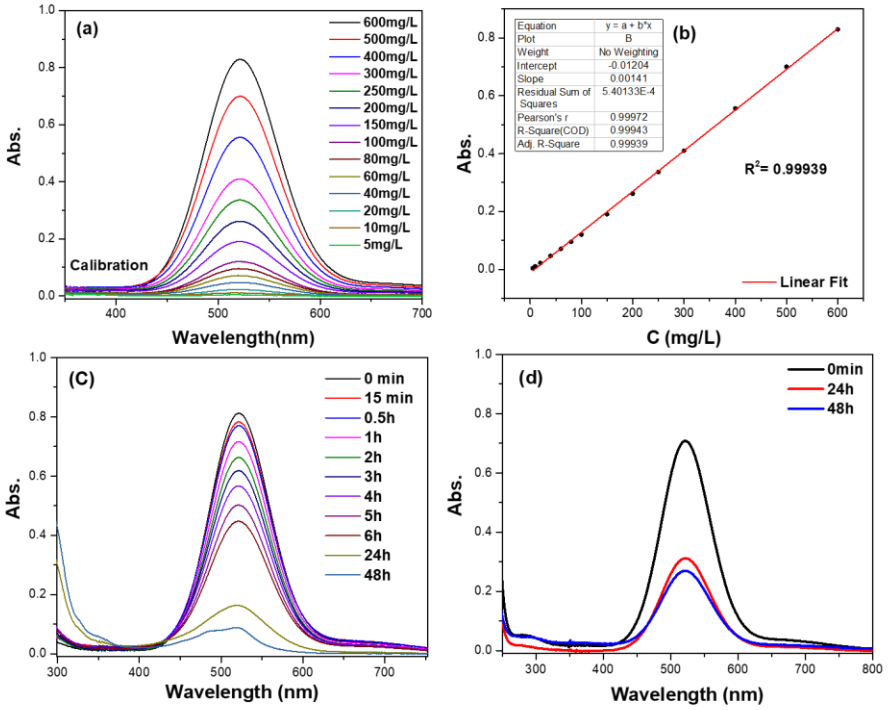

Fig. 5.48 (a) UV−Vis of iodine solution of n-hexane in different concentrations, (b) Linear curve of UV−Vis absorption of iodine in different concentrations of n-hexane solution at 525 nm, (c) UV−vis spectra for TPB-QOT COP (1 mg) and iodine (1.2 mg/2ml) in n-hexane solution, (d) UV−vis spectra for TPB-QOT COP (5 mg) and iodine (20mg/2ml) in n-hexane solution

5.4 Conclusion and Outlook

In this study, novel 2-D covalent organic polymers containing quinoidal moieties were developed and their optical properties were investigated. The first study was inspired by self-assembly of 2'-carbaldehyde-3,4-ethylenedioxythiophene (EDOT-aldehyde) (Fig. 5.7). Based on this study, we attempted to synthesize 2-D methine-

bridge polymer containing quinoid form by co-condensation of tris(4-(thiophen-2-yl)phenyl)amine (TTPA) and terephthaldehyde (1,4-dibenzaldehyde) (Fig. 5.9). As a beginning, we have tried to obtain and optimize the reaction conditions of our target structure of methine bridged-TTPAQ COP, for this purpose we have carried out various experiments using different conditions. The polymerisation was performed both by conventional thermal and microwave-assisted approaches and satisfied results were obtained under microwave irradiation in a short time. The polymerisation was accomplished through the reaction of TPAT and terephthalaldehyde in presence of methanesulfonic acid, obtaining black precipitate which is the doped form, then this doped form was turned into dedoped which is quinoid form using hydrazine solution and elucidated with FT-IR and elemental analysis. The broad and intense ‘‘conductance band’’ in the doped polymer spreading from Vis to the mid-IR region was identified by diffuse reflectance spectrometer and unexpectedly, this band disappears during the dedoping. Even if the predominantly doped form was achieved, mixtures such as alcohol, and doped form with methane sulfonate were observed (Fig. 5.21). However, these findings suggest that making methine-bridged polymers would indeed be an important development as long as an efficient dynamic equilibrium reaction to make such connections can be developed. For instance, it can be proper for implementing in electrochemical applications and its doped form might be suitable for the recovery of priceless elements by anionic exchange.

In the first study, we aimed to create 2D polymers by obtaining quinoid form during reaction in 2 steps; doped and de-doped according to the reference study.[289] However, occurrence of reaction mixtures and being obtained narrow absorbance causing larger band-gap of quinoid form than its doped form indicates

that creating a quinoid form in 2D polymers based on reference study might not be appropriate. Thus, we mainly focused on creating building blocks containing quinoidal segments to incorporate into a covalent organic framework using tritopic linker based on imine linkage. According to this purpose, a novel imine-linked 2-D covalent organic framework containing quinoid-oligothiophene linear building blocks has been developed. Four different quinoid-oligothiophene compounds were designed and one of them, composed of thiophene and its quinoid form including aromatic units connected with methine bridge (Fig. 5.10), has been used for the construction of a 2-D polymer. It was characterized by ^{1}H-NMR, FT-IR, UV-Vis, LC-MS spectroscopies. Obtained Isomers were isolated by a heating process (or column chromatography) to convert into one stable isomer. The relative energies of the isomers of building blocks and also relative energies of their model compounds were calculated and one of them (C^{I}, Fig. 5.26, Table 5.4) was found having the most low energy and being the most stable. In this form, thiophene units rotate opposite to the quinoid form and strained conformation takes place. When this reacts with tris(aminotriphenyl) benzene (TAPB) linker, it is estimated that the building block bends inside pore and causes distorted micropore surface. SEM images and CO_2 adsorption/desorption isotherm confirms this formation indicating micro-spherical surfaces with pore size of 0.56-0.80 nm. For investigating the thermal stability of the TPB-QOT polymer material, thermogravimetric analysis (TGA) under nitrogen atmosphere was performed. Obtained polymer exhibited almost no weight loss up to 380-400 ^{o}C retaining its 90% weight. This shows

superior thermal stability and such promising thermal stability is highly suitable for optoelectronic application.

Since these quinoid structures have high conjugation causing large absorption, the TPB-QOT COP demonstrated also a larger absorbance edge. Solid state UV-Vis-NIR diffuse reflectance spectroscopy was used to evaluate its band gap and measured as nearly 1.43 (direct) eV by Tauc`s plot. This is highly satisfied result in terms of optical properties, the obtainment of a band gap lower than 2 eV is still challenging in covalent organic frameworks or polymers so, this kind of highly conjugated 2D covalent organic polymer can be very suitable in optoelectronic especially energy storage devices.

We developed and worked on the TPB-QOT COP not only for the optical properties that can be suitable for electrochemical applications but also for the iodine uptake which is highly risky as environmental. Integrated building block into 2D polymer is highly appropriate for the iodine uptake due to containing high sulfur and aromatic contents, imine bond, active sites like alkene as well as its micro-spherical surfaces. The polymer exhibited high iodine adsorption capacity of 428 wt% in the vapor phase of molecular iodine, this is higher than most of those porous polymers.[188] Moreover, after five cycles of iodine adsorption, it still retained its capacity as 79% according to its initial adsorption. This shows that polymer is highly stable by adsorbing the iodine as mainly physisorption instead of chemisorption. Furthermore, its adsorption capacity in iodine solution of n-hexane was calculated as 248 wt% indicating that it still retains its high capacity even if it is lower than the former one and this might be owing to the effect of the solvent encapsulation. However, such a high capacity demonstrates that the micropore surface of polymer can enable mostly adsorption of iodine instead of solvent in the

solution. These results suggest that these kinds of building blocks can be very suitable when incorporated into 2D polymers in terms of gas storage capacities.

Apart from the asymmetric building blocks, we also synthesized symmetric building block to avoid formation of isomers and it is composed of quinoid-thienothiophene containing four aromatic units linked with methine bridge. In the future, we are planning to functionalize this building block with reactive groups such as aldehyde or amine and then we can use it to build 2D COFs based on different geometric shapes such as Kagome or tetragonal using various linear linkers. These kinds of shaped-COFs have demonstrated high electron and charge transfer than its hexagonal-shaped one. These kagome-shaped COFs have heteropores and can exhibit also high iodine uptake with our proposed building block. In addition, this TPB-QOT COP can be suitable for energy storage devices such as Li-ion batteries and supercapacitors due to redox-active feature of the quinoid building block. For this purpose, we are also planning to investigate the electron storage of the polymer.

CHAPTER 6

Conclusion and Outlook

Throughout the present thesis, the aim was to develop new 2D COFs which are addressing to different applications such as optoelectronic, energy storage devices as well as iodine uptake studies, basing on their molecular structure and properties. In the first and second chapter, the design, synthesis and technological applications of covalent organic frameworks have been introduced and then we focused on electrochemical biosensors. In the third chapter, two triazine based covalent organic frameworks were synthesized and utilized as conductive materials for biosensor applications. The biosensor was assembled using screen-printed carbon electrodes (SPCEs) and covalent triazine frameworks are exploited as electro-active material due to their high conjugation and donor-acceptor relation. Indeed, superoxide radicals, usually present in Cancerous tissues were successfully detected by prepared biosensor using synthesized covalent-triazine based COFs. This shows that 2D COFs can be useful in electrochemical biosensor in future.

In the fourth chapter, the synthesis of novel 2D squaraine-based covalent organic polymers have been discussed. In their synthesis, tritopic linkers were used as donor groups with squaric acid as acceptor group to obtain COFs with donor-acceptor geometry. The employment of different donor or acceptor units leads to tunable optical properties and low-band gap systems were obtained. Since these optical features are suitable for electrochemical applications, they are under investigation as hole transport layer in perovskite solar cell. In the future, their knots can be altered to be used in different optoelectronic applications. For this purpose, we are planning to work on modified linkers

to create a library of Squaraine-linked covalent organic frameworks which can be suitable for optoelectronic devices.

In the fifth chapter, novel 2D imine-linked covalent organic polymers have been proposed. A series of new building blocks have been designed and the most promising one has been integrated into 2D covalent organic polymer. The building block is coloured and conjugated, when used in 2D polymer it demonstrated a low band gap. The building block is redox active, and it might be suitable for energy storage devices. In addition, its 2D structure leads to the formation of micro-spherical morphologies and to the exposition of many active sites that have been proved to have a strong interaction with iodine. After a thoughtful design of the COF and its precursor, we created a building block embodying a relatively high percentage of sulfur, being the latter known to strongly interact with iodine. Indeed, it exhibited a very high iodine uptake feature (about 500% w/w), hence it can be an adsorbent material to uptake volatile toxic gases like iodine which is environmentally risky but also for other volatile compounds (formaldehyde, polycyclic aromatiic hydrocarbons (PAH)) or toxic gases (Carbon Monoxide (CO), Carbon Dioxide (CO_2), Hydrogen Fluoride (HF), Hydrogen Sulfide (H_2S)).

Appendix

Academic Activity

Pubblications;

- **O. Yildirim,** and B. Derkus, Triazine-based 2D Covalent Organic Frameworks Improve the Electrochemical Performance of Enzymatic Biosensors, J Mater Sci, 2020, 55, 3034–3044
- **O. Yildirim,** M. Bonomo, N. Barbero, C. Atzori, B. Civalleri, F. C. Bonino, G. Viscardi, C. Barolo, Application of Metal Organic Frameworks and Covalent Organic Frameworks as (photo)active Material in Hybrid Photovoltaic Technologies (Review), Energies, 2020, 13, 5602
- O. Yildirim et al., 2D Squaraine-based Covalent Organic Polymers as Hole Transport Layers in Perovskite Solar Cells (manuscript in preparation)
- O. Yildirim et al., Imine-Linked 2D Covalent Organic Polymer Containing Quinoid-Oligothiophene with High Iodine Uptake (manuscript has been prepared)

Conferences, Symposiums and Presentations;

- **Flash Communication + Poster** at Merck Young Chemists Symposium, Milano Marritima /ITALY, 13-15/10/2017

  O. Yildirim, B. Derkus, "Triazine-Based 2D-Covalent Organic Framework Enhances Electrochemical Performance of Enzymatic Biosensor"
- **Poster** at Conference, Giornate dell'Elettrochimica Italiana – GEI 2018, Sestriere/ITALY, 21-25/01/2018

  O. Yildirim, B. Derkus, C. Barolo, "Enzymatic Electrochemical Biosensor Based on a 2D-Covalent Triazine Framework"

- **Poster** at Conference IX Giornote Italo-Francesi di Chimico (lournées Franco-Italiennes de Chimie), Genova/ITALY, 16-18/04/2018

  O. Yildirim, R. Buscaino, N. Barbero, C. Barolo, G. Viscardi, "Synthesis of Covalent Organic Frameworks Containing Structural Linkers with Donor-Acceptor Characteristics and Investigation of Their Optoelectronic and Energy Storage Properties"
- **Poster** at Conference, SupraChem2019, University of Wurzburg, Wurzburg/GERMANY, 24-26/02/2019

  O. Yildirim, A. Fin, G. Viscardi, C. Barolo, "Synthesis of Covalent Organic Frameworks Based on Squarine Dye and Quinoid Form of Thiophene Having Donor-Acceptor Properties"
- **Poster** at Conference XXXIX National Conference of the Division of Organic Chemistry of the Italian Chemical Society, Torino/ITALY, 08-12/09/2019

  O. Yildirim, C. Atzori, F. Bonino, M. Chierotti, M. Zanetti, C. Barolo, G. Viscardi, "Squaraine-Based Porous Organic Polymers Containing Trigonal Linkers"
- **Poster** at International Winter School, Innovative Catalysis and Sustainability, Bardonecchia/ITALY,

  O. Yildirim, C. Barolo, A. Fin, G. Viscardi, "Synthesis of Covalent Organic Frameworks with Donor-Acceptor Structural Linkers"

Ph.D. Schools;

- **Crystallography School 2018, CrisDi -** Interdepartmental Centre for Crystallography University of Torino, Turin/ITALY, (Attended 8 courses, 48 hours), 29.05-25.06/2018
- **Summer School, SAMSET 2018,** Advanced Materials for Sustainable Energy

Technologies, University of Salento, CNR NANOTEC, Lecce/ITALY, 11-15/06/2018

Courses;

- **Raman Day 2018** Alessandro Damin, Eliano Diana, Sergio Favero-Longo, Simona Ferrando, Paolo Olivero, Federico Picollo, Piergiorgio Rossetti, Francesco Turci, University of Turin / Earth Sciences, 8 hours, 2 CFU
- **Introduction to Crystallography** Piera Benna, University of Turin / Crisdi - Interdepartmental Centre for Crystallography, 6 hours, 1.5 CFU
- **Instrumentation for X-RAY Diffraction** Angelo Agostino, University of Turin / Crisdi-Interdepartmental Centre for Crystallography, 4 hours, 1 CFU
- **X-RAY Diffraction** Alessandro Pavese, University of Turin / Crisdi-Inter departmental Centre for Crystallography, 4 hours, 1 CFU
- **X-RAY Diffraction Methods: Single Crystal** Domenica Marabello, University of Turin / Crisdi-Interdepartmental Centre for Crystallography 10 hours, 2.5 CFU
- **Introduction to Crystal Growth** Emanuele Costa, University of Turin / Crisdi-Interdepartmental Centre for Crystallography, 6 hours, 1.5 CFU
- **X-RAYS Diffraction Methods: Polycrystalline** Marco Milanesio, University of Piemonte Orientale / Crisdi-Interdepartmental Centre for Cryst., 10 hours, 2.5 CFU
- **Solid State Properties: Modelization** Anna Maria Ferrari, University of Turin / Crisdi-Interdepartmental Centre for Crystallography, 8 hours, 2 CFU
- **Electrochemical Energy Storage and Conversion Systems** Mauro Sgroi University of Turin / Department of Chemistry, 12 hours, 3 CFU
- **Corso di formazione generale alla salute e scurezza per i lavoratori,** University of Turin, 4 hours, 1 CFU

- **English Academic Course,** Jemma Robinson, University of Turin, 30 hours, 7.5 CFU
- **Solid state NMR:** basics and applications, Roberto Gobetto, Michele Chierotti, 3 CFU
- **Corso Di Lingua Italiana** (PhD School), 40 hours, 10 CFU

Teaching support assignments;

- **Chemistry and Chemical Technologies Organic and Inorganic Laboratory for synthesis of industrial interest,** Responsible Professor: Prof. Guido VISCARDI, 40 hours, 4 CFU

Total amount of CFU: 72.5/60

References

1. Patel N. G., Haydak M. H. and Gochnauer T. A., Electrophoretic components of the proteins in honeybee larval food. *Nature.* **186,** 633–634 (1960).
2. Brodschneider R. and Crailsheim, K. Nutrition and health in honeybees, *Apidologie.* **41,** 278−294 (2010).
3. Buzea C., Pacheco I. I.and Robbie K. Nanomaterials and nanoparticles: Sources and toxicity. *Biointerphases.* **2,** MR17–MR71 (2007).
4. Hyeon T., Lee S. S., Park J., Chung Y. and Na H. Bin. Synthesis of highly crystalline and monodisperse maghemite nanocrystallites without a size-selection process. *J. Am. Chem. Soc.* **123,** 12798–12801 (2001).
5. Long J. R. and Yaghi O. M. The pervasive chemistry of metal–organic frameworks. *Chem. Soc. Rev.* **38,** 1213–1214 (2009).
6. Zhou H. C., Long, J. R. and Yaghi, O. M. Introduction to Metal–Organic Frameworks. *Chem. Rev.* **112,** 673–674 (2012).
7. Davis M. E. Ordered porous materials for emerging applications. *Nature.* **417**, 813–821 (2002).
8. Greim, J. and Schwetz, K. A. Boron carbide, boron nitride, and etal borides. *Ullmann's Encyclopedia of Industrial Chemistry* (2006). doi:https://doi.org/10.1002/14356007.a04_295.pub2
9. Côté, A. P. *et al.* Porous, Crystalline, Covalent Organic Frameworks. *Science (80-.).* **310**, 1166 LP – 1170 (2005).
10. Blake A. J., Champness N. R., Crew M. and Parsons S, Sawhorse connections in a Ag(I)-nitrite coordination network: {[Ag(pyrazine)]NO2}∞. *New J. Chem.* **23**, 13–15 (1999).
11. Dawson R., Cooper A. I. and Adams D. J., Nanoporous organic polymer networks. *Prog. Polym. Sci.* **37**, 530–563 (2012).

12. Whitesides G., Simanek E., Mathias J., Seto C., Chin D., Mammen M., Gordon D. Noncovalent synthesis: using physical-organic chemistry to make aggregates. *Acc. Chem. Res.* **28**, 37–44 (1995).
13. Zang L., Che Y. and Moore J. S. One-Dimensional self-assembly of planar π-conjugated molecules: adaptable building blocks for organic nanodevices. *Acc. Chem. Res.* **41**, 1596–1608 (2008).
14. Hiemstra H., The logic of chemical synthesis. E. J. Corey and Xue-Min Cheng. John Wiley & Sons Ltd, Chichester, 1989. 436 pp., £19.15/$34.45. ISBN 0-471-50979-5. *Recl. des Trav. Chim. des Pays-Bas* **109**, 364–365 (1990).
15. Thomas A. Functional Materials: from hard to soft porous frameworks. *Angew. Chemie Int. Ed.* **49**, 8328–8344 (2010).
16. Ding, S. Y. and Wang W. Covalent organic frameworks (COFs): from design to applications. *Chem. Soc. Rev.* **42**, 548–568 (2013).
17. Diercks, C. S. and Yaghi, O. M. The atom, the molecule, and the covalent organic framework. *Science (80-.).* **355**, eaal1585 (2017).
18. Huang N., Wang P. and Jiang D. Covalent organic frameworks: a materials platform for structural and functional designs. *Nat. Rev. Mater.* **1**, 16068 (2016).
19. Colson, J. W. and Dichtel, W. R. Rationally synthesized two-dimensional polymers. *Nat. Chem.* **5**, 453–465 (2013).
20. Geng K., He T., Liu R., Dalapati S., Tan K., Li Z., Tao S., Gong Y., Jiang Q., Jiang D. Covalent Organic Frameworks: design, synthesis, and functions. *Chem. Rev.* **120**, 8814–8933 (2020).
21. Zhang K.-D. and Matile S., Complex functional systems with three different types of dynamic covalent bonds. *Angew. Chemie Int. Ed.* **54**, 8980–8983 (2015).

22. Wilson A., Gasparini G. and Matile S. Functional systems with orthogonal dynamic covalent bonds. *Chem. Soc. Rev.* **43**, 1948–1962 (2014).

23. Bi S., Yang C., Zhang W., Xu J., Liu L., Wu D., Wang X., Han Y., Liang Q., Zhang F. Two-dimensional semiconducting covalent organic frameworks via condensation at arylmethyl carbon atoms. *Nat. Commun.* **10**, 2467 (2019).

24. Zhang B., Wei M., Mao H., Pei X., Alshmimri S., Reimer J., Yaghi O. Crystalline dioxin-linked covalent organic frameworks from irreversible reactions. *J. Am. Chem. Soc.* **140**, 12715–12719 (2018).

25. Jin E., Asada M., Xu Q., Dalapati S., Addicoat M., Brady M., Xu H., Nakamura T., Heine T., Chen Q., Jiang D. Two-dimensional sp2 carbon–conjugated covalent organic frameworks. *Science (80-.).* **357**, 673 – 676 (2017).

26. Zhuang X., Zhao W., Zhang F., Cao Y., Liu F., Bi S., Feng X. A two-dimensional conjugated polymer framework with fully sp2-bonded carbon skeleton. *Polym. Chem.* **7**, 4176–4181 (2016).

27. Campbell N. L., Clowes R., Ritchie L. K. and Cooper A. I. Rapid microwave synthesis and purification of porous covalent organic frameworks. *Chem. Mater.* **21**, 204–206 (2009).

28. Wei H., Chai S., Hu N., Yang Z., Wei L. and Wang L. The microwave-assisted solvothermal synthesis of a crystalline two-dimensional covalent organic framework with high CO_2 capacity, *Chem. Commun.* **51,** 12178–12181 (2015).

29. Ren S., Bojdys M., Dawson R., Laybourn A., Khimyak Y., Adams D., Cooper A. Porous, fluorescent, covalent triazine-based frameworks via room-temperature and microwave-assisted synthesis. *Adv. Mater.* **24**, 2357–2361 (2012).

30. Kuhn, P., Antonietti, M. and Thomas, A. Porous, covalent triazine-based

frameworks prepared by ionothermal synthesis. *Angew. Chemie Int. Ed.* **47**, 3450–3453 (2008).

31. Bojdys, M. J., Jeromenok, J., Thomas, A. and Antonietti, M. Rational extension of the family of layered, covalent, triazine-based frameworks with regular porosity. *Adv. Mater.* **22**, 2202–2205 (2010).
32. Guan X., Ma Y., Li H., Yusran Y., Xue M., Fang Q., Yan Y., Valtchev V., Qiu S. Fast, ambient temperature and pressure ionothermal synthesis of three-dimensional covalent organic frameworks. *J. Am. Chem. Soc.* **140**, 4494–4498 (2018).
33. Chandra S., Kandambeth S., Biswal B., Lukose B., Kunjir S., Chaudhary M., Babarao R., Heine T., Banerjee R. Chemically stable multilayered covalent organic nanosheets from covalent organic frameworks via mechanical delamination. *J. Am. Chem. Soc.* **135**, 17853–17861 (2013).
34. Biswal B., Chandra S., Kandambeth S., Lukose B., Heine T., Banerjee R. Mechanochemical synthesis of chemically stable isoreticular covalent organic frameworks. *J. Am. Chem. Soc.* **135**, 5328–5331 (2013).
35. Shinde D., Aiyappa H. Bhadra M., Biswal B., Wadge P., Kandambeth S., Garai B., Kundu T., Kurungot S., Banerjee R. A mechanochemically synthesized covalent organic framework as a proton-conducting solid electrolyte. *J. Mater. Chem. A* **4**, 2682–2690 (2016).
36. Peng Y., Xu G., Hu Z., Cheng Y., Chi C., Yuan D., Cheng H., Zhao D. Mechanoassisted synthesis of sulfonated covalent organic frameworks with high intrinsic proton conductivity. *ACS Appl. Mater. Interfaces* **8**, 18505–18512 (2016).
37. Das G., Balaji Shinde D., Kandambeth S., Biswal B. P. and Banerjee R. Mechanosynthesis of imine, β-ketoenamine, and hydrogen-bonded imine-

linked covalent organic frameworks using liquid-assisted grinding. *Chem. Commun.* **50**, 12615–12618 (2014).

38. Medina D., Rotter J., Hu Y., Dogru M., Werner V., Auras F., Markiewicz J., Knochel P., Bein T. Room temperature synthesis of covalent–organic framework films through vapor-assisted conversion. *J. Am. Chem. Soc.* **137**, 1016–1019 (2015).

39. Matsumoto M., Dasari R., Ji W., Feriante C., Parker T., Marder S., Dichtel W. Rapid, low temperature formation of imine-linked covalent organic frameworks catalyzed by metal triflates. *J. Am. Chem. Soc.* **139**, 4999–5002 (2017).

40. Zhang F., Zhang J., Zhang B., Tan X., Shao D., Shi J., Tan D., Liu L., Feng J., Han B., Yang G., Zheng L., Zhang J. Room-temperature synthesis of covalent organic framework (COF-LZU1) nanobars in CO_2/water solvent. *ChemSusChem* **11**, 3576–3580 (2018).

41. Delapeñaruigõmez A., Rodríguez-San-Miguel D., Stylianou K., Cavallini M., Gentili D., Liscio F., Milita S., Roscioni O., Ruiz-González M., Carbonell C., Maspoch D., Mas-Ballesté R., Segura J., Zamora F. Direct on-surface patterning of a crystalline laminar covalent crganic framework synthesized at room temperature. *Chem. – A Eur. J.* **21**, 10666–10670 (2015).

42. Rodríguez-San-Miguel D., Abrishamkar A., Navarro J., Rodriguez-Trujillo R., Amabilino D., Mas-Ballesté R., Zamora F., Puigmartí-Luis J. Crystalline fibres of a covalent organic framework through bottom-up microfluidic synthesis. *Chem. Commun.* **52**, 9212–9215 (2016).

43. Zhang M., Li L., Lin Q., Tang M., Wu Y., Ke C. Hierarchical-coassembly-enabled 3D-printing of omogeneous and heterogeneous covalent organic frameworks. *J. Am. Chem. Soc.* **141**, 5154–5158 (2019).

44. Wan S., Guo J., Kim J., Ihee H. and Jiang D. A Belt-shaped, blue luminescent, and semiconducting covalent organic framework. *Angew. Chemie Int. Ed.* **47**, 8826–8830 (2008).

45. Haishen Y., Ya D., Shun W., George D. T., Yinghua J. and Wei Z. Mesoporous 2D covalent organic frameworks based on shape-persistent arylene-ethynylene macrocycles. *Chem. Sci.* **6**, 4049–4053 (2015).

46. Maria S. L., Julian M. R., Johannes T. M., Veronika W., Matthias B., Simon H., Paul K., Timothy C., Thomas B. and Dana D. M. From benzodithiophene to diethoxy-benzodithiophene covalent organic frameworks – structural investigations. *CrystEngComm* **18**, 4295–4302 (2016).

47. Hunt J. R., Doonan C. J., LeVangie J. D., Côté A. P. and Yaghi O. M. Reticular synthesis of covalent organic borosilicate frameworks. *J. Am. Chem. Soc.* **130**, 11872–11873 (2008).

48. Uribe-Romo F. J., Hunt J. R., Furukawa H., Klöck C., O'Keeffe M., Yaghi O. M. A Crystalline imine-linked 3-D porous covalent organic framework. *J. Am. Chem. Soc.* **131**, 4570–4571 (2009).

49. Chen X., Addicoat M., Irle S., Nagai A. and Jiang D. Control of crystallinity and porosity of covalent organic frameworks by managing interlayer interactions based on self-complementary π-electronic force. *J. Am. Chem. Soc.* **135**, 546–549 (2013).

50. Song J.-R., Sun J., Liu J., Huang Z.-T. and Zheng Q.-Y. Thermally/hydrolytically stable covalent organic frameworks from a rigid macrocyclic host. *Chem. Commun.* **50**, 788–791 (2014).

51. Uribe-Romo F. J., Doonan C. J., Furukawa H., Oisaki K. and Yaghi O. M. Crystalline covalent organic frameworks with hydrazone linkages. *J. Am. Chem. Soc.* **133**, 11478–11481 (2011).

52. Jackson K. T., Reich T. E. and El-Kaderi H. M. Targeted synthesis of a porous borazine-linked covalent organic framework. *Chem. Commun.* **48**, 8823–8825 (2012).

53. Nagai A., Chen X., Feng X., Ding X., Guo Z., Jiang D. A Squaraine-linked mesoporous covalent organic framework. *Angew. Chemie Int. Ed.* **52**, 3770–3774 (2013).

54. Dalapati S., Jin S., Gao J., Xu Y., Nagai A., Jiang D. An Azine-linked covalent organic framework. *J. Am. Chem. Soc.* **135**, 17310–17313 (2013).

55. Guo J., Xu Y., Jin S., Chen L., Kaji T., Honsho Y., Addicoat M. A., Kim J., Saeki A., Ihee H., Seki S., Irle S., Hiramoto M., Gao J., Jiang D. Conjugated organic framework with three-dimensionally ordered stable structure and delocalized π clouds. *Nat. Commun.* **4**, (2013).

56. Fang Q., Zhuang Z., Gu S., Kaspar R. B., Zheng J., Wang J., Qiu S., Yan Y. Designed synthesis of large-pore crystalline polyimide covalent organic frameworks. *Nat. Commun.* **5**, 4503 (2014).

57. Chen X., Addicoat M., Jin E., Xu H., Hayashi T., Xu F., Huang N., Irle S., Jiang D. Designed synthesis of double-stage two-dimensional covalent organic frameworks. *Sci. Rep.* **5**, 14650 (2015).

58. Zeng Y., Zou R., Luo Z., Zhang H., Yao X., Ma X., Zou R., Zhao Y. Covalent organic frameworks formed with two types of covalent bonds based on orthogonal reactions. *J. Am. Chem. Soc.* **137**, 1020–1023 (2015).

59. Du Y., Yang H., Whiteley J. M., Wan S., Jin Y., Lee S. H., Zhang W. Ionic covalent organic frameworks with spiroborate linkage. *Angew. Chemie Int. Ed.* **55**, 1737–1741 (2016).

60. Lyu H., Diercks C. S., Zhu C. and Yaghi O. M. Porous crystalline olefin-linked covalent organic frameworks. *J. Am. Chem. Soc.* **141**, 6848–6852 (2019).

61. Waller P. J., Lyle S. J., Osborn Popp T. M., Diercks C. S., Reimer J. A., Yaghi O. M. Chemical conversion of linkages in covalent organic frameworks. *J. Am. Chem. Soc.* **138**, 15519–15522 (2016).

62. Das G., Skorjanc T., Sharma S. K., Gándara F., Lusi M., Shankar Rao D. S., Vimala S., Krishna Prasad S., Raya J., Han D. S., Jagannathan R., Olsen J. C., Trabolsi A. Viologen-based conjugated covalent organic networks via zincke reaction. *J. Am. Chem. Soc.* **139**, 9558–9565 (2017).

63. Yahiaoui O., Fitch A. N., Hoffmann F., Fröba M., Thomas A., Roeser J. 3D anionic silicate covalent organic framework with srs topology. *J. Am. Chem. Soc.* **140**, 5330–5333 (2018).

64. Zhao C., Diercks C. S., Zhu C., Hanikel N., Pei X., Yaghi O. M., Urea-linked covalent organic frameworks. *J. Am. Chem. Soc.* **140**, 16438–16441 (2018).

65. Guan X., Li H., Ma Y., Xue M., Fang Q., Yan Y., Valtchev V., Qiu S. Chemically stable polyarylether-based covalent organic frameworks. *Nat. Chem.* **11**, 587–594 (2019).

66. El-Kaderi H. M., Hunt J. R., Mendoza-Cortés J. L., Côté A. P., Taylor R. E., O'Keeffe M., Yaghi O. M. Designed synthesis of 3D covalent organic frameworks. *Science (80-.).* **316**, 268 LP – 272 (2007).

67. Wan S., Guo J., Kim J., Ihee H. and Jiang D. A photoconductive covalent organic framework: Self-condensed arene cubes composed of eclipsed 2D polypyrene sheets for photocurrent generation. *Angew. Chemie - Int. Ed.* **48**, 5439–5442 (2009).

68. Dogru M., Sonnauer A., Gavryushin A., Knochel P. and Bein T. A covalent organic framework with 4 nm open pores. *Chem. Commun.* **47**, 1707–1709 (2011).

69. Ritchie L. K., Trewin A., Reguera-Galan A., Hasell T. and Cooper A. I. Synthesis

of COF-5 using microwave irradiation and conventional solvothermal routes. *Microporous Mesoporous Mater.* **132**, 132–136 (2010).

70. Côté A. P., El-Kaderi H. M., Furukawa H., Hunt J. R. and Yaghi, O. M. Reticular synthesis of microporous and mesoporous 2D covalent organic frameworks. *J. Am. Chem. Soc.* **129**, 12914–12915 (2007).

71. Feng X., Chen L., Honsho Y., Saengsawang O., Liu L., Wang L., Saeki A., Irle S., Seki S., Dong Y., Jiang D. An ambipolar conducting covalent organic framework with self-sorted and periodic electron donor-acceptor ordering. *Adv. Mater.* **24**, 3026–3031 (2012).

72. Dalapati S., Jin E., Addicoat M., Heine T. and Jiang, D. Highly emissive covalent organic frameworks. *J. Am. Chem. Soc.* **138**, 5797–5800 (2016).

73. Ma H., Ren H., Meng S., Yan Z., Zhao H., Sun F., Zhu G. A 3D microporous covalent organic framework with exceedingly high C_3H_8/CH_4 and C2 hydrocarbon/CH_4 selectivity. *Chem. Commun.* **49**, 9773–9775 (2013).

74. Dogru M., Handloser M., Auras F., Kunz T., Medina D., Hartschuh A., Knochel P., Bein T. A photoconductive thienothiophene-based covalent organic framework showing charge transfer towards included fullerene. *Angew. Chemie - Int. Ed.* **52**, 2920–2924 (2013).

75. Jin S., Furukawa K., Addicoat M., Chen L., Takahashi S., Irle S., Nakamura T., Jiang D. Large pore donor—acceptor covalent organic frameworks. *Chem. Sci.* **4**, 4505–4511 (2013).

76. Spitler E. L. and Dichtel W. R. Lewis acid-catalysed formation of two-dimensional phthalocyanine covalent organic frameworks. *Nat. Chem.* **2**, 672–677 (2010).

77. Spitler E. L., Giovino M. R., White S. L. and Dichtel W. R. A mechanistic study of Lewis acid-catalyzed covalent organic framework formation. *Chem. Sci.* **2**,

1588–1593 (2011).

78. Ding S. Y., Gao J., Wang Q., Zhang Y., Song W. G., Su C. Y., Wang W. Construction of covalent organic framework for catalysis: Pd/COF-LZU1 in Suzuki-Miyaura coupling reaction. *J. Am. Chem. Soc.* **133**, 19816–19822 (2011).

79. Bai L., Phua S. Z. F., Lim W. Q., Jana A., Luo Z., Tham H. P., Zhao L., Gao Q., Zhao Y. Nanoscale covalent organic frameworks as smart carriers for drug delivery. *Chem. Commun.* **52**, 4128–4131 (2016).

80. Fang Q., Gu S., Zheng J., Zhuang Z., Qiu S., Yan Y. 3D microporous base-functionalized covalent organic frameworks for size-selective catalysis. *Angew. Chemie Int. Ed.* **53**, 2878–2882 (2014).

81. Xu L., Zhou X., Tian W. Q., Gao T., Zhang Y. F., Lei S., Liu Z. F. Surface-confined single-layer covalent organic framework on single-layer graphene grown on copper foil. *Angew. Chemie Int. Ed.* **53**, 9564–9568 (2014).

82. Xu H.-S., Ding S.-Y., An W.-K., Wu H. and Wang W. Constructing crystalline covalent organic frameworks from chiral building blocks. *J. Am. Chem. Soc.* **138**, 11489–11492 (2016).

83. Zou L., Yang X., Yuan S. and Zhou H.-C. Flexible monomer-based covalent organic frameworks: design, structure and functions. *CrystEngComm* **19**, 4868–4871 (2017).

84. Ascherl L., Sick T., Margraf J. T., Lapidus S. H., Calik M., Hettstedt C., Karaghiosoff K., Döblinger M., Clark T., Chapman K. W., Auras F., Bein T. Molecular docking sites designed for the generation of highly crystalline covalent organic frameworks. *Nat. Chem.* **8**, 310–316 (2016).

85. Li Z.-J., Ding S.-Y., Xue H.-D., Cao W. and Wang, W. Synthesis of –CN– linked covalent organic frameworks via the direct condensation of acetals and

amines. *Chem. Commun.* **52**, 7217–7220 (2016).

86. Smith B. J., Overholts A. C., Hwang N. and Dichtel W. R. Insight into the crystallization of amorphous imine-linked polymer networks to 2D covalent organic frameworks. *Chem. Commun.* **52**, 3690–3693 (2016).

87. Xu H., Gao J. and Jiang D. Stable, crystalline, porous, covalent organic frameworks as a platform for chiral organocatalysts. *Nat. Chem.* **7**, 905–912 (2015).

88. Kandambeth S., Venkatesh V., Shinde D. B., Kumari S., Halder A., Verma S., Banerjee R. Self-templated chemically stable hollow spherical covalent organic framework. *Nat. Commun.* **6**, 6786 (2015).

89. Liu X. H., Guan C. Z., Ding S. Y., Wang W., Yan H. J., Wang D., Wan L. J. On-surface synthesis of single-layered two-dimensional covalent organic frameworks via solid-vapor interface reactions. *J. Am. Chem. Soc.* **135**, 10470–10474 (2013).

90. Yue J.-Y., Liu X.-H., Sun B. and Wang D. The on-surface synthesis of imine-based covalent organic frameworks with non-aromatic linkage. *Chem. Commun.* **51**, 14318–14321 (2015).

91. Xu H., Tao S. and Jiang D. Proton conduction in crystalline and porous covalent organic frameworks. *Nat. Mater.* **15**, 722–726 (2016).

92. Huang N., Zhai L., Xu H. and Jiang D. Stable covalent organic frameworks for exceptional mercury removal from aqueous solutions. *J. Am. Chem. Soc.* **139**, 2428–2434 (2017).

93. Halder A., Kandambeth S., Biswal B. P., Kaur G., Roy N. C., Addicoat M., Salunke J. K., Banerjee S., Vanka K., Heine T., Verma S., Banerjee R. Decoding the morphological diversity in two dimensional crystalline porous polymers by core planarity modulation. *Angew. Chemie Int. Ed.* **55**, 7806–7810 (2016).

94. Gao Q., Bai L., Zhang X., Wang P., Li P., Zeng Y., Zou R., Zhao Y., Synthesis of microporous nitrogen-rich covalent-organic framework and Its application in CO_2 capture. *Chinese J. Chem.* **33**, 90–94 (2015).

95. Vyas V. S., Lau V. W. and Lotsch B. V. Soft photocatalysis: organic polymers for solar fuel production. *Chem. Mater.* **28**, 5191–5204 (2016).

96. Sun B., Liu J., Cao A., Song W. and Wang, D. Interfacial synthesis of ordered and stable covalent organic frameworks on amino-functionalized carbon nanotubes with enhanced electrochemical performance. *Chem. Commun.* **53**, 6303–6306 (2017).

97. Xiong C., Ning H., Jia G., Hong X., Fei X., Donglin J. Towards covalent organic frameworks with predesignable and aligned open docking sites. *Chem. Commun.* **50**, 6161–6163 (2014).

98. Auras F., Ascherl L., Hakimioun A. H., Margraf J. T., Hanusch F. C., Reuter S., Bessinger D., Döblinger M., Hettstedt C., Karaghiosoff K., Herbert S., Knochel P., Clark T., Bein T. Synchronized offset stacking: a concept for growing large-domain and highly crystalline 2D covalent organic frameworks. *J. Am. Chem. Soc.* **138**, 16703–16710 (2016).

99. Jin S., Sakurai T., Kowalczyk T., Dalapati S., Xu F., Wei H., Chen X., Gao J., Seki S., Irle S., Jiang D. Two-dimensional tetrathiafulvalene covalent organic frameworks: Towards latticed conductive organic salts. *Chem. – A Eur. J.* **20**, 14608–14613 (2014).

100. Wu Y., Xu H., Chen X., Gao J. and Jiang D. A π-electronic covalent organic framework catalyst: π-walls as catalytic beds for Diels–Alder reactions under ambient conditions. *Chem. Commun.* **51**, 10096–10098 (2015).

101. Leng W., Peng Y., Zhang J., Lu H., Feng X., Ge R., Dong B., Wang B., Hu X., Gao Y. Sophisticated design of covalent organic frameworks with controllable

bimetallic docking for a cascade reaction. *Chem. – A Eur. J.* **22**, 9087–9091 (2016).

102. Zhou T.-Y., Xu S.-Q., Wen Q., Pang Z.-F. and Zhao X. One-step construction of two different kinds of pores in a 2D covalent crganic framework. *J. Am. Chem. Soc.* **136**, 15885–15888 (2014).
103. Zhong Fu P., Shun Qi X., Tian You Zh., Rong Ran L., Tian Guang Z., Xin Z., Construction of covalent organic frameworks bearing three different kinds of pores through the heterostructural mixed linker strategy. *J. Am. Chem. Soc.* **138**, 4710–4713 (2016).
104. Fei X., Shuhao Y., Xiong C., Qianhui L., Hejun L., Hongqiang W., Bingqing W., Donglin J. Energy-storage covalent organic frameworks: improving performance via engineering polysulfide chains on walls. *Chem. Sci.* **10**, 6001–6006 (2019).
105. Song Liang C., Yue Biao Z., Andrew B. P., Bo H., Jinhui Y., Francesca M. T., Ian D. S., Omar M. Y., Jun F., Sheng Run Z., Wei Guang Z., Yi L. Tunable electrical conductivity in oriented thin films of tetrathiafulvalene-based covalent organic framework. *Chem. Sci.* **5**, 4693–4700 (2014).
106. Huimin D., Yonghai L., Hui H., Yimeng S., Jianguo W., Caixing W., Cheng W., Guanxin Z., Baoshan W., Wei X., Deqing Z. A tetrathiafulvalene-based electroactive covalent organic framework. *Chem. – A Eur. J.* **20**, 14614–14618 (2014).
107. Song L., Christian S. D., Yue Biao Z., Nikolay K., Eva M. N., Yingbo Z., Aubrey R. P., Dohyung K., Peidong Y., Omar M. Y., Christopher J. C. Covalent organic frameworks comprising cobalt porphyrins for catalytic CO_2 reduction in water. *Science (80-.).* **349**, 1208 LP – 1213 (2015).
108. Huaping L., Hongmin W., Huimin D., Xiangshi M., Hai X., Baoshan W., Xinping

A., Cheng W. A 2D porous porphyrin-based covalent organic framework for sulfur storage in lithium–sulfur batteries. *J. Mater. Chem. A* **4**, 7416–7421 (2016).

109. Shun W., Felipe G., Atsushi A., Hiroyasu F., Akinori S., Sanjeev K. D., Lei L., Michael W. A., Youssry Y. B., Xiangfeng D., Shu S., J. Fraser S., Omar M. Y. Covalent organic frameworks with high charge carrier mobility. *Chem. Mater.* **23**, 4094–4097 (2011).
110. Huang N., Chen X., Krishna R. and Jiang D. Two-Dimensional covalent organic frameworks for carbon dioxide capture through channel-wall functionalization. *Angew. Chemie Int. Ed.* **54**, 2986–2990 (2015).
111. Xu S.-Q., Zhan T.-G., Wen Q., Pang Z.-F. and Zhao X. Diversity of covalent organic frameworks (COFs): a 2D COF containing two kinds of triangular micropores of different sizes. *ACS Macro Lett.* **5**, 99–102 (2016).
112. Xu S.-Q., Liang R.-R., Zhan T.-G., Qi Q.-Y. and Zhao X. Construction of 2D covalent organic frameworks by taking advantage of the variable orientation of imine bonds. *Chem. Commun.* **53**, 2431–2434 (2017).
113. Sasanka D., Matthew A., Shangbin J., Tsuneaki S., Jia G., Hong X., Stephan I., Shu S., Donglin J. Rational design of crystalline supermicroporous covalent organic frameworks with triangular topologies. *Nat. Commun.* **6**, 7786 (2015).
114. Cheng Q., Qiao Yan Q., Guo Fang J., Fu Zhi C., Yuan T., Xin Z. Toward covalent organic frameworks bearing three different kinds of pores: the strategy for construction and COF-to-COF transformation via heterogeneous linker exchange. *J. Am. Chem. Soc.* **139**, 6736–6743 (2017).
115. Peng Y., Wong W., Hu Z., Cheng Y., Yuan D., Khan S., Zhao D. Room temperature batch and continuous flow synthesis of water-stable covalent

organic frameworks (COFs). *Chem. Mater.* **28**, 5095–5101 (2016).

116. Sharath K., Digambar Balaji S., Manas K. P., Binit L., Thomas H., Rahul Banerjee. Enhancement of chemical stability and crystallinity in porphyrin-containing covalent organic frameworks by intramolecular hydrogen bonds. *Angew. Chemie Int. Ed.* **52**, 13052–13056 (2013).
117. Qi S., Briana A., Jason P., Lyndsey D. E., Carter W. A., Yuchuan C., Hao W., Nicholas N., Lukasz W., Shengqian Ma. Postsynthetically modified covalent organic frameworks for efficient and effective mercury removal. *J. Am. Chem. Soc.* **139**, 2786–2793 (2017).
118. Jianqiang Z., Yongsheng P., Wenguang L., Yanan G., Feifei X., Jinling Chai Nitrogen ligands in two-dimensional covalent organic frameworks for metal catalysis. *Chinese J. Catal.* **37**, 468–475 (2016).
119. Mohammad Gulam R., Ali Kemal S., Zafer K., Thomas E. R., Ransheng D., Hani M. El-Kaderi A 2D mesoporous imine-linked covalent organic framework for high pressure gas storage applications. *Chem. – A Eur. J.* **19**, 3324–3328 (2013).
120. Qiang G., Linyi B., Yongfei Z., Peng W., Xiaojing Z., Ruqiang Z., Yanli Z. Reconstruction of covalent organic frameworks by dynamic equilibrium. *Chem. – A Eur. J.* **21**, 16818–16822 (2015).
121. Shichen Y., Xinyu G., Hui L., Daohao L., Ming X., Yushan Y., Valentin V., Shilun Q., Qianrong F. Three-dimensional salphen-based covalent–organic frameworks as catalytic antioxidants. *J. Am. Chem. Soc.* **141**, 2920–2924 (2019).
122. Yuwei Z., Xiaochen S., Xiao F., Hong X., Ying M., Xiaoming L. Covalent organic frameworks as pH responsive signaling scaffolds. *Chem. Commun.* **52**, 11088–11091 (2016).

123. Zhu Y., Wan S., Jin Y. and Zhang W. Desymmetrized vertex design for the synthesis of covalent organic frameworks with periodically heterogeneous pore structures. *J. Am. Chem. Soc.* **137**, 13772–13775 (2015).

124. Linus S., Maximilian W. H., Andreas J., Gökcen S., Christian O., Johannes A. L., Bettina V. L. Tunable water and CO_2 sorption properties in isostructural azine-based covalent organic frameworks through polarity engineering. *Chem. Mater.* **27**, 7874–7881 (2015).

125. Kewei W., Li Ming Y., Xi W., Liping G., Guang C., Chun Z., Shangbin J., Bien T., Andrew C. Covalent triazine frameworks via a low-temperature polycondensation approach. *Angew. Chemie Int. Ed.* **56**, 14149–14153 (2017).

126. Soo Young Y., Javeed M., Hyuk Jun N., Jeong Min S., Sun Min J., Sun Hee S., Yoon K., ImIn Yup J., Jong B. Baek direct synthesis of a covalent triazine-based framework from aromatic amides. *Angew. Chemie Int. Ed.* **57**, 8438–8442 (2018).

127. Qianrong F., Junhua W., Shuang G., Robert B. K., Zhongbin Z., Jie Z., Hongxia G., Shilun Q., Yushan Y. 3D Porous crystalline polyimide covalent organic frameworks for drug delivery. *J. Am. Chem. Soc.* **137**, 8352–8355 (2015).

128. Enquan J., Juan L., Keyu G., Qiuhong J., Hong X., Qing X., Donglin J. Designed synthesis of stable light-emitting two-dimensional sp2 carbon-conjugated covalent organic frameworks. *Nat. Commun.* **9**, 4143 (2018).

129. Chen R., Shi J., Ma Y., Lin G., Lang X., Wang C. Designed synthesis of a 2D porphyrin-based sp^2 carbon-conjugated covalent organic framework for heterogeneous photocatalysis. *Angew. Chemie Int. Ed.* **58**, 6430–6434 (2019).

130. Shunqi X., Gang W., Bishnu P. B., Matthew A., Silvia P., Wenbo S., Xiaodong

Z., Eike B., Thomas H., Reinhard B., Xinliang F. A nitrogen-rich 2D sp^2-carbon-linked conjugated polymer framework as a high-performance cathode for lithium-ion batteries. *Angew. Chemie Int. Ed.* **58**, 849–853 (2019).

131. Meng Z., Stolz R. M. and Mirica K. A. Two-dimensional chemiresistive covalent organic framework with high intrinsic conductivity. *J. Am. Chem. Soc.* **141**, 11929–11937 (2019).

132. Rao M. R., Fang Y., De Feyter S. and Perepichka D. F. Conjugated covalent organic frameworks via michael addition–elimination. *J. Am. Chem. Soc.* **139**, 2421–2427 (2017).

133. Wei L., Xin L., Yang B., Yan Peng L., Guo Hong N., Ibrahim A., Linjun L., Chang Tai N., Zhi Gang H., Dan Z., Bin L., Su Ying Q., Kian Ping L. A two-dimensional conjugated aromatic polymer via C–C coupling reaction. *Nat. Chem.* **9**, 563–570 (2017).

134. Zhou D., Tan X., Wu H., Tian L. and Li M. Synthesis of C−C bonded two-dimensional conjugated covalent organic framework films by suzuki polymerization on a liquid–liquid interface. *Angew. Chemie Int. Ed.* **58**, 1376–1381 (2019).

135. Shaofei W., Minchan L., Hoa P., Dingguan W., Tun Seng H., Jun D., Zhouguang L., Jishan W. Toward two-dimensional π-conjugated covalent organic radical frameworks. *Angew. Chemie Int. Ed.* **57**, 8007–8011 (2018).

136. Mona C., Florian A., Laura M. S., Kathrin B., Irene G., Matthias H., Dana D. M., Mirjam D., Florian L., Dirk T., Achim H., Thomas B., Extraction of photogenerated electrons and holes from a covalent organic framework integrated heterojunction. *J. Am. Chem. Soc.* **136**, 17802–17807 (2014).

137. Bessinger D., Ascherl L., Auras F. and Bein T. Spectrally switchable photodetection with near-infrared-absorbing covalent Organic frameworks.

J. Am. Chem. Soc. **139**, 12035–12042 (2017).

138. Shangbin J., Mustafa S., Matthew A., Ko F., Long C., Toshikazu N., Shunichi F., Stephan I., Donglin J. Creation of superheterojunction polymers via direct polycondensation: segregated and bicontinuous donor-acceptor π-columnar arrays in covalent organic frameworks for long-lived charge separation. *J. Am. Chem. Soc.* **137**, 7817–7827 (2015).
139. Shangbin J., Xuesong D., Xiao F., Mustafa S., Ko F., Seiya T., Matthew A., Mohamed E. El-K., Toshikazu N., Stephan I., Shunichi F., Atsushi N., Donglin J. Charge dynamics in a donor-acceptor covalent organic framework with periodically ordered bicontinuous heterojunctions. *Angew. Chemie - Int. Ed.* **52**, 2017–2021 (2013).
140. Haase F., Gottschling K., Stegbauer L., Germann L., Gutzler R., Duppel V., Vyas V., Kern K., Dinnebier R., Lotsch B. Tuning the stacking behaviour of a 2D covalent organic framework through non-covalent interactions. *Mater. Chem. Front.* **1**, 1354–1361 (2017).
141. Huiqing L., Pengpeng S., Shuqi C., Guosheng L., Xiao F., Xiong C., Hui Jun Z., Jianbin L., Yun Bao J. Supramolecular alternating donor–acceptor assembly toward intercalated covalent organic frameworks. *J. Am. Chem. Soc.* **142**, 3712–3717 (2020).
142. Junpei S., Christina S., Xiaozhang Z., Hayato T., Dirk M. G., Eiichi N. Electron transfer through rigid organic molecular wires enhanced by electronic and electron–vibration coupling. *Nat. Chem.* **6**, 899–905 (2014).
143. Long C., Ko F., Jia G., Atsushi N., Toshikazu N., Yuping D., Donglin J. Photoelectric covalent organic frameworks: Converting open lattices into ordered donor-acceptor heterojunctions. *J. Am. Chem. Soc.* **136**, 9806–9809 (2014).

144. Gabrielle A. L., Allison M. R., Brandon J. Y., Anna A. B., Richard T. L., Charles N. B., Denis C., Amy J. B., Donna A. C., Benjamin W. L., Morgan S., Kenneth S. S., Mark D. S., Aaron K. V., Perry J. P., Sophya G., Natalia B. S. A dual threat: redox-activity and electronic structures of well-defined donor–acceptor fulleretic covalent-organic materials. *Angew. Chemie Int. Ed.* **59**, 6000–6006 (2020).

145. Geng K., Arumugam V., Xu H., Gao Y. and Jiang D. Covalent organic frameworks: Polymer chemistry and functional design. *Prog. Polym. Sci.* **108**, 101288 (2020).

146. Ruoyang L., Ke Tian T., Yifan G., Yongzhi C., Zhuoer L., Shuailei X., Ting H., Zhen L., Hao Y., Donglin J. Covalent organic frameworks: an ideal platform for designing ordered materials and advanced applications. *Chem. Soc. Rev.* **50**, 120–242 (2021).

147. Carmen C., Francesco Di P., Alessandro L., Matteo B., Danilo D. Nanostructured semiconductor materials for dye-sensitized solar cells. *J. Nanomater.* **2017**, 5323164 (2017).

148. Byung Wook P., Meysam P., Kerttu A., Seunghee J., Erik M. J. J., Anders H., Gerrit B. Understanding interfacial charge transfer between metallic PEDOT counter electrodes and a cobalt redox shuttle in dye-sensitized solar cells. *ACS Appl. Mater. Interfaces* **6**, 2074–2079 (2014).

149. Tian Y.-B., Wang Y.-Y., Chen S.-M., Gu Z.-G. & Zhang J. Epitaxial growth of highly transparent metal–porphyrin framework thin films for efficient bifacial dye-sensitized solar cells. *ACS Appl. Mater. Interfaces* **12**, 1078–1083 (2020).

150. Xiaodan C., Zhiqiang X., Ying W. Novel CoS_2 embedded carbon nanocages by direct sulfurizing metal-organic frameworks for dye-sensitized solar cells.

Nanoscale **8**, 11984–11992 (2016).

151. Yu L., Han S., Huashang R., Zhonglin D., Zhenxiao P., Xinhua Z., MOF-derived Co, N, Co doped Carbon/Ti mesh counter electrode for high-efficiency quantum dot sensitized solar cells. *J. Phys. Chem. Lett.* **10**, 4974–4979 (2019).

152. Dou J., Li Y., Xie F., Ding X. and Wei M. Metal-Organic framework derived hierarchical porous anatase TiO_2 as a photoanode for dye-sensitized solar cell. *Cryst. Growth Des.* **16**, 121–125 (2016).

153. Jin Soo K., Jiho K., Dong Young C., Yoon Jun S., Seoni K., Sungjun K., Jin K., Juwon J., Myeong Jae L., Heejong S., Subin P., Sung Jong Y., Min Jae KoJeyong Y., Yung Eun S. Tailoring the porosity of MOF-derived N-doped carbon electrocatalysts for highly efficient solar energy conversion. *J. Mater. Chem. A* **6**, 20170–20183 (2018).

154. Yuan W., Mingshui Y., Lianjing Z., Wei W., Weinan X., Yan L., CuxS nanoparticle@carbon nanorod composites prepared from metal–organic frameworks as efficient electrode catalysts for quantum dot sensitized solar cells. *J. Mater. Chem. A* **7**, 2210–2218 (2019).

155. Yongjian L., Xiufeng L., Hansheng L., Daxin S., Qingze J., Yun Z., Caihong F., Xiaoping B., Hongxia W., Qin W. Rational design of metal organic framework derived hierarchical structural nitrogen doped porous carbon coated CoSe/nitrogen doped carbon nanotubes composites as a robust Pt-free electrocatalyst for dye-sensitized solar cells. *J. Power Sources* **422**, 122–130 (2019).

156. Tai Ying C., Yi June H., Chun Ting L., Chung Wei K., R. V., Kuo Chuan H. Metal-organic framework/sulfonated polythiophene on carbon cloth as a flexible counter electrode for dye-sensitized solar cells. *Nano Energy* **32**, 19–27

(2016).

157. Xiancai J., Hongmei L., Shuolin L., Shaowei H., Changli Z., Linxi H., Metal-organic framework-derived Ni–Co alloy@carbon microspheres as high-performance counter electrode catalysts for dye-sensitized solar cells. *Chem. Eng. J.* **334**, 419–431 (2018).

158. Zhang W., Wu Z. Y., Jiang H. L. and Yu S. H. Nanowire-directed templating synthesis of metal-organic framework nanofibers and their derived porous doped carbon nanofibers for enhanced electrocatalysis. *J. Am. Chem. Soc.* **136**, 14385–14388 (2014).

159. Qiulong W., Fangyu X., Shuangshuang T., Lei H., Esther H. L., Bruce D., Liqiang M. Porous one-dimensional nanomaterials: Design, fabrication and applications in electrochemical energy storage. *Adv. Mater.* **29**, (2017).

160. Park S.-H., Kim B.-K. and Lee W.-J. Electrospun activated carbon nanofibers with hollow core/highly mesoporous shell structure as counter electrodes for dye-sensitized solar cells. *J. Power Sources* **239**, 122–127 (2013).

161. Xuesong D., Jia G., Xiao F., Yoshihito Ho., Jingdong G., Shu S., Phornphimon M., Akinori S., Shigeru N., Donglin J. Synthesis of metallophthalocyanine covalent organic frameworks that exhibit high carrier mobility and photoconductivity. *Angew. Chemie Int. Ed.* **50**, 1289–1293 (2011).

162. Xuesong D., Long C., Yoshihito H., Xiao F., Oraphan S., Jingdong G., Akinori S., Shu S., Stephan I., Shigeru N., Vudhichai P., Donglin J., An n -channel two-dimensional covalent organic framework. *J. Am. Chem. Soc.* **133**, 14510–14513 (2011).

163. Xiao F., Lili L., Yoshihito H., Akinori S., Shu S., Stephan I., Yuping D., Atsushi N., Donglin J., High-rate charge-carrier transport in porphyrin covalent organic frameworks: Switching from hole to electron to ambipolar

conduction. *Angew. Chemie Int. Ed.* **51**, 2618–2622 (2012).

164. Ren Y., Yu C., Chen Z. and Xu Y. Two-dimensional polymer nanosheets for efficient energy storage and conversion. *Nano Res.* **14**, 2023–2036 (2021).
165. Chen Z., Chen J., Bu F., Agboola P., Shakir I., Xu Y. Double-holey-heterostructure frameworks enable fast, stable, and simultaneous ultrahigh gravimetric, areal, and volumetric lithium storage. *ACS Nano* **12**, 12879–12887 (2018).
166. Lili L., Yuyang H., Xiongwei W., Shiying X., Zheng C., Yaqiong Y., Yuping W. Nanoporous selenium as a cathode material for rechargeable lithium–selenium batteries. *Chem. Commun.* **49**, 11515–11517 (2013).
167. Yan Shuai H., Chen Zi Z., Ye X., Rui X., Jing Jing X., Jia Qi H., Qiang Z., Xiqian YuHong L., Safe lithium-metal anodes for Li–O_2 batteries: from fundamental chemistry to advanced characterization and effective protection. *Batter. Supercaps* **2**, 638–658 (2019).
168. Dandan Y., Hongyang Z., Na L., Rui S., Xiaolei S., Xinghua L., Yaping D. Enhancing the rate capability of niobium oxide electrode through rare-earth doping engineering. *Batter. Supercaps* **2**, 924–928 (2019).
169. Xiao P. and Xu Y. Recent progress in two-dimensional polymers for energy storage and conversion: design, synthesis, and applications. *J. Mater. Chem. A* **6**, 21676–21695 (2018).
170. Chen Z., An X., Dai L. and Xu Y. Holey graphene-based nanocomposites for efficient electrochemical energy storage. *Nano Energy* **73**, 104762 (2020).
171. Yan B., Chen Z. and Xu Y. Amorphous and crystalline 2D polymeric carbon nitride nanosheets for photocatalytic hydrogen/oxygen evolution and hydrogen peroxide production. *Chem. – An Asian J.* **15**, 2329–2340 (2020).
172. Bai L., Gao Q. and Zhao Y. Two fully conjugated covalent organic frameworks

as anode materials for lithium ion batteries. *J. Mater. Chem. A* **4**, 14106–14110 (2016).

173. Fei X., hangbin J., Hui Z., Dingcai W., Xiaoqing Y., Xiong C., Hao W., Ruowen F., Donglin J. Electrochemically active, crystalline, mesoporous covalent organic frameworks on carbon nanotubes for synergistic lithium-ion battery energy storage. *Sci. Rep.* **5**, 8225 (2015).
174. Shan W., Qianyou W., Pengpeng S., Yuzhen H., Xing GaoLi M., Shuai Y., Xiaojie M., Junwen Z., Xiao F., Bo W. Exfoliation of covalent organic frameworks into few-layer redox-active nanosheets as cathode materials for lithium-ion batteries. *J. Am. Chem. Soc.* **139**, 4258–4261 (2017).
175. Zhonghui C., Shuo L., Yong Z., Mohamed F. Aly A., Imran S., Yuxi X. Ultrafine FeS_2 nanocrystals/porous nitrogen-doped carbon hybrid nanospheres encapsulated in three-dimensional graphene for simultaneous efficient lithium and sodium ion storage. *J. Mater. Chem. A* **7**, 26342–26350 (2019).
176. Jihui L., Jinrui L., Fan Z., Xuan D., Juan A. Z., Yongbing T. Sodium-ion hybrid battery combining an anion-intercalation cathode with an adsorption-type anode for enhanced rate and cycling performance. *Batter. Supercaps* **2**, 440–447 (2019).
177. Zhao S., Qin B., Chan K.-Y., Li C.-Y. V. and Li F. Recent development of aprotic Na−O_2 batteries. *Batter. Supercaps* **2**, 725–742 (2019).
178. Liu J., Lyu P., Zhang Y., Nachtigall P. and Xu Y. New layered triazine framework/exfoliated 2D polymer with superior sodium-storage properties. *Adv. Mater.* **30**, 1705401 (2018).
179. Duan H., Lyu P., Liu J., Zhao Y. and Xu Y. Semiconducting crystalline two-dimensional polyimide nanosheets with superior sodium storage properties. *ACS Nano* **13**, 2473–2480 (2019).

180. Yuan C., Wu H., Bin Xie Y. and Lou X. W. (David). Mixed transition-metal oxides: design, synthesis, and energy-related applications. *Angew. Chemie Int. Ed.* **53**, 1488–1504 (2014).

181. Wang Y., Song Y. and Xia Y. Electrochemical capacitors: mechanism, materials, systems, characterization and applications. *Chem. Soc. Rev.* **45**, 5925–5950 (2016).

182. Jinfeng S., Lingzhi G., Xuan S., Jinyang Z., Linrui H., Li L., Shuhua Y., Changzhou Y. One-dimensional nanostructured pseudocapacitive materials: design, synthesis and applications in supercapacitors. *Batter. Supercaps* **2**, 820–841 (2019).

183. DeBlase C. R., Silberstein K. E., Truong T.-T., Abruña H. D. and Dichtel W. R. β-Ketoenamine-linked covalent organic frameworks capable of pseudocapacitive energy storage. *J. Am. Chem. Soc.* **135**, 16821–16824 (2013).

184. Abdul Muqsit K., Zahid Ali G., Bin L., Niaz Ali K., Azhar I., Lianshan L., Zhiyong T. A redox-active 2D covalent organic framework with pyridine moieties capable of faradaic energy storage. *J. Mater. Chem. A* **4**, 16312–16317 (2016).

185. Suman C., Debarati Roy C., Matthew A., Thomas H., Amit P., Rahul B. Molecular level control of the capacitance of two-dimensional covalent organic frameworks: role of hydrogen bonding in energy storage materials. *Chem. Mater.* **29**, 2074–2080 (2017).

186. Catherine R. D., Kenneth Hernández-B., Katharine E. S., Gabriel G. Rodríguez-C., Ryan P. B., Héctor D. A., William R. D., Rapid and efficient redox processes within 2D covalent organic framework thin films. *ACS Nano* **9**, 3178–3183 (2015).

187. Yusran Y., Hui L., Xinyu G., Daohao L., Lingxue T., Ming X., Zhongbin Z., Yushan Y., Valentin V., Shilun Q., Qianrong F. Exfoliated mesoporous 2D covalent organic frameworks for high-rate electrochemical double-layer capacitors. *Adv. Mater.* **32**, 1907289 (2020).

188. Xie W., Cui D., Zhang S. R., Xu Y. H. and Jiang D. L. Iodine capture in porous organic polymers and metal-organic frameworks materials. *Mater. Horizons* **6**, 1571–1595 (2019).

189. Zhi Jian Y., Shun Qi X., Tian Guang Z., Qiao Yan Q., Zong Quan W., Xin Zhao Ultrahigh volatile iodine uptake by hollow microspheres formed from a heteropore covalent organic framework. *Chem. Commun.* **53**, 7266–7269 (2017).

190. Chang W., Yu W., Rile G., Xuedan S., Xueqing X., Qike J., Hui L., Ce H., Xinwen G., Yanan G., Donglin J. A 3D Covalent organic framework with exceptionally high iodine capture capability. *Chem. – A Eur. J.* **24**, 585–589 (2018).

191. Ping W., Qing X., Zhongping L., Weiming J., Qiuhong J., Donglin J. Exceptional iodine capture in 2D covalent organic frameworks. *Adv. Mater.* **30**, 1801991 (2018).

192. Jinheng L., Huixin Z., Lingyan Z., Ke W., Zhengkang W., Guiyan L., Yanli Z., Yongfei Z. Two-dimensional covalent–organic frameworks for ultrahigh iodine capture. *J. Mater. Chem. A* **8**, 9523–9527 (2020).

193. Xinghua G., Yin T., Meicheng Z., Yang L., Rui W., Xing L., Xiaofeng L., Ying X., Lijian M., Chuanqin X., Shoujian L. Mechanistic insight into hydrogen-bond-controlled crystallinity and adsorption property of covalent organic frameworks from flexible building blocks. *Chem. Mater.* **30**, 2299–2308 (2018).

194. Yunxiao L., Xuanfeng J., Samuel T. K., Sampath B. A., Xisen H., Zhiyun Z.,

Christina M. T., Ronald A. S., Chenfeng K. An elastic hydrogen-bonded cross-linked organic framework for effective iodine capture in water. *J. Am. Chem. Soc.* **139**, 7172–7175 (2017).

195. Gobinda D., Thirumurugan P., Selbi N., Dong Suk H., Ahmed Abdel-WahabJohn Carl O., Kyriaki P., Carlos Platas-I., Florent R., Mustapha J., Ali T. Multifunctional redox-tuned viologen-based covalent organic polymers. *J. Mater. Chem. A* **4**, 15361–15369 (2016).
196. Lan Y., Tong M., Yang Q. and Zhong C. Computational screening of covalent organic frameworks for the capture of radioactive iodine and methyl iodide. *CrystEngComm* **19**, 4920–4926 (2017).
197. Xu Y., Yingpan S., Jiameng L., Nan Z., Chunlin Z., Linghao H., Zhihong Z., Zhongyi L. Two-dimensional porphyrin-based covalent organic framework: A novel platform for sensitive epidermal growth factor receptor and living cancer cell detection. *Biosens. Bioelectron.* **126**, 734–742 (2019).
198. Linyu W., Yi X., Yuxi Y., Huihui L., Li W., Yonghai S. Electroactive covalent organic frameworks/carbon nanotubes composites for electrochemical sensing. *ACS Appl. Nano Mater.* **3**, 1412–1419 (2020).
199. Yi X., Mengli X., Li W., Huihui L., Linyu W., Yonghai S. Iron-porphyrin-based covalent-organic frameworks for electrochemical sensing H_2O_2 and pH. *Mater. Sci. Eng. C* **112**, 110864 (2020).
200. Mengli X., Linyu W., Yi X., Yonghai S., Li W. Ratiometric electrochemical sensing and biosensing based on multiple redox-active state COF-DHTA-TTA. *Sensors Actuators B Chem.* **281**, 1009–1015 (2019).
201. Yildirim O. and Derkus B. Triazine-based 2D covalent organic frameworks improve the electrochemical performance of enzymatic biosensors. *J. Mater. Sci.* **55**, 3034–3044 (2020).

202. Möller K. and Bein T. Mesoporosity – a new dimension for zeolites. *Chem. Soc. Rev.* **42**, 3689–3707 (2013).

203. Stock N. and Biswas S. Synthesis of metal-organic frameworks (MOFs): routes to various MOF topologies, morphologies, and composites. *Chem. Rev.* **112**, 933–969 (2012).

204. Vincent G., Dongwook K., Jarrod F. E., Ryan L., Xinfang L., Karim A., Myoung Soo L., Mohamed E. A supermolecular building approach for the design and construction of metal–organic frameworks. *Chem. Soc. Rev.* **43**, 6141–6172 (2014).

205. Eddaoudi M., Sava D. F., Eubank J. F., Adil K. and Guillerm V. Zeolite-like metal–organic frameworks (ZMOFs): design, synthesis, and properties. *Chem. Soc. Rev.* **44**, 228–249 (2015).

206. Waller P. J., Gándara F. and Yaghi O. M. Chemistry of covalent organic frameworks. *Acc. Chem. Res.* **48**, 3053–3063 (2015).

207. Sakaushi K. and Antonietti M. Carbon- and nitrogen-based organic frameworks. *Acc. Chem. Res.* **48**, 1591–1600 (2015).

208. Segura J. L., Mancheño M. J. and Zamora F. Covalent organic frameworks based on Schiff-base chemistry: synthesis, properties and potential applications. *Chem. Soc. Rev.* **45**, 5635–5671 (2016).

209. Das S., Heasman P., Ben T. and Qiu S. Porous organic materials: strategic design and structure–function correlation. *Chem. Rev.* **117**, 1515–1563 (2017).

210. Dogru M. and Bein T. On the road towards electroactive covalent organic frameworks. *Chem. Commun.* **50**, 5531–5546 (2014).

211. Long H., Jing N., Bin L., Bin W., Yunbo Z., Zhihong T., Junhe Y., Arne T., Linjie Z. Structural evolution of 2D microporous covalent triazine-based

framework toward the study of high-performance supercapacitors. *J. Am. Chem. Soc.* **137**, 219–225 (2015).

212. Ling P., Lei J. and Ju H. Porphyrinic metal-organic framework as electrochemical probe for DNA sensing via triple-helix molecular switch. *Biosens. Bioelectron.* **71**, 373–379 (2015).

213. Xianbo L., Xue W., Lidong W., Lingxia W., Dhanjai, Lei F., Yuan G., Jiping C. Response characteristics of bisphenols on a metal–organic framework-based tyrosinase nanosensor. *ACS Appl. Mater. Interfaces* **8**, 16533–16539 (2016).

214. Deep A., Bhardwaj S. K., Paul A. K., Kim K.-H. and Kumar P. Surface assembly of nano-metal organic framework on amine functionalized indium tin oxide substrate for impedimetric sensing of parathion. *Biosens. Bioelectron.* **65**, 226–231 (2015).

215. Hadi H., Hamid A., Ali D., Akbar B., Azadeh T., Ali Reza F. A novel electrochemical sensor based on metal-organic framework for electro-catalytic oxidation of L-cysteine. *Biosens. Bioelectron.* **42**, 426–429 (2013).

216. Wang X., Lu X., Wu L. and Chen J. 3D metal-organic framework as highly efficient biosensing platform for ultrasensitive and rapid detection of bisphenol A. *Biosens. Bioelectron.* **65**, 295–301 (2015).

217. Cheng Z., Xuerui W., Miao H., Xiaoyang L., Xiaoling W., Jun G. Immobilization on metal–organic framework engenders high sensitivity for enzymatic electrochemical detection. *ACS Appl. Mater. Interfaces* **9**, 13831–13836 (2017).

218. Wu Y., Han J., Xue P., Xu R. and Kang Y. Nano metal–organic framework (NMOF)-based strategies for multiplexed microRNA detection in solution and living cancer cells. *Nanoscale* **7**, 1753–1759 (2015).

219. Miller S. E., Teplensky M. H., Moghadam P. Z. and Fairen-Jimenez D. Metal-organic frameworks as biosensors for luminescence-based detection and imaging. *Interface Focus* **6**, 20160027 (2016).

220. Liao H., Ding H., Li B., Ai X. and Wang C. Covalent-organic frameworks: potential host materials for sulfur impregnation in lithium–sulfur batteries. *J. Mater. Chem. A* **2**, 8854–8858 (2014).

221. Jinhong B., Wei F., Liuyi LiJinyun W., Shijing L., Yunhui H., Minghua L., Ling W. Covalent Triazine-Based Frameworks as visible light photocatalysts for the splitting of water. *Macromol. Rapid Commun.* **36**, 1799–1805 (2015).

222. Gomes R., Bhanja P. and Bhaumik A. A Triazine-based covalent organic polymer for efficient CO2 adsorption. *Chem. Commun.* **51**, 10050–10053 (2015).

223. Fei C., Jianping G., Guotao W., Lin L., Miao Z., Teng H., Peikun W., Pei Y., Ping C. Covalent triazine-based framework as an efficient catalyst support for ammonia decomposition. *RSC Adv.* **5**, 3605–3610 (2015).

224. Kuecken S., Schmidt J., Zhi L. and Thomas A. Conversion of amorphous polymer networks to covalent organic frameworks under ionothermal conditions: a facile synthesis route for covalent triazine frameworks. *J. Mater. Chem. A* **3**, 24422–24427 (2015).

225. Laviron E. General expression of the linear potential sweep voltammogram in the case of diffusionless electrochemical systems. *J. Electroanal. Chem. Interfacial Electrochem.* **101**, 19–28 (1979).

226. Jin Y., Zhu Y. and Zhang W. Development of organic porous materials through Schiff-base chemistry. *CrystEngComm* **15**, 1484–1499 (2013).

227. Maahs G. and Hegenberg P. Syntheses and derivatives of squaric acid. *Angew. Chemie Int. Ed. English* **5**, 888–893 (1966).

228. Xia L., Zhifang W., Jiaxing S., Jia G., Yu Z., Peng C., Briana A., Shengqian M., Yao C., Zhenjie Z. Squaramide-decorated covalent organic framework as a new platform for biomimetic hydrogen-bonding organocatalysis. *Chem. Commun.* **55**, 5423–5426 (2019).

229. Kayaramkodath Chandran R., Leena G., Vivek Chandrakant W., Goudappagouda, R. Nandini D., Sukumaran Santhosh B. A squaraine-linked metalloporphyrin two-dimensional polymer photocatalyst for hydrogen and oxygen evolution reactions. *Chem. Commun.* **55**, 1627–1630 (2019).

230. Ranjeesh K. C., George L., Maibam A., Krishnamurty S. and Babu S. S. A durable metalloporphyrin 2D-polymer for photocatalytic hydrogen and oxygen evolution from river and sea waters. *ChemCatChem* **13**, 1717–1721 (2021).

231. Zhang W., Jiang P., Wang Y., Zhang J. and Zhang P. Bottom-up approach to engineer two covalent porphyrinic frameworks as effective catalysts for selective oxidation. *Catal. Sci. Technol.* **5**, 101–104 (2015).

232. Ian Storer R., Aciro C. and Jones L. H. Squaramides: physical properties, synthesis and applications. *Chem. Soc. Rev.* **40**, 2330–2346 (2011).

233. Huang L. and Cao G. 2D Squaraine-bridged covalent organic polymers with promising CO_2 storage and separation properties. *ChemistrySelect* **1**, 533–538 (2016).

234. Liu Y., Zhu Y., Alahakoon S. B. and Egap E. Synthesis of imine-based covalent organic frameworks catalyzed by metal halides and in situ growth of perovskite@COF composites. *ACS Mater. Lett.* **2**, 1561–1566 (2020).

235. Li Y., Chen W., Xing G., Jiang D. and Chen L. New synthetic strategies toward covalent organic frameworks. *Chem. Soc. Rev.* **49**, 2852–2868 (2020).

236. Wurm F. R. and Klok H.-A. Be squared: expanding the horizon of squaric acid-

mediated conjugations. *Chem. Soc. Rev.* **42**, 8220–8236 (2013).

237. Dong J., Wang Y., Liu G., Cheng Y. and Zhao D. Isoreticular covalent organic frameworks for hydrocarbon uptake and separation: the important role of monomer planarity. *CrystEngComm* **19**, 4899–4904 (2017).
238. Chunhui D., Ting H., Lixiang Z., Xingang L., Wenlong Z., Can X., Shuzhou L., Donglin J., Bin L. 2,4,6-Triphenyl-1,3,5-Triazine based covalent organic frameworks for photoelectrochemical H_2 evolution. *Adv. Mater. Interfaces* **8**, 2002191 (2021).
239. Law K.-Y. and Bailey F. C. Squaraine chemistry. Synthesis and characterization of squaraine dyes having self-organizing properties. *Dye. Pigment.* **20**, 25–40 (1992).
240. Basma N., Cullen P. L., Clancy A. J., Shaffer M. S.P., Skipper N. T., Headen T. F., Howard, C. A. The liquid structure of the solvents dimethylformamide (DMF) and dimethylacetamide (DMA). *Mol. Phys.* **117**, 3353–3363 (2019).
241. Bras J. L. and Muzart J. N,N-Dimethylformamide and N,N-Dimethylacetamide as carbon, hydrogen, nitrogen, and/or oxygen sources. *Solvents as Reagents in Organic Synthesis* 199–314 (2017).
242. Infrared Spectroscopy. in *ACS Reagent Chemicals* (American Chemical Society, 2017). doi:doi:10.1021/acsreagents.2008
243. Holder C. F. and Schaak R. E. Tutorial on Powder X-ray diffraction for characterizing nanoscale materials. *ACS Nano* **13**, 7359–7365 (2019).
244. Weinberger P. Revisiting Louis de Broglie's famous 1924 paper in the philosophical magazine . *Philos. Mag. Lett.* **86**, 405–410 (2006).
245. Xing L., Hai Sen X., Kai L., See Wee C., Xiaoxu Z., Noopur J., Hai X., Jingsi Q., Qiang G., In Hyeok P., Su Ying Q., Utkur M., Kian Ping L. Partitioning the interlayer space of covalent organic frameworks by embedding

pseudorotaxanes in their backbones. *Nat. Chem.* **12**, 1115–1122 (2020).

246. Kawal P., Girish G., Moumita K., Sushil Kumar K., Deepak B. S., Harish K. S., Subash Chandra S., Pascal Van Der V., Sandipan R., Mechanochemical synthesis of a new triptycene-based imine-linked covalent organic polymer for degradation of organic dye. *Cryst. Growth Des.* **19**, 2525–2530 (2019).

247. Lukose B., Kuc A. and Heine T. The structure of layered covalent-organic frameworks. *Chem. – A Eur. J.* **17**, 2388–2392 (2011).

248. Na Z., Taisheng W., Xing W., Chen J., Fang C., Wei B., Ruke B. Self-exfoliation of 2D covalent organic frameworks: morphology transformation induced by solvent polarity. *RSC Adv.* **8**, 3803–3808 (2018).

249. Huang N., Wang P., Addicoat M. A., Heine T. and Jiang D. Ionic covalent organic frameworks: design of a charged interface aligned on 1D channel walls and its unusual electrostatic functions. *Angew. Chemie Int. Ed.* **56**, 4982–4986 (2017).

250. Wu X., Han X., Liu Y., Liu Y. and Cui Y. Control interlayer stacking and chemical stability of two-dimensional covalent organic frameworks via steric tuning. *J. Am. Chem. Soc.* **140**, 16124–16133 (2018).

251. Vardhan H., Nafady A., Al-Enizi A. M. and Ma, S. Pore surface engineering of covalent organic frameworks: structural diversity and applications. *Nanoscale* **11**, 21679–21708 (2019).

252. Langmuir, I. The constitution and fundemental properties of solids and liquids. PART I. SOLIDS. *J. Am. Chem. Soc.* **38**, 2221–2295 (1916).

253. Brunauer S., Emmett P. H. and Teller E. Adsorption of gases in multimolecular layers. *J. Am. Chem. Soc.* **60**, 309–319 (1938).

254. Feng X., Ding X. and Jiang D. Covalent organic frameworks. *Chem. Soc. Rev.* **41**, 6010–6022 (2012).

255. Mohammad Adil A., Nabin G., Khan Mamun R., Behzad B., Raja Sekhar B., Ashim G., Ashraful Haider C., Parameswar Krishnan I., Qiquan Q., Thermal stability and performance enhancement of perovskite solar cells through oxalic acid-induced perovskite formation. *ACS Appl. Energy Mater.* **3**, 2432–2439 (2020).

256. Maji T. K. and Kitagawa S. Chemistry of porous coordination polymers. *Pure Appl. Chem.* **79**, 2155–2177 (2007).

257. Thanasekaran P., Su C.-H., Liu Y.-H. and Lu K.-L. Weak interactions in conducting metal–organic frameworks. *Coord. Chem. Rev.* **442**, 213987 (2021).

258. Cox J. R., Müller P. and Swager T. M. Interrupted energy transfer: highly selective detection of cyclic ketones in the vapor phase. *J. Am. Chem. Soc.* **133**, 12910–12913 (2011).

259. Taihong L., Mykhailo V. B., Kevin D. B., Dane A., Artëm E. M., David J. H., Eric W. Van S., Linear photophysics and femtosecond nonlinear spectroscopy of a star-shaped squaraine derivative with efficient two-photon absorption. *J. Phys. Chem. C* **120**, 11099–11110 (2016).

260. Taihong L., Xinglei L., Weina W., Zhipu L., Muqiong L., Shengli Z., Cristina S., Anna P., Yuanwei Z., Mikas V., Mykhailo V. B., David J. H., Eric W. Van S., Yu F., Kevin D. B. Systematic molecular engineering of a series of aniline-based squaraine dyes and their structure-related properties. *J. Phys. Chem. C* **122**, 3994–4008 (2018).

261. Manman M., Yanwen W., Yutian Q., Xilong Y., Yang L., Ligong C. Two-dimensional imine-linked covalent organic frameworks as a platform for selective oxidation of olefins. *ACS Appl. Mater. Interfaces* **9**, 22856–22863 (2017).

262. Park S., Kim M.-S., Jang W., Park J. K. and Wang D. H. Covalent organic nanosheets for effective charge transport layers in planar-type perovskite solar cells. *Nanoscale* **10**, 4708–4717 (2018).

263. Xing L., Qiang G., J. A., Hai Sen X., Zhongxin C., Wei T., Cuibo L., Xiangyan S., K. V. Adarsh., Yixin L., Kian Ping L. Molecular engineering of bandgaps in covalent organic frameworks. *Chem. Mater.* **30**, 5743–5749 (2018).

264. Olena Y., David F., Lisa Zur B., Rudolf Z., Jürgen H., Sabine L., Electrochemically induced reversible and irreversible coupling of triarylamines. *J. Phys. Chem. B* **116**, 30–39 (2012).

265. Te Fang Y., Kuo Yuan C., Hsu Chun C., Yen Wei L., Ming Yu K., Yuhlong Oliver S. Studies on the structure of N-phenyl-substituted hexaaza[1 6]paracyclophane: Synthesis, electrochemical properties, and theoretical calculation. *J. Org. Chem.* **77**, 8627–8633 (2012).

266. Sunny K.S. F., Felipe L. O., Thiago C. dos S., Danilo H., Claudia M., Célia M. R., Pierre M. E. A carbocationic triarylmethane-based porous covalent organic network. *Chem. – A Eur. J.* **27**, 2342–2347 (2021).

267. A. Alec T., Andrea C., Alexandra C. F., Michael E. F., Vitalie S., Paul H., R. Adam K., Veronika S., Farid El G., Heayoung P. Y., François L., Mark D. A., Tunable electrical conductivity in metal-organic framework thin-film devices. *Science (80-.).* **343**, 66 LP – 69 (2014).

268. Bertrand G. H. V, Michaelis V. K., Ong T.-C., Griffin R. G. and Dincă M. Thiophene-based covalent organic frameworks. *Proc. Natl. Acad. Sci.* **110**, 4923 – 4928 (2013).

269. Xiaoyan W., Linjiang C., Samantha Y. C., Marc A. L., Yongzhen W., Wei Hong Z., Rob C., Yong Y., Martijn A. Z., Reiner Sebastian S., Andrew I. C. Sulfone-containing covalent organic frameworks for photocatalytic hydrogen

evolution from water. *Nat. Chem.* **10**, 1180–1189 (2018).

270. Torben S., Alexander G. H., Jonathan KampmannIlina K., Mona C., Julian M. R., Austin E., Markus D., Simon H., Kristina P., Daniel B., Paul K., Dana D. M., Dina Fattakhova-R., Thomas B., Oriented films of conjugated 2D covalent organic frameworks as photocathodes for water splitting. *J. Am. Chem. Soc.* **140**, 2085–2092 (2018).
271. Enquan J., Keyu G., Ka Hung L., Weiming J., Juan L., Qiuhong J., Stephan I., Donglin J., Topology-templated synthesis of crystalline porous covalent organic frameworks. *Angew. Chemie Int. Ed.* **59**, 12162–12169 (2020).
272. Niklas K., Derya B., Stephan R., Mona C., Laura A., Fabian C. H., Florian A., Thomas B. Oligothiophene-bridged conjugated covalent organic frameworks. *J. Am. Chem. Soc.* **139**, 8194–8199 (2017).
273. Bappaditya G., Vladimir S., Sabrina R., Matthias G., Dana D. M., Thomas B., Frank W., Florian B. Microtubular self-assembly of covalent organic frameworks. *Angew. Chemie Int. Ed.* **57**, 846–850 (2018).
274. Fei Y., Wenbo L., Bang L., Dan T., Jing Lin Z., Qichun Z. Photostimulus-responsive large-area two-dimensional covalent organic framework films. *Angew. Chemie Int. Ed.* **58**, 16101–16104 (2019).
275. Shunqi X., Hanjun S., Matthew A., Bishnu P. B., Fan H., Sang Wook P., Silvia P., Tao Z., Wenbo S., Eike B., Yang H., Marcus R., Xinliang F. Thiophene-bridged donor–acceptor sp2-carbon-linked 2D conjugated polymers as photocathodes for water reduction. *Adv. Mater.* **33**, 2006274 (2021).
276. Liu M., Yao C., Liu C. and Xu Y. Thiophene-based porous organic networks for volatile iodine capture and effectively detection of mercury ion. *Sci. Rep.* **8**, 14071 (2018).
277. Xiaowei P., Xihao Q., Qiheng Z., Yuansheng G., Hanzhong K., Guoe C. N- and

S-rich covalent organic framework for highly efficient removal of indigo carmine and reversible iodine capture. *Microporous Mesoporous Mater.* **296**, 109990 (2020).

278. Du W., Qin Y., Ni C., Dai W. and Zou J. Efficient capture of volatile iodine by thiophene-containing porous organic polymers. *ACS Appl. Polym. Mater.* **2**, 5121–5128 (2020).
279. Huang J. and Yu G. Recent progress in quinoidal semiconducting polymers: structural evolution and insight. *Mater. Chem. Front.* **5**, 76–96 (2021).
280. Chen W.-C. and Jenekhe S. A. Small-bandgap conducting polymers based on conjugated poly(heteroarylene methines). 2. Synthesis, structure, and properties. *Macromolecules* **28**, 465–480 (1995).
281. Tomokazu U., Yusuke W., Masaaki O., Douvogianni E., Tetsuya S., Hiroshi I. Synthesis of low bandgap polymers based on thienoquinodimethane units and their applications in bulk heterojunction solar cells. *J. Mater. Chem.* **22**, 24394–24402 (2012).
282. Chen W.-C. and Jenekhe S. A. Model compound studies of small bandgap conjugated poly(heteroarylene methines). *Macromol. Chem. Phys.* **199**, 655–666 (1998).
283. Jenekhe S. A. A class of narrow-band-gap semiconducting polymers. *Nature* **322**, 345–347 (1986).
284. Lee Y. and Kertesz M. The effect of heteroatomic substitutions on the band gap of polyacetylene and polyparaphenylene derivatives. *J. Chem. Phys.* **88**, 2609–2617 (1988).
285. Montgomery L. K., Huffman J. C., Jurczak E. A. and Grendze M. P. The molecular structures of Thiele's and Chichibabin's hydrocarbons. *J. Am. Chem. Soc.* **108**, 6004–6011 (1986).

286. Mulvaney J. E. and Green G. D. Polyesters from α,α′-dicarbomethoxy-α,α′-diphenyl-p-xylylene and the synthesis and properties of a new quinodimethane. *J. Polym. Sci. Part A Polym. Chem.* **26**, 2597–2602 (1988).

287. Brandt M. W., Mulvaney J. E., Hall Jr., H. K. and Green G. D. Synthesis and polymerizability of 7,8-dicyano-7,8-diphenylquinodimethane. *J. Polym. Sci. Part A Polym. Chem.* **27**, 1957–1965 (1989).

288. Moreno P. A., Rodero A. and Fernandez J. E. Synthesis of 1,4-cyclohexadienylbis(benzylidene). *J. Org. Chem.* **47**, 3986–3987 (1982).

289. Zaman M. B. and Perepichka D. F. A new simple synthesis of poly(thiophene-methine)s. *Chem. Commun.* 4187–4189 (2005). doi:10.1039/B506138E

290. Kai G., Botao W., Yu J., Zhongli W., Ziqi L., Yuning L., Yunfeng D., Yanhou G., Synthesis of an isomerically pure thienoquinoid for unipolar n-type conjugated polymers: effect of backbone curvature on charge transport performance. *J. Mater. Chem. C* **7**, 10352–10359 (2019).

291. Mushkacheva G., Rabinovich E., Privalov V., Povolotskaya S., Shorokhova V. Sokolova S., Turdakova V., Ryzhova E., Hall P., Schneider A. B., Preston D. L. Ron E. Thyroid abnormalities associated with protracted childhood exposure to ^{131}I from atmospheric emissions from the mayak weapons facility in russia. *Radiat. Res.* **166**, 715–722 (2006).

292. Riley B. J., Vienna J. D., Strachan D. M., McCloy J. S. and Jerden J. L. Materials and processes for the effective capture and immobilization of radioiodine: A review. *J. Nucl. Mater.* **470**, 307–326 (2016).

293. Pei C., Ben T., Xu S. and Qiu S. Ultrahigh iodine adsorption in porous organic frameworks. *J. Mater. Chem. A* **2**, 7179–7187 (2014).